IMPROVED RF NOISE MODELING FOR SILICON-GERMANIUM

HETEROJUNCTION BIPOLAR TRANSISTORS

Except where reference is made to the work of others, the work described in this dissertation is my own or was done in collaboration with my advisory committee. This dissertation does not include proprietary or classified information.

_____

Kejun Xia

Certificate of Approval:

_____

Richard C. Jaeger
Distinguished University Professor
Electrical and Computer Engineering

_____

Guofu Niu, Chair
Professor
Electrical and Computer Engineering

_____

Fa Foster Dai
Associate Professor
Electrical and Computer Engineering

_____

Stuart Wentworth
Associate Professor
Electrical and Computer Engineering

_____

Joe F. Pittman
Interim Dean
Graduate School

# IMPROVED RF NOISE MODELING FOR SILICON-GERMANIUM HETEROJUNCTION BIPOLAR TRANSISTORS

Kejun Xia

A Dissertation

Submitted to

the Graduate Faculty of

Auburn University

in Partial Fulfillment of the

Requirements for the

Degree of

Doctor of Philosophy

Auburn, Alabama
December 15, 2006

IMPROVED RF NOISE MODELING FOR SILICON-GERMANIUM

HETEROJUNCTION BIPOLAR TRANSISTORS

Kejun Xia

Permission is granted to Auburn University to make copies of this dissertation at its discretion, upon the request of individuals or institutions and at their expense. The author reserves all publication rights.

_____

Signature of Author

_____

Date of Graduation

# VITA

Kejun Xia, elder son of Shengbin Xia and Meiqin Zhu, was born in Shanxi Town, Wenzhou City, Zhejiang Province, China on June 25, 1978. Upon graduation from Wenzhou No. 1 High School in 1996, he entered Tianjin University, Tianjin, China, from which he received the B.E. and M.S. degrees in electronics in 2000 and 2003, respectively. He entered Electrical and Computer Engineering Department graduate program of Auburn University in 2003 to work towards the Ph.D. degree.

DISSERTATION ABSTRACT

# IMPROVED RF NOISE MODELING FOR SILICON-GERMANIUM HETEROJUNCTION BIPOLAR TRANSISTORS

Kejun Xia

Doctor of Philosophy, December 15, 2006
(M.S., Tianjin University, 2003)
(B.E., Tianjin University, 2000)

232 Typed Pages

Directed by Guofu Niu

Accurate radio frequency (RF) noise models for individual transistors are critical to minimize noise during mixed-signal analog and RF circuit design. This dissertation proposes two improved RF noise models for SiGe Heterojunction Bipolar Transistors (SiGe HBTs), a semi-empirical model and a physical model. A new parameter extraction method for small signal equivalent circuit of SiGe HBT has also been developed.

The semi-empirical model extracts intrinsic base and collector current noise from measured device noise parameters using standard noise de-embedding method based on a quasi-static input equivalent circuit. Equations are then developed to model these noise sources by examining the frequency and bias dependences. The model is shown to work at frequencies up to at least half of the peak unit-gain cutoff frequency ($f_T$), and at biasing currents below high injection $f_T$ roll off. The model is scalable for emitter geometry, and can be easily implemented using currently available CAD tools.

For the physical model, improved electron and hole noise models are developed. The impact of the collector-base space charge region (CB SCR) on electron RF noise is examined to determine

its importance for scaled SiGe HBTs. The van Vliet model is then improved to take into account the CB SCR effect. The fringe EB junction effect is included to improve base hole noise. The base noise resistance is found to be different from the AC intrinsic base resistance, which cannot be explained by the fringe effect. Applying a total of four bias-independent model parameters, the combination of new electron and hole noise models based on a non-quasistatic input equivalent circuit provides excellent noise parameter fittings for frequencies up to 26 GHz and all biases before $f_T$ roll off for three generations of SiGe HBTs. The model also has a good emitter geometry scaling ability.

The new small signal parameter extraction method developed here is based on a Taylor expansion analysis of transistor Y-parameters. This method is capable of extracting both input non-quasistatic effect and output non-quasistatic effect, which are not available for any of the existing extraction methods.

## ACKNOWLEDGMENTS

The author would like to acknowledge his parents and his wife for their unconditional love and continuous support. He would like to thank his advisor Prof. Guofu Niu for the precious opportunity to conduct the interesting RF noise research and for the wide-scope instruction on semiconductor devices. He also thanks his advisory committee, Dr. Richard C. Jaeger, Dr. Fa Foster Dai, and Dr. Stuart Wentworth for their interests and comments. He is grateful to the outside reader Dr. An-Ban Chen for the discussions on Green's functions. He would like to acknowledge financial support from SRC under grant #2003-NJ-1133 and IBM under an IBM Faculty Partnership Award.

The author would like to thank the semiconductor device physics / TCAD research group members, especially Yan Cui and Yun Shi, for their help in microscopic device simulation using software DESSIS. In addition, he is grateful to J. Cressler, D. Sheridan, S. Sweeney and the IBM SiGe team for their data support and contributions.

Style manual or journal used IEEE Transactions on Electron Devices (together with the style known as "auphd"). Bibliography follows van Leunen's *A Handbook for Scholars*.

Computer software used The document preparation package TEX (specifically LATEX) together with the departmental style-file `auphd.sty`. The plots were generated using Microsoft Viso® and MATLAB®.

TABLE OF CONTENTS

LIST OF FIGURES xiii

LIST OF TABLES xix

1 INTRODUCTION 1
1.1 Motivation . . . 1
1.2 SiGe HBT fundamentals . . . 2
1.2.1 SiGe as base material . . . 2
1.2.2 Performance parameters . . . 5
1.2.3 Improving $f_T$ and $f_{max}$ . . . 6
1.2.4 SiGe BiCOMS technology . . . 8
1.3 Noise parameters for two-port network . . . 9
1.4 Frequency and bias dependence of noise parameters for SiGe HBTs . . . 12
1.5 Noise performance trends for SiGe HBTs . . . 14
1.6 Noise modeling considerations and methodology for SiGe HBTs . . . 15
1.7 Summary . . . 16

2 RF NOISE THEORY FOR SIGE HBTS 17
2.1 RF noise sources . . . 17
2.1.1 Velocity fluctuation noise . . . 21
2.1.2 GR noise . . . 29
2.2 Electron noise of base region without distributive effect . . . 30
2.2.1 1-D solution . . . 30
2.2.2 General 3-D solution by van Vliet . . . 45
2.2.3 Evaluation of van Vliet solution for finite exit velocity boundary condition 46
2.3 Extension to including emitter hole noise . . . 47
2.3.1 3-D van Vliet model . . . 47
2.3.2 1-D solution . . . 50
2.3.3 Evaluation of finite surface recombination velocity effect . . . 51
2.3.4 Comparison of base electron and emitter hole contributions to $S_{ib}$ . . . 52
2.4 Compact noise model including distributive effect . . . 53
2.4.1 Compact noise model assuming uniform $f_T$ across EB junction . . . 53
2.4.2 NQS and QS base resistance . . . 56
2.5 Present noise models and implementation problems . . . 59
2.5.1 SPICE model . . . 59
2.5.2 Transport noise model . . . 59
2.5.3 Brutal use of van Vliet model . . . 60

2.5.4 $4kTr_{bi}$ for $r_{bi}$ noise . . . 61
2.6 Methodologies to improve noise modeling . . . 61
2.7 Summary . . . 62

3 SMALL SIGNAL PARAMETER EXTRACTION 64
3.1 Necessity of including input NQS effect in equivalent circuit . . . 65
3.2 NQS Equivalent circuit . . . 66
3.2.1 CB SCR effect . . . 67
3.2.2 NQS equivalent circuit . . . 69
3.3 Parameter extraction . . . 71
3.3.1 $C_{cs}$, $r_{cs}$, $\gamma$ and $r_e$ extraction . . . 73
3.3.2 $C_{bct}$, $C_{bcx}$, $C_{bci}$, $r_c$ and $g_m$ extraction . . . 74
3.3.3 $r_{bx}$ and $r_{bi}$ extraction . . . 75
3.3.4 $C_{bex}$ and $C_{bej}$ extraction . . . 77
3.3.5 $C_{bed}$, $r_d$, $g_{be}$ and $\tau_d$ extraction . . . 79
3.4 Results and discussions . . . 81
3.4.1 Extraction and modeling results . . . 81
3.4.2 Discussions . . . 81
3.5 Extraction of bias dependent $r_{bi}$ . . . 86
3.6 Summary . . . 89

4 SEMI-EMPIRICAL NOISE MODEL BASED ON EXTRACTION 91
4.1 Intrinsic noise extraction . . . 92
4.1.1 Two basic noise de-embedding techniques . . . 92
4.1.2 SiGe HBT noise calculation . . . 94
4.1.3 Extracted intrinsic noise . . . 96
4.2 Semi-empirical intrinsic noise model . . . 99
4.2.1 $S_{ib}$ . . . 99
4.2.2 $S_{ic}$ . . . 102
4.2.3 Imaginary part of $S_{icib^*}$ [$\Im(S_{icib^*})$] . . . 103
4.2.4 Real Part of $S_{icib^*}$ [$\Re(S_{icib^*})$] . . . 106
4.2.5 Generalized Model Equations . . . 108
4.2.6 Noise Parameter Modeling Results . . . 111
4.2.7 Sensitivity Analysis . . . 112
4.3 Emitter geometry scaling . . . 114
4.3.1 Intrinsic noise scaling . . . 115
4.3.2 Extrinsic noise scaling . . . 117
4.3.3 Comparison of intrinsic noise with resistance noise . . . 119
4.4 Implementation in CAD tools . . . 119
4.5 Summary . . . 123

5 IMPROVED PHYSICAL NOISE MODEL 125
5.1 CB SCR effect on electron noise . . . 125
5.1.1 Model equation derivation . . . 127
5.1.2 Verification and discussion . . . 131
5.2 Fringe BE junction effect on base hole noise . . . 133

5.2.1 Physical considerations . . . 135
5.2.2 Model equation derivation . . . 136
5.2.3 $R_{bn}$, instead of $r_{bi}$, as base noise resistance . . . 141
5.3 Improved physical noise model . . . 142
5.3.1 Implementation technique . . . 142
5.3.2 Modeling results . . . 144
5.3.3 Geometry scaling . . . 149
5.3.4 Model parameter impacts and extraction guidelines . . . 150
5.4 Summary . . . 152

BIBLIOGRAPHY 154

APPENDICES 159

A REPRESENTATION TRANSFORMATION FOR TWO-PORT NETWORK 160
A.1 T-matrix for noise representation transformation . . . 160
A.2 Derivation of Noise Parameters . . . 160

B APPROXIMATION OF INTRINSIC BASE RESISTANCE NOISE CONSIDERING CURRENT CROWDING EFFECT 162
B.1 General Principles . . . 162
B.2 Circular Emitter BJT . . . 163
B.3 Rectangular Emitter BJT . . . 164

C DERIVATION OF NQS DELAY TIME WITH CB SCR 166

D ANALYTICAL Y-PARAMETERS 167
D.1 Manual Derivation of Analytical Y-parameters . . . 167
D.2 MATLAB Code for Analytical Y-parameters Derivation . . . 168
D.3 MATLAB code for Taylor expansion . . . 169

E MATLAB CODE FOR SMALL SIGNAL PARAMETER EXTRACTION 171

F MATLAB CODE FOR INTRINSIC NOISE EXTRACTION 177
F.1 MATLAB code . . . 177
F.2 Data of S-parameters and noise . . . 179

G VERILOG-A CODE OF VBIC MODEL FOR SEMI-EMPIRICAL NOISE MODEL IMPLEMENTATION 195

H DERIVATION OF LOW INJECTION VAN VLIET MODEL IN ADMITTANCE REPRESENTATION 196
H.1 Fundamentals . . . 196
H.1.1 Operator . . . 196
H.1.2 Green's theorem for $L_p$ . . . 197
H.1.3 Dirac delta function . . . 197
H.1.4 $\Lambda$ theorem . . . 198

H.2 Problem setup for base low injection noise of PNP transistor . . . . . 198
H.3 Green's function of homogeneous boundary . . . . . 200
H.4 Hole concentration fluctuation and its spectrum . . . . . 202
H.4.1 van Vliet - Fasset form of noise spectrum . . . . . 203
H.4.2 Solution for $\Lambda$ theorem at low injection . . . . . 206
H.5 Terminal noise current spectrum . . . . . 207
H.5.1 Spectrum due to $j^o$ . . . . . 208
H.5.2 Spectrum due to correlation of $j^o$ and $\gamma$ . . . . . 209
H.5.3 Terminal total noise current density spectrum . . . . . 210
H.6 Y-parameters in homogeneous Green's function . . . . . 210
H.7 Relation between Y-parameter and noise spectrum . . . . . 211
H.7.1 Common-base noise for BJTs . . . . . 212
H.7.2 Common-emitter noise for BJTs . . . . . 212

## LIST OF FIGURES


1.1 Energy band diagram of a graded-base SiGe HBT. . . . . 3

1.2 Cross section of a raised-base SiGe HBT. . . . . 4

1.3 Vertical scaling strategy for SiGe HBT. . . . . 6

1.4 Two-port noise representations. (a) Admittance (Y-) representation, (b) Impedance (Z-) representation, (c) Chain (ABCD-) presentation, and (d) hybrid (H-) representation. . . . . 10

1.5 Noise parameters versus $I_c$ for a 50 GHz SiGe HBT with $A_E = 0.24 \times 20 \times 2\ \mu m^2$. Six frequency points (2 GHz, 5 GHz, 10 GHz, 15 GHz, 20 GHz and 25 GHz) are measured. . . . . 12

1.6 Simplified common-emitter small signal equivalent circuit with noise sources for SiGe HBTs. . . . . 13

1.7 HBT optimized noise figure *Opt*. $F_{min}$ versus frequency for four SiGe HBT BiCMOS technologies, including three high performance variants at the 0.5-, 0.18-, and 0.13- $\mu$m nodes as well as a cost-reduced (and slightly higher breakdown voltage) variant at the 0.18- $\mu$m node. . . . . 15

2.1 Illustration of vector dipole current. . . . . 25

2.2 Illustration of base region with built-in electric field. . . . . 30

2.3 Equivalent circuit for intrinsic base of bipolar transistor without $r_{bi}$. (a) With NQS input. (b) With QS input. . . . . 35

2.4 Y-parameter modeling result using equivalent circuit with NQS input. $\mu_0$=270 cm/vs$^2$. $\tau_n = 1.54 \times 10^-7 s$. $n_{00} = 50/cm^3$. $T = 300K$. $d_B$=45 nm. $V_{BE}$=0.8 V. $v_{exit} = 1 \times 10^7$ cm/s. $f_T = g_m/C^b_{bed}$=184 GHz for $\eta = 5$. $f_T = g_m/C^b_{bed}$=83 GHz for $\eta = 0$. $A_E$=1 cm$^2$. . . . . 36

2.5 Delay times of base region. $\mu_0$=270 cm/vs$^2$. $\tau_n = 1.54 \times 10^-7 s$. $n_{00} = 50/cm^3$. $T = 300K$. $d_B$=45 nm. $A_E$=1 cm$^2$. . . . . 37

2.6 Input NQS delay resistance $r_d^b$ versus $\eta$ at $V_{BE}$=0.8 V. $\mu_0$=270 cm/vs$^2$. $\tau_n = 1.54 \times 10^-7s$. $n_{00} = 50\ /cm^3$ ($N_A = 2 \times 10^{18}\ /cm^3$). $T = 300K$. $d_B$=45 nm. $W_E$=0.24 $\mu$m. $L_E$=20 $\mu$m. $A_E$=1 cm$^2$. . . . . 38

2.7 Setup for solving Langevin equation. . . . . 41

2.8 Scalar Green functions. . . . . 42

2.9 Vector Green functions. . . . . 43

2.10 Evaluation of van Vliet model for base region noise under $d_B = 100nm$, $\eta = 5.4$ ($|E|$=70.2 kV/cm), $V_{BE}$=0.8V, where "$f_T$"$\equiv g_m/C_{be}$=698 GHz. $A_E$=1 cm$^2$. . . . 47

2.11 Evaluation of van Vliet model for base region noise under $d_B = 20nm$, $\eta = 5.4$ ($|E|$=0 kV/cm), $V_{BE}$=0.8V, where "$f_T$"$\equiv g_m/C_{be}$=698 GHz. $A_E$=1 cm$^2$. . . . . 48

2.12 Evaluation of van Vliet model for base region noise under $d_B = 20nm$, $\eta = 5.4$ ($|E|$=70.2 kV/cm), $V_{BE}$=0.8V. $A_E$=1 cm$^2$. . . . . 49

2.13 Evaluation of emitter hole noise model. $\tau_p = 1.54 \times 10^-7s$. $\eta_E$=0. $p_{00} = 6.66/cm^3$. $T = 300K$. $d_E$=120 nm. $V_{BE}$=0.8 V. $\mu_p$=220 cm/cs$^2$. $A_E$=1 cm$^2$. . . . . 51

2.14 Comparison of base electron and emitter hole contributions to $S_{ib}$. $\tau_p = 1.54 \times 10^-7s$. $\eta_E$=0. $p_{00} = 6.66/cm^3$. $T = 300K$. $d_E$=120 nm. $V_{BE}$=0.8 V. $\mu_p$=220 cm/cs$^2$. $\tau_n = 1.54 \times 10^-7s$. $\eta_B$=5.4. $n_{00} = 333/cm^3$. $d_E$=20 nm. $\mu_n$=450 cm/cs$^2$. $V_{exit} = 1 \times 10^7\ cm/s$. $\tau_c = 0.57ps$. $A_E$=1 cm$^2$. . . . . 52

2.15 Small signal equivalent circuit for a transistor divided into 1-D sub-transistors. . . . 53

2.16 Compact noise model assuming uniform $f_T$ for whole EB junction. . . . . 54

2.17 Equivalent circuit for intrinsic base of bipolar transistor with $r_{bi}$: (a) With NQS input; (b) With QS input. . . . . 57

2.18 Comparison between $r_{bi}$, $r_{bi,QS}$ and $r_d^b$. $\tau_p = 1.54 \times 10^-7s$. $\eta_E$=0. $p_{00} = 0.466\ /cm^3$. $T = 300K$. $d_E$=120 nm. $\mu_{p0}$=225 cm/cs$^2$. $\tau_n = 1.54 \times 10^-7s$. $\eta_B$=5.4. $n_{00} = 23.3\ /cm^3$ ($N_A = 4.3 \times 10^18\ /cm^3$). $d_E$=20 nm. $\mu_{n0}$=450 cm/cs$^2$. $V_{exit} = 1 \times 10^7\ cm/s$. $\tau_c = 0.57ps$. $C_{bej}$=38 fF. $W_E$=0.12 $\mu$m. $L_E$=18 $\mu$m. $A_E$=1 cm$^2$. . . . . 58

3.1 Intrinsic NQS small signal equivalent circuit of SiGe HBTs: (a) without $\tau_c$; (b) with $\tau_c$. . . . . 68

3.2 CB SCR effect on $\tau_{in}$ and $\tau_{out}$. For the 1-D base region, $V_{sat}^{bs} = 1 \times 10^7$ cm/s, $\mu_{n0}$ = 270 cm/Vs$^2$, $\tau_n$=0.154 $\mu$s, $T$=300 K. . . . . 68

3.3 CB SCR and Ge gradient impacts on the importance of input NQS effect. For the 1-D base region, $d_B$=20 nm, $V_{sat}^{bs} = 1 \times 10^7$ cm/s, $\mu_{n0} = 270$ cm/Vs$^2$, $\tau_n$=0.154 $\mu$s, $T$=300 K. $V_{BE}$ =0.8 V. . . . . 69

3.4 Small signal equivalent circuit of SiGe HBTs with substrate tied to emitter. . . . . 70

3.5 Illustration of Taylor expansions coefficient extraction for (a) $\Re(Y_{11}^{BM} + Y_{12}^{BM})_2$, and (b) $\Im(Y_{22}^{BM})_1$. . . . . 73

3.6 Small signal equivalent circuit of SiGe HBTs for block $B_M$. . . . . 75

3.7 $\Im(Y_{21}^{BM} - Y_{12}^{BM})_1/g_m$ versus $\Im(Y_{11}^{BM} + Y_{12}^{BM})_1$. The slope of fitting line gives $r_{bx}+r_{bi}$. 76

3.8 $\Im(Y_{22}^{BM})_1$ versus $g_m C_{bct}$. The slope of fitting line gives $r_{bx} + \gamma r_{bi}$. . . . . 77

3.9 Illustration of low current limit extraction for (a) $\Re(Y_{11}^{BM} + Y_{12}^{BM})_2$, and (b) $\Im(Y_{11}^{BM} + Y_{12}^{BM})_1$. . . . . 78

3.10 Illustration of $C_{bet}$ splitting: (a) Linear fitting for $C_{bet}$ versus $g_m$; (b) Extracted $C_{bed}$ and $C_{bej}$ versus $g_m$. . . . . 80

3.11 Extracted $r_d$ versus $1/I_C$. $r_{bx}$ and $r_{bi}$ are shown for reference. . . . . 81

3.12 Comparison of Y-parameters for experimental data and modeling results at high bias. . . . . 83

3.13 Intrinsic $\Re(Y_{11}^{BI})$ extraction and modeling results for three biases. . . . . 84

3.14 Comparison of $S_{ib}$ obtained from noise de-embedding of experimental noise data and van Vliet model $S_{ib} = 4kT\Re(Y_{11}^{BI}) - 2qI_B$ for a 50 GHz $A_E = 0.24 \times 20 \times 2$ $\mu$m$^2$ SiGe HBT at three biases. . . . . 85

3.15 Comparison of $r_{bi}$ extracted using equivalent circuit with and without including input NQS effect. . . . . 86

3.16 Extracted delay times and modeling results for three biases. . . . . 87

3.17 NQS delay time ($\tau_{in}$ and $\tau_d$ or $\tau_{out}$) extraction. . . . . 88

3.18 Bias dependent $r_{bi}$ compared with $\overline{r_{bi}}$ for (a) 50 GHz SiGe HBT and (b) 180 GHz SiGe HBTs. . . . . 90

4.1 Series block de-embedding using impedance representation. . . . . 93

4.2 Parallel block de-embedding using admittance representation. . . . . 93

4.3 Small signal equivalent circuit of SiGe HBT used for Y-parameter and noise parameters de-embedding. . . . . 95

4.4 Extracted intrinsic noise sources as a function of frequency. . . . . 99

4.5 (a) $(S_{ib} - 2qI_B)$ versus $\omega^2$ at $I_c$=4.9 mA and 17.9 mA. (b) $C_{ib}$ (denoted as $(S_{ib} - 2qI_B)/\omega^2$) versus $g_m$. . . . . 101

4.6 (a) Measured $S_{ic}$ versus frequency at $I_c$=1.40 mA, 10.6 mA and 19.4 mA. (b) $C_{ic}$ (denoted as $S_{ic}/\Re(Y_{21})$) versus $g_m$. . . . . 103

4.7 Simulated $S_{ic}$ versus frequency at different $I_c$ level. . . . . 104

4.8 (a) $\Im(S_{icib^*})$ versus $\omega$ at $I_C$=4.9 mA and 17.9 mA. (b) $C^i_{icib^*}$ (denoted as $\Im(S_{icib^*}/\omega)$) versus $g_m^{1.8}$. . . . . 105

4.9 $\Re(S_{icib^*})$ versus $\omega^2$ at $I_c$=4.9 mA and 17.9 mA. . . . . 107

4.10 (a) $C^{r2}_{icib^*}$ (denoted as $\Re(S_{icib^*})/\omega^2$) versus $g_m^2$. (b) $C^{r1}_{icib^*}$ (denoted as $\Re(S_{icib^*})[\omega = 0]$) versus $g_m$. . . . . 108

4.11 Normalized correlation $c$ of the extracted intrinsic noise for $0.24 \times 20 \times 2\mu m^2$ device: (a) $\Re(c)$ and $\Im(c)$ versus frequency at $I_c$=17.9 mA; (b) Magnitude of $c$ versus frequency at $I_c$=17.9 mA; (c) $\Re(c)$ and $\Im(c)$ versus $I_c$ at $f$=25 GHz; (d) Magnitude of $c$ versus $I_c$ at $f$=25 GHz. . . . . 110

4.12 Noise parameters versus frequency for the measured noise data. $I_c$=17.9 mA. $A_E$=$0.24 \times 20 \times 2\mu m^2$. . . . . 112

4.13 Noise parameters versus collector current for the measured noise data. $f$=25 GHz. $A_E$=$0.24 \times 20 \times 2\mu m^2$. . . . . 113

4.14 Extracted intrinsic noise divided by M vs $I_c/M$ at $f$=15 GHz, where M is the emitter geometry scaling factor. . . . . 116

4.15 Noise parameters versus frequency for $0.24 \times 10 \times 2\mu m^2$ SiGe HBT at $I_c$=1.6 mA and 8.0 mA. $V_{CE}$=2.0 V. . . . . 117

4.16 Noise parameters versus frequency for $0.24 \times 20 \times 1\mu m^2$ SiGe HBT at $I_c$=1.6 mA and 8.0 mA. $V_{CE}$=3.0 V. . . . . 118

4.17 Noise parameters versus frequency for $0.48 \times 10 \times 1\mu m^2$ SiGe HBT at $I_c$=1.6 mA and 7.8 mA. $V_{CE}$=2.0 V. . . . . 119

4.18 Normalized noise parameters versus $I_c/M$ at f=15 GHz. . . . . 120

4.19 $NF_{min}$ versus $I_c$, determined by intrinsic noise only, resistance noise only and both of intrinsic and resistance noise for different geometry SiGe HBTs: (a) $0.24 \times 20 \times 2\mu m^2$; (b)$0.24 \times 10 \times 2\mu m^2$; (c) $0.24 \times 20 \times 1\mu m^2$; (d) $0.48 \times 10 \times 1\mu m^2$ . . . . . 121

4.20 Technique of insertion of correlated noise sources into the intrinsic transistor of VBIC model. . . . . 122

4.21 Noise parameters versus frequency simulated by ADS using semi-empirical noise model at $I_C$=15.1 mA. . . . . 123

4.22 Noise parameters versus frequency simulated by ADS using SPICE noise model at $I_C$=15.1 mA. . . . . 124

5.1 Illustration of AC or noise current flows in ideal 1-D intrinsic SiGe HBT. . . . . 126

5.2 Comparison of the intrinsic noise with $\tau_c$=0 and $\tau_c$=0.75$\tau_{tr}$. For $\tau_c$=0.75$\tau_{tr}$, $f_T$=174 GHz. . . . . 128

5.3 Comparison between the brutal used van Vliet model and the improved model under $\tau_c$=0.75$\tau_{tr}$. $f_T$=174 GHz. . . . . 130

5.4 Comparison between van Vliet model, new model and the extracted intrinsic noise from DESIS simulation results. $\tau_c$=0.75($\tau_b$+$\tau_c$) is used in the new model. Effective $d_B$=20nm, $\eta$=5.4, $|E|$=70.2 kV/cm. . . . . 131

5.5 Illustration of base distribution effect by dividing the base resistances into five segments of three types. . . . . 134

5.6 Small signal equivalent circuit of five segments model. . . . . 135

5.7 Comparison of simulation and new model for base hole noise in hybrid representation at one bias $V_{BE}$=0.90V. . . . . 140

5.8 Comparison of simulation and new model for base hole noise in chain representation at one bias $V_{BE}$=0.90V. . . . . 141

5.9 (a) $K_1$ extracted for simulated 85 GHz and 183 GHz peak $f_T$ SiGe HBTs. (b) $K_2$ extracted for simulated 85 GHz and 183 GHz peak $f_T$ SiGe HBTs . . . . . 142

5.10 Comparison between thermal resistances $R_{bn}$ and small signal resistance $r_{bi}$. . . . . 143

5.11 Noise parameters versus frequency for $A_E = 0.24 \times 20 \times 2\mu\text{m}^2$ 50 GHz SiGe HBT at $I_c$=19.4 mA. . . . . 144

5.12 Noise parameters versus $I_C$ for $A_E = 0.24 \times 20 \times 2\ \mu\text{m}^2$ 50 GHz SiGe HBT at f=15 GHz. . . . . 145

5.13 Comparison between thermal resistances $R_{bn}$ and small signal resistance $r_{bi}$. . . . . 146

5.14 Noise parameters versus frequency for $A_E = 0.12 \times 18\ \mu\text{m}^2$ 160 GHz SiGe HBT at $I_c$=11.7 mA. . . . . 147

5.15 Noise parameters versus $I_c$ for $A_E = 0.12 \times 18$ $\mu$m$^2$ 160 GHz SiGe HBT at f=26 GHz. . . . . 148

5.16 Noise parameters versus frequency for $0.12 \times 20 \times 4$ 90 GHz SiGe HBT at $I_C$=34.8 mA. . . . . 149

5.17 Noise parameters versus $I_C$ for $0.12 \times 20 \times 4$ 90 GHz SiGe HBT at f=20 GHz. . . . 150

5.18 Noise parameters versus frequency for scaled 50 GHz SiGe HBTs ($A_E = 0.24 \times 10 \times 2\mu$m$^2$). . . . . 151

5.19 Noise parameters versus frequency for scaled 90 GHz SiGe HBTs ($A_E$=$0.12 \times 8 \times 4\mu m^2$). . . . . 152

5.20 Noise parameters versus frequency for scaled 160 GHz SiGe HBTs ($A_E$=$0.12 \times 12\mu m^2$). . . . . 153

A.1 Noise Figure . . . . . 161

B.1 Approximation induced error versus $V_{B_x B_i}$ for rectangular emitter BJT. . . . . 165

B.2 Comparison between approximation method and the traditional $4kT/r_{bi}$ method for rectangular emitter BJT. . . . . 165

H.1 Schematic geometry of a PNP transistor. . . . . 199

H.2 Illustration of surface integral. . . . . 202

H.3 Admittance representation for BJT noise: (a) Common-base; (b) Common-emitter. 212

## LIST OF TABLES


1.1 Comparison of key performance parameters for different SiGe HBT generations . . 8

3.1 Extracted small signal parameter values of $A_E = 0.12 \times 6 \times 1\ \mu m^2$ SiGe HBT . . . 82

4.1 Extracted small signal parameter values of $0.24 \times 20 \times 2\mu m^2$ SiGe HBT . . . . . 97

4.2 Parameter values of the simplified noise model for Experiment $0.24 \times 20 \times 2\ \mu m^2$ 50 GHz SiGe HBT . . . . . 111

4.3 Parameter sensitivity at $I_C$=17.9mA, $f$=25GHz. $A_E$=$0.24 \times 20 \times 2\mu m^2$. . . . . 114

4.4 Extracted $r_{bx}$, $r_{bi}$ for 50 GHz SiGe HBTs with different emitter geometries . . . . . 117

5.1 Extracted delay time from DESSIS simulation data . . . . . 130

5.2 Model parameters, $r_{bi}$* and $r_{bx}$* for reference . . . . . 151

A.1 Transformation Matrices to Calculate Noise Matrices . . . . . 160

# CHAPTER 1

# INTRODUCTION

This chapter opens with a discussion of the motivation for this research on improving RF noise modeling for SiGe Heterojunction Bipolar Transistors (SiGe HBTs). The fundamentals of SiGe HBT physics and the two-port noise representation theory are then introduced, followed by a description of the basic characteristics of noise parameters for SiGe HBTs and the noise performance scaling trend. Finally the chapter is summarized and the organization of this dissertation is provided.

## 1.1 Motivation

The rapidly developing wireless communication systems have given the human race an information net composed of thousands of communication satellites in space, millions of base-stations on the ground and billions of personal communicators in people's hands. Detailed studies on reducing the noise in the mixed-signal analog and RF circuits used in wireless systems are therefore vital to improve the sensitivity of transceivers, and thus save base-station density and enhance the flexibility of handsets. One of the key concerns is the minimization of RF noise in transistor amplifiers through device level design and circuit level design.

By introducing a graded germanium profile in the base and a higher level of base doping, SiGe HBT enjoys a higher unit-gain cutoff frequency and a smaller base resistance than traditional Silicon Bipolar Transistors (Si BJTs) and maintains a comparable current gain [1]. All these features contribute to the lower noise level of SiGe HBTs compared to Si BJTs.

For RF circuits based on SiGe HBTs, optimizing the design is very important to reduce noise. This clearly requires accurate SiGe HBT noise models and efficient parameter extraction techniques, particularly at the increasingly higher frequencies. The noise modeling approaches currently used for the compact bipolar models are not sufficiently accurate for robust circuit simulation [1], and must be refined to make possible predictive low-noise RF circuit design.

The purpose of this study is to improve RF noise modeling for SiGe HBTs by developing more accurate compact models for intrinsic transistor noise sources. A semi-empirical noise model and a physical noise model are presented in this dissertation. A novel small signal parameter extraction method is also presented. These results were presented in the 2006 *IEEE Transactions on Electron Devices* [2], the 2004, 2005 and 2006 *IEEE BCTM Conference Proceedings* [3–6], and the 2006 *IEEE SiRF Conference Proceedings* [7], while others are forth coming [8, 9].

## 1.2 SiGe HBT fundamentals

### 1.2.1 SiGe as base material

The key feature of SiGe HBT is the use of SiGe alloy as the base. Since the energy bandgap of Ge (0.66 eV) is smaller than that of Si (1.12 eV), the bandgap of SiGe is smaller than that of silicon and depends on the Ge mole composition $x$ ($\Delta E_{g,SiGe} = 0.74x$). The Ge-induced band offset occurs predominantly in the valence band. A properly defined base Ge profile determines the DC, AC and noise characteristics of SiGe HBTs, and gives SiGe HBTs performance advantages over silicon BJTs [1]. Fig. 1.1 shows a typically graded Ge profile and the resulting energy band diagram for a SiGe HBT. The band diagram shows a finite band offset at the EB junction, denoted as $\Delta E_{g0}$, along with a larger band offset at the CB junction, leading to a built-in electric field in the neutral base region that facilitates electron transport from emitter to collector and hence reduces base transit time and improves AC frequency response. If the profile is linear and the base doping

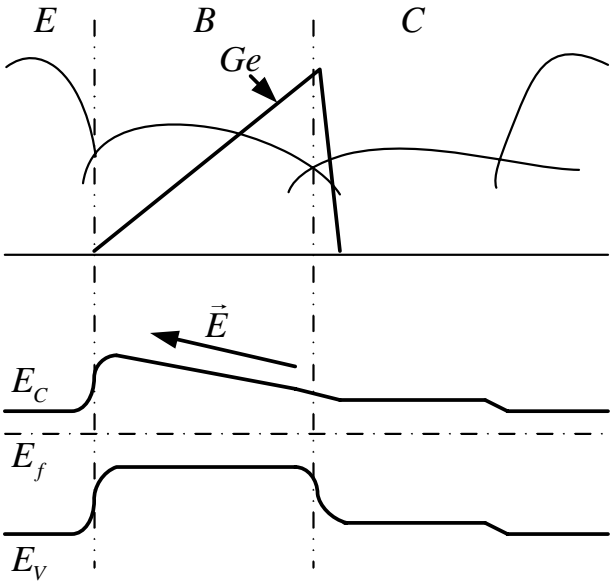


Figure 1.1: Energy band diagram of a graded-base SiGe HBT.

is uniform, the built-in field is homogeneous within the base region, that is

$$E = -\frac{\eta V_T}{d_B}, \tag{1.1}$$

where $d_B$ is the base width, $\eta$ denotes the difference between the bandgaps at the two base ends in unit of thermal voltage, i.e. $\eta = \Delta E_{g,Ge}(grade)/V_T$. Another important consequence of a graded Ge profile is the exponentially decreasing output conductance $g_o$, which is reflected by the Early voltage, $V_A$. $g_o$ is negligible for SiGe HBTs.

The concept of adding a *drift* field in the base is surprisingly old, and was pioneered by Kroemer [10, 11]. However, it took 30 years to realize due to material growth limitations. Nowadays, SiGe alloy can be grown epitaxially on silicon using the ultrahigh vacuum / chemical vapor deposition (UHV/CVD) technique.

For SiGe HBT, the addition of Ge in the base increases the collector current density, $J_C$. This is made possible by the increased electron injection at the EB junction, which yields more

emitter-to-collector charge transport for a given BE voltage. Such an increase in $J_C$ also results in an increase in the DC current gain, $\beta$. Consequently the base doping can be increased if the DC current gain is maintained at the same level as for Si BJTs. This reduces the base resistance, leading to further improved AC performance and reduced RF noise.

Fig. 1.2 shows the cross-sectional structure of a raised-base SiGe HBT [12]. Carbon is doped during SiGe epitaxy to prevent boron backward diffusion into collector. Selectively Implanted Collector (SIC) [13] and Shallow Trench Isolation (STI) [14] are used to improve transistor performance. These techniques will be described in detail below. The most important parasitics are labeled in Fig. 1.2 and consist of the emitter resistance $r_e$, extrinsic base resistance $r_{bx}$, extrinsic collector resistance $r_{cx}$, substrate resistance $r_{cs}$, extrinsic EB capacitance $C_{bex}$, extrinsic CB capacitance $C_{bcx}$, and collector-substrate junction capacitance $C_{cs}$. The intrinsic base resistance $r_{bi}$, intrinsic CB capacitance $C_{bci}$ and intrinsic collector resistance $r_{ci}$ are also shown for reference.

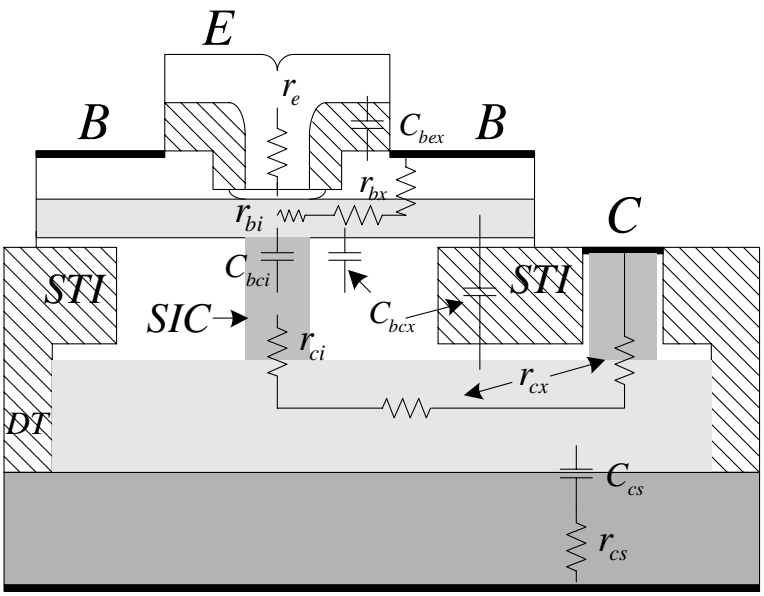


Figure 1.2: Cross section of a raised-base SiGe HBT. Main parasitics are labeled.

### 1.2.2 Performance parameters

For low injection, a key SiGe HBT AC figure-of-merit, the unity-gain cutoff frequency ($f_T$), can be written generally as [1]

$$f_T = \frac{1}{2\pi\tau_{ec}} \approx \frac{1}{2\pi}\left[\frac{C_{bej}+C_{bcx}+C_{bci}}{g_m} + \tau_{tr}^{b} + \tau_e + \tau_c + (r_e + r_{cx} + r_{ci})(C_{bcx}+C_{bci})\right]^{-1}, \quad (1.2)$$

where $\tau_{ec}$ is the total emitter-to-collector delay time, $g_m$ ($\approx qI_c/kT$) is the intrinsic transconductance at low injection, $C_{bej}$ is the EB depletion capacitance, $\tau_{tr}^{b}$ is the base transit time, $\tau_e$ is the emitter charge storage delay time, and $\tau_c$ is the collector transit time due to the CB space charge region (CB SCR). Physically, $f_T$ is the common-emitter, unity current gain cutoff frequency ($H_{21} = 1$), and can be conveniently measured using S-parameter techniques. $f_T$ can be improved by reducing transit times and using a smaller resistive collector. For an ideal HBT, $f_T$ increases versus collector current $I_c$ and finally saturates, a direct result of (1.2). However in reality, $f_T$ will roll-off when $I_c$ exceeds some threshold value due to the Kirk effect or base push-out [15]. That is, $f_T$ has a peak value at certain current density $J_{C,peak}$.

Another figure-of-merit that is often used to describe device AC performance is the maximum oscillation frequency $f_{max}$, reflecting the power gain of a transistor. $f_{max}$ is the common-emitter, unity power gain frequency, and can be related to $f_T$ by a first order equation [1]

$$f_{max} \approx \sqrt{\frac{f_T}{8\pi(C_{bci}+C_{bcx})(r_{bx}+r_{bi})}}. \quad (1.3)$$

There are various definitions of power gain (e.g. U, MAG, MSG), all of which can be measured from the S-parameters [1]. Clearly $f_{max}$ depends not only on the intrinsic transistor performance ($f_T$), but also on the device parasitics associated with the process technology and its structural implementation. Reducing the base resistance and CB capacitance is decisive for improving $f_{max}$.

For general applications, the CB junction is reversely biased. If $V_{CB}$ is high enough, ionization occurs within the CB SCR. $I_c$ increases dramatically due to carrier multiplication, resulting in device breakdown. $BV_{CBO}$ is the CB breakdown voltage when the emitter is floated. $BV_{CEO}$ is the CB breakdown voltage when the base floats. As shown below, increasing $BV_{CEO}$ will decrease $f_T$. Product $BV_{CEO} \times f_T$, the so-called Johnson limit, is a physical constraint on device optimization.

### 1.2.3 Improving $f_T$ and $f_{max}$

Common sense dictates that for transistors, the smaller they are, the faster they will perform. Indeed, the performance of SiGe HBTs has been greatly enhanced by scaling down accompanied with innovative structure designs, both in vertical and lateral dimensions. The $f_T$ of the first functional SiGe HBT demonstrated in 1987 [16] is about 50 GHz. Nowadays, SiGe HBTs with both $f_T$ and $f_{max}$ greater than 300 GHz have been achieved [17], and this trend continues.

#### Vertical scaling

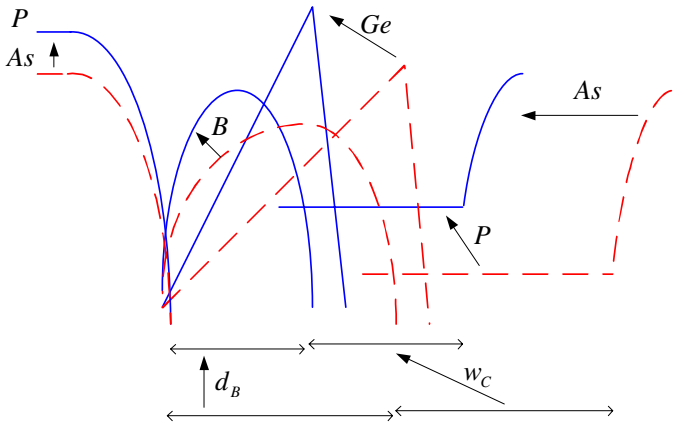


Figure 1.3: Vertical scaling strategy for SiGe HBT.

Fig. 1.3 illustrates the vertical scaling strategy.

- *Base* Here the base width $d_B$ is reduced, and a higher Ge ramp is applied, both of which help to reduce base transit time $\tau_{tr}^b$. For advanced devices, e.g. 200 GHz SiGe HBTs, $\tau_{tr}^b$ is less than the total of other transit times. Base doping is also increased to reduce base resistance.

- *Collector* A higher collector doping $N_C$ and a narrower lightly doped collector thickness $w_C$ are used to reduce collector transit time $\tau_c$. For aggressively scaled devices, $\tau_c$ dominates the total transit time. A higher level of doping also helps to defer the Kirk effect. However, the breakdown voltage is reduced due to the higher CB SCR electric field. Additionally, higher collector doping leads to larger CB capacitance, which reduces $f_{max}$. Therefore, there is a trade off between $f_T$, $f_{max}$ and breakdown voltage for $N_C$.

- *Emitter* The doping is increased to reduce $r_e$ and $\tau_e$, and the arsenic dopant can be replaced with phosphorus to obtain higher doping concentrations. Generally speaking, $\tau_e$ is negligible due to HBT's high DC current gain $\beta$.

**Lateral scaling**

The emitter width $W_E$ is the key factor for lateral scaling, and generally serves as an indicator of the technology generation. When $W_E$ is narrowed, both the intrinsic base resistance $r_{bi}$ and the intrinsic CB capacitance $C_{bci}$ are reduced, and hence $f_{max}$ is improved. $f_T$, however, cannot be improved by this approach. With $W_E$ scaled down, extrinsic base and collector parasitics become significant for $f_{max}$, and must be reduced by scaling and *ad hoc* techniques .

- $R_{bx}$ Increasing base doping will reduce $R_{bx}$, but at the price of increasing the CB capacitance. The solution to this dilemma is to use the so called raised base technique, as shown in Fig. 1.2 [12], where highly doped polysilicon is deposited on top of the SiGe:C layer. Self-aligned low resistive silicide is generally used for such a raised extrinsic base, and a double base contact can be used to reduce the base resistance further.

- $C_{bcx}$ Using implantation through the emitter window, only the collector of the intrinsic device is highly doped to obtained high $f_T$. The remainder of the collector, which is on top of the highly doped collector buried layer, is lightly doped to obtain small $C_{bcx}$. This is known as the Selectively Implanted Collector (SIC) technique [13]. Shallow trench isolation [14], as shown in Fig. 1.2, can be used to reduce $C_{bcx}$ further by reducing the extrinsic CB junction area.

Table 1.1 summarizes the key performance parameters for the five generations of SiGe HBTs readily fabricated in industry [18].

Table 1.1: Comparison of key performance parameters for different SiGe HBT generations [18]

| Generation | I | II | III | IV | V |
|---|---|---|---|---|---|
| $W_E$ ($\mu$m) | 0.5 | 0.25 | 0.18 | 0.13 | 0.12 |
| $f_T$ (GHz) | 47 | 47 | 120 | 210 | 375 |
| $f_{max}$ (GHz) | 65 | 65 | 100 | 285 | 210 |
| $\beta$ | 100 | 100 | 350 | 300 | 3500 |
| $BV_{CEO}$ (V) | 3.4 | 3.4 | 1.8 | 1.7 | 1.4 |
| $BV_{CBO}$ (V) | 10.5 | 10.5 | 6.5 | 5.5 | 5.0 |
| $J_{C,peak}$ (mA/$\mu$m$^2$) | 1.5 | 1.5 | 8 | 12 | 23 |

### 1.2.4 SiGe BiCOMS technology

Today's SiGe HBT technology combines the high speed, low noise SiGe HBTs, aggressively scaled Si CMOS, and a full-suite of on-chip passives together, to create the so-called SiGe BiCMOS technology. SiGe technology has thus emerged as a serious contender for many high-speed digital, RF, analog and microwave applications [1]. At present, there are more than 25 SiGe HBT industrial fabrication facilities on line, and their numbers are growing steadily. Design kits for first four generations of SiGe BiCMOS systems have already been released by IBM. More details of the industrial "state-of-the-art" for SiGe HBT BiCMOS technology can be found in [19].

### 1.3 Noise parameters for two-port network

In this study, the substrate of the SiGe HBT is always tied to its collector to facilitate S-parameter measurements using a GSG probing system. The resulting SiGe HBT is a two-port network. The noise level of such two-port networks can be measured in terms of *Noise Factor*, $F$, which is defined as

$$F = \frac{(SNR)_{signal\ source}}{(SNR)_{output}}. \tag{1.4}$$

Here $SNR$ is the signal-to-noise power ratio. $F$ is usually measured in dB and its value is referred to as the *Noise Figure* $NF$, i.e. $NF = 10Log10(F)$. For a two-port network connected to a signal source, $F$ is determined by both the *noise parameters* ($F_{min}$ or $NF_{min}$, $R_n$ and $Y_{opt}$) of the two-port network and the signal source admittance $Y_S$ as [20]

$$NF = NF_{min} + \frac{R_n}{G_S}|Y_S - Y_{opt}|^2, \tag{1.5}$$

where $G_S$ is the real part of $Y_S$. The noise parameters can be measured using noise measurement facilities, and their meanings can be explained as follows:

- $F_{min}$, the minimum noise factor. Its value in dB is the so called minimum noise figure $NF_{min}$, i.e. $10Log10(F_{min})$.

- $R_n$, the noise resistance, is commonly normalized by the intrinsic impedance $Z_0$, and thus is unitless.

- $Y_{opt}$, the optimum noise matching admittance, is a complex number with a real part $G_{opt}$ and an imaginary part $B_{opt}$. Its inverse value is denoted as $Z_{opt}$. Experimentally, the reflection coefficient $\Gamma_{opt}$ is measured instead of $Y_{opt}$. Note that $\Gamma_{opt} = Mag \cdot e^{(j \cdot Angle/180 \cdot \pi)}$. $Y_{opt}$ can

be obtained from $\Gamma_{opt}$ as

$$Y_{opt} = \frac{1}{Z_0} \cdot \frac{1 - \Gamma_{opt}}{1 + \Gamma_{opt}}.$$

(1.5) implies that if a two-port network is noise matched ($Y_S = Y_{opt}$), the noise figure is minimized. The available power gain under noise matching conditions is known as the associated power gain, $G_A^{ass}$. It can be calculated by

$$G_A^{ass} = \left| \frac{Y_{21}}{Y_{11} + Y_{opt}} \right|^2 \frac{G_{opt}}{\Re[Y_{22} - (Y_{12}Y_{21})/(Y_{11} + Y_{opt})]}.$$

The noise parameters of a two-port network are fully determined by the noise sources that are distributed within the network. All of the distributive noises can be lumped into two equivalent noise sources located at the port terminals, and they are generally correlated [20]. Fig.1.4 shows four commonly used representations for lumped noise sources, (a) admittance or Y- representation, (b) impedance or Z- representation, (c) chain or ABCD- or A- presentation, and (d) hybrid or H-representation. Note the source polarities in (c) and (d). For each representation, the noise Power

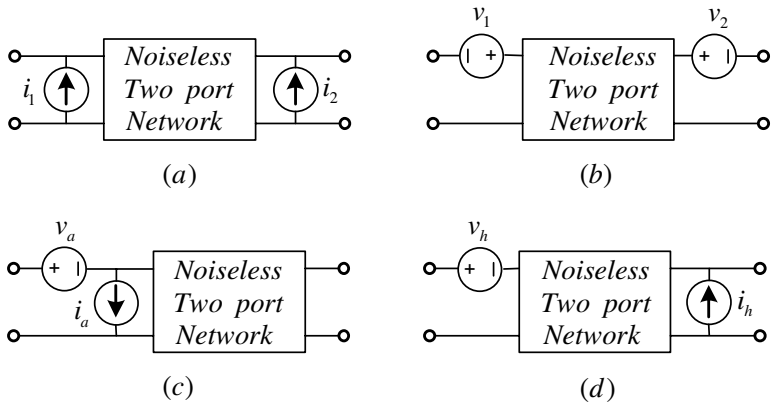


Figure 1.4: Two-port noise representations. (a) Admittance (Y-) representation, (b) Impedance (Z-) representation, (c) Chain (ABCD-) presentation, and (d) hybrid (H-) representation.

Spectral Density (PSD) of the two noise sources, as well as their correlation, can be described by a noise correlation matrix at each frequency point ($\omega$). PSD matrices for the four representations are defined as

$$S^Y(\omega) = \begin{bmatrix} S_{i_1 i_1^*}(\omega) & S_{i_1 i_2^*}(\omega) \\ S_{i_1 i_1^*}(\omega) & S_{i_2 i_2^*}(\omega) \end{bmatrix}, \quad S^Z(\omega) = \begin{bmatrix} S_{v_1 v_1^*}(\omega) & S_{v_1 v_2^*}(\omega) \\ S_{v_2 v_1^*}(\omega) & S_{v_2 v_2^*}(\omega) \end{bmatrix},$$
$$S^A(\omega) = \begin{bmatrix} S_{v_a v_a^*}(\omega) & S_{v_a i_a^*}(\omega) \\ S_{i_a v_a^*}(\omega) & S_{i_a i_a^*}(\omega) \end{bmatrix}, \quad S^H(\omega) = \begin{bmatrix} S_{v_h v_h^*}(\omega) & S_{v_h i_h^*}(\omega) \\ S_{i_h v_h^*}(\omega) & S_{i_h i_h^*}(\omega) \end{bmatrix}. \tag{1.6}$$

Each of these matrices, denoted as $S^{origin}$, can be transformed into another, denoted as $S^{destination}$, by

$$S^{destination} = T S^{origin} T^{\dagger}. \tag{1.7}$$

Here the superscript † represents the transpose conjugate operator. The T-matrices are summarized in Appendix A.

Noise parameters, determined by lumped noise sources, can be directly calculated from the chain representation noise matrix elements, i.e. $S_v$, $S_i$ and $S_{iv^*}$ as [20]

$$\begin{aligned} R_n &= \frac{S_v}{4kT}, \\ G_{opt} &= \sqrt{\frac{S_i}{S_v} - \left[\frac{\Im(S_{iv^*})}{S_v}\right]^2}, \\ B_{opt} &= -\frac{\Im(S_{iv^*})}{S_v}, \\ NF_{min} &= 1 + 2R_n\left[G_{opt} + \frac{\Re(S_{iv^*})}{S_v}\right]. \end{aligned} \tag{1.8}$$

The derivation is given in Appendix A. Inversely, the chain representation noise matrix can be calculated from noise parameters using (1.8) as

$$S^A = \begin{bmatrix} S_v & S_{vi^*} \\ S_{iv^*} & S_i \end{bmatrix} = 4kT \begin{bmatrix} R_n & \frac{NF_{min}-1}{2} - R_n Y_{opt}^* \\ \frac{NF_{min}-1}{2} - R_n Y_{opt} & R_n |Y_{opt}|^2 \end{bmatrix}. \tag{1.9}$$

(1.9) will be used in the noise de-embedding procedure described in Chapter 4.

## 1.4 Frequency and bias dependence of noise parameters for SiGe HBTs

Generally speaking, all the noise parameters are both frequency and bias dependent. Fig. 1.5 shows the measured noise parameters versus collector current $I_c$ for a 50 GHz SiGe HBT with emitter area $A_E = 0.24 \times 20 \times 2\ \mu m^2$. Six frequency points (2 GHz, 5 GHz, 10 GHz, 15 GHz, 20 GHz and 25 GHz) are shown.

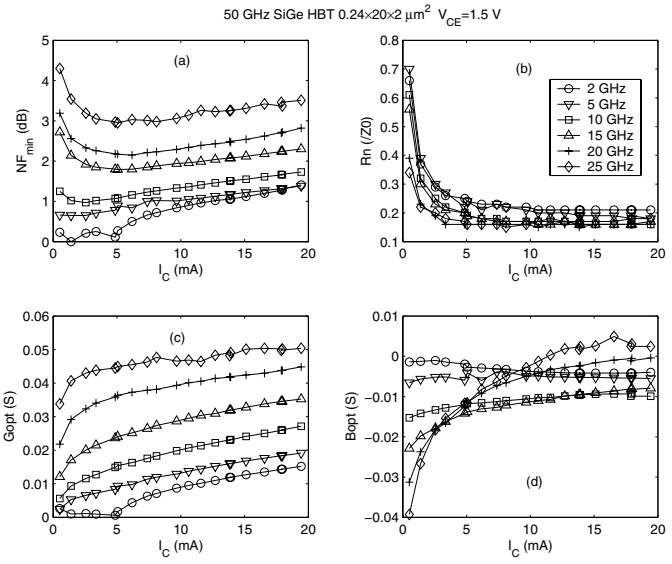


Figure 1.5: Noise parameters versus $I_c$ for a 50 GHz SiGe HBT with $A_E = 0.24 \times 20 \times 2\ \mu m^2$. Six frequency points (2 GHz, 5 GHz, 10 GHz, 15 GHz, 20 GHz and 25 GHz) are measured.

To qualitatively understand these frequency and bias dependence, it is necessary to derive the noise parameters analytically. Fig. 1.6 shows a *simplified* common-emitter small signal equivalent circuit with noise sources for SiGe HBTs. $C_{bct}$ is the total CB capacitance ($= C_{bci} + C_{bcx}$) and $r_{bt}$ is the total base resistance. Since $r_e$ is not included in Fig. 1.6, $r_{bt} \approx r_{bx} + r_{bi} + r_e(1+\beta)$. $C_{bet}$ is the total EB capacitance, and is the sum of the EB diffusion capacitance $C_{bed}$ and the EB junction depletion capacitance $C_{bej}$. $g_{be}$ is the EB low frequency conductance. $r_{bt}$ is assumed to have $4kTR$ noise PSD, i.e. $S_{vrbt} = 4kTr_{bt}$. Uncorrelated $2qI$ shot noise PSDs are assumed for the base and collector current noises, i.e. $S_{ib} = 2qI_b$, $S_{ic} = 2qI_c$ and $S_{icib^*} = 0$. CB ionization noise is not taken into account here and throughout this work, since only low $V_{CB}$ operation is concerned. Using the

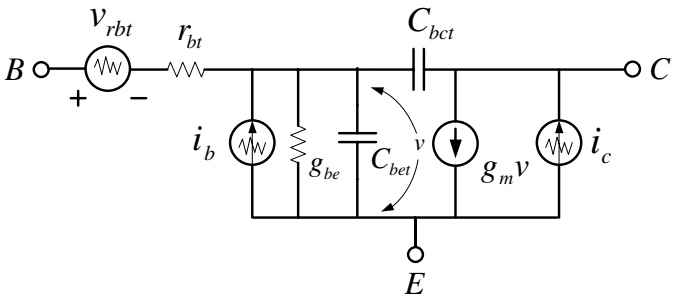


Figure 1.6: Simplified common-emitter small signal equivalent circuit with noise sources for SiGe HBTs.

two-port network noise theory in Section 1.3, the noise parameters can be derived as [19]

$$F_{min} \approx 1 + \frac{N}{\beta} + \sqrt{\frac{2I_c}{V_T} r_{bt} \left( \frac{f^2}{f_T^2} + \frac{1}{\beta} + \frac{N^2}{\beta} \right)} \approx 1 + \sqrt{\frac{2I_c}{V_T} r_{bt} \left( \frac{f^2}{f_T^2} + \frac{1}{\beta} \right)}, \tag{1.10}$$

$$R_n \approx \frac{V_T}{2I_c} + r_{bt}, \tag{1.11}$$

$$Y_{opt} \approx \frac{F_{min} - 1}{2R_n}, \tag{1.12}$$

where $N$ is the EB junction ideality factor and $N \approx 1$.

- $NF_{min}$ or $F_{min}$ (1.10) means that at a fixed bias, $NF_{min}$ increases versus frequency as shown in Fig. 1.5 (a). At low biases, $f_T \propto 1/I_c$ according to (1.2), consequently $F_{min}-1 \propto 1/\sqrt{I_c}$. Therefore $NF_{min}$ increases when $I_c$ decreases at very low $I_c$ levels. For high biases before $f_T$ roll-off, $f_T$ is nearly constant, hence $F_{min} - 1 \propto \sqrt{I_c}$, meaning that $NF_{min}$ increases versus $I_c$. These trends are indeed shown in Fig. 1.5 (a). Analysis shows that $F_{min}$ has a minimum value, the so-called optimized noise figure ($Opt.\ F_{min}$), which is approximately $\sqrt{f}\sqrt{8\pi^2 r_{bt}(C_{bej}+C_{bct})/\beta^{1/2}}$ at low frequencies and $f4\pi\sqrt{2r_{bt}(C_{bej}+C_{bct})(\tau_b+\tau_e+\tau_c)}$ at high frequencies. Increasing $f_T$ and decreasing $r_{bt}$ can significantly reduce the optimized noise figure ($Opt.\ F_{min}$).

- $R_n$ (1.11) shows that $R_n$ drops versus $I_c$ and saturates to the value of $r_{bt}$, which is consistent with Fig. 1.5 (b). The frequency dependence cannot be explained using this simplified equivalent circuit.

- $Y_{opt}$ (1.12) shows that the imaginary part of $Y_{opt}$ or $B_{opt}$ is negligible. This is qualitatively true, as can be seen by comparing Fig. 1.5 (d) with Fig. 1.5 (c). The real part of $Y_{opt}$ or $G_{opt}$ increases versus frequency, as shown by Fig. 1.5 (c), which is consistent with (1.12). The bias dependence of $G_{opt}$, however, cannot be easily explained since both $F_{min}$ and $R_n$ are bias dependent. As Fig. 1.5 (c) shows, $G_{opt}$ increases versus $I_c$.

## 1.5 Noise performance trends for SiGe HBTs

Advances in scaling technology and a series of innovations in processing and structure have led to a steady increase in the peak $f_T$ and a reduction in the base resistance $r_{bt}$. According to the discussion above, these $f_T$ and $r_{bt}$ trends will improve noise performance, driving a reduction in $NF_{min}$ with each generation. SiGe BiCOMS technologies thus enable circuit designers to implement noise-sensitive applications at an increasingly broader frequency range based on silicon technology. Fig. 1.7 shows the optimized noise figure $Opt.\ F_{min}$ versus frequency for four SiGe

HBT BiCMOS technology generations, including three high performance variants at the 0.5-, 0.18-, and 0.13- $\mu$m nodes as well as a cost-reduced (and slightly higher breakdown voltage) variant at the 0.18- $\mu$m node. The performance of GaAs PHEMT is also illustrated for reference. The noise figure has been greatly decreased for the 0.13- $\mu$m node. $F_{min}$ remains below 0.4 dB beyond 12 GHz, rising to only 1.3 dB at 26.5 GHz. This level of performance falls within the range established using the data sheets for GaAs PHEMT currently on the commercial market, placing silicon within one generation of this benchmark [19].

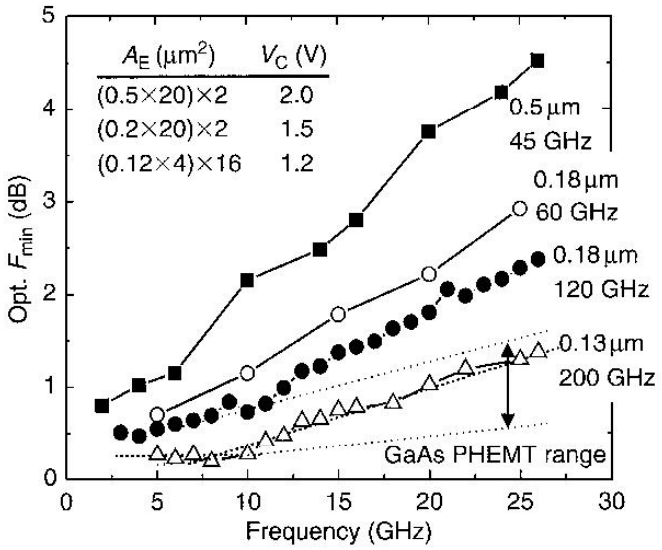


Figure 1.7: HBT optimized noise figure *Opt*. $F_{min}$ versus frequency for four SiGe HBT BiCMOS technologies, including three high performance variants at the 0.5-, 0.18-, and 0.13- $\mu$m nodes as well as a cost-reduced (and slightly higher breakdown voltage) variant at the 0.18- $\mu$m node. (Original figure was shown by D. Greenberg at IEEE MTT-S International Microwave Symposium, Fort Worth, 2004. The above figure is copied from [19])

.

## 1.6 Noise modeling considerations and methodology for SiGe HBTs

A good noise model should give an excellent fit for all the noise parameters. This calls for an accurate compact noise model for device noise. The noise models used for extrinsic parasitics are

well established and are sufficiently accurate for this purpose, so for this study the only concern is the intrinsic device noise modeling. As we are developing models for the wide sense steady (WSS) RF noise, the noise modeling can be completely based on small signal equivalent circuit due to the small signal nature of RF noise. Both semi-empirical and physical noise models are developed here. Emitter geometry scaling, especially emitter length scaling are examined for both models. MATLAB programs are used for small signal parameter extraction and noise calculation. The Verilog-A language is used to implement the new semi-empirical noise model in VBIC, a large signal BJT model applicable for circuit simulators such as Advanced Design System (ADS) supplied by Agilent Technologies.

## 1.7 Summary

This chapter describes the motivation for the research and the theoretical background for SiGe HBTs and RF noise modeling. In this dissertation, Chapter 2 gives the RF noise theory for SiGe HBTs. Chapter 3 explores the small signal extraction method for a small signal equivalent circuit including the input non-quasistatic effect. Chapter 4 describes the intrinsic noise source extraction technique and the new semi-empirical noise model developed based on the extraction results. Chapter 5 describes the new physical noise model developed for this study based on the improved electron and base hole noise models.

# CHAPTER 2

# RF NOISE THEORY FOR SIGE HBTS

This chapter opens with a description of two noise sources that are important for semiconductors, namely carrier velocity fluctuation and carrier population density fluctuation. Then two sets of base electron noise PSDs are presented without including the distributive effect, one of which is the solution for a new 1-D Langevin equation including finite exit velocity boundary condition for CB junction, the other is van Vliet's general solution for 3-D Langevin equation without including finite exit velocity boundary condition for CB junction. The 1-D solution is used to evaluate van Vliet's 3-D solution for the finite exit velocity effect. Both solutions are extended to include emitter hole noise. The crowding theory that deals with base distributive effect using segmentation method is then described. The compact noise model with three noise sources derived from the crowding theory by assuming uniform $f_T$ across the whole EB junction is discussed in detail. Finally the disadvantages of previous noise models used in CAD tools and the literatures are reviewed, and new methods are proposed, with which to develop improved models.

## 2.1 RF noise sources

During the motions induced by external forces, carriers in semiconductors inevitably interact with lattice perturbations, impurities or other carriers, leading to observable terminal voltage or current variations from their ideal values. The noise measured at device terminals is referred to as *macroscopic noise*, while the spatially distributive fluctuations, such as carrier velocity, position, population density, are referred to as *microscopic noise*. To mathematically describe

the microscopic noise, two approaches can be followed, the microscopic and mesoscopic methods [21, 22]. The quantum mechanical microscopic method describes statistical carrier distributions within whole phase space or states based on Liouville / von Neumann's equations. Both the fluctuation-transportation equation and characterization of microscopic noise sources can be obtained in terms of Markov random processes. For example, a semi-classical k-space Boltzmann transport equation (BTE) with appropriate Langevin source has been derived [23–26], from which it is possible to obtain hydrodynamic or more simplified drift-diffusion models that include the microscopic noise sources. This approach is beyond the scope of this dissertation, and will not be further discussed. The *mesoscopic* approach deals with carrier fluctuations within coarse-grained time and space limits, e.g. $t >> \tau_{cs}$ and $l >> l_0$, where $\tau_{cs}$ is the expected collision time and $l_0$ is the expected free path distance. By satisfying such limits, the impact of the carrier's initial state vanishes. Different carriers may have the same statistical characterizations, so for carriers contained within a small mesoscopic volume, it is only necessary to study the statistical characterizations of one electron in order to know the statistical characterizations of the whole volume.

There are two main microscopic noise sources in semiconductor materials or devices. They are *generation-recombination (GR) noise*, which represents the carrier population density fluctuation due to transitions between bands and localized states (donors, traps, Shockley-Read-Hall centers, etc.), and *velocity fluctuation or diffusion noise*, which is associated with the Brownian motion of free carriers in the classical treatment or electron-phonon and electron-impurity scattering in the quantum treatment [21]. The underlying microscopic events are interband transitions for GR noise and intraband transitions for velocity fluctuation noise. To describe each of the two noise sources mesoscopically, two methods can be used: the coarse-grained mesoscopic Master equation (ME) approach and the Langevin approach.

The ME describes how the transition probability density evolves versus time for Markov processes as

$$\frac{\partial P(a,t|a')}{\partial t} = \int da''[P(a'',t|a')W_{a''a'} - P(a,t|a')W_{aa''}], \tag{2.1}$$

where $P(a,t|a')$ is the probability density of state $a$ at time $t$ with initial state of $a'$ at time zero, $W_{aa''}$ is the probability (density) per unit time of an instantaneous transition at time $t$ from $a$ to $a''$, and similarly for $W_{a''a'}$. $a$ and $a'$ are the state vectors. (2.1) can be transformed into the Kramer-Moyal expansion. Often only the first and the second orders of such expansions are important. Truncating all higher orders (>2) yields the Fokker-Planck equation (FPE)

$$\frac{\partial P(a,t|a')}{\partial t} = -\sum_i \frac{\partial}{\partial a_i}[A_i(a)P] + \frac{1}{2}\sum_{ij}\frac{\partial}{\partial a_i \partial a_j}[B_{ij}(a)P], \tag{2.2}$$

where $i$ and $j$ denote different variables of state $a$, and $A$ and $B$ are the first and second order Fokker-Planck moments, explicitly

$$A_i(a) = \int (a_i' - a_i)W_{aa'}da', \quad B_{ij}(a) = \int (a_i' - a_i)(a_j' - a_j)W_{aa'}da'. \tag{2.3}$$

Moments $A$ and $B$ fully describe the stochastic process $a$, and hence determine the phenomenological noise source in the Langevin description, as shown below. From (2.2) and applying a Laplace transformation gives [21]

$$\frac{\partial < \Delta a(t) >_{a'}}{\partial t} = -M < \Delta a(t) >_{a'}, \quad M_{ij} = -\frac{\partial A_i(a')}{\partial a_j}. \tag{2.4}$$

This is the *phenomenological equation* that gives the average behavior of deviation for $a(t)$ from its initial state $a'(0)$. Such phenomenological equations may involve external or internal driving forces and sometimes friction forces. Theoretically, any higher order moment, such as covariances

and correlations, can be obtained in the same way as (2.4). Note that the Fourier transform of an autocorrelation gives the power spectrum density (PSD).

In the Langevin approach, (2.4) is written without the conditional averaging bracket by adding Langevin sources as

$$\frac{\partial \Delta a(t)}{\partial t} = -M\Delta a(t) + \xi(t). \tag{2.5}$$

Clearly $\xi(t)$ is used to *mimic* the random forces that produce the fluctuation of $a(t)$. Two necessary and sufficient requirements for $\xi(t)$ to provide the same first order and second order moments of $\Delta a(t)$, are [21]

$$< \xi(t) >= 0, \quad < \xi(t)\xi(t') >= B[a'(0)]\delta(t - t'). \tag{2.6}$$

From (2.6), the PSD of $\xi(t)$ can be obtained by performing a Fourier transformation as

$$S_{\xi,\xi} = 2B[a'(0)]. \tag{2.7}$$

The coefficient is 2, since single side band PSD is considered here (for measurement only positive frequencies are allowed). (2.7) explains the meaning of the Langevin force and how to obtain the PSD of such a force from the Master equation. The advantage of the Langevin approach is that the calculation of fluctuation-transportation can then be fully resolved based on familiar partial differential equations (PDEs).

The next section describes the PSD of the microscopic noise sources using these two methods. The emphasis here is on velocity fluctuation noise since it is the major noise source for modern SiGe HBTs with narrow base widths.

### 2.1.1 Velocity fluctuation noise

In the mesoscopic approach, carrier velocity fluctuations are modeled as the Brownian motion of a single particle that takes place in the corresponding band [21], i.e. electrons in the conductance band and holes in the valence band. The ground breaking work on the theory of Brownian motion was conducted by Einstein in 1905 in one of the classic papers he published that year [27] using a Fokker-Planck PDE he had derived, where the relation $< x^2 >= 2Dt$ was first established. Another breakthrough was made in 1908 by Langevin using what is now called Langevin force method [28]. The Brownian motion theory was further elucidated by Uhlenbeck and Ornstein in 1930 [29], where the motion was treated using both the Langevin method and the Fokker-Planck method and the motion was proved to be Gaussian. A complete analysis of Brownian motion can be found in the 1943 classic paper by Chandrasekar [30]. The results of the PSD of velocity fluctuations, $S_{\delta v,\delta v}(\omega)$, are shown below using the ME/Fokker-Planck and Langevin methods respectively, after which the methods to establish the microscopic noise source representations for velocity fluctuations will be discussed.

Brownian motion, which is assumed to be a Markov stochastic process in phase space ($\overrightarrow{r}$, $\overrightarrow{v}$), can be described by the Fokker-Planck equation (2.2). Further assuming that the scattering events are characterized by a collision time $\tau_{cs}$, and that the carrier effective mass $m^*$ is isotropic, the Fokker-Planck moment $\boldsymbol{A}$ and $\boldsymbol{B}$ can be derived as [29, 30]

$$\boldsymbol{A} = \begin{bmatrix} \overrightarrow{v} \\ -\frac{1}{\tau_{cs}}\overrightarrow{v} \end{bmatrix}, \quad \boldsymbol{B} = \begin{bmatrix} \mathbb{O} & \mathbb{O} \\ \mathbb{O} & \frac{2}{\tau_{cs}}\frac{kT}{m^*}\mathbb{I} \end{bmatrix}, \tag{2.8}$$

where $\mathbb{O}$ and $\mathbb{I}$ are rank-two zero and unitary tensors, respectively. The solution $P(\overrightarrow{r}, \overrightarrow{v}, t|\overrightarrow{r_0}, \overrightarrow{v_0})$ for (2.2) and (2.8) can be found in [22, 30]. Using the obtained solution and the $< x^2 >= 2Dt$

relation, the diffusion coefficient can be obtained as

$$D = \frac{\tau_{cs} kT}{m^*} = V_T \mu, \tag{2.9}$$

where $\mu$ is the carrier mobility defined as $e\tau_{cs}/m^*$. (2.9) states the Einstein relation. More accurate $D$ and $\mu$ expressions can be derived from the Boltzmann transport equation. It shows that (2.9) holds only when carriers satisfy the Boltzmann statistics [31]. Therefore (2.9) is only valid for low field transport. As only the velocity of $(\overrightarrow{r}, \overrightarrow{v})$ is interested here, (2.2) is integrated through the whole $\overrightarrow{r}$ space to obtain the equation for $P(\overrightarrow{v}, t|, \overrightarrow{v_0})$, briefly designated as $P_v$,

$$\frac{\partial P_v}{\partial t} = \frac{1}{\tau_{cs}} \nabla_v \cdot (\overrightarrow{v} P_v) + \frac{1}{\tau_{cs}} \frac{kT}{m^*} \nabla_v^2 P_v. \tag{2.10}$$

The solution is [21, 30]

$$P(\overrightarrow{r}, \overrightarrow{v}, t|\overrightarrow{r_0}, \overrightarrow{v_0}) = \left[ \frac{m^*}{2\pi kT(1 - e^{-2t/\tau_{cs}})} \right]^{1/2} exp \left[ -\frac{m^*}{2kT} \frac{\left| \overrightarrow{v} - \overrightarrow{v_0} e^{-t/\tau_{cs}} \right|^2}{1 - e^{-2t/\tau_{cs}}} \right]. \tag{2.11}$$

The conditional mean velocity and variance can then be obtained as

$$\begin{aligned} &< \overrightarrow{v}(t) >_{\overrightarrow{v}_0} = \overrightarrow{v}_0 e^{-t/\tau_{cs}}, \\ &< \delta v(t)^2 >_{\overrightarrow{v}_0} \equiv < (\overrightarrow{v}(t) - < \overrightarrow{v}(t) >_{\overrightarrow{v}_0})^2 >_{\overrightarrow{v}_0} = \frac{kT}{m^*} (1 - e^{-2t/\tau_{cs}}) \mathbb{I}. \end{aligned} \tag{2.12}$$

(2.12) approaches Maxwell's equilibrium distribution when $t >> \tau_{cs}$. From (2.11), the autocorrelation function of velocity can be obtained through integration as [22, 32]

$$R_{\delta v, \delta v}(t, t') = \left[ -\frac{kT}{m^*} e^{-(t+t')/\tau_{cs}} + \frac{kT}{m^*} e^{-|t-t'|/\tau_{cs}} \right] \mathbb{I}. \tag{2.13}$$

By setting $t = t'$, (2.13) is correctly reduced to (2.12). Due to the coarse-grain procedure inherent in mesoscopic method, i.e. $t, t' >> \tau_{cs}$, the stationary autocorrelation function is obtained from (2.13)

$$R_{\delta v,\delta v}(\tau) = \frac{1}{\tau_{cs}} D e^{-|\tau|/\tau_{cs}} \mathbb{I}, \tag{2.14}$$

where $\tau \equiv t - t'$ and $D$ is given in (2.9). Now the single side band PSD of velocity fluctuation can be readily obtained from a Fourier transformation of (2.14) multiplied by two. The result is

$$S_{\delta v,\delta v}(\omega) = \frac{4D}{1 + \omega^2 \tau_{cs}^2} \mathbb{I}, \tag{2.15}$$

Since $\tau_{cs}$ is of the order of picoseconds, $S_{\delta v,\delta v}(\omega) \approx 4D\mathbb{I}$ is valid up to one hundred GHz.

For the Langevin method, two white-noise sources are introduced for $\overrightarrow{r}$ and $\overrightarrow{v}$. The equations for the fluctuations of $\overrightarrow{r}$ and $\overrightarrow{v}$ are

$$\frac{d\delta\overrightarrow{r}}{dt} = \delta\overrightarrow{v} + \xi_r, \quad \frac{d\delta\overrightarrow{v}}{dt} = -\frac{1}{\tau_{cs}}\overrightarrow{v} + \xi_v. \tag{2.16}$$

$\xi_v$ has a physical meaning of the *stochastic collision force*. According to (2.7), the PSD of $\xi_r$ and $\xi_v$ must obey

$$S_{\xi,\xi} = 2B = \begin{bmatrix} \mathbb{O} & \mathbb{O} \\ \mathbb{O} & \frac{4}{\tau_{cs}}\frac{kT}{m^*}\mathbb{I} \end{bmatrix}, \tag{2.17}$$

which means $S_{\xi_v,\xi_v}(\omega) = 4D/\tau_{cs}^2 \mathbb{I}$. Fourier transformation of (2.16) gives

$$\delta v = \frac{\tau_{cs}}{1 + j\omega\tau_{cs}} \xi_v. \tag{2.18}$$

The PSD of velocity fluctuation is therefore

$$S_{\delta v,\delta v}(\omega) = \frac{\tau_{cs}^2}{1+\omega^2\tau_{cs}^2} S_{\xi_v,\xi_v} = \frac{4D}{1+\omega^2\tau_{cs}^2}\mathbb{I}, \tag{2.19}$$

which is consistent with the ME/Fokker-Planck result in (2.15). Since the noise power spectrum density is directly related to the diffusion coefficient, velocity fluctuation noise is also called *diffusion noise*.

The PSD of velocity fluctuation in (2.15) is true only for low electric field case. For modern SiGe HBTs, the built-in field in the base due to Ge gradient is quite strong. The high field impacts on diffusion, drift, and noise are no longer negligible. For example, the driving force for velocity saturation equation is approximated to be the gradient of carrier fermi level $\bigtriangledown E_f$, instead of the gradient of electric potential $\bigtriangledown\phi$. (2.15) is a very rough approximation for the PSD of velocity fluctuation due to non-equilibrium effects. A self-consistent development of $S_{\delta v,\delta v}$ for high electric field can be followed from the full band Monte Carlo simulation under homogeneous bulk conditions [33]. In this work, (2.15) is used for simplicity.

Now the problem is to determine how the velocity fluctuation should be described as microscopic noise source. There are two possible kinds of descriptions, the physical *vector dipole current* noise source developed by Shockley [34] and the phenomenological *current density* Langevin noise source [35]. These are, of course, equivalent.

- Vector dipole current description

  Due to velocity fluctuation $\delta\vec{v}$, a carrier labeled with $m$ traveling between $t_1$ and $t_2$ has a disturbance from its ideal position as if the carrier is displaced by

$$\delta\vec{r}_m = \int_{t_1}^{t_2} \delta\vec{v}_m dt \approx \delta\vec{v}_m(t_2 - t_1).$$

as shown in Fig. 2.1. This means that *the carrier with charge e is taken from its ideal position and injected into a disturbed position*. The current produced by this procedure $\delta I_m$ is $e/(t_2 - t_1)$.

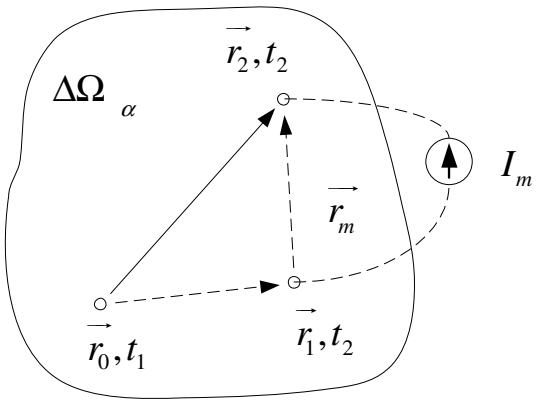


Figure 2.1: Illustration of vector dipole current.

Therefore

$$e\delta\vec{v}_m = e\frac{\delta\vec{r}_m}{t_2 - t_1} = \frac{e}{t_2 - t_1}\delta\vec{r}_m = \delta I_m \delta\vec{r}_m. \tag{2.20}$$

(2.20) clearly reveals that *velocity fluctuation has a physical meaning of vector dipole current*. Now at any given instant in a small volume satisfying the mesoscopic requirement,

$$(\Delta\Omega)_\alpha = \Delta x \Delta y \Delta z,$$

consider the total vector current dipole

$$\delta\dot{\mathfrak{P}}_\alpha = e\sum_m \delta\vec{v}_m(t) = \delta I_\alpha \delta\vec{r}_\alpha. \tag{2.21}$$

$\delta\dot{\mathfrak{P}}_\alpha$ includes all the noise generated within $(\Delta\Omega)_\alpha$. For the mesoscopic domain, fluctuations of all particles are independent and the same. The PSD of $\delta\dot{\mathfrak{P}}_\alpha$ is thus directly obtained as

$$S_{\delta\dot{\mathfrak{P}}_\alpha,\delta\dot{\mathfrak{P}}_\alpha} = e^2 \sum_m S_{\delta v,\delta v} = \frac{4e^2 nD}{1+\omega^2\tau_{cs}^2}(\Delta\Omega)_\alpha, \tag{2.22}$$

where $n$ is the carrier concentration at any position within the small volume $(\Delta\Omega)_\alpha$. For convenience, define the local noise source $K_\gamma(\vec{r}\,,\omega)$ as

$$K_\gamma(\vec{r}\,,\omega) \equiv \frac{4e^2 nD}{1+\omega^2\tau_c^2}\mathbb{I} \approx 4e^2 nD\mathbb{I}, \tag{2.23}$$

so that

$$S_{\delta\dot{\mathfrak{P}}_\alpha,\delta\dot{\mathfrak{P}}_\alpha} = K_\gamma(\vec{r}\,,\omega)(\Delta\Omega)_\alpha. \tag{2.24}$$

Such vector dipole current noise representation can be very easily used to calculate its contribution to the terminal macroscopic noise. For example, to examine the noise voltage at terminal $N$, $\delta v_N$, inject noise current $\delta I_\alpha$ at $\vec{r}_1$, and subtract the same amount of noise current at $\vec{r}_2$ ($\delta\vec{r}_\alpha = \vec{r}_2 - \vec{r}_1$). Supposing the transfer impedance $Z_{N\alpha} \equiv \delta v_N/\delta I_\alpha$ is known for all positions within device, this gives

$$\delta v_N = [Z_{N\alpha}(\vec{r}_1) - Z_{N\alpha}(\vec{r}_2)]\delta I_\alpha = \nabla Z_{N\alpha}\cdot\delta\vec{r}_\alpha\delta I_\alpha = \nabla Z_{N\alpha}\cdot\delta\dot{\mathfrak{P}}_\alpha. \tag{2.25}$$

Consequently, the total terminal noise voltage PSD can be obtained as

$$S_{v_N,v_N}(\omega) = \sum_\alpha S_{\delta v_N,\delta v_N}(r_\alpha,\omega) = \sum_\alpha |\nabla Z_{Nr}|^2 S_{\delta\dot{\mathfrak{P}}_\alpha,\delta\dot{\mathfrak{P}}_\alpha} = \int |\nabla Z_{Nr}|^2 K_\gamma(\vec{r}\,,\omega)d\Omega \tag{2.26}$$

This is the so-called *impedance field method* for noise calculation [34].

- Current density description

  As the treatment of noise transport is based on the drift-diffusion (DD) model, the velocity fluctuation must be expressed in terms of current density fluctuations, denoted as $\overrightarrow{\gamma}(t)$ at a certain spatial position at time $t$, which can be directly inserted into the continuity equations. Again, considering a small volume $(\Delta\Omega)_\alpha$, the current density fluctuations induced by the $m$th carrier velocity fluctuations is represented by

$$\delta\overrightarrow{j}_m = \frac{e}{(\Delta\Omega)_\alpha}\delta\overrightarrow{v}_m. \tag{2.27}$$

  The charge $e$ is distributed uniformly within the whole small volume to obtain the charge density due to the $m$th carrier, since $\delta\overrightarrow{j}_m$ is the current density for any point within the small volume. Then

$$S_{\delta j_m,\delta j_m}(\omega) = \frac{e^2}{(\Delta\Omega)_\alpha^2} S_{\delta v_m,\delta v_m}(\omega). \tag{2.28}$$

  Since the velocity fluctuations of different carriers within $(\Omega)_\alpha$ are uncorrelated, the total power spectrum of the current density fluctuations generated by $(\Omega)_\alpha$ is

$$S_\gamma(\omega) = \sum_m S_{\delta j_m,\delta j_m}(\omega) = n(\Delta\Omega)_\alpha S_{\delta j_m,\delta j_m}(\omega) = \frac{ne^2}{(\Delta\Omega)_\alpha} S_{\delta v,\delta v}(\omega) = \frac{K_\gamma(\overrightarrow{r},\omega)}{(\Delta\Omega)_\alpha}. \tag{2.29}$$

  Curiously, the current density fluctuation is the inverse of small volume. The problem will be clear after an examination of the averaged velocity for $(\Delta\Omega)_\alpha$

$$\delta\bar{v} = \frac{1}{N_\alpha}\sum_m \delta\overrightarrow{v}_m. \tag{2.30}$$

As

$$S_{\delta\bar{v},\delta\bar{v}} = \frac{1}{N_\alpha}\sum_m S_{\delta v_m,\delta v_m} = \frac{1}{n}\frac{S_{\delta v,\delta v}}{(\Delta\Omega)_\alpha}, \tag{2.31}$$

the averaged velocity fluctuation becomes stronger for smaller volume or fewer carriers. This is consistent with the intuitive concepts. As $\vec{\gamma} = \pm en\vec{\bar{v}}$, this once again gives

$$S_\gamma(\omega) = e^2n^2S_{\delta\bar{v},\delta\bar{v}} = \frac{ne^2}{(\Delta\Omega)_\alpha}S_{\delta v,\delta v}(\omega) = \frac{K_\gamma(\vec{r},\omega)}{(\Delta\Omega)_\alpha}. \tag{2.32}$$

The $S_\gamma(\omega)$ in (2.33) is the PSD of auto-correlation for the current density fluctuations $j(\vec{r})$ at any point $\vec{r}$ within the small volume, i.e. $< j(\vec{r})j(\vec{r}) >$. Since the current density fluctuation is uniform within the small volume, the current density fluctuations at any given two points within the same small volume, $j(\vec{r})$ and $j(\vec{r}\,')$, are correlated, and $< j(\vec{r})j(\vec{r}\,') >= < j(\vec{r})j(\vec{r}) >$. It can be assumed that the current density fluctuations at different small volumes are independent, that is, if $\vec{r}$ is inside of $(\Delta\Omega)_\alpha$ while $\vec{r}\,'$ is outside of $\vec{r}\,'$ then $< j(\vec{r})j(\vec{r}\,') >=0$. Therefore the PSD of the current correlation at any given two points $\vec{r}$ and $\vec{r}\,'$ is

$$S_\gamma(\vec{r},\vec{r}\,',\omega) = \frac{K_\gamma(\vec{r},\omega)}{(\Delta\Omega)_{\vec{r}}}U_{(\Delta\Omega)_{\vec{r}}}(\vec{r}\,') = K_\gamma(\vec{r},\omega)\frac{U_{(\Delta\Omega)_{\vec{r}}}(\vec{r}\,')}{(\Delta\Omega)_{\vec{r}}}, \tag{2.33}$$

where $(\Delta\Omega)_{\vec{r}}$ is the small volume containing $\vec{r}$, $U_{(\Delta\Omega)_{\vec{r}}}(\vec{r}\,')$ is a unit step function: it is one when $\vec{r}\,'$ is inside of $(\Delta\Omega)_{\vec{r}}$ otherwise zero. (2.33) is already a Langevin source. However, it is not convenient to use due to the segmentation (divide the whole device into sufficient small volumes) needed before solving Langevin equations. Further, the size of the small volumes

should be infinite small to obtain exact results, which is the idea of integration. Note that

$$\lim_{(\Delta\Omega)_{\overrightarrow{r}}\to 0} \frac{U_{(\Delta\Omega)_{\overrightarrow{r}}}(\overrightarrow{r}')}{(\Delta\Omega)_{\overrightarrow{r}}} = \delta(\overrightarrow{r} - \overrightarrow{r}'), \tag{2.34}$$

the infinite small limit of (2.33) gives

$$S_\gamma(\overrightarrow{r}, \overrightarrow{r}', \omega) = K_\gamma(\overrightarrow{r}, \omega)\delta(\overrightarrow{r} - \overrightarrow{r}'), \tag{2.35}$$

where $K_\gamma(\overrightarrow{r}, \omega)$ is given in (2.23). (2.35) is the Langevin source for the diffusion noise in current density representation. Since this discussion is not confined to either electrons or holes, (2.35) is applicable to both carriers.

### 2.1.2 GR noise

GR noise induces population fluctuations within devices. Hence, the stochastic quantity *population changing rate* $\zeta(t)$ is a good description for such noise. $\zeta(t)$ has the physical meaning of *the injected current density fluctuation* at a given spatial position at time $t$. As with the velocity fluctuation noise, the power spectrum density of $\zeta(t)$, $S_\zeta(\overrightarrow{r}, \overrightarrow{r}', \omega)$, can be derived through either the ME/Fokker-Planck method or the Langevin method. Details can be found in [21, 22]. By considering only the band-to-band transitions and symmetric Shockley-Read-Hall (SRH) transitions, the result is

$$S_\zeta(\overrightarrow{r}, \overrightarrow{r}', \omega) = K_\zeta(\overrightarrow{r}, \omega)\delta(\overrightarrow{r} - \overrightarrow{r}'), \quad K_\zeta(\overrightarrow{r}, \omega) = \frac{2(n_0 + n)}{\tau}, \tag{2.36}$$

where $\tau$ is the carrier life time, $n_0$ is the DC equilibrium carrier concentration, $n$ is the total carrier concentration, and $K_\zeta(\overrightarrow{r}, \omega)$ is the local noise source for population fluctuation. (2.36) is again applicable to both electrons and holes.

## 2.2 Electron noise of base region without distributive effect

This section first solves a 1-D Langevin equation to obtain the electron noise PSD for *base region*. The impact of finite exit velocity boundary condition at CB junction is considered. The general 3-D solution derived by van Vliet is then introduced although the finite exit velocity boundary condition is not considered. Finally, the van Vliet model is evaluated using the 1-D solution derived for the finite exit velocity condition. The CB SCR effect and base distributive effect are not considered in either case.

### 2.2.1 1-D solution

Assume a uniform base built-in field $E$ induced by either the Ge gradient or the doping gradient, as shown in Fig. 2.2. $E$ is measured using parameter $\eta$ as in (1.1). The minus sign in (1.1)

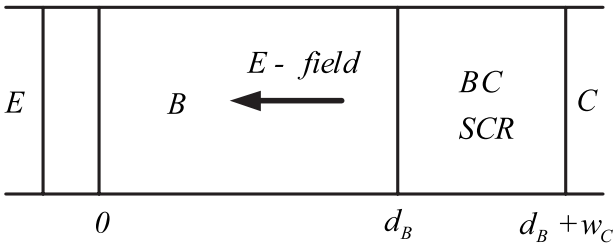


Figure 2.2: Illustration of base region with built-in electric field.

indicates an acceleration field for the electron from the emitter to the collector. The following are the parameters and variables used

- $A_E$ – cross-sectional area of the 1-D device
- $d_B$ – neutral base width.
- $\eta$ – related to electrical field strength.
- $\mu_n$ – electron mobility.

- $V_T$ – thermal voltage.
- $D_n$ – electron diffusion coefficient, which is related to mobility through the Einstein relation, i.e. $D_n = V_T \mu_n$.
- $v_{exit}$ – electron finite exit velocity at the CB junction, which is close to the electron saturation velocity.
- $\tau_n$ – electron life time.
- $L_n$ – electron diffusion length, $L_n = \sqrt{D_n \tau_n}$.
- $n_{00}$ – equilibrium electron concentration at the base beginning point ($x = 0$).

$$n_{00} = \frac{N_c N_v e^{\frac{-E_{g,si}+\Delta E_{g0}}{V_T}}}{N_A} = \frac{n_i^2 e^{\frac{\Delta E_{g0}}{V_T}}}{N_A}, \tag{2.37}$$

  where $N_A$ is the base doping concentration.
- $n$ – electron concentration.
- $n_0$ – equilibrium electron concentration, given by

$$n_0 = n_{00} e^{\eta \frac{x}{d_B}}. \tag{2.38}$$

- $\Delta n$ – excess electron concentration, $\Delta n = n - n_0$.
- $n_1$ – $\Delta n$ at $x = 0$.
- $\widetilde{n}$ – AC electron concentration.
- $\widetilde{n}_1$ – $\widetilde{n}$ at $x = 0$.

Solving the DC, AC continuity equations and Langevin equation gives the DC current, Y-parameters and the PSDs of the intrinsic base and collector noise currents. The electron finite exit velocity

boundary condition is forced at the end of the base for all three cases. The high field mobility model is used

$$\mu_n = \frac{\mu_{n0}}{\sqrt[\beta]{1 + \left(\frac{\mu_{n0} E}{v_{sat}}\right)^{\beta}}}.$$

Drift-Diffusion (DD) model is applied, i.e.

$$J_n = e\mu En + eD_n \frac{d}{dx} n. \tag{2.39}$$

**DC solution**

$V_{BE}$ is applied to the EB junction. Solving the continuity equation

$$D_n \frac{\partial^2}{\partial x^2}\Delta n + \mu_n E \frac{\partial}{\partial x}\Delta n - \frac{\Delta n}{\tau_n} = 0, \tag{2.40}$$

with the boundary conditions

$$\Delta n|_{x=0} \equiv n_1 = n_{00}\left(e^{\frac{V_{BE}}{V_T}} - 1\right), \quad \Delta n|_{x=d_B} = -\frac{J_n|_{x=d_B}}{e v_{exit}},$$

gives the electron concentration and terminal current densities

$$\begin{aligned}
\Delta n(x) &= \left(\frac{e^{\frac{\alpha_1 x}{d_B}}}{1 - \kappa^{-1} e^{2\theta}} + \frac{e^{\frac{\alpha_2 x}{d_B}}}{1 - \kappa e^{-2\theta}}\right) n_1, \\
J_C &= J_n|_{x=d_B} = -en_1 \frac{v_{exit}}{\delta - \alpha_2}\left(\frac{\alpha_1 - \alpha_2}{e^{-\alpha_2} - \kappa e^{-\alpha_1}}\right), \\
J_E &= J_n|_{x=0} = -en_1 \frac{v_{exit}}{\delta}\left(\frac{\eta}{2} + \theta \frac{e^{-\alpha_2} + \kappa e^{-\alpha_1}}{e^{-\alpha_2} - \kappa e^{-\alpha_1}}\right), \\
J_B &= J_C - J_E,
\end{aligned} \tag{2.41}$$

where

$$\kappa = \frac{\alpha_1 - \delta}{\alpha_2 - \delta}, \quad \delta = \frac{v_{exit} d_B}{\mu_n V_T}, \quad \alpha_1 = \frac{\eta}{2} + \theta, \quad \alpha_2 = \frac{\eta}{2} - \theta, \quad \theta = \sqrt{\left(\frac{\eta}{2}\right)^2 + \left(\frac{d_B}{L_n}\right)^2}.$$

The base transit time can be obtained from (2.41) as

$$\tau_B = \frac{Q_B}{J_C} = \frac{d_B(\delta - \alpha_2)}{v_{exit}} \frac{\frac{1-e^{-\alpha_2}}{\alpha_2} - \frac{1-e^{-\alpha_1}}{\alpha_1}\kappa}{\alpha_1 - \alpha_2}, \tag{2.42}$$

With $v_{exit} \to \infty$ and $d_B << L_n$, (2.42) is reduced to the Kramer equation

$$\tau_{b0} = \left(\frac{1}{\eta} - \frac{1 - e^{-\eta}}{\eta^2}\right) \frac{d_B^2}{D_n}. \tag{2.43}$$

**AC solution**

Here a small signal $\widetilde{v}_{be}$ is applied to EB junction. Solving the AC continuity equation

$$D_n \frac{\partial^2}{\partial x^2}\widetilde{n} + \mu_n E \frac{\partial}{\partial x}\widetilde{n} - \frac{\widetilde{n}}{\tau_n} - j\omega\widetilde{n} = 0, \tag{2.44}$$

with the boundary conditions

$$\widetilde{n}|_{x=0} \equiv \widetilde{n}_1 = \frac{n_{00}}{V_T} e^{\frac{V_{BE}}{V_T}} \widetilde{v}_{be}, \quad \widetilde{n}|_{x=d_B} = -\frac{\widetilde{j}_n|_{x=d_B}}{e v_{exit}}.$$

leads to the electron concentration and terminal current densities as follows

$$\begin{aligned}
\widetilde{n}(x) &= \left( \frac{e^{\frac{\widetilde{\alpha}_1 x}{d_B}}}{1-\widetilde{\kappa}^{-1}e^{2\widetilde{\theta}}} + \frac{e^{\frac{\widetilde{\alpha}_2 x}{d_B}}}{1-\widetilde{\kappa}e^{-2\widetilde{\theta}}} \right) \widetilde{n}_1, \\
\widetilde{j}_c &= \widetilde{j}_n|_{x=d_B} = -e\widetilde{n}_1 \frac{v_{exit}}{\delta-\widetilde{\alpha}_2} \left( \frac{\widetilde{\alpha}_1-\widetilde{\alpha}_2}{e^{-\widetilde{\alpha}_2}-\widetilde{\kappa}e^{-\widetilde{\alpha}_1}} \right), \\
\widetilde{j}_e &= \widetilde{j}_n|_{x=0} = -e\widetilde{n}_1 \frac{v_{exit}}{\delta} \left( \frac{\eta}{2} + \widetilde{\theta}\frac{e^{-\widetilde{\alpha}_2}+\widetilde{\kappa}e^{-\widetilde{\alpha}_1}}{e^{-\widetilde{\alpha}_2}-\widetilde{\kappa}e^{-\widetilde{\alpha}_1}} \right), \\
\widetilde{j}_b &= \widetilde{j}_c - \widetilde{j}_e,
\end{aligned} \tag{2.45}$$

where

$$\widetilde{\kappa} = \frac{\widetilde{\alpha}_1-\delta}{\widetilde{\alpha}_2-\delta},\ \ \delta = \frac{v_{exit}d_B}{\mu_n V_T},\ \ \widetilde{\alpha}_1 = \frac{\eta}{2}+\widetilde{\theta},\ \ \widetilde{\alpha}_2 = \frac{\eta}{2}-\widetilde{\theta},\ \ \widetilde{\theta} = \sqrt{\left(\frac{\eta}{2}\right)^2 + \left(\frac{d_B}{L_n}\right)^2 + j\omega\frac{d_B^2}{D_n}}. \tag{2.46}$$

From (2.45), the common-emitter Y-parameters for base region can be derived

$$\begin{aligned}
Y^B_{11,CE} &\equiv \frac{A_E\widetilde{j}_b}{\widetilde{v}_{be}} = A_E e\frac{n_{00}}{V_T}e^{\frac{V_{BE}}{V_T}} \left[ \frac{v_{exit}}{\delta}\left( \frac{\eta}{2} + \widetilde{\theta}\frac{e^{-\widetilde{\alpha}_2}+\widetilde{\kappa}e^{-\widetilde{\alpha}_1}}{e^{-\widetilde{\alpha}_2}-\widetilde{\kappa}e^{-\widetilde{\alpha}_1}} \right) - \frac{v_{exit}}{\delta-\widetilde{\alpha}_2}\left( \frac{\widetilde{\alpha}_1-\widetilde{\alpha}_2}{e^{-\widetilde{\alpha}_2}-\widetilde{\kappa}e^{-\widetilde{\alpha}_1}} \right) \right], \\
Y^B_{21,CE} &\equiv \frac{-A_E\widetilde{j}_c}{\widetilde{v}_{be}} = A_E e\frac{n_{00}}{V_T}e^{\frac{V_{BE}}{V_T}} \frac{v_{sat}}{\delta-\widetilde{\alpha}_2}\left( \frac{\widetilde{\alpha}_1-\widetilde{\alpha}_2}{e^{-\widetilde{\alpha}_2}-\widetilde{\kappa}e^{-\widetilde{\alpha}_1}} \right).
\end{aligned} \tag{2.47}$$

An equivalent circuit is needed to model these Y-parameters. The commonly used one is shown in Fig. 2.3 (b), where the $\Re(Y_{11})$ is frequency independent. The input network of Fig. 2.3 (b) is quasi-static (QS). Of particular interest for modeling the RF noise in the base current is the frequency dependence of the real part of the input admittance ($\Re(Y_{11})$) due to the base electron transport, as shown below. The frequency dependence of $\Re(Y_{11})$ for the base was first examined by Winkel [36] using (2.47). The results show that the base minority carrier charge responds to the base emitter voltage with an input delay time $\tau^b_{in}$, after which the collector current at the end of base region responds to the stored base minority carrier charge with another delay time $\tau^b_{out}$. $\tau^b_{in}$ represents the input non-quasistatic (NQS) effect and $\tau^b_{out}$ represents the output excess phase

delay. In an equivalent circuit, $\tau_{in}^{b}$ can be modeled by an input delay resistance $r_{d}^{b}$ in series with EB junction diffusion capacitance $C_{bed}^{b}$ as illustrated by Fig. 2.3 (a) [37,38]. $\tau_{in}^{b} = r_{d}^{b}C_{bed}^{b}$. Here the EB depletion capacitance $C_{bej}$ is also included. As depletion capacitance is charged through majority carrier movement, $C_{bej}$ does not experience an NQS delay, and should therefore be separated from $C_{bed}^{b}$. Note that $C_{bej} = 0$ and $C_{bed} = g_m\tau_{tr}^{b}$ for (2.47). $\tau_{tr}^{b}$ is the base transit time. $\tau_{out}^{b}$ can be included as a delay term in the transconductance. Fig. 2.4 shows the result of (2.47) together with

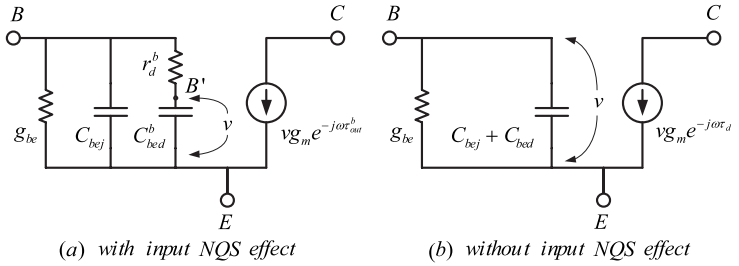


Figure 2.3: Equivalent circuit for intrinsic base of bipolar transistor without $r_{bi}$. (a) With NQS input. (b) With QS input.

the modeling result of Fig. 2.3 (a). Clearly, Fig. 2.3 (a) is accurate for frequencies up to $f_T$. The input NQS effect becomes more important at a given frequency for a larger Ge gradient device, as shown by $\Re(Y_{11})$ in Fig. 2.4. However, the modeling error due to using the QS equivalent circuit for a real device with a base resistance becomes smaller at high current levels for larger Ge gradient devices (see Section 2.4.2). Fig. 2.5 shows the extracted delay times for the base region. The solid line is the result of finite $v_{exit}$. The dashed line is the result of infinite $v_{exit}$. The finite $v_{exit}$ will increase $\tau_{tr}^{b}$ by $d_B/v_{exit}$, as shown in Fig. 2.5 (a). Fig. 2.5 (b) shows the $\tau_{tr}^{b}$ normalized $\tau_{in}^{b}$ and $\tau_{out}^{b}$. Finite $v_{exit}$ has a subtle effect on the normalized value, and the finite $v_{exit}$ does not change the importance of input and output NQS delay times. Note that the normalized NQS delay times increase versus $\eta$, with the result that $\tau_{in}^{b}$ and $\tau_{out}^{b}$ are weakly dependent on the Ge gradient. For

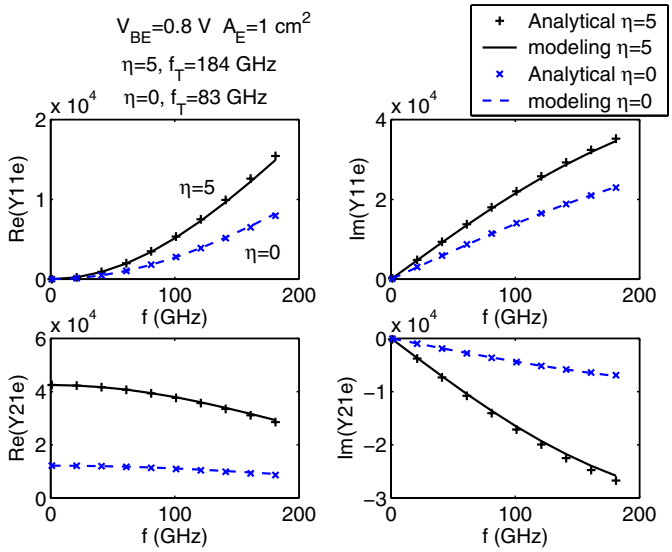


Figure 2.4: Y-parameter modeling result using equivalent circuit with NQS input. $\mu_0$=270 cm/vs$^2$. $\tau_n = 1.54 \times 10^{-}7s$. $n_{00} = 50/cm^3$. $T = 300K$. $d_B$=45 nm. $V_{BE}$=0.8 V. $v_{exit} = 1 \times 10^7$ cm/s. $f_T = g_m/C^b_{bed}$=184 GHz for $\eta = 5$. $f_T = g_m/C^b_{bed}$=83 GHz for $\eta = 0$. $A_E$=1 cm$^2$.

input NQS delay resistance,

$$
\begin{aligned}
r^b_d &= \frac{\tau^b_{in}}{C^b_{bed}} = \frac{1}{g_m}\frac{\tau^b_{in}}{\tau^b_{tr}} \approx \frac{1}{W_E L_E J_c/V_T}\frac{\tau^b_{in}}{\tau^b_{tr}} \approx \frac{1}{W_E L_E n_1/(d_B V_T)}\frac{\tau^b_{in}}{\tau^b_{tr}} \\
&\approx \frac{1}{W_E L_E n_{00} e^{V_{BE}/V_T}/(d_B V_T)}\frac{\tau^b_{in}}{\tau^b_{tr}} = \frac{d_B V_T}{W_E L_E n_{00} e^{V_{BE}/V_T}}\frac{\tau^b_{in}}{\tau^b_{tr}} \\
&= \left(\frac{d_B}{W_E L_E}\right)\left(\frac{n_i^2}{N_A}\right)\left(\frac{\tau^b_{in}}{\tau^b_{tr}}\right) e^{\Delta E_{g0}/V_T} V_T e^{-V_{BE}/V_T}. \qquad (2.48)
\end{aligned}
$$

The impacts of base geometry, base doping and bias on $r^b_d$ are clear from (2.48). However the $\eta$ and finite $v_{exit}$ impacts are not clear due to the approximations made. Fig. 2.6 shows the input NQS delay resistance $r^b_d$ versus $\eta$ at $V_{BE}$=0.8 V. Both the finite and infinite $v_{exit}$ are shown. By increasing the Ge gradient, $r^b_d$ is reduced. A finite CB exit velocity increases $r^b_d$. This is discussed further in Section 2.4.2.

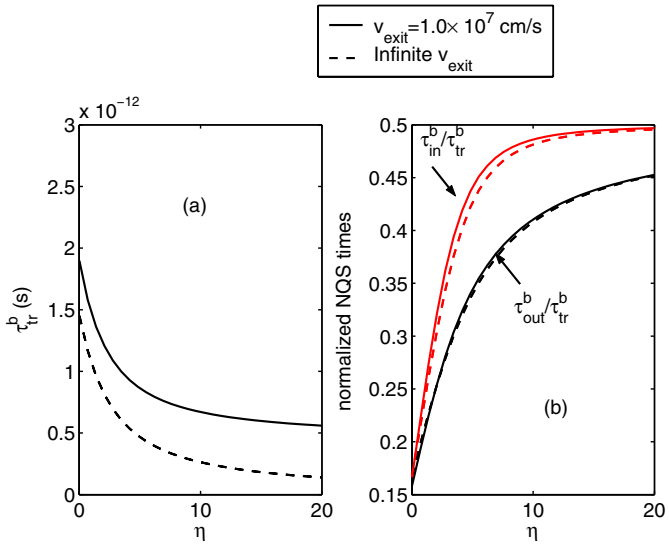


Figure 2.5: Delay times of base region. $\mu_0$=270 cm/vs$^2$. $\tau_n = 1.54 \times 10^{-}7s$. $n_{00} = 50/cm^3$. $T = 300K$. $d_B$=45 nm. $A_E$=1 cm$^2$.

**Noise solution**

The 1-D Langevin equation for the base electron noise is

$$-D_n \frac{\partial^2}{\partial x^2}\widetilde{n} - \mu_n E \frac{\partial}{\partial x}\widetilde{n} + \frac{\widetilde{n}}{\tau_n} + j\omega\widetilde{n} = \xi(x,\omega), \tag{2.49}$$

where

$$\xi(x,\omega) = \zeta(x,\omega) + \frac{1}{e}\frac{\partial}{\partial x}\gamma(x,\omega). \tag{2.50}$$

The Langevin noise sources $\xi(\omega)$ is the sum of the GR noise $\zeta(\omega)$ and the gradient of diffusion noise $\gamma(\omega)$, which have been described in Section 2.1. The boundary condition for (2.49) is

$$\widetilde{n}|_{x=0} = 0, \widetilde{n}|_{x=d_B} = -\frac{\widetilde{j}_n}{ev_{exit}}. \tag{2.51}$$

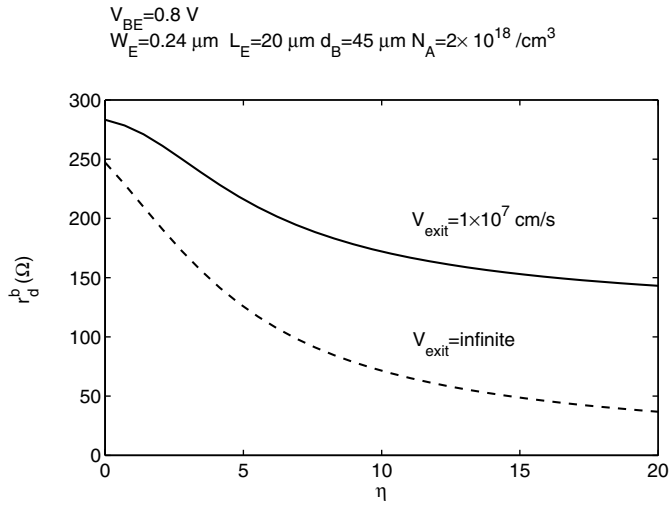


Figure 2.6: Input NQS delay resistance $r_d^b$ versus $\eta$ at $V_{BE}$=0.8 V. $\mu_0$=270 cm/vs$^2$. $\tau_n = 1.54 \times 10^{-}7s$. $n_{00} = 50\ /cm^3$ ($N_A = 2 \times 10^{18}\ /cm^3$). $T = 300K$. $d_B$=45 nm. $W_E$=0.24 $\mu$m. $L_E$=20 $\mu$m. $A_E$=1 cm$^2$.

To solve (2.49)-(2.50), the Green function method [22] is used. First, we define a carrier density Green function $G_n(x, x')$, which satisfies

$$- D_n \frac{\partial^2}{\partial x^2} G_n(x, x') - \mu_n E \frac{\partial}{\partial x} G_n(x, x') + \frac{G_n(x, x')}{\tau_n} + j\omega G_n(x, x') = \delta(x - x'), \tag{2.52}$$

$$G_n(x, x') = 0|_{x=0}, \quad G_n(x, x') = -\frac{\widetilde{j}_n(x)}{e v_{exit}}|_{x=d_B}, x \in [0, d_B], \ x' \in (0, d_B).$$

Clearly $G_n(x, x')$ is the electron density change at position $x$ responding to the unity point carrier flux density injection at position $x'$, The total carrier density fluctuation $\widetilde{n}$ for (2.49) can then be obtained as

$$\widetilde{n}(x) = \int_0^{d_B} G_n(x, x') \xi(x', \omega) dx'. \tag{2.53}$$

However, the PSD for terminal current instead of carrier density is needed. To provide this, operate $e\mu E + eD_n\frac{d}{dx}$ on both sides of (2.53)

$$\widetilde{j}_n(x) = \int_0^{d_B} \left( e\mu E + eD\frac{d}{dx} \right) G_n(x, x')\xi(x', \omega)dx'. \tag{2.54}$$

For convenience, we define terminal carrier flux density ( current density divided by -$e$) Green functions (scalar)

$$G_e(x') = \left( \mu E + D_n\frac{d}{dx} \right) G_n(x, x')|_{x=0}, \tag{2.55}$$

$$G_c(x') = -\left( \mu E + D_n\frac{d}{dx} \right) G_n(x, x')|_{x=d_B}. \tag{2.56}$$

$G_e(x')$ and $G_e(x')$ are thus the emitter and collector *outflow* carrier flux densities responding to the unity point carrier flux density injection at position $x'$, respectively. The base terminal *outflow* carrier flux density responding to the unity point carrier flux density injection at position $x'$, denoted as $G_b(x')$ can be obtained directly from the quasi-neutral condition, that is

$$G_b(x') = 1 - G_c(x') - G_e(x'). \tag{2.57}$$

The terminal *inflow* noise current density fluctuations are

$$\widetilde{j}_e = e\int_0^{d_B} G_e(x')\xi(x', \omega)dx', \;\; \widetilde{j}_c = e\int_0^{d_B} G_c(x')\xi(x', \omega)dx', \;\; \widetilde{j}_b = e\int_0^{d_B} G_b(x')\xi(x', \omega)dx', \tag{2.58}$$

The PSD for the correlation between the noise current densities of terminal $\alpha$ and $\beta$ ($\alpha, \beta = e, c, b$) can be obtained via the following integration

$$\begin{aligned}
S_{j_\alpha, j_\beta^*}(\omega) \equiv <\widetilde{j}_\alpha \widetilde{j}_\beta^* > &= e^2 \int_0^{d_B}\int_0^{d_B} G_\alpha(x) < \xi(x)\xi(x') > G_\beta^*(x')dxdx' \\
&= e^2 \int_0^{d_B}\int_0^{d_B} G_\alpha(x) < \zeta(x)\zeta(x') > G_\beta^*(x')dxdx' \\
&\quad + \int_0^{d_B}\int_0^{d_B} G_\alpha(x)\frac{\partial}{\partial x}\frac{\partial}{\partial x'} < \gamma(x)\gamma(x') > G_\beta^*(x')dxdx' \\
&\approx e^2 \int_0^{d_B}\int_0^{d_B} G_\alpha(x) < \zeta(x)\zeta(x') > G_\beta^*(x')dxdx' \\
&\quad + \int_0^{d_B}\int_0^{d_B} \frac{\partial G_\alpha(x)}{\partial x} < \gamma(x)\gamma(x') > \frac{\partial G_\beta^*(x')}{\partial x'}dxdx' \\
&= e^2 \int_0^{d_B}\int_0^{d_B} G_\alpha(x) K_\zeta(x,\omega)\delta(x-x')G_\beta^*(x')dxdx' \\
&\quad + \int_0^{d_B}\int_0^{d_B} \frac{\partial G_\alpha(x)}{\partial x} K_\gamma(x,\omega)\delta(x-x')\frac{\partial G_\beta^*(x')}{\partial x'}dxdx' \\
&= e^2 \int_0^{d_B} G_\alpha(x') K_\zeta(x',\omega) G_\beta(x')^* dx' \\
&\quad + \int_0^{d_B} \overrightarrow{G}_\alpha(x') K_\gamma(x',\omega)\overrightarrow{G}_\beta(x')^* dx', \qquad (2.59)
\end{aligned}$$

where $\overrightarrow{G}_{\alpha,\beta}(x')$ are vector Green functions:

$$\overrightarrow{G}_e(x') \equiv \frac{\partial}{\partial x'}G_e(x'), \quad \overrightarrow{G}_c(x') \equiv \frac{\partial}{\partial x'}G_c(x'), \quad \overrightarrow{G}_b(x') \equiv \frac{\partial}{\partial x'}G_b(x') = -\overrightarrow{G}_e(x') - \overrightarrow{G}_c(x'). \quad (2.60)$$

The approximation made for the third step in (2.59) is the neglecting of two complex surface integrations when using Gauss theorem when the finite exit velocity boundary condition is not considered. (2.59) shows that the scalar Green functions should be used for GR noise and the vector Green functions should be used for diffusion noise.

Now to solve $G_n(x, x')$, a unity current pulse is inserted at position $x'$ as shown in Fig. 2.7. Note $\delta i$ =1. The boundary condition in (2.51) changes to

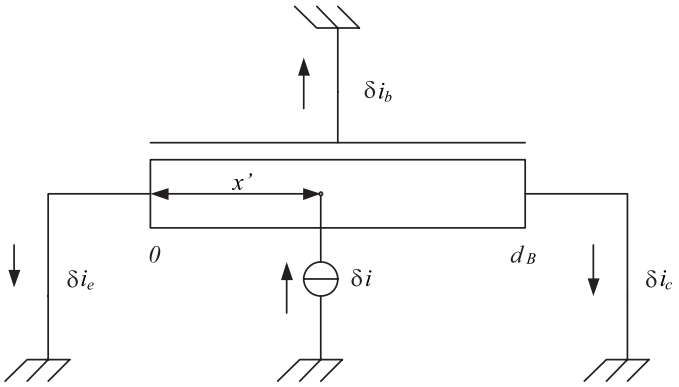


Figure 2.7: Setup for solving Langevin equation.

$$G_n(x,x')|_{x=0}=0, \quad G_n(x,x')|_{x=x'_-}=G_n(x,x')|_{x=x'_+},$$
$$\frac{\partial G_n(x,x')}{\partial x}|_{x=x'_+}-\frac{\partial G_n(x,x')}{\partial x}|_{x=x'_-}=\frac{\delta i}{D_n}, \quad G_n(x,x')|_{x=d_B}=-\frac{\widetilde{j}_n}{ev_{exit}}. \tag{2.61}$$

The third condition in (2.61) can be obtained by integrating (2.49) over the area around $x'$. The solutions for (2.49) and (2.61) are

$$G_n(x,x')=\begin{cases}\frac{d_B}{2D_n}\frac{\left(e^{-\frac{\widetilde{\alpha}_1 x'}{d_B}}-\widetilde{\kappa}e^{-2\widetilde{\theta}}e^{-\frac{\widetilde{\alpha}_2 x'}{d_B}}\right)\left(-e^{\frac{\widetilde{\alpha}_1 x}{d_B}}+e^{\frac{\widetilde{\alpha}_2 x}{d_B}}\right)}{\widetilde{\theta}(1-\widetilde{\kappa}e^{-2\widetilde{\theta}})}, & \text{if } x\in[0\ \ x'];\\ \frac{d_B}{2D_n}\frac{\left(e^{\frac{\widetilde{\alpha}_2 x}{d_B}}-\widetilde{\kappa}e^{-2\widetilde{\theta}}e^{\frac{\widetilde{\alpha}_1 x}{d_B}}\right)\left(e^{-\frac{\widetilde{\alpha}_1 x'}{d_B}}-e^{-\frac{\widetilde{\alpha}_2 x'}{d_B}}\right)}{\widetilde{\theta}(1-\widetilde{\kappa}e^{-2\widetilde{\theta}})}, & \text{if } x\in(x'\ \ d_B],\end{cases} \tag{2.62}$$

where $\widetilde{\alpha}_1$, $\widetilde{\alpha}_2$, $\widetilde{\kappa}$ and $\widetilde{\theta}$ are given in 2.46.

With $G_n(x, x')$, the scalar and vector Green functions can be calculated from (2.55), (2.56), (2.57) and (2.60). The results are

$$
\begin{aligned}
G_e(x') &= \frac{e^{-\frac{\widetilde{\alpha}_1 x'}{d_B}} - \widetilde{\kappa} e^{-2\widetilde{\theta}} e^{-\frac{\widetilde{\alpha}_2 x'}{d_B}}}{1 - \widetilde{\kappa} e^{-2\widetilde{\theta}}}, \\
G_c(x') &= \frac{e^{-\frac{\widetilde{\alpha}_1 x'}{d_B}} - e^{-\frac{\widetilde{\alpha}_2 x'}{d_B}}}{1 - \widetilde{\kappa} e^{-2\widetilde{\theta}}} \frac{(\widetilde{\alpha}_1 - \widetilde{\kappa}\widetilde{\alpha}_2) e^{\widetilde{\alpha}_2}}{\widetilde{\alpha}_2 - \widetilde{\alpha}_1}, \\
G_b(x') &= 1 - G_e(x') - G_c(x'), \\
\overrightarrow{G}_e(x') &= -\frac{\widetilde{\alpha}_1 e^{-\frac{\widetilde{\alpha}_1 x'}{d_B}} - \widetilde{\alpha}_2 \widetilde{\kappa} e^{-2\widetilde{\theta}} e^{-\frac{\widetilde{\alpha}_2 x'}{d_B}}}{d_B(1 - \widetilde{\kappa} e^{-2\widetilde{\theta}})} \hat{x}, \\
\overrightarrow{G}_c(x') &= -\frac{\widetilde{\alpha}_1 e^{-\frac{\widetilde{\alpha}_1 x'}{d_B}} - \widetilde{\alpha}_2 e^{-\frac{\widetilde{\alpha}_2 x'}{d_B}}}{d_B(1 - \widetilde{\kappa} e^{-2\widetilde{\theta}})} \frac{(\widetilde{\alpha}_1 - \widetilde{\kappa}\widetilde{\alpha}_2) e^{\widetilde{\alpha}_2}}{\widetilde{\alpha}_2 - \widetilde{\alpha}_1} \hat{x}, \\
\overrightarrow{G}_b(x') &= -\overrightarrow{G}_e(x') - \overrightarrow{G}_c(x').
\end{aligned}
\tag{2.63}
$$

Figs. 2.8 and 2.9 show the scalar Green functions and vector Green functions, respectively, plotted versus base position. For the solid lines, $v_{exit} = 1 \times 10^7$ cm/s, and for the dashed lines, $v_{exit} \to \infty$.

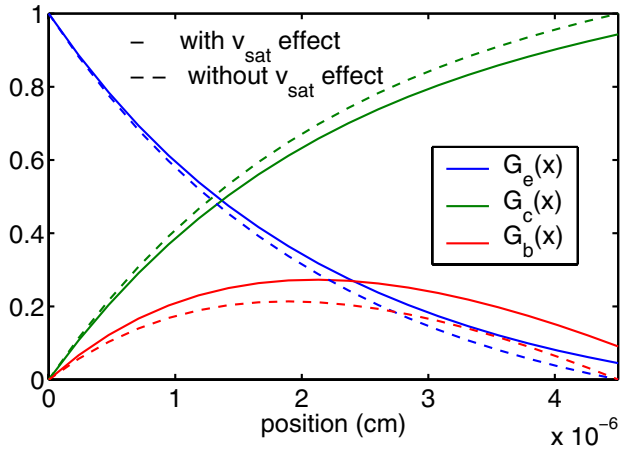


Figure 2.8: Scalar Green functions.

Given the Green functions in (2.63) and DC electron concentration in (2.41), all the noise PSDs can be obtained by integrating (2.59). Since the diffusion noise dominates for the base

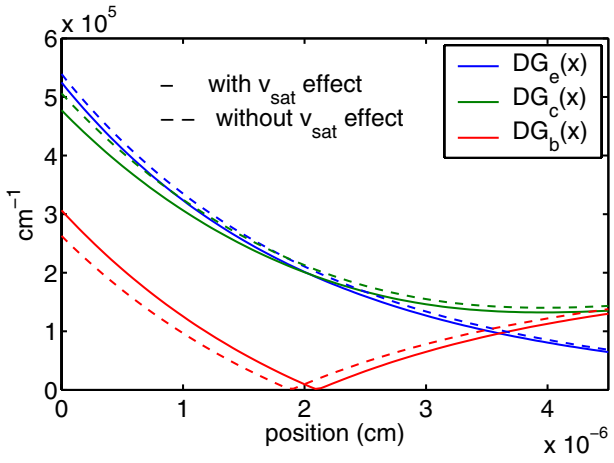


Figure 2.9: Vector Green functions.

region of SiGe HBT, only the analytical results for diffusion noise are given here:

$$
\begin{aligned}
S_{ib}^{B} \equiv S_{ibib^*}^{B} = A_E \Bigg[ & |A+C|^2 \bar{K} \frac{d_B}{-\widetilde{\alpha}_1 - \widetilde{\alpha}_1^* + \alpha_1} \left( e^{-\widetilde{\alpha}_1 - \widetilde{\alpha}_1^* + \alpha_1} - 1 \right) \\
& + |B+D|^2 \bar{K} \frac{d_B}{-\widetilde{\alpha}_2 - \widetilde{\alpha}_2^* + \alpha_1} \left( e^{-\widetilde{\alpha}_2 - \widetilde{\alpha}_2^* + \alpha_1} - 1 \right) \\
& + (A^*+C^*)(B+D) \bar{K} \frac{d_B}{-\widetilde{\alpha}_1^* - \widetilde{\alpha}_2 + \alpha_1} \left( e^{-\widetilde{\alpha}_1^* - \widetilde{\alpha}_2 + \alpha_1} - 1 \right) \\
& + (A+C)(B^*+D^*) \bar{K} \frac{d_B}{-\widetilde{\alpha}_1 - \widetilde{\alpha}_2^* + \alpha_1} \left( e^{-\widetilde{\alpha}_1 - \widetilde{\alpha}_2^* + \alpha_1} - 1 \right) \\
& + first\ 4\ lines, substitute\ \alpha_1 \rightarrow \alpha_2\ and\ \bar{K} \rightarrow \bar{L} \\
& + first\ 4\ lines, substitute\ \alpha_1 \rightarrow \eta\ and\ \bar{K} \rightarrow \overline{KL} \Bigg],
\end{aligned}
\tag{2.64}
$$

$$
\begin{aligned}
S^B_{icib^*} = A_E \Bigg[ & - C(A^* + C^*)\bar{K}\frac{d_B}{-\widetilde{\alpha}_1 - \widetilde{\alpha}_1^* + \alpha_1}\left(e^{-\widetilde{\alpha}_1 - \widetilde{\alpha}_1^* + \alpha_1} - 1\right) \\
& - D(B^* + D^*)\bar{K}\frac{d_B}{-\widetilde{\alpha}_2 - \widetilde{\alpha}_2^* + \alpha_1}\left(e^{-\widetilde{\alpha}_2 - \widetilde{\alpha}_2^* + \alpha_1} - 1\right) \\
& - D(A^* + C^*)\bar{K}\frac{d_B}{-\widetilde{\alpha}_1^* - \widetilde{\alpha}_2 + \alpha_1}\left(e^{-\widetilde{\alpha}_1^* - \widetilde{\alpha}_2 + \alpha_1} - 1\right) \\
& - C(B^* + D^*)\bar{K}\frac{d_B}{-\widetilde{\alpha}_1 - \widetilde{\alpha}_2^* + \alpha_1}\left(e^{-\widetilde{\alpha}_1 - \widetilde{\alpha}_2^* + \alpha_1} - 1\right) \\
& + first\ 4\ lines, substitute\ \alpha_1 \rightarrow \alpha_2\ and\ \bar{K} \rightarrow \bar{L} \\
& + first\ 4\ lines, substitute\ \alpha_1 \rightarrow \eta\ and\ \bar{K} \rightarrow \overline{KL}\Bigg],
\end{aligned} \tag{2.65}
$$

$$
\begin{aligned}
S^B_{ic} \equiv S^B_{icic^*} = A_E \Bigg[ & |C|^2\bar{K}\frac{d_B}{-\widetilde{\alpha}_1 - \widetilde{\alpha}_1^* + \alpha_1}\left(e^{-\widetilde{\alpha}_1 - \widetilde{\alpha}_1^* + \alpha_1} - 1\right) \\
& + |D|^2\bar{K}\frac{d_B}{-\widetilde{\alpha}_2 - \widetilde{\alpha}_2^* + \alpha_1}\left(e^{-\widetilde{\alpha}_2 - \widetilde{\alpha}_2^* + \alpha_1} - 1\right) \\
& + C^*D\bar{K}\frac{d_B}{-\widetilde{\alpha}_1^* - \widetilde{\alpha}_2 + \alpha_1}\left(e^{-\widetilde{\alpha}_1^* - \widetilde{\alpha}_2 + \alpha_1} - 1\right) \\
& + CD^*\bar{K}\frac{d_B}{-\widetilde{\alpha}_1 - \widetilde{\alpha}_2^* + \alpha_1}\left(e^{-\widetilde{\alpha}_1 - \widetilde{\alpha}_2^* + \alpha_1} - 1\right) \\
& + first\ 4\ lines, substitute\ \alpha_1 \rightarrow \alpha_2\ and\ \bar{K} \rightarrow \bar{L} \\
& + first\ 4\ lines, substitute\ \alpha_1 \rightarrow \eta\ and\ \bar{K} \rightarrow \overline{KL}\Bigg],
\end{aligned} \tag{2.66}
$$

where

$$
A = -\frac{\widetilde{\alpha}_1}{d_B\left(1 - \widetilde{\kappa}e^{-2\widetilde{\theta}}\right)},\quad B = \frac{\widetilde{\kappa}e^{-2\widetilde{\theta}}\widetilde{\alpha}_2}{d_B\left(1 - \widetilde{\kappa}e^{-2\widetilde{\theta}}\right)},\quad C = A\frac{(\widetilde{\alpha}_1 - \widetilde{\kappa}\widetilde{\alpha}_2)e^{\widetilde{\alpha}_2}}{\widetilde{\alpha}_2 - \widetilde{\alpha}_1},\quad D = -C\frac{\widetilde{\alpha}_2}{\widetilde{\alpha}_1},
$$

$$
\bar{K} = \frac{4q^2D_n n_{00}e^{\frac{V_{BE}}{V_T}}}{1 - \kappa^{-1}e^{2\theta}},\quad \bar{L} = \frac{4q^2D_n n_{00}e^{\frac{V_{BE}}{V_T}}}{1 - \kappa e^{-2\theta}},\quad \overline{KL} = 4q^2D_n n_{00}.
$$

$$
\alpha_1 = \widetilde{\alpha}_1|_{\omega=0},\quad \alpha_2 = \widetilde{\alpha}_2|_{\omega=0},\quad \kappa = \widetilde{\kappa}|_{\omega=0}.
$$

The last two lines in each PSD represent eight terms that are obtained by a parameter substitution procedure performed on the first four lines. The velocity saturation boundary condition is involved through parameter $\kappa$. $\kappa = 1$ if such a condition is neglected.

### 2.2.2 General 3-D solution by van Vliet

The 3-D Langevin equation for base electron noise is solved by van Vliet using Green's function method in [39]. The adiabatic (homogeneous) boundary condition, i.e. $\widetilde{n}$=0 or zero electron density fluctuation, is used for both ends of the base region. The built-in field can be position dependent. It is important to note that the base distributive effect is not considered in van Vliet's derivation in spite of the 3-D analysis because the AC bias voltage for the whole EB junction is assumed to be uniform. In the derivation, the Y-parameters are expressed by Green's functions in *linear* fashion using the extended Green theorem. The power spectrum densities of noise are initially *quadratic* in Green's functions. In order to make the connection between noise PSD and the Y-parameter, it is convenient to transform the noise PSD into a result whose main part is linear in the Green's functions. This is accomplished using the $\Lambda$ theorem in [40]. Finally the base electron noises are related to the Y-parameters of the base region. The detailed derivation is given in Appendix H. The original results are in common-base configuration but can be readily transformed into common-emitter configuration. The results are

$$\begin{aligned} S_{ib}^{B} &= 4kT\Re(Y_{11}^{B}) - 2qI_{b}^{B}, \\ S_{ic}^{B} &= 4kT\Re(Y_{22}^{B}) + 2qI_{c}, \\ S_{icib^*}^{B} &= 2kT(Y_{21}^{B} + Y_{12}^{B^*} - g_m), \end{aligned} \tag{2.67}$$

where $I_b^B$ is the DC base recombination current. Here, the frequency dependence of $S_{ib}^B$ and $S_{ic}^B$, as well as their correlation $S_{icib^*}^B$, are taken into account through the frequency dependence of the Y-parameters of base $Y^B$. For SiGe HBTs, or modern transistors, $I_b^B$ is negligible. Instead, the base

current due to hole injection into the emitter, $I_b^E$, dominates $I_b$. Also van Vliet's derivation failed to consider electron transport in the CB SCR, which is noticeable for aggressively scaled HBTs. This is because the van Vliet model was derived for early transistors in which the base current is dominated by base recombination. The 3-D Langevin equation was solved only for base minority carriers, which in the case of SiGe HBTs is the electrons. Therefore, the base DC recombination current and Y-parameters of base region should be used in (2.67). In practice, however, the total base current $I_b$ ($I_b^B + I_b^E$) and the Y-parameters of whole transistor are brutally used in (2.67), and the results are recognized as the noise of whole transistor, which is not justified. These issues will be discussed in detail in Chapter 5.

### 2.2.3 Evaluation of van Vliet solution for finite exit velocity boundary condition

Using the 1-D Langevin equation solution derived above,for cases where the finite exit velocity is not included in the boundary conditions, the van Vliet model gives the base electron noise exactly, as expected. When such boundary condition is applied, however, the van Vliet model deviates from the analytical results when the base width becomes narrow. Fig. 2.10 shows the wide base case ($d_B$=100 nm), where the van Vliet model is consistent with the 1-D solution. Fig. 2.11 shows the narrow base case ($d_B$=20 nm). The van Vliet model clearly overestimates $S_{ib}$ and $|\Re(S_{icib^*})|$ while underestimating $|\Im(S_{icib^*})|$.

However, with a strong base built-in field, typically the case in graded SiGe HBTs, the deviation is significantly reduced, as shown in Fig. 2.12, where $\eta = 5.4$. A careful inspection of the solution process does not yield an intuitive explanation for this observation, but calculations show that this is generally true for all practical values of built-in field found in modern SiGe HBTs with graded bases. Therefore, it is reasonable to continue to use the van Vliet model to describe the relationship between noise and Y-parameters of the intrinsic base for graded SiGe HBTs. This is the starting point for the analysis of the CB SCR effect given in Chapter 5.

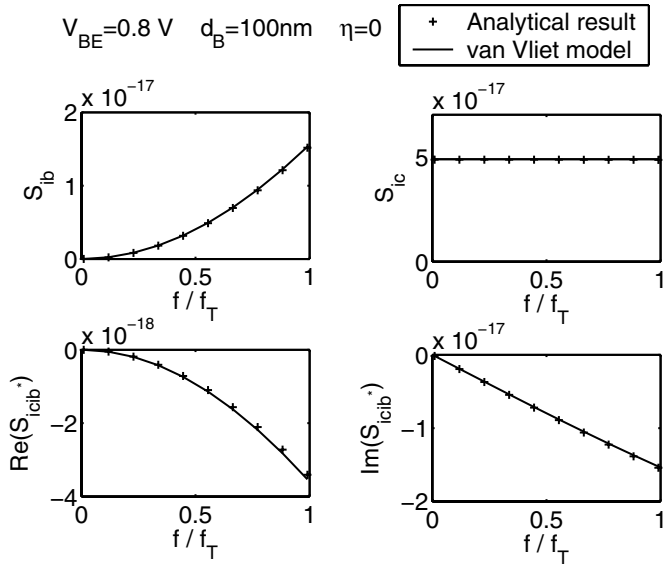


Figure 2.10: Evaluation of van Vliet model for base region noise under $d_B = 100nm$, $\eta = 5.4$ ($|E|$=70.2 kV/cm), $V_{BE}$=0.8V, where "$f_T$"$\equiv g_m/C_{be}$=698 GHz. $A_E$=1 cm$^2$.

## 2.3 Extension to including emitter hole noise

For modern transistors, the base current due to hole injection into the emitter, $I_b^E$, dominates the base current. At low frequency, the PSD of $i_b^E$ should be $2qI_b^E$ to first order, which is much larger than the PSD of base recombination current $2qI_b^B$. Therefore it is important to include base hole noise.

### 2.3.1 3-D van Vliet model

To obtain the emitter hole noise induced base noise current $i_b^E$, and denote its PSD as $S_{ib}^E$, it is necessary to solve a 3-D Langevin equation for emitter minority carriers (holes here as NPN HBTs are of interest) with a boundary condition $\Delta p = 0$ at both the emitter contact and the neutral to depletion boundary of the EB junction. $\Delta p$ is the hole density fluctuation. $\Delta p = 0$ at the emitter contact as infinite surface recombination velocity is assumed. $\Delta p = 0$ at the neutral to depletion boundary of the EB junction, as the same adiabatic boundary condition used in [39] is assumed.

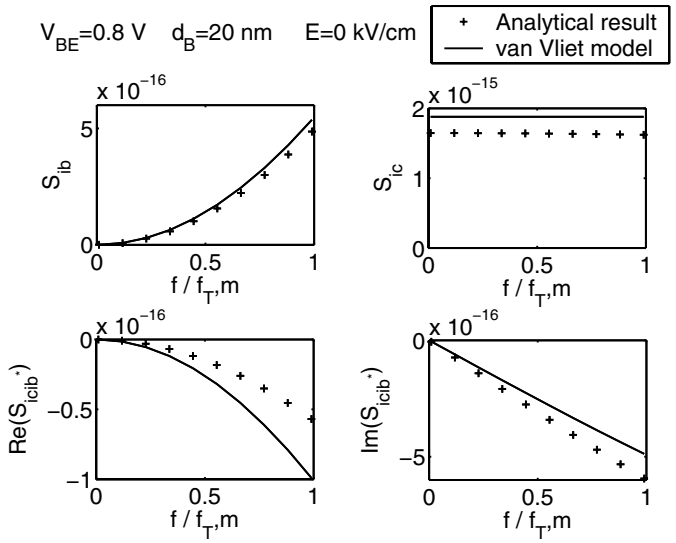


Figure 2.11: Evaluation of van Vliet model for base region noise under $d_B = 20nm$, $\eta = 5.4$ ($|E|$=0 kV/cm), $V_{BE}$=0.8V, where "$f_T$"$\equiv g_m/C_{be}$=698 GHz. $A_E$=1 cm$^2$.

The solution can be obtained following van Vliet's derivation for base minority carrier noise [39]. The Langevin equation for minority holes in the emitter of NPN HBT solved here is exactly the same Langevin equation for minority holes in the base of PNP transistor solved in [39] with the same adiabatic condition $\Delta p = 0$ is used in [39]. The emitter minority carrier induced noise current at the emitter-side neutral to depletion boundary of the EB junction, $i_b^E$, is analogous to the base minority carrier induced noise current at the base-side neutral to depletion boundary of the EB junction, $i_e^B$ ($= i_b^B + i_c^B$). Therefore, the PSD of $i_b^E$ takes the functional form of the PSD of $i_e^B$ in [39], that is,

$$S_{ib}^E = 4kT\Re(Y_{11}^E) - 2qI_b^E, \tag{2.68}$$

where $Y_{11}^E$ is the input admittance seen by the base terminal due to emitter hole injection. At low frequency limit, $Y_{11}^E \approx qI_b^E/kT$, hence $S_{ib}^E \approx 2qI_b^E$.

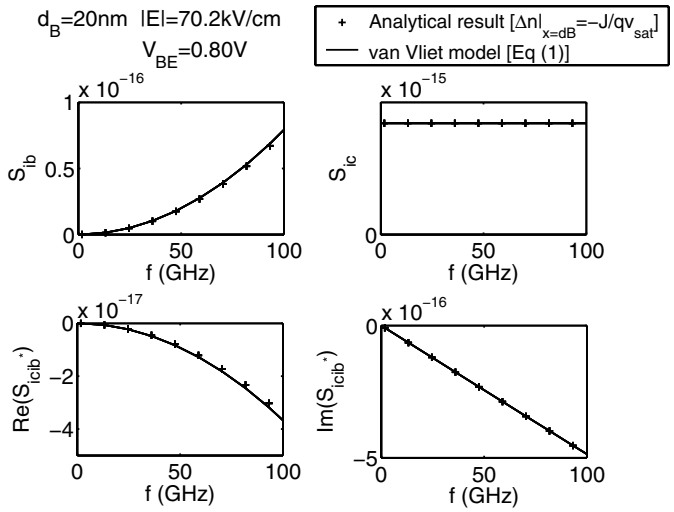


Figure 2.12: Evaluation of van Vliet model for base region noise under $d_B = 20nm$, $\eta = 5.4$ ($|E|$=70.2 kV/cm), $V_{BE}$=0.8V. $A_E$=1 cm$^2$.

The emitter hole density fluctuations induce emitter electron density fluctuations to maintain quasi-neutrality due to dielectric relaxation. The electron density fluctuations, however, induce electron current fluctuation only at the emitter contact but not at the depletion to neutral boundary, because electrons are majority carriers in the emitter. Therefore the emitter hole noise only contributes to the base current noise $i_b$, but not the collector current noise $i_c$. The PSDs of the total $i_b$ and $i_c$ can then be obtained as

$$S_{ib}^{EB} = 4kT\Re(Y_{11}^{EB}) - 2qI_b, \; S_{ic}^{EB} = 4kT\Re(Y_{22}^{EB}) + 2qI_c \approx 2qI_c,$$
$$S_{icib^*}^{EB} = 2kT(Y_{21}^{EB} + Y_{12}^{EB*} - g_m) \approx 2kT(Y_{21}^{EB} - g_m), \tag{2.69}$$

where

$$Y_{11}^{EB} = Y_{11}^{E} + Y_{11}^{B}, \quad I_b = I_b^E + I_b^B,$$
$$Y_{21}^{EB} = Y_{21}^{B}, \quad Y_{22}^{EB} = Y_{22}^{B}, \quad Y_{12}^{EB} = Y_{12}^{B}.$$

Interestingly, (2.69) has the same functional form as (2.67), meaning that the van Vliet model in (2.67) can be directly applied to include emitter hole noise by simply replacing $Y^B$ with $Y^{EB}$, the Y-parameters of base and emitter regions. So far, the effect of electron transport in the CB SCR on Y-parameters and noise has not been taken into account.

### 2.3.2 1-D solution

Similarly, the PSD for emitter hole noise $S_{ib}^E$ of the 1-D Langevin equation solution for the emitter can be obtained from the $S_{ie}^B$ of the 1-D Langevin equation solution for the base. That is

$$\begin{aligned}
S_{ib}^E = A_E \Bigg[ & |E|^2 \bar{K} \frac{d_E}{-\widetilde{\alpha}_1 - \widetilde{\alpha}_1^* + \alpha_1} \left( e^{-\widetilde{\alpha}_1 - \widetilde{\alpha}_1^* + \alpha_1} - 1 \right) \\
& + |F|^2 \bar{K} \frac{d_E}{-\widetilde{\alpha}_2 - \widetilde{\alpha}_2^* + \alpha_1} \left( e^{-\widetilde{\alpha}_2 - \widetilde{\alpha}_2^* + \alpha_1} - 1 \right) \\
& + E^* F \bar{K} \frac{d_E}{-\widetilde{\alpha}_1^* - \widetilde{\alpha}_2 + \alpha_1} \left( e^{-\widetilde{\alpha}_1^* - \widetilde{\alpha}_2 + \alpha_1} - 1 \right) \\
& + E F^* \bar{K} \frac{d_E}{-\widetilde{\alpha}_1 - \widetilde{\alpha}_2^* + \alpha_1} \left( e^{-\widetilde{\alpha}_1 - \widetilde{\alpha}_2^* + \alpha_1} - 1 \right) \\
& + first\ 4\ lines, substitute\ \alpha_1 \rightarrow \alpha_2\ and\ \bar{K} \rightarrow \bar{L} \\
& + first\ 4\ lines, substitute\ \alpha_1 \rightarrow \eta\ and\ \bar{K} \rightarrow \overline{KL} \Bigg],
\end{aligned} \tag{2.70}$$

where

$$\begin{aligned}
& E = -\frac{\widetilde{\alpha}_1}{d_E \left( 1 - \widetilde{\kappa} e^{-2\widetilde{\theta}} \right)}, \quad F = \frac{\widetilde{\kappa} e^{-2\widetilde{\theta}} \widetilde{\alpha}_2}{d_E \left( 1 - \widetilde{\kappa} e^{-2\widetilde{\theta}} \right)}, \\
& \bar{K} = \frac{4q^2 D_p p_{00} e^{\frac{V_{BE}}{V_T}}}{1 - \kappa^{-1} e^{2\theta}}, \quad \bar{L} = \frac{4q^2 D_p p_{00} e^{\frac{V_{BE}}{V_T}}}{1 - \kappa e^{-2\theta}}, \quad \overline{KL} = 4q^2 D_p p_{00}. \\
& \alpha_1 = \widetilde{\alpha}_1|_{\omega=0}, \quad \alpha_2 = \widetilde{\alpha}_2|_{\omega=0}, \quad \kappa = \widetilde{\kappa}|_{\omega=0}. \\
& \widetilde{\kappa} = \frac{D_p \widetilde{\alpha}_1 - v_{sr} d_E}{D_p \widetilde{\alpha}_2 - v_{sr} d_E}, \quad \widetilde{\alpha}_1 = \frac{\eta_E}{2} + \widetilde{\theta}, \quad \widetilde{\alpha}_2 = \frac{\eta_E}{2} - \widetilde{\theta}, \quad \widetilde{\theta} = \sqrt{\left( \frac{\eta_E}{2} \right)^2 + \frac{d_E^2}{D_p \tau_p} + \frac{j\omega d_E^2}{D_p}}.
\end{aligned} \tag{2.71}$$

Here $v_{sr}$ is the emitter surface recombination velocity, $d_E$ is emitter thickness, $\eta_E$ represents the emitter built-in field due to non-uniform doping, $D_p$ is the emitter hole diffusion coefficient, and $\tau_p$ is the emitter hole life time. Consequently, the total base and collector current noise PSDs can be obtained by adding $S_{ib}^E$ to $S_{ib}$ only. In order to evaluate (2.68), $Y_{11}^E$ and $I_b^E$ are derived as

$$Y_{11}^E = e\frac{p_{00}}{V_T}e^{\frac{V_{BE}}{V_T}}\frac{v_{sr}}{\delta}\left(\frac{\eta}{2}+\widetilde{\theta}\frac{e^{-\widetilde{\alpha}_2}+\widetilde{\kappa}e^{-\widetilde{\alpha}_1}}{e^{-\widetilde{\alpha}_2}-\widetilde{\kappa}e^{-\widetilde{\alpha}_1}}\right), \tag{2.72}$$

$$I_b^E = ep_{00}\left(e^{\frac{V_{BE}}{V_T}}-1\right)\frac{v_{sr}}{\delta}\left(\frac{\eta}{2}+\theta\frac{e^{-\alpha_2}+\kappa e^{-\alpha_1}}{e^{-\alpha_2}-\kappa e^{-\alpha_1}}\right), \tag{2.73}$$

where all parameters are given in (2.71).

### 2.3.3 Evaluation of finite surface recombination velocity effect

Fig. 2.13 compares two $S_{ib}^E$ values versus frequency, which are the analytical results of (2.70) and the modeling result using (2.70), (2.72) and (2.73). Three values for the surface recombination velocity are used. Clearly the finite surface recombination velocity has only a negligible effect on the accuracy of (2.68). Furthermore, the frequency dependence of $S_{ib}^E$ is weak. Since only

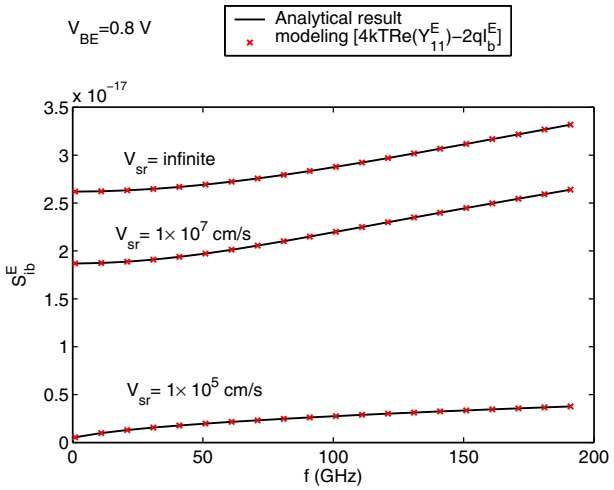


Figure 2.13: Evaluation of emitter hole noise model in (2.68). $\tau_p = 1.54 \times 10^{-}7s$. $\eta_E$=0. $p_{00} = 6.66/cm^3$. $T = 300K$. $d_E$=120 nm. $V_{BE}$=0.8 V. $\mu_p$=220 cm/cs$^2$. $A_E$=1 cm$^2$.

the diffusion noise is taken into account here, the result above is not exact for the emitter where GR noise is non-negligible. However, when the GR current is significant, the effect of surface recombination velocity is reduced.

### 2.3.4 Comparison of base electron and emitter hole contributions to $S_{ib}$

This comparison is based on an HBT constructed for this study with $\beta$=235 and $f_T$=200 GHz. A CB SCR delay is included as detailed in Chapter 5. Fig. 2.14 shows a plot of $S_{ib}^E$ and $S_{ib}^B$ versus frequency at $V_{BE}$=0.8 V. The graph shows that only for $f$<15 GHz is $S_{ib}^B$ negligible. For $f$>30 GHz, $S_{ib}^B$ dominates $S_{ib}$. $S_{ib}$ has a strong frequency dependence due to base electron noise.

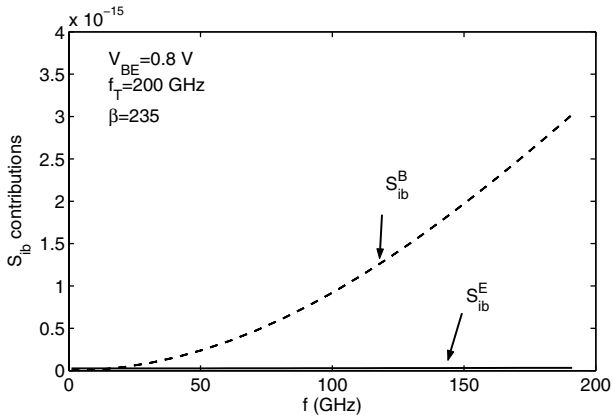


Figure 2.14: Comparison of base electron and emitter hole contributions to $S_{ib}$. $\tau_p = 1.54 \times 10^{-}7s$. $\eta_E$=0. $p_{00} = 6.66/cm^3$. $T = 300K$. $d_E$=120 nm. $V_{BE}$=0.8 V. $\mu_p$=220 cm/cs$^2$. $\tau_n = 1.54 \times 10^{-}7s$. $\eta_B$=5.4. $n_{00} = 333/cm^3$. $d_E$=20 nm. $\mu_n$=450 cm/cs$^2$. $V_{exit} = 1 \times 10^7\ cm/s$. $\tau_c = 0.57ps$. $A_E$=1 cm$^2$. The units of y-axis is A$^2$/Hz. $A_E$=1 cm$^2$.

## 2.4 Compact noise model including distributive effect

### 2.4.1 Compact noise model assuming uniform $f_T$ across EB junction

The technique commonly used to deal with transistor distributive effects is the segmentation method, where the transistor is divided into many narrow 1-D sub-transistors and these sub-transistors are then connected by divided base resistances. Fig. 2.15 shows the small signal equivalent circuit for this method. $Y_{11}$ and $Y_{21}$ of each sub-transistor naturally include non-quasistatic (NQS) effect. $Y_{11}$ includes the input NQS effect, while $Y_{21}$ includes the output NQS effect. The resistances have $4kTR$ thermal noise. The base and collector current noises of each segment can be described by the van Vliet model if the CB SCR effect is not important.

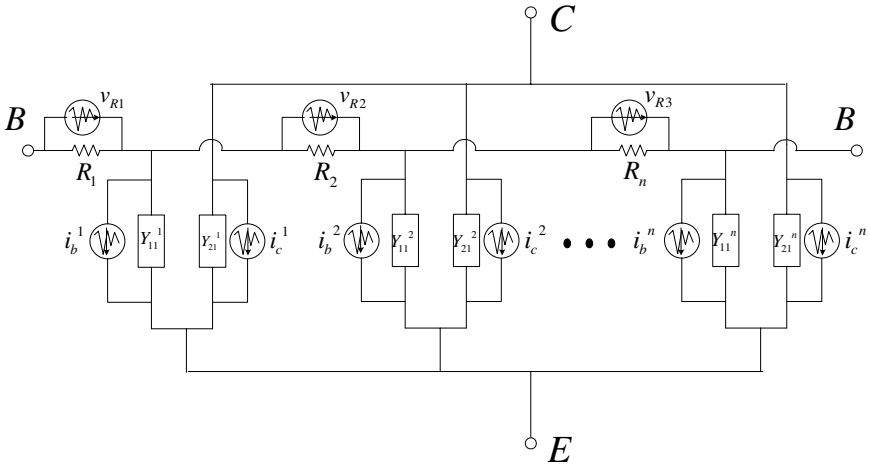


Figure 2.15: Small signal equivalent circuit for a transistor divided into 1-D sub-transistors.

The objective is to develop a compact noise model that includes as few noise sources as possible, with their analytical expressions. Although a general analytical solution is hard to achieve, a compact noise model with only three noise sources can be derived by assuming the same $f_T$ for all of the 1-D sub-transistors according to the crowding theory in [41]. Fig. 2.16 shows the lumped small signal equivalent circuit, together with the lumped noise sources.

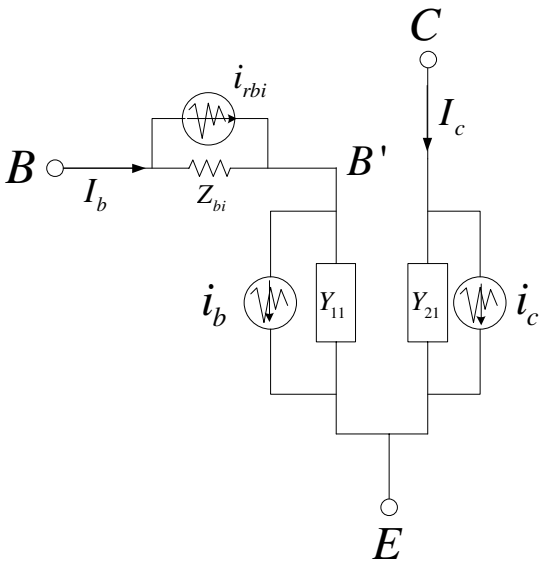


Figure 2.16: Compact noise model assuming uniform $f_T$ for whole EB junction [41].

Since the output conductance $g_o$ is negligible for SiGe HBTs, the lumped $Y_{11}$ and $Y_{21}$ can be chosen to be the sum of $Y_{11}$ and $Y_{21}$ for all the sub-transistors, explicitly,

$$Y_{11} = Y_{11}^1 + Y_{11}^2 + ... + Y_{11}^n,$$
$$Y_{21} = Y_{21}^1 + Y_{21}^2 + ... + Y_{21}^n.$$

The lumped base impedance $Z_{bi}$ has a complex expression, which relates to the distributive base resistances and EB capacitances. Denote the low frequency limit of the real part of $Z_{bi}$ as $r_{bi}$, the lumped AC small signal value of the intrinsic base resistance. For transistors with double base contacts and at low current levels,

$$r_{bi} = R_{BV} \equiv \frac{1}{12} R_{\square} \frac{W_E}{L_E}, \tag{2.74}$$

where $L_E$ and $W_E$ are the base length and base width, respectively, and $R_{\square}$ is the base sheet resistance.

The lumped base and collector current noises $i_b$ and $i_c$ are the sum of the noise currents of the 1-D sub-transistors with no crowding effect

$$i_b = i_b^1 + i_b^2 + ... + i_b^n,$$
$$i_c = i_c^1 + i_c^2 + ... + i_c^n.$$

$i_b$ and $i_c$ are correlated.

The noise current assigned to $Z_{bi}$, $i_{rbi}$ , lumps together all the distributive noise effects, and therefore contains not only the distributive base resistance thermal noise, but also the distributive intrinsic base current noise. It is an important result of [41] that $i_{rbi}$ is not correlated with either $i_b$ and $i_c$ once a uniform $f_T$ across EB junction is assumed. Thus, the PSD of $i_{rbi}$, $S_{i_{rbi}}$, is generally frequency dependent through the frequency dependence of the intrinsic base current noise and has a complex expression [41]. Denote the DC voltage drop across $Z_{bi}$ as $V_{B_x B_i}$. For a circular emitter BJT, the low frequency limit of $S_{i_{rbi}}$ is given as

$$S_{irbi,cir} = \frac{4kT}{R_{BV}} \Delta f \frac{5e^{V_{B_x B_i}/V_T} + 1}{6}. \tag{2.75}$$

For a rectangular emitter BJT, the low frequency limit of $S_{i_{rbi}}$ is given as

$$S_{irbi,rec} = \frac{4kT}{R_{BV}} \Delta f \frac{5e^{V_{B_x B_i}/V_T} + 4}{9}. \tag{2.76}$$

These expressions are hard to use for noise modeling based on small signal equivalent circuits, because the parameters used are not available in a small signal equivalent circuit. At low frequencies, $S_{i_{rbi}}$ can be related to $r_{bi}$ by

$$S_{i_{rbi}} = 4kT/r_{bi} - 2qI_B/3. \tag{2.77}$$

The derivation is given in Appendix B based on [41]. (2.77) is exact for circular emitter BJTs, and has less than a 3% error for rectangular BJTs. At low current levels or under weak crowding strength, (2.77) simplifies to become $4kT/r_{bi}$, the traditional thermal noise model for $r_{bi}$. Note that (2.77) is accurate only when the input NQS effect is included in the intrinsic transistor model, as assumed by [41]. However, in current CAD tools, QS equivalent circuits are used, which cause some problems for $r_{bi}$ noise modeling. Even when the NQS equivalent circuit is used, the $r_{bi}$ needed for $R_n$ fitting is not always equal to $r_{bi}$. These issues are discussed in more detail in Chapter 5.

### 2.4.2 NQS and QS base resistance

Based on the crowding theory [41], Fig. 2.17 (a) with NQS input is the correct equivalent circuit for intrinsic transistor where $r_{bi}$ is the true lumped intrinsic base resistance. $r_{bi}$ is generally dependent on $I_b$. If the carrier density modulation in base is not considered, according to Appendix B

$$r_{bi} \approx \frac{R_{BV}}{1 + I_b R_{BV}/V_T}. \tag{2.78}$$

(2.78) implies that $r_{bi}$ can be modeled by $R_{BV}$ paralleled with $g_{be}$. Clearly the $I_b$ dependence is more severe at low temperatures. An exact consideration of carrier density modulation is difficult, but if an averaged $V_{BE}$ is used to measure the level of carrier density modulation, the $r_{bi}$ can be derived as

$$\begin{aligned} \frac{1}{r_{bi}} &\approx \frac{1}{R_{BV}} \left( \frac{3 + \sqrt{1 + I_b \frac{4n_i^2}{N_A^2 I_{bs}}}}{4} \right) + \frac{I_b}{V_T} \\ &= \frac{1}{R_{BV}} \left( \frac{3 + \sqrt{1 + \frac{I_b}{I_{bk}}}}{4} \right) + \frac{I_b}{V_T}, \end{aligned} \tag{2.79}$$

where $N_A$ is the base doping concentration, $I_{bs}$ is the base saturation current, and

$$I_{bk} \equiv \frac{4n_i^2}{N_A^2 I_{bs}} \approx A_E \frac{4}{\beta} \frac{eD_n N_A}{d_B}. \tag{2.80}$$

$A_E$ is the emitter area. Two parameters, $R_{BV}$ and $I_{bk}$, are needed to model the bias dependence of $r_{bi}$. For high speed SiGe HBTs at room temperature, $R_{BV}$ is quite small, and the carrier density modulation is negligible, leading to the weak $I_b$ dependence of $r_{bi}$ as shown in the experimental extraction in Chapter 3 and in Fig. 2.18 below by analytical calculation.

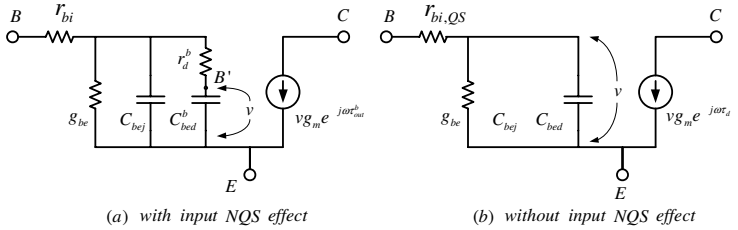


Figure 2.17: Equivalent circuit for intrinsic base of bipolar transistor with $r_{bi}$: (a) With NQS input; (b) With QS input.

If the QS and NQS equivalent circuits in Fig. 2.17 are used to model the same Y-parameters, $r_{bi,QS}$ becomes a lumped resistance related to the true intrinsic resistance $r_{bi}$ and the NQS delay resistance $r_d^b$ ($r_d^b = \tau_{in}^b / C_{bed}^b$). Applying the Taylor expansion method described in Chapter 3 yields

$$r_{bi,QS} \approx r_{bi} + r_d^b \left( \frac{C_{bed}^b}{C_{bed}^b + C_{bej}} \right)^2. \tag{2.81}$$

At low biases $r_d^b C_{bed}^b = \tau_{in}^b$ is a constant. Since $C_{bed}^b$ increases versus bias and $C_{bej}$ is nearly constant, the ratio $C_{bed}^b/(C_{bed}^b + C_{bej})^2$ has a maximum value at $C_{bed}^b = C_{bej}$. This means that $r_{bi,QS}$ should increase at low biases and fall at high biases. $r_{bi,QS}$ is clearly larger than $r_{bi}$. Fig. 2.18 compares $r_{bi}$, $r_{bi,QS}$ and $r_d^b$ extracted from the 1-D Y-parameters in (2.47). $f_T$ is shown for reference. $r_{bi}$ is calculated using (2.79). Peak $f_T$=186 GHz. Note $f_T$ roll off is not included.

$\beta$=235. $\tau_c = 0.57ps$. $C_{bej}$=38 fF. $W_E$=0.12 $\mu$m. $L_E$=18 $\mu$m. These parameters are consistent with those for experimental 200 GHz SiGe HBTs. $V_{BE}$=1.02 V when $\Delta n = N_A$ for base injection. For 200 GHz SiGe HBTs, $f_T$ rolls off around this $V_{BE}$. So the $V_{BE}$<1.02 V range is concerned for AC performance, where $r_{bi}$ is closely bias independent. $r_{bi,QS}$ indeed shows a bell shape and deviates from $r_{bi}$ by 43% at the bias when $C^b_{bed} = C_{bej}$.

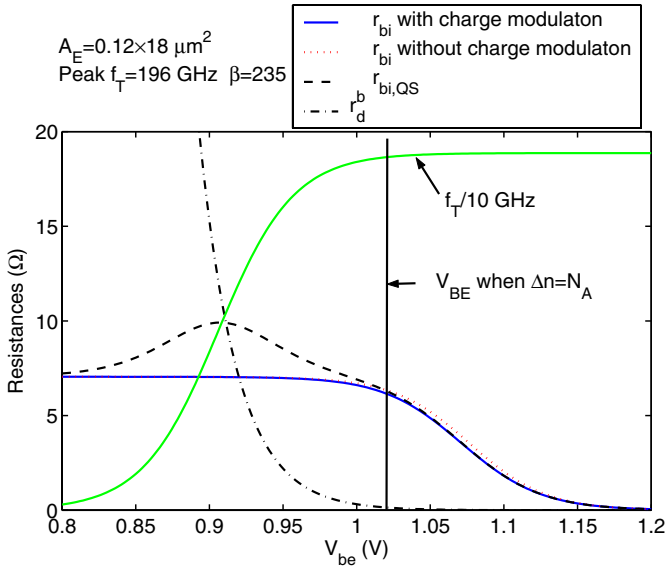


Figure 2.18: Comparison between $r_{bi}$, $r_{bi,QS}$ and $r^b_d$. $\tau_p = 1.54 \times 10^-7s$. $\eta_E$=0. $p_{00} = 0.466\ /cm^3$. $T = 300K$. $d_E$=120 nm. $\mu_{p0}$=225 cm/cs$^2$. $\tau_n = 1.54 \times 10^-7s$. $\eta_B$=5.4. $n_{00} = 23.3\ /cm^3$ ($N_A = 4.3 \times 10^18\ /cm^3$). $d_E$=20 nm. $\mu_{n0}$=450 cm/cs$^2$. $V_{exit} = 1 \times 10^7\ cm/s$. $\tau_c = 0.57ps$. $C_{bej}$=38 fF. $W_E$=0.12 $\mu$m. $L_E$=18 $\mu$m. $A_E$=1 cm$^2$.

At high current levels, $r_{bi,QS} \approx r_{bi} + r^b_d$. Thus, it is meaningful and interesting to compare $r_{bi}$ with $r^b_d$ under different parameter changes.

- $W_E$, $d_B$ (2.48) shows that $r^b_d \propto d_B/W_E$. On the contrary, $r_{bi} \propto W_E/d_B$. During device scaling, both $W_E$ and $d_B$ are scaled. Therefore, for different generation devices, it is difficult to compare the relative importance of $r^b_d$. For the same generation devices, however, the smaller the emitter width, the more important $r^b_d$.

- $L_E$, $N_A$ (2.48) shows that $r^b_d \propto 1/L_E N_A$, the same as $r_{bi}$.

- *Ge gradient* ($\eta$) As shown in Fig. 2.6, $\eta$ reduces $r_d^b$. However $\eta$ has little effect on $r_{bi}$. Therefore, for two devices that only differ in terms of Ge gradient, the one with the larger Ge gradient will have less modeling error using QS equivalent circuit at high current levels.

Overall, unlike $f_T$, *one cannot compare the relative importance of* $r_d^b$ *for different generations of devices without knowing the design details of each generation*.

## 2.5 Present noise models and implementation problems

### 2.5.1 SPICE model

The default $i_b$ and $i_c$ noise models in current CAD tools are the same as those used in SPICE [42]. $i_b$ and $i_c$ are assumed to be shot like and uncorrelated. This is denoted as SPICE model and the PSDs are given by

$$S_{ib}^{SPICE} = 2qI_B, \quad S_{ic}^{SPICE} = 2qI_C, \quad S_{icib^*}^{SPICE} = 0. \tag{2.82}$$

Both the theoretical analysis above and experimental data have shown that this highly simplified model is not sufficient for high frequency applications, particularly at the higher biasing currents required to achieve high speed operation [43–48]. In particular, $S_{ib}$ has been shown to increase with frequency, and the correlation $S_{icib^*}$ is significant and cannot be neglected [43, 45–47, 49].

### 2.5.2 Transport noise model

The transport noise model [43] [44] has recently been shown to work better than the SPICE model [43,45] by taking into account the correlation. The essence of this model is that the collector current noise is transported from the electron current shot noise in the emitter-base junction, with

a noise transit time $\tau_n$ [43]:

$$
\begin{aligned}
S_{ib}^{Tran} &= 2qI_B + 4qI_C[1 - \Re(e^{j\omega\tau_n})], \\
S_{ic}^{Tran} &= 2qI_C, \\
S_{icib^*}^{Tran} &= 2qI_C(e^{-j\omega\tau_n} - 1).
\end{aligned} \tag{2.83}
$$

However, in practical devices, with only a single parameter $\tau_n$, simultaneous fitting of measured $S_{ib}$ and $S_{icib^*}$ can become difficult. Simultaneous fitting of $NF_{min}$, $R_n$, $G_{opt}$ and $B_{opt}$ is challenging in some cases.

### 2.5.3 Brutal use of van Vliet model

The van Vliet model serves as the basis of several other models, e.g. [47, 50–53]. Since the van Vliet derivation does not consider electron transport in the collector-base space charge region (CB SCR), characterized by transit time $\tau_c$, (2.67) cannot be automatically extended to include the CB SCR effect simply by replacing $Y_B$ with Y-parameters of whole intrinsic transistor [5]. In the literature [50–53], the van Vliet model is often used unphysically:

- $Y_B$ should explicitly include the input NQS effect, that is, $\Re(Y_{11}^B)$ should be frequency dependent, so that the frequency dependence of $S_{bi}^B$ can be modeled. However, all the implementations reported use QS equivalent circuits whose $\Re(Y_{11}^B)$ is frequency independent.

- The Y-parameters of the whole intrinsic transistor, including the CB SCR, are used in (2.67), the results are recognized as the noise of whole transistor without justification. For scaled bipolar transistors, CB SCR electron transport becomes more significant than base electron transport. The van Vliet model must be improved to including this effect.

### 2.5.4 $4kTr_{bi}$ for $r_{bi}$ noise

With the uniform $f_T$ assumption, the noise PSD of $i_{rbi}$ can be approximated with $4kT/r_{bi}$ for SiGe HBTs whose crowding effect is negligible. This is the base resistance noise model commonly used in CAD tools and in the literature [42, 50–53]. However, problems were encounted when using $4kTr_{bi}$ for noise modeling based on either QS or NQS lumped equivalent circuits: First, the noise resistance $R_n$ cannot be well modeled, as it is sensitive to base hole noise. One has to use an empirical $S_{ic}$ based on noise extraction, which is unphysically larger than $2qI_c$ for 50 GHz SiGe HBTs ( see Chapter 4). Another problem is that the absolute value of the imaginary part of the noise parameter $Y_{opt}$, i.e. $B_{opt}$, is overestimated by the van Vliet model based on NQS equivalent circuit. The deviation cannot be eliminated by choosing an appropriate $r_{bi}$.

The uniform $f_T$ assumption is not justified for high speed SiGe HBTs with narrow emitter width ($\leq 0.24\mu m$). The $f_T$ within the fringe transistor is smaller than that in the main transistor due to larger base width. Such non-uniform $f_T$ does not have a significant effect on $i_b$ and $i_c$ noises. However, the base hole noise now has to be modeled by a noise source at the input together with a *correlated* noise current source at the output [6].

## 2.6 Methodologies to improve noise modeling

Two methods are proposed to improve noise modeling in this work:

- The first method is to implement a semi-empirical model for the intrinsic transistor noise based on noise extraction for the QS equivalent circuit, as detailed in Chapter 4. Eq. (2.77) is used for $S_{i_{rbi}}$ and then the intrinsic noise $S_{ib}$, $S_{icib^*}$ and $S_{ic}$ are extracted from device noise parameters using standard noise de-embedding methods [54]. Equations can then be developed to model these noise sources. The deviation caused by the use of a QS input equivalent circuit, and hence the lumping of input NQS resistance into $r_{bi}$, as well as the use of (2.77), is all included in the intrinsic noise. The extracted $S_{ib}$ and $S_{ic}$ are thus not

precisely the physical intrinsic transistor noises, which can only be obtained through higher order modeling that includes input NQS and noise crowding effects. The noise sources and their correlation, are first modeled as functions of frequency ($\omega$). The coefficients are then extracted and modeled as a function of biasing current through $g_m$. As the QS equivalent circuit is used, existing parameter extraction methods can be applied, and the proposed model can be readily implemented in current compact models. This method was verified in VBIC model using Verilog-A by Advance Design System (ADS) circuit simulator.

- The second method improves compact RF noise modeling for SiGe HBTs based on NQS equivalent circuit using new electron and hole noise models as detailed in Chapter 5. The impact of CB SCR on electron RF noise is examined to be important for scaled SiGe HBTs. The van Vliet model is then improved to account for the CB SCR effect. The impact of the fringe BE junction on base hole noise is further investigated. Due to the fringe effect, the base hole noise should be modeled with correlated noise voltage source and noise current source in hybrid representation. The base noise resistance is found to be different from $r_{bi}$, and cannot be explained by fringe effect alone. An extra parameter $R_{bn}$ is included for base noise resistance. With a total of four bias-independent model parameters, the combination of electron and hole noise model provides excellent noise parameter fittings for frequencies up to 26 GHz and all biases before $f_T$ roll off for three generations of SiGe HBTs.

## 2.7 Summary

Diffusion noise is the major noise source in SiGe HBTs. The van Vliet model is still applicable for typical SiGe HBTs with a base built-in field, and can be directly extended to include emitter hole noise. The CB SCR effect is important for aggressively scaled devices, and should be included in noise modeling. The fringe BE junction effect impacts base hole noise, and should be included for noise modeling. Present noise models are not sufficiently accurate for RF noise modeling at

high frequencies. Both semi-empirical and physical methods are used in this work to improve RF noise modeling.

# CHAPTER 3

# SMALL SIGNAL PARAMETER EXTRACTION

Small-signal equivalent circuit accurately modeling both AC and noise characteristics of SiGe HBTs is very useful for RF circuit design as well as understanding of device physics. The topology of equivalent circuit determines the physics effects that can be accounted for, accuracy of final AC and noise characteristics, and affects circuit parameter extraction procedure as well as the physical soundness of extracted equivalent circuit parameters. Microscopic noise physics based noise models of bipolar transistors described in Chapter 2 require modeling of input NQS effect. This chapter examines small signal equivalent circuit modeling of input NQS effect including CB CSR delay, and its parameter extraction.

Accurate parameter extraction is challenging in practice due to the large number of parameters involved, in spite of the various methods proposed, including both direct or analytical methods and numerical optimization based methods. Including the input NQS effect makes the circuit topology even more complex. Numerical methods often lead to physically meaningless values, as reviewed in [55]. The full analytical expressions of Y/Z-parameters are too complex to be directly used for extraction. This chapter presents a new direct extraction method based on Taylor series expansion analysis of Y/Z-parameter expressions [8]. The real part of Y/Z-parameters is approximated up to second order of frequency. The imaginary part is approximated up to first order. The expansion coefficients are obtained as simple functions of equivalent circuit parameters, allowing straightforward parameter extraction. The extracted parameters, such as intrinsic base resistance and excess phase delay time, show more physical bias dependences compared to conventional extraction. The

utility of this method is demonstrated using SiGe HBTs of different sizes from different technology generations, a SiGe HBT with 180 GHz peak $f_T$ is used below for illustration of extraction procedure.

### 3.1 Necessity of including input NQS effect in equivalent circuit

Of particular interest to modeling of the RF noise in the base current is the frequency dependence of the real part of the input admittance, $\Re(Y_{11})$, due to base electron transport, which is responsible for the frequency dependence of base current noise as well as the correlation between base and collector current RF noises as discussed in Chap 2. We have also show the NQS equivalent circuit for base region in Fig. 2.3. The base minority carrier charge responds to base emitter voltage by the input NQS delay time $\tau_{in}^b$, then the collector current at the end of base region responds to the stored base minority carrier charge by the output NQS delay time $\tau_{out}^b$. For a real device, particularly modern SiGe HBTs, the output collector current is further delayed, compared to the current at the end of the base, by the CB SCR transit time $\tau_c$. Although the circuit topology of Fig. 2.3 (a) was derived for the base region, the same circuit topology is capable of including $\tau_{in}^b$, $\tau_{out}^b$ and $\tau_c$ delays, as shown below, with proper modifications to values of its elements.

However, in present BJT models e.g. SPICE Gummel-Poon and VBIC, and all the recent direct parameter extraction methods [55–61], a circuit topology of Fig. 2.3 (b) is used for the intrinsic transistor. Although $\tau_{out}^b$ has been included in Fig. 2.3 (b), the input NQS effect is neglected. We found problems in using such circuit topology for both AC and noise modeling of high peak $f_T$ SiGe HBTs. First of all, with Fig. 2.3 (b), the real part of $Y_{11}$ of intrinsic device, $\Re(Y_{11})$, is frequency independent [3, 4]. Correct modeling of $\Re(Y_{11})$ is crucial for a physically meaningful implementation of microscopic noise physics based base and collector current RF noise models [2],

such as the van Vliet model, see (2.67). The increase of base current noise with frequency is directly proportional to the $\Re(Y_{11})$ of the base and this part of the base current noise is correlated with the collector current noise.

Another major problem with using the circuit topology with QS input is extraction of intrinsic base resistance, which we denote as $r_{bi,QS}$. $r_{bi,QS}$ is often extracted using impedance semicircle fitting method [62], which determines base resistance from the x-axis intercept of a semicircle fitted to ($\Re[H_{11}]$,$\Im[H_{11}]$) points of different frequencies on a complex impedance plane for an equivalent circuit excluding the extrinsic base resistance and CB capacitance. We find that the $r_{bi,QS}$ extracted increases unphysically at low base currents because $r_d^b$ is lumped into $r_{bi}$ [4]. Such unphysical result in $r_{bi}$ extraction was also observed by others, e.g. in [63], and is typical of existing $r_{bi}$ or $r_b$ extraction. The use of $r_{bi,QS}$ also leads to an overestimation of minimum noise figure [4]. The extracted excess phase delay time of the intrinsic device shows a strong bias-dependence even at low current levels, a clearly unphysical result. The inaccurate excess phase delay time directly affects the correlation between base current noise and collector current noise through $\Im(Y_{21})$ in van Vliet model, see (2.67). Using an equivalent circuit based on Fig. 2.3 (a) which explicitly includes the input NQS effect, the abnormal bias dependence of $r_{bi,QS}$ can be explained and avoided. A more physical value of $r_{bi}$ is obtained, which also helps improving noise modeling. The extracted excess phase delay time shows a more physical bias-dependence [8].

### 3.2 NQS Equivalent circuit

The input NQS equivalent circuit of Fig. 2.3 (a) proposed by Winkel was based on frequency domain solution in the base only. For modern SiGe HBTs, it is necessary to include the impact of CB SCR.

### 3.2.1 CB SCR effect

The Y-parameters of base, $Y^{bs}$, can be obtained from Fig. 2.3 (a) as

$$Y_{11}^{bs} = g_{be} + j\omega C_{bej} + \frac{j\omega C_{bed}^{b}}{1 + j\omega\tau_{in}^{b}}, \quad Y_{21}^{bs} = g_m \frac{e^{-j\omega\tau_{out}^{b}}}{1 + j\omega\tau_{in}^{b}}. \tag{3.1}$$

$Y_{12}^{bs}$ and $Y_{22}^{bs}$ are equal to zero. With CB SCR, the Y-parameters of whole transistor, $Y^{al}$, can be calculated from $Y^{bs}$ and $\tau_c$ as [5]

$$Y_{11}^{al} = Y_{11}^{bs} + (1 - \lambda)Y_{21}^{bs}, \qquad Y_{21}^{al} = \lambda Y_{21}^{bs}, \tag{3.2}$$

where $\lambda = (1 - e^{-2j\omega\tau_c})/(2j\omega\tau_c)$. (More details in (5.1)). A close inspection shows that we can still use the circuit topology of Fig. 2.3 (a) or Fig. 3.1 (a) to describe $Y^{al}$ with an accuracy up to the second order in frequency. The intrinsic NQS equivalent circuit including CB SCR is shown in Fig. 3.1 (b). The equivalent circuit parameters of whole transistor ($C_{bed}$, $r_d$ or $\tau_{in}$, and $\tau_{out}$) are related to those of base region ($C_{bed}^{b}$, $r_d^{b}$ or $\tau_{in}^{b}$, and $\tau_{out}^{b}$) and $\tau_c$. Denoting $\tau_{tr} \equiv C_{bed}/g_m$ and $\tau_{tr}^{b} \equiv C_{bed}^{b}/g_m$, we find

$$\begin{aligned}
\tau_{tr} &= \tau_{tr}^{b} + \tau_c, \\
\tau_{in} &= \tau_{in}^{b} + \tau_c \frac{\tau_{out}^{b} + 2\tau_c/3}{\tau_{tr}^{b} + \tau_c}, \\
\tau_{out} &= \tau_{out}^{b} + \tau_c \frac{\tau_{tr}^{b} - \tau_{out}^{b} + \tau_c/3}{\tau_{tr}^{b} + \tau_c}.
\end{aligned} \tag{3.3}$$

Detailed derivation is given in Appendix C. (3.3) reveals that $\tau_{in} \to 2/3\tau_{tr}$ and $\tau_{out} \to 1/3\tau_{tr}$ when $\tau_c >> \tau_{tr}^{b}, \tau_{in}^{b}, \tau_{out}^{b}$, the case of SiGe HBTs with ultra narrow base.

To further investigate the $\tau_c$ effect, we use analytical Y-parameter expressions of ideal 1-D base region derived from frequency domain solution of the drift-diffusion equations in (2.47). First, we extract $\tau_{tr}^{b}$, $\tau_{in}^{b}$ and $\tau_{out}^{b}$ from the analytical Y-parameters. Then $\tau_{tr}$, $\tau_{in}$ and $\tau_{out}$ are evaluated

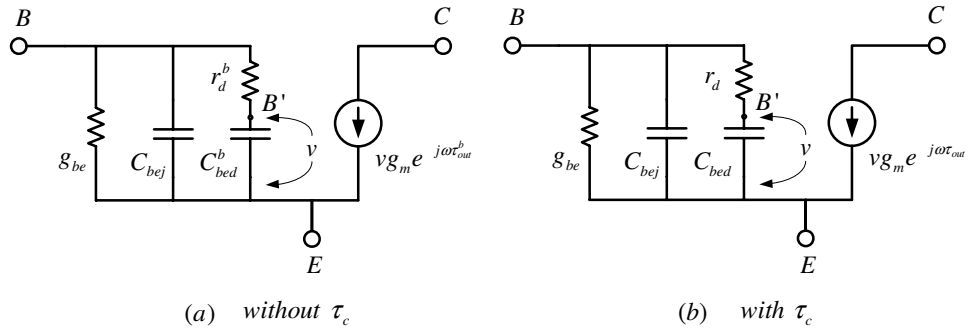


Figure 3.1: Intrinsic NQS small signal equivalent circuit of SiGe HBTs: (a) without $\tau_c$; (b) with $\tau_c$.

using (3.3). Fig. 3.2 (a) shows $\tau_{in}/\tau_{tr}$ and $\tau_{out}/\tau_{tr}$ versus base width for different $\tau_c$ at $\eta = 6$, the typical value for SiGe HBTs. $\tau_c$ increases the input NQS effect and decreases excess phase delay time for narrow base transistor. Fig. 3.2 (b) shows $\tau_{in}/\tau_{tr}$ and $\tau_{out}/\tau_{tr}$ versus base width for different $\eta$ at $\tau_c$=0.6 ps. For SiGe HBTs with higher Ge grading, i.e. larger $\eta$, the normalized input NQS effect becomes larger.

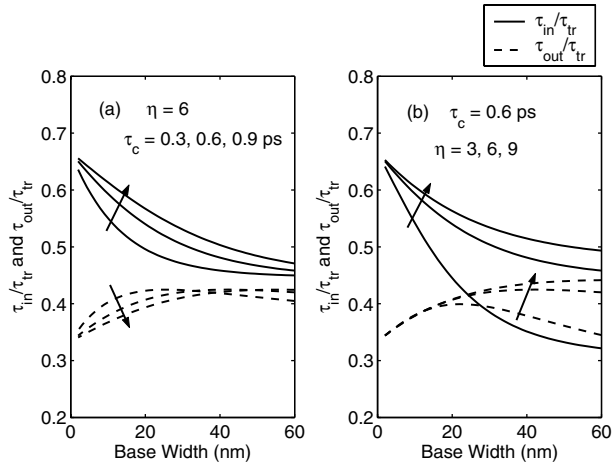


Figure 3.2: CB SCR effect on $\tau_{in}$ and $\tau_{out}$. For the 1-D base region, $V_{sat}^{bs} = 1 \times 10^7$ cm/s, $\mu_{n0} = 270$ cm/Vs$^2$, $\tau_n$=0.154 $\mu$s, $T$=300 K.

The importance of input NQS can be measured by comparing the frequency dependent part of $\Re(Y_{11})$ with $g_{be}$ ($\approx I_b/V_T$). The frequency dependent part of $\Re(Y_{11})$ can be calculated from (3.2)

as $\omega^2 C_{bed}\tau_{in}$. For fixed frequency, bias, and emitter design, the importance of input NQS can thus be measured by $C_{bed}\tau_{in}$. Fig. 3.3 shows $C_{bed}\tau_{in}$ versus $\eta$ for different $\tau_c$. The larger $\tau_c$ or the larger base Ge gradient, the more important the input NQS effect.

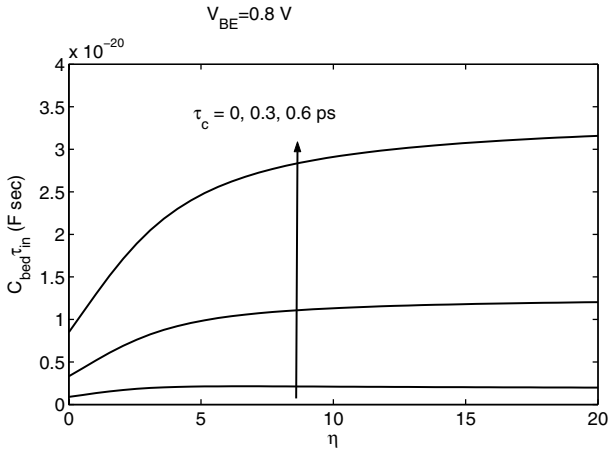


Figure 3.3: CB SCR and Ge gradient impacts on the importance of input NQS effect. For the 1-D base region, $d_B$=20 nm, $V_{sat}^{bs} = 1\times10^7$ cm/s, $\mu_{n0} = 270$ cm/Vs$^2$, $\tau_n$=0.154 $\mu$s, $T$=300 K. $V_{BE}$ =0.8 V.

### 3.2.2 NQS equivalent circuit

Fig. 3.4 shows the small signal equivalent circuit used. The substrate is tied to emitter to facilitate two-port RF measurements using two GSG probes. Block $B_X$ is the equivalent circuit excluding $r_e$ and substrate network from the full circuit. $B_M$ is the block obtained by excluding $r_c$ from $B_X$. Block $B_{IR}$ is the intrinsic device with $r_{bi}$. Block $B_I$ is the intrinsic device without $r_{bi}$. Note that the control voltage for the transconductance term is the total intrinsic BE voltage drop across $r_d$ and $C_{bed}$, instead of the voltage across $C_{bed}$ as done in Fig. 2.3 (a). This makes the total excess phase delay time $\tau_{in} + \tau_{out}$, designated as $\tau_d$ below. Lumping $\tau_{in}$ and $\tau_{out}$ into $\tau_d$ does not lose modeling accuracy and is advantageous for extraction, as the input NQS and output excess phase delays are now separated. $C_{bex}$ is the extrinsic BE capacitance, for example, the capacitance between base and emitter through spacer, and is non-negligible for small devices of

high $f_T$ SiGe HBTs. The output conductance $r_o$ is neglected due to the large Early voltage in SiGe HBTs. Parameter $r_u$ relating to the $V_{CB}$ modulation of neutral base recombination current has no significant effect on either Y-parameters or RF noise at frequencies above 1 GHz, and is neglected. All other extrinsic parameters have their conventional meanings. For convenience, we define total BE capacitance, total BC capacitance and its partition factor $\gamma$ as

$$C_{bet} \equiv C_{bed} + C_{bej}, C_{bct} \equiv C_{bcx} + C_{bci}, \gamma \equiv C_{bci}/C_{bct}.$$

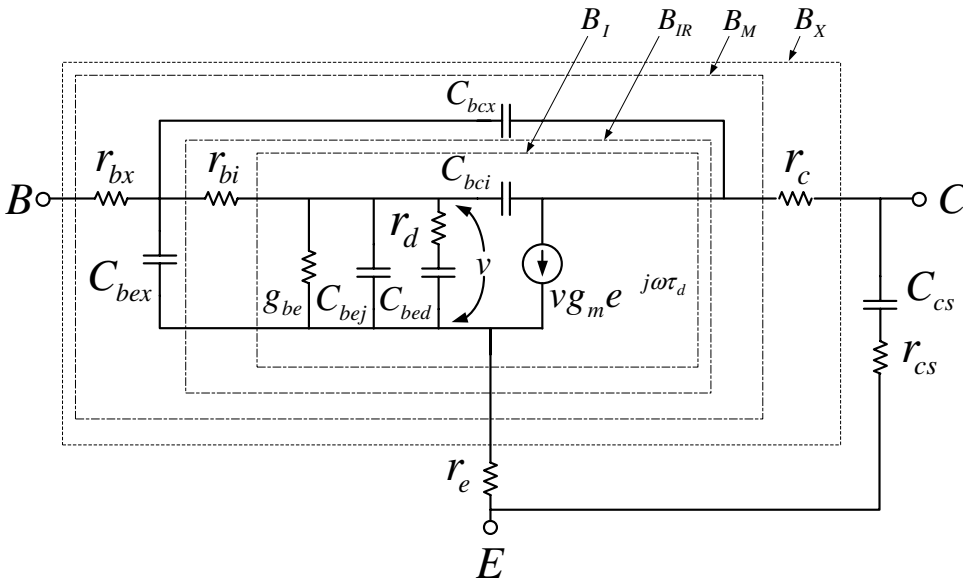


Figure 3.4: Small signal equivalent circuit of SiGe HBTs with substrate tied to emitter.

Now we discuss a few assumptions we will make on the bias dependence of small signal parameters. Extrinsic element $r_{bx}, r_c, C_{bex}$ are considered as bias-independent. $\gamma$ is also considered as bias-independent. Strictly speaking, BE depletion capacitance $C_{bej}$ is a function of $V_{BE}$. However, for the RF bias range across which $f_T$ is high, the variation of $V_{BE}$ (0.80–0.92 V) is small, and $C_{bej}$ can be considered bias-independent. The base charge modulation and DC crowding effect are

negligible for SiGe HBTs because of the high base doping [1]. Consequently $r_{bi}$ is weakly bias dependent before high injection base push out occurs. In our extraction method, we first consider $r_{bi}$ as bias-independent during extrinsic parameter extraction. Bias-independent $r_{bi}$ is extracted. Such assumption is justified for high $f_T$ SiGe HBTs due to the high base doping as discussed in Chapter 2. It is important to note that the bias dependent $r_{bi,QS}$ extracted using equivalent circuit without including input NQS effect is a lumped parameter involving $r_d$ and $r_{bi}$ [4]. The bias dependence of $r_{bi,QS}$ can be well reproduced by our NQS circuit with bias-independent $r_{bi}$ as discussed in Section IV. To make our method more general, we also give a method that can extract bias-dependent $r_{bi}$, where the delay time ratios $\tau_{in}/\tau_{tr}$ and $\tau_d/\tau_{tr}$ are considered as constant for all biases.

### 3.3 Parameter extraction

S-parameters are measured for SiGe HBTs of different process generations with different emitter geometries. Only a 180 peak $f_T$ device is used below for illustration of parameter extraction. The HBT has an emitter area $A_E = 0.12 \times 6 \times 1\ \mu\text{m}^2$. S-parameters are measured on-chip using a 8510C Vector Network Analyzer (VNA) from 1-48 GHz. The S-parameters are de-embedded using standard OPEN/SHORT structures. "Active" measurement is made by sweeping $V_{BE}$ (0.80–0.98 V) with $V_{CE}$=1.5 V. The $f_T$ rolls off at $V_{BE}$=0.921 V. "Cold" measurement ($V_{BE}$=0 V, $V_{CE}$=1.5 V) is also made to extract the substrate network and the $C_{bc}$ partition factor $\gamma$.

The analytical Y/Z-parameter expressions for each block in Fig. 3.4 can be derived in a way very similar to the derivation in [3]. Note that $C_{bej}$ is not explicitly split from $C_{bed}$ in [3]. The results are shown in Appendix D. We also use the symbolic analysis of MATLAB to obtain these results. The source code is given in Appendix D. Some of the Y-parameters and the inverse of Z-parameters, or their linear combinations, can be used for parameter extraction. We denote them as $T$. Due to the complexity of equivalent circuit, the exact $T$ expressions, however, are difficult to use for direct parameter extraction. We notice that all of the $T$ expressions are functions of

frequency or $\omega$, and have no singularities at $\omega$=0. Hence we can make Taylor expansions for them at $\omega$=0. The real part of $T$ is expanded up to the second order of $\omega$ and the imaginary part up to the first order of $\omega$,

$$\begin{aligned}\Re(T) =&[\Re(T)_0] + [\Re(T)_2]\omega^2 + o(\omega^2),\\ \Im(T) =&[\Im(T)_1]\omega + o(\omega).\end{aligned} \tag{3.4}$$

We emphasize that the real part expansion consists of only even orders of $\omega$ terms and the imaginary part consists of only odd orders of $\omega$ terms. Any admittance, impedance or transconductance element containing $\omega$ in Fig. 3.4 contains $j\omega$. Since the real part of $T$ only contains even order terms of $j$, the real part must only contain even order terms of $\omega$. Similarly, the imaginary part of $T$ only contains odd order terms of $j$, hence the imaginary part must only contain odd order terms of $\omega$. The coefficients directly relate to small signal equivalent circuit parameters and can then be used for parameter extraction, as detailed below. It is critical to accurately extract these coefficients for certain Y/Z-parameter. To extract $\Re(T)_0$ and $\Re(T)_2$, we plot $\Re(T)$ versus $\omega^2$. A linear relation should be observed at low frequencies. With a linear fitting, the y-axis intercept gives $\Re(T)_0$, and the slope gives $\Re(T)_2$. Fig. 3.5 (a) illustrates the extraction of $\Re(Y_{11}^{BM} + Y_{12}^{BM})_2$ at low, medium and high biases. To extract $\Im(T)_1$, we plot $\Im(T)/\omega$ versus $\omega^2$. A linear relation is observed at low frequencies. With a linear fitting, the y-axis intercept gives $\Im(T)_1$. Fig. 3.5 (b) illustrates the extraction of $\Im(Y_{22}^{BM})_1$ at low, medium and high biases. One could also extract $\Im(T)_1$ from the slope of $\Im(T)$ versus $\omega$ at lower frequencies where the third order term is weak. This, however, is not necessary when plotting $\Im(T)/\omega$ versus $\omega^2$. We now detail the extraction procedure parameter by parameter.

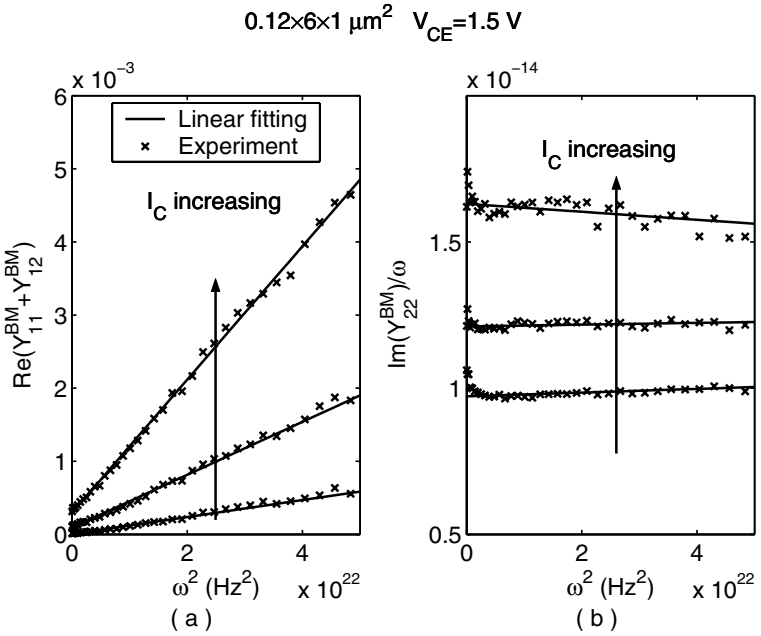


Figure 3.5: Illustration of Taylor expansions coefficient extraction for (a) $\Re(Y_{11}^{BM} + Y_{12}^{BM})_2$, and (b) $\Im(Y_{22}^{BM})_1$.

### 3.3.1 $C_{cs}$, $r_{cs}$, $\gamma$ and $r_e$ extraction

Cold measurement data is used to extract substrate network ($r_{cs}$, $C_{cs}$) using the method in [64], that is

$$C_{cs} = \frac{\Im(Y_{22}^{Cold} + Y_{12}^{Cold})}{\omega}, \quad r_{cs} = \frac{\Re(Y_{22}^{Cold} + Y_{12}^{Cold})}{\left[\Im(Y_{22}^{Cold} + Y_{12}^{Cold})\right]^2}. \tag{3.5}$$

The CB capacitance partition factor $\gamma$ can also be extracted from cold measurement data using the method in [65], explicitly

$$\gamma \approx \frac{\Im(Y_{11}^{Cold} + Y_{12}^{Cold})}{\Im(Y_{12}^{Cold})} \frac{\Re(Y_{12}^{Cold})}{\Re(Y_{11}^{Cold} + Y_{12}^{Cold})}. \tag{3.6}$$

$\gamma$ usually is small for SiGe HBTs. For example, $\gamma$=0.21 for the device used for illustration. $r_e$ is determined by the y-axis intercept of $\Re(Z_{12})$ versus $1/I_c$.After de-embedding the substrate network and $r_e$, the Z-parameters of block $B_X$ are known, explicitly,

$$Z_{11}^{BX} = \frac{Y_{22} - \frac{j\omega C_{cs}}{1+j\omega C_{cs} r_{cs}}}{Y_{11}Y_{22} - Y_{12}Y_{21} - Y_{11}\frac{j\omega C_{cs}}{1+j\omega C_{cs} r_{cs}}} - r_e, \quad Z_{12}^{BX} = -\frac{Y_{12}}{Y_{11}Y_{22} - Y_{12}Y_{21} - Y_{11}\frac{j\omega C_{cs}}{1+j\omega C_{cs} r_{cs}}} - r_e,$$
$$Z_{21}^{BX} = -\frac{Y_{21}}{Y_{11}Y_{22} - Y_{12}Y_{21} - Y_{11}\frac{j\omega C_{cs}}{1+j\omega C_{cs} r_{cs}}} - r_e, \quad Z_{22}^{BX} = \frac{Y_{11}}{Y_{11}Y_{22} - Y_{12}Y_{21} - Y_{11}\frac{j\omega C_{cs}}{1+j\omega C_{cs} r_{cs}}} - r_e. \tag{3.7}$$

### 3.3.2 $C_{bct}$, $C_{bcx}$, $C_{bci}$, $r_c$ and $g_m$ extraction

For block $B_X$, we obtain the following Taylor expansion coefficients using symbolic analysis in MATLAB (code is given in Appendix D)

$$\Im\left[1/(Z_{22}^{BX} - Z_{21}^{BX})\right]_1 = C_{bct}, \tag{3.8}$$
$$\Re\left[1/(Z_{22}^{BX} - Z_{21}^{BX})\right]_2 = C_{bct}^2\left(r_c - \gamma r_{bi}\frac{C_{bcx} + C_{bex}}{C_{bct}}\right), \tag{3.9}$$
$$\Re\left[1/Z_{12}^{BX}\right]_0 = g_m. \tag{3.10}$$

The basic idea is that $r_{bx}$ does not impact the above Z-parameters. Therefore, the coefficients are not affected by $r_{bx}$. $C_{bct}$ can be directly obtained from (3.8), which essentially is the method reported in [66]. With $C_{bct}$ and $\gamma$ known, $C_{bcx}$ and $C_{bci}$ are obtained. $g_m$ can be directly obtained from (3.10). $r_c$ can be extracted from (3.9) by neglecting the term related to small $\gamma$ as

$$r_c \approx \frac{\Re\left[1/(Z_{22}^{BX} - Z_{21}^{BX})\right]_2}{C_{bct}^2}. \tag{3.11}$$

Note that (3.11) is sensitive to substrate network de-embedding. Inaccurate $C_{cs}$ and $r_{cs}$ will result in unphysical bias dependence of $r_c$. Now the Z-parameters of block $B_M$ can be obtained

$$Z_{11}^{BM} = Z_{11}^{BX},\ \ Z_{12}^{BM} = Z_{12}^{BX},\ \ Z_{21}^{BM} = Z_{21}^{BX},\ \ Z_{22}^{BM} = Z_{22}^{BX} - r_c. \tag{3.12}$$

Consequently, the Y-parameters of block $B_M$ are known.

### 3.3.3 $r_{bx}$ and $r_{bi}$ extraction

Fig. 3.6 shows the block $B_M$ of the small signal equivalent circuit. We have the following

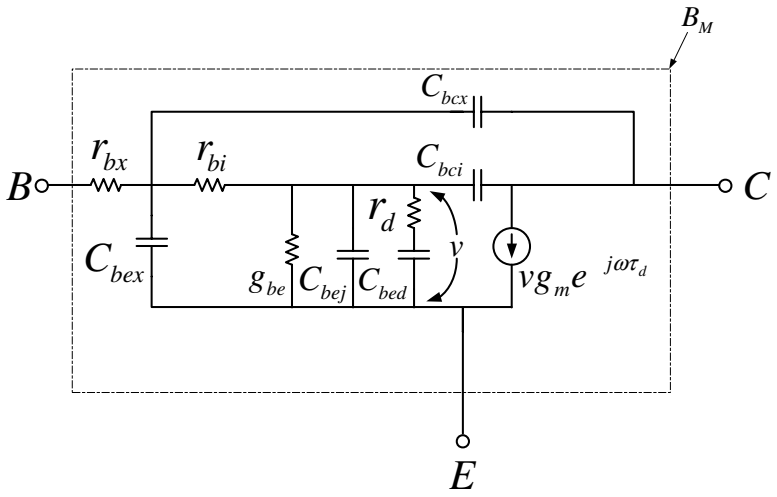


Figure 3.6: Small signal equivalent circuit of SiGe HBTs for block $B_M$.

Taylor expansion coefficients for block $B_M$ using symbolic analysis

$$\Im(Y_{11}^{BM} + Y_{12}^{BM})_1 \approx C_{bet} + C_{bex}, \tag{3.13}$$

$$\begin{aligned}\Im(Y_{21}^{BM} - Y_{12}^{BM})_1 \approx & g_m\{(r_{bx} + r_{bi})(C_{bet} + C_{bex}) \\ & + [\tau_d + (r_{bx} + \gamma r_{bi})C_{bct} - r_{bi}C_{bex}]\},\end{aligned} \tag{3.14}$$

$$\Im(Y_{22}^{BM})_1 \approx C_{bct} + g_m C_{bct}(r_{bx} + \gamma r_{bi}). \tag{3.15}$$

Approximation $(r_{bx}+r_{bi})g_{be} << 1$ is used, meaning that these expressions are less accurate at high biases. For SiGe HBTs, due to high base doping, this approximation is valid for low and medium biases, where we extract $r_{bx}$. According to (3.13) and (3.14), we have

$$\frac{\Im(Y_{21}^{BM} - Y_{12}^{BM})_1}{g_m} \approx (r_{bx} + r_{bi})\Im(Y_{11}^{BM} + Y_{12}^{BM})_1 + U, \tag{3.16}$$

where $U \equiv \tau_d + (r_{bx} + \gamma r_{bi})C_{bct} - r_{bi}C_{bex}$ is bias independent at low biases since all the parameters involved are bias independent at low biases. Fig. 3.7 plots $\Im(Y_{21}^{BM} - Y_{12}^{BM})_1/g_m$ versus $\Im(Y_{11}^{BM} + Y_{12}^{BM})_1$. A linear relation is observed. $r_{bx} + r_{bi}$ is determined by the slope of fitting line according to (3.16). According to (3.15), if we plot $\Im(Y_{22}^{BM})_1$ versus $g_m C_{bct}$, a linear relation can be obtained

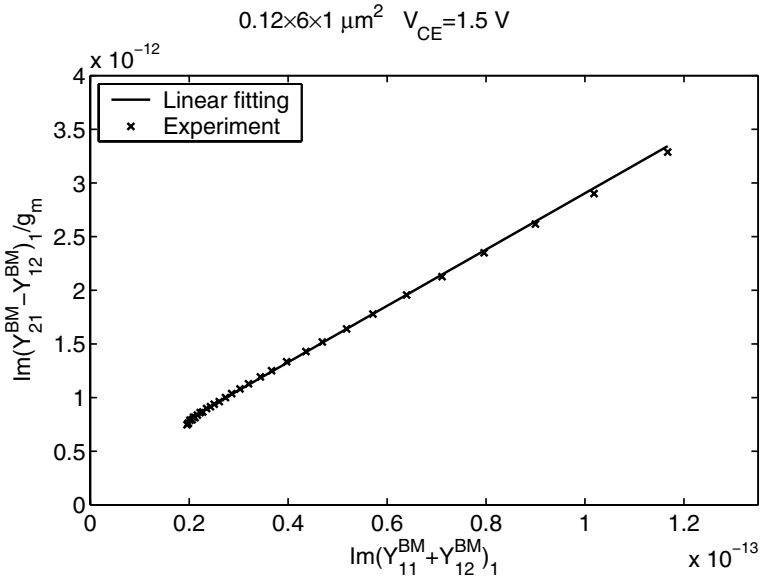


Figure 3.7: $\Im(Y_{21}^{BM} - Y_{12}^{BM})_1/g_m$ versus $\Im(Y_{11}^{BM} + Y_{12}^{BM})_1$. The slope of fitting line gives $r_{bx} + r_{bi}$.

as shown in Fig. 3.8. The slope gives $r_{bx} + \gamma r_{bi}$. With $\gamma$ known, $r_{bx}$ and $r_{bi}$ can then be calculated from $r_{bx} + \gamma r_{bi}$ and $r_{bx} + r_{bi}$.

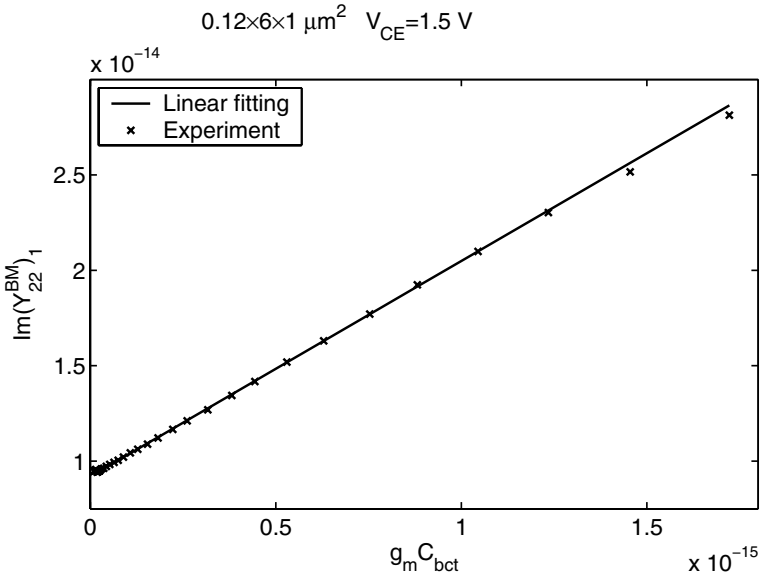


Figure 3.8: $\Im(Y_{22}^{BM})_1$ versus $g_m C_{bct}$. The slope of fitting line gives $r_{bx} + \gamma r_{bi}$.

### 3.3.4 $C_{bex}$ and $C_{bej}$ extraction

As $C_{bej}$ is the low current limit of $C_{bet}$, the low current limit of $\Im(Y_{11}^{BM} + Y_{12}^{BM})_1$ gives $C_{bex} + C_{bej}$ according to (3.13). For block $B_M$, we have

$$\begin{aligned}\Re(Y_{11}^{BM} + Y_{12}^{BM})_2 \approx & r_{bx}(C_{bej} + C_{bex})(C_{bej} + C_{bex} + C_{bct}) \\ & + r_{bi}C_{bej}^2 + (\gamma r_{bi}C_{bct})C_{bej} + g_m W, \end{aligned} \tag{3.17}$$

where $W$ is a complex function of circuit parameters. Again $(r_{bx} + r_{bi})g_{be} << 1$ is used. Consider now the low current limit of (3.17),

$$\begin{aligned}&\{r_{bi}\}C_{bej}^2 + \{(\gamma r_{bi}C_{bct})\}C_{bej} + \{r_{bx}(C_{bej} + C_{bex})(C_{bej} + C_{bex} + C_{bct}) \\ &- \Re(Y_{11}^{BM} + Y_{12}^{BM})_2|_{g_m \to 0}\} = 0. \end{aligned} \tag{3.18}$$

This is a quadratic equation for $C_{bej}$ with all the coefficients in the curly brackets known. $C_{bej}$ corresponds to the positive root. $C_{bex}$ is then obtained.

To extract the low current limits for Taylor expansion coefficients, $\Im(Y_{11}^{BM} + Y_{12}^{BM})_1$ and $\Re(Y_{11}^{BM} + Y_{12}^{BM})_2$, we make a linear fitting versus $g_m$ within *low current* domain for these coefficients. The y-axis intercepts give the corresponding low current limits. Fig. 3.9 illustrates the low current limit extraction of $\Re(Y_{11}^{BM} + Y_{12}^{BM})_2$ and $\Im(Y_{11}^{BM} + Y_{12}^{BM})_1$.

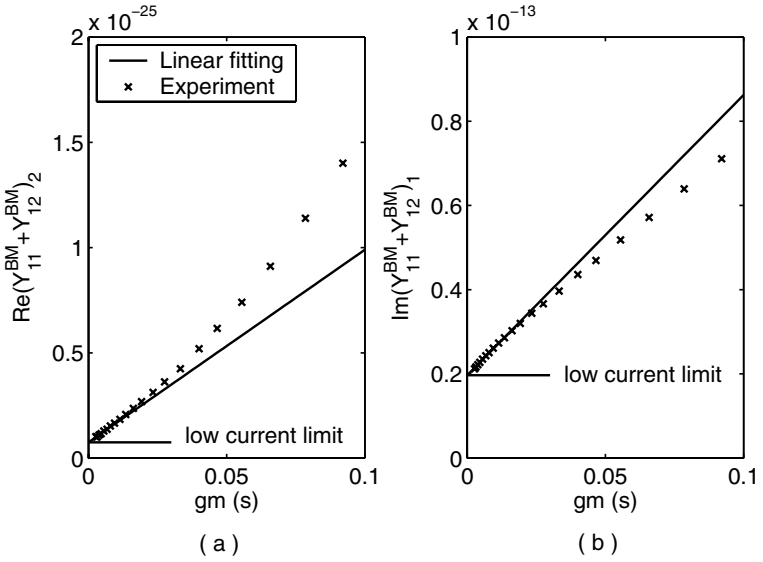


Figure 3.9: Illustration of low current limit extraction for (a) $\Re(Y_{11}^{BM} + Y_{12}^{BM})_2$, and (b) $\Im(Y_{11}^{BM} + Y_{12}^{BM})_1$.

So far we have extracted all the extrinsic parameters and intrinsic parameter $r_{bi}$. The Y-parameters of block $B_{IR}$ can be obtained as

$$\begin{aligned} Y_{11}^{BIR} &= \frac{Y_{11}^{BM}}{1 - r_{bx}Y_{11}^{BM}} - j\omega(C_{bex} + C_{bcx}), \quad Y_{12}^{BIR} = \frac{Y_{12}^{BM}}{1 - r_{bx}Y_{11}^{BM}} + j\omega C_{bcx}, \\ Y_{21}^{BIR} &= \frac{Y_{21}^{BM}}{1 - r_{bx}Y_{11}^{BM}} + j\omega C_{bcx}, \quad Y_{22}^{BIR} = \frac{Y_{12}^{BM} - r_{bx}(Y_{11}^{BM}Y_{22}^{BM} - Y_{12}^{BM}Y_{21}^{BM})}{1 - r_{bx}Y_{11}^{BM}} - j\omega C_{bcx}, \end{aligned} \tag{3.19}$$

which can be transformed into Z-parameters. The Z-parameters of the intrinsic transistor, block $B_I$, are

$$Z_{11}^{BI} = Z_{11}^{BIR} - r_{bi}, \quad Z_{12}^{BI} = Z_{12}^{BIR}, \quad Z_{21}^{BI} = Z_{21}^{BIR}, \quad Z_{22}^{BI} = Z_{22}^{BIR}. \tag{3.20}$$

Consequently, the Y-parameters of block $B_I$ are now known.

### 3.3.5 $C_{bed}$, $r_d$, $g_{be}$ and $\tau_d$ extraction

The Y-parameter Taylor expansion coefficients of block $B_I$ are obtained as

$$\Im(Y_{11}^{BI} + Y_{12}^{BI})_1 = C_{bet}, \quad \Im(Y_{21}^{BI} - Y_{12}^{BI})_1 = g_m\tau_d, \tag{3.21}$$

$$\Re(Y_{11}^{BI})_0 = g_{be}, \qquad \Re(Y_{11}^{BI})_2 = C_{bed}\tau_{in}. \tag{3.22}$$

These expressions are accurate for all biases because the factor $(r_{bx} + r_{bi})g_{be}$ does not exist any more.

$C_{bet}$ is given by $\Im(Y_{11}^{BI} + Y_{12}^{BI})_1$. Strictly speaking, $C_{bed}$ can be directly calculated from $C_{bet} - C_{bej}$ as $C_{bej}$ is known. This is, however, not accurate for low biases where $C_{bed} < C_{bej}$. For these biases, we make a linear fitting for $C_{bet}$ versus $g_m$. The slope gives low bias $\tau_{tr}$. $C_{bed}$ is evaluated by $g_m\tau_{tr}$. $C_{bej}$ is then updated as $C_{bet} - C_{bed}$. Fig. 3.10 (a) illustrates the splitting

procedure for low bias. Clearly $\tau_{tr}$, indicated by the curve slope, increases for the biases after $f_T$ roll off due to Kirk effect. Fig. 3.10 (b) shows the extracted $C_{bed}$ and $C_{bej}$.

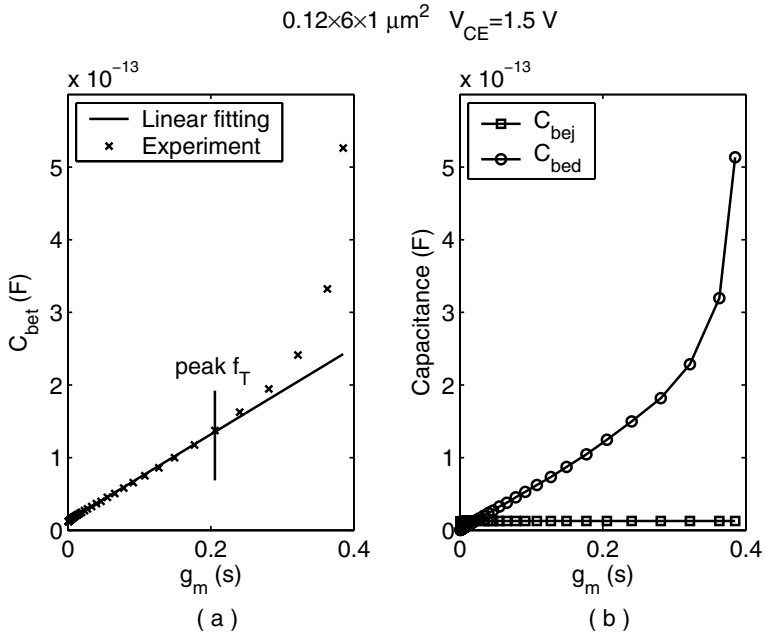


Figure 3.10: Illustration of $C_{bet}$ splitting: (a) Linear fitting for $C_{bet}$ versus $g_m$; (b) Extracted $C_{bed}$ and $C_{bej}$ versus $g_m$.

With $C_{bet}$ split, $\tau_{in}$ can be calculated from $\Re(Y_{11}^{BI})_2/C_{bed}$. $r_d$ is then obtained from $\tau_{in}/C_{bed}$. Fig. 3.11 shows the extracted $r_d$ versus $1/I_C$. The resulting curve is linear at low biases where $\tau_{in}$ is a constant.

The MATLAB program of small signal parameter extraction for the above illustration device is not attached in this dissertation, instead, the similar program for a 50 GHz SiGe HBT is given in Appendix E, since the data of the same device is used to illustrate noise de-embedding in Chapter 4.

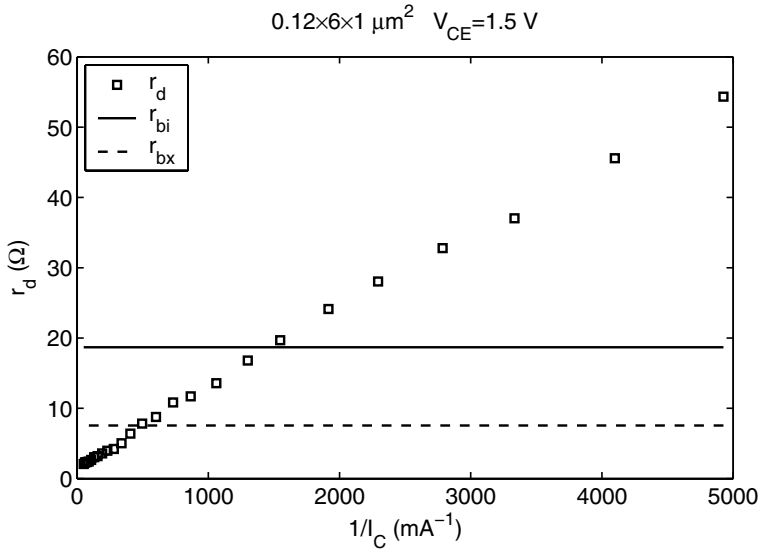


Figure 3.11: Extracted $r_d$ versus $1/I_C$. $r_{bx}$ and $r_{bi}$ are shown for reference.

## 3.4 Results and discussions

### 3.4.1 Extraction and modeling results

Table 4.1 summarizes the extracted small signal parameters for the $A_E = 0.12 \times 6 \times 1$ $\mu$m$^2$ SiGe HBTs at three $V_{BE}$, representing low, medium and high biases, respectively. Fig. 3.12 shows the Y-parameters for both experimental data and simulation results at $V_{BE}$=0.921 V. Excellent fitting has been obtained up to 50 GHz.

### 3.4.2 Discussions

Fig. 3.13 shows the frequency dependence of intrinsic $\Re(Y_{11}^{BI})$ at three biases for both extracted and modeling results. $\Re(Y_{11}^{BI})$ increases versus frequency. Such frequency dependence cannot be modeled for an equivalent circuit without including input NQS effect.

Table 3.1: Extracted small signal parameter values of $A_E = 0.12 \times 6 \times 1\ \mu m^2$ SiGe HBT

| | | | |
|---|---|---|---|
| $V_{CE}$ (V) | 1.5 | 1.5 | 1.5 |
| $V_{BE}$ (V) | 0.828 | 0.867 | 0.921 |
| $I_C$ (mA) | 0.44 | 1.7 | 7.7 |
| $I_B$ ($\mu$A) | 0.0 | 4.0 | 46 |
| $f_T$ (GHz) | 60.1 | 127 | 183 |
| $r_{bx}(\Omega)$ | 7.56 | 7.56 | 7.56 |
| $r_{bi}(\Omega)$ | 18.7 | 18.7 | 18.7 |
| $r_e(\Omega)$ | 4.0 | 4.0 | 4.0 |
| $r_c(\Omega)$ | 7.2 | 7.2 | 7.2 |
| $r_d$ ($\Omega$) | 28.0 | 8.76 | 3.04 |
| $r_{cs}$(k$\Omega$) | 1.8 | 1.8 | 1.8 |
| $g_{be}$(mS) | 0.0572 | 0.257 | 1.81 |
| $g_m$(S) | 0.0163 | 0.0554 | 0.206 |
| $\tau_d$(ps) | 0.43 | 0.40 | 0.56 |
| $C_{bed}$(fF) | 9.946 | 32.61 | 124.6 |
| $C_{bej}$(fF) | 12.74 | 12.74 | 12.74 |
| $C_{bex}$(fF) | 7.585 | 7.585 | 7.585 |
| $C_{bcx}$(fF) | 7.614 | 7.646 | 7.848 |
| $C_{bci}$(fF) | 1.877 | 1.855 | 1.912 |
| $C_{cs}$(fF) | 2.380 | 2.380 | 2.380 |

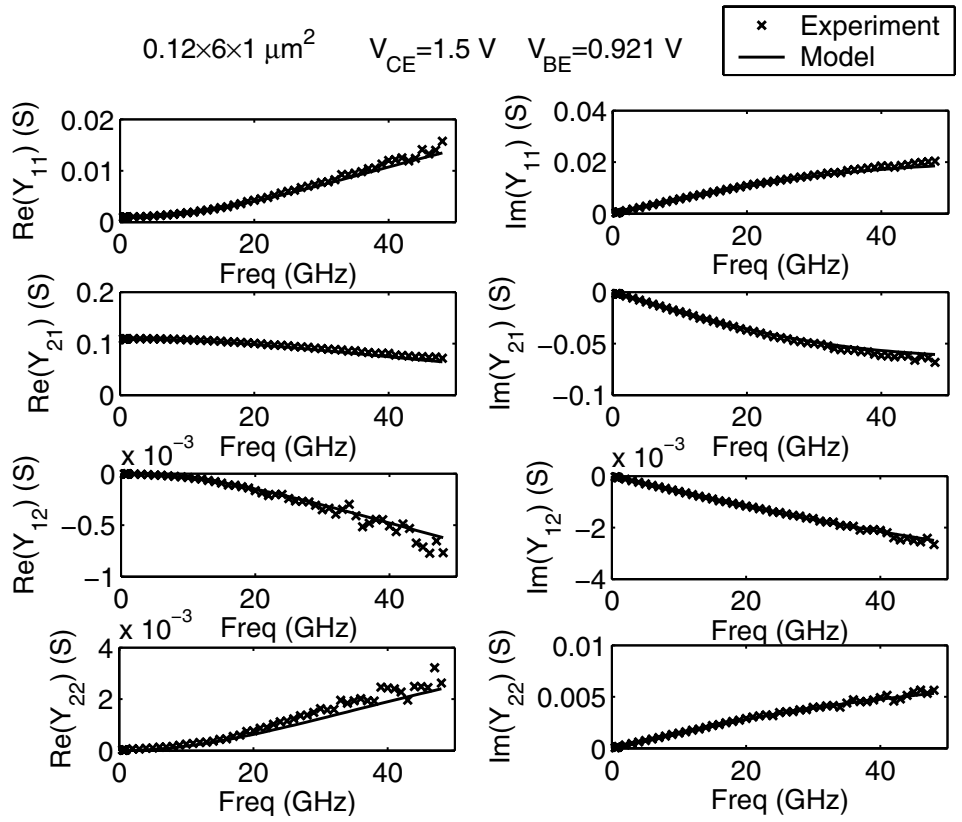


Figure 3.12: Comparison of Y-parameters for experimental data and modeling results at high bias.

The frequency dependence of $\Re(Y_{11}^{BI})$ is important for noise modeling [2, 39]. Fig. 3.14 compares the power spectrum density of intrinsic base current noise $S_{ib}$ obtained from noise de-embedding of experimental noise data and the $S_{ib}$ from van Vliet model $S_{ib} = 4kT\Re(Y_{11}^{BI}) - 2qI_B$, for a 50 GHz $A_E = 0.24 \times 20 \times 2\ \mu\text{m}^2$ SiGe HBT at three biases. $r_{bi}$ of this device is 2.03 Ω, while the thermal base resistance, $r_{bn}$ is set to be 3.0 Ω for the reasons discussed in [6] and Chapter 5. Clearly $S_{ib}$ is frequency dependent and can be modeled by the frequency dependent $\Re(Y_{11}^{BI})$. We choose a 50 GHz device for illustration because CB SCR has significant impact on 180 GHz device noise, consequently $S_{ib}$ cannot be simply modeled with $4kT\Re(Y_{11}^{BI}) - 2qI_B$ ( [5], also Chapter 5).

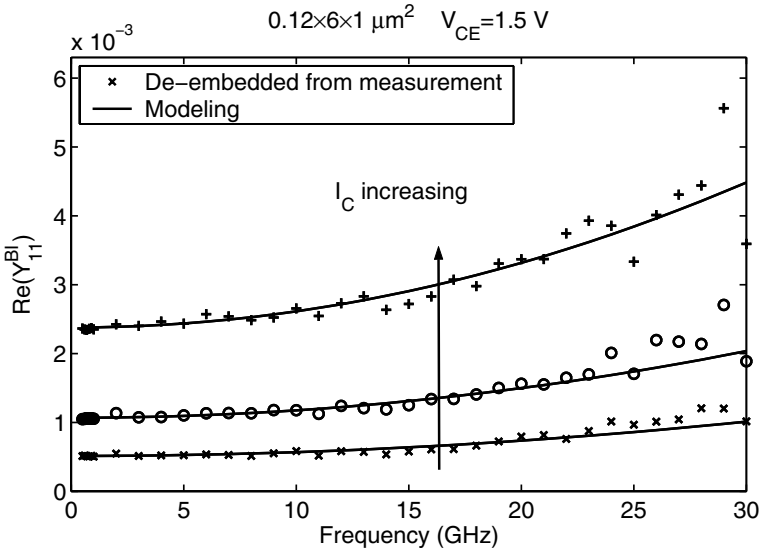


Figure 3.13: Intrinsic $\Re(Y_{11}^{BI})$ extraction and modeling results for three biases.

Fig. 3.15 shows the extracted intrinsic base resistances using equivalent circuit with and without including input NQS effect. $r_{bi,QS}$ is extracted from the Y-parameters of block $B_{IR}$ using circle fitting method [62], which assumes an equivalent circuit *without* including input NQS effect. For the $r_{bi,QS}$ of circle symbol, the Y-parameters of $B_{IR}$ are obtained from experimental data by de-embedding. For the $r_{bi,QS}$ of solid line, the Y-parameters of $B_{IR}$ are calculated using the extracted NQS small signal parameters within $B_{IR}$. $r_{bi,QS}$ shows a bell-shaped bias dependence that is typical of extraction using an equivalent circuit without input NQS effect. Using a bias-independent $r_{bi}$ (the square symbols), the equivalent circuit including input NQS effect can well reproduce the bias dependence of $r_{bi,QS}$ as shown by the good fitting of solid line to circle symbols. The bias dependence of $r_{bi,QS}$ can be explained by the lumping effect of $r_{bi}$ and $r_d$, which can be

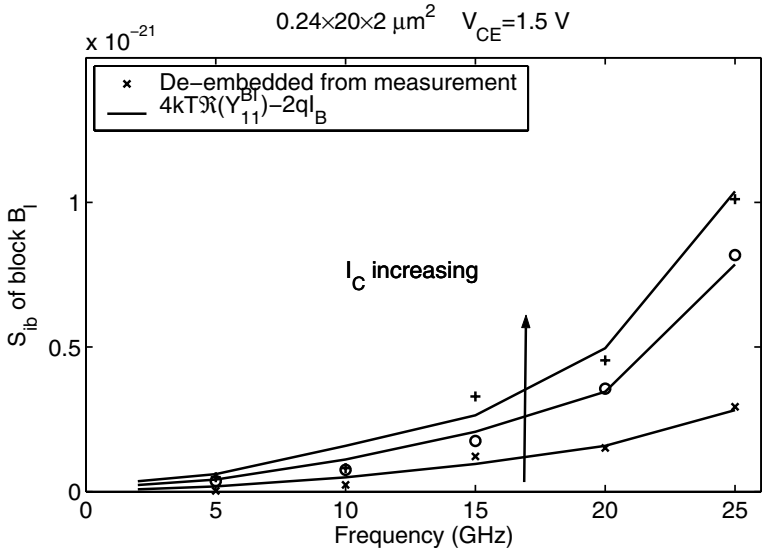


Figure 3.14: Comparison of $S_{ib}$ obtained from noise de-embedding of experimental noise data and van Vliet model $S_{ib} = 4kT\Re(Y_{11}^{BI}) - 2qI_B$ for a 50 GHz $A_E = 0.24 \times 20 \times 2$ $\mu$m$^2$ SiGe HBT at three biases.

approximately described by [4]

$$r_{bi,QS} \approx r_{bi} + r_d C_{bed} \frac{C_{bed}}{\left(C_{bed} + C_{bej}\right)^2}. \tag{3.23}$$

At low biases $r_d C_{bed} = \tau_{in}$ is a constant [37]. Since $C_{bed}$ increases versus bias and $C_{bej}$ is nearly constant, the ratio $C_{bed}/(C_{bed}+C_{bej})^2$ has a maximum value at $C_{bed} = C_{bej}$. This means that $r_{bi,QS}$ should increase at low biases and drop at high biases. $r_{bi,QS}$ is clearly larger than $r_{bi}$. The star symbols in Fig. 3.15 show the extracted $r_{bi,QS}$ from experimental data with $C_{bex}$=0. The strong bias dependence of the extraction results suggests the necessity of including $C_{bex}$ in even equivalent circuits without input NQS effect.

Fig. 3.16 shows the extracted delay times. The square represents the effective base transit time $\tau_{tr}$. The down-triangle represents $\tau_{in}$ and the up-triangle represents $\tau_d$. The circle represents $\tau_d$ extracted using equivalent circuit without including input NQS effect. $\tau_{tr}$ is the maximum one as

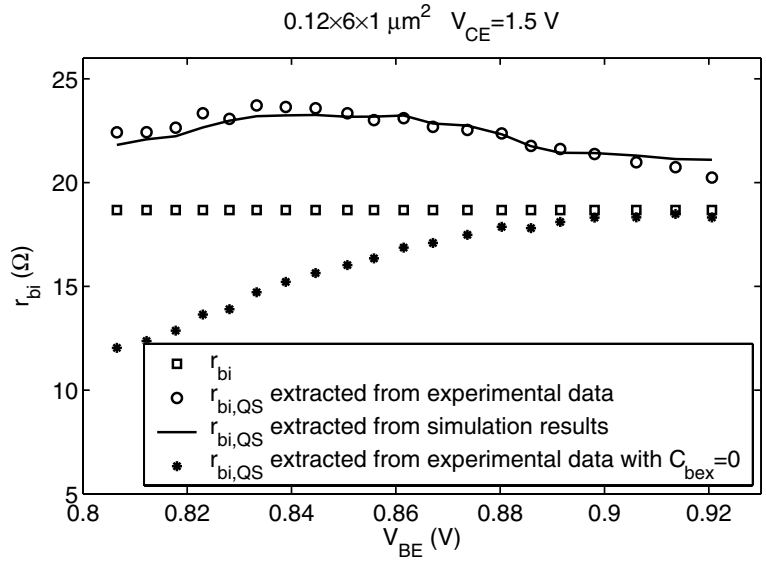


Figure 3.15: Comparison of $r_{bi}$ extracted using equivalent circuit with and without including input NQS effect.

expected by theory in (3.3). It is shown that $\tau_{tr}$, $\tau_{in}$ and $\tau_d$ are bias independent at low to medium biases and increase dramatically for biases after $f_T$ roll off due to base push out. However, $\tau_{d,QS}$ is strongly bias dependent and non-monotonic for all biases due to the unphysical bias dependence of $r_{bi,QS}$. This further demonstrates that the extracted parameters for the equivalent circuit with input NQS effect are more physical.

### 3.5 Extraction of bias dependent $r_{bi}$

In the above sections, we have assumed the bias independence condition for $r_{bi}$. Such condition is not valid for transistors with lower base doping, e.g. 50 GHz SiGe HBTs. The $r_{bi}$ extracted using the above method, denoted as $\overline{r_{bi}}$, is the approximated $r_{bi}$ value of high bias. That is, we treat $\overline{r_{bi}}$ as initial guess of $r_{bi}$, which is used to extract $r_{bx}$ and $C_{bex}$. To obtain bias dependent $r_{bi}$ for full bias range, we start from known block $B_{IR}$. Equivalently speaking, all the parameters outside of

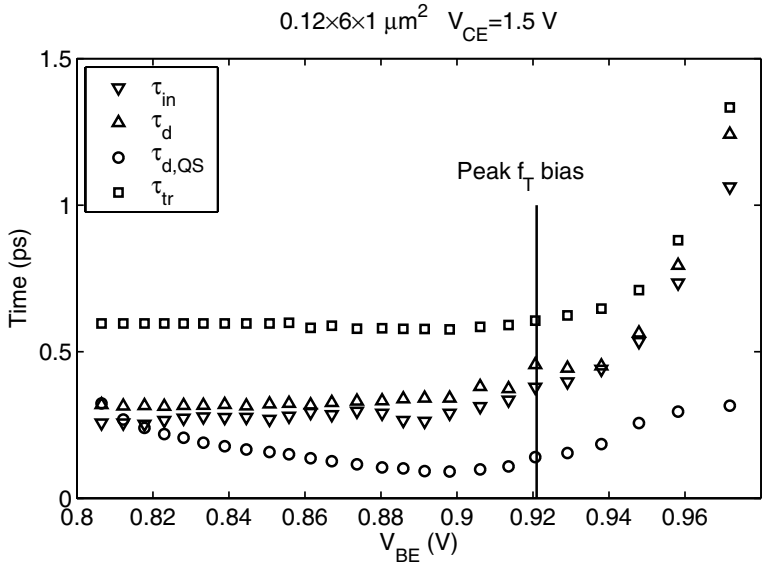


Figure 3.16: Extracted delay times and modeling results for three biases.

block $B_{IR}$ are obtained using the above extraction method. We have

$$\Im\left[\frac{Y_{11}^{BIR}+Y_{12}^{BIR}}{Y_{21}^{BIR}-Y_{12}^{BIR}}\right]_1 = \frac{C_{bed}+C_{bej}}{g_m}, \tag{3.24}$$

$$\Re\left[\frac{Y_{11}^{BIR}+Y_{12}^{BIR}}{Y_{21}^{BIR}-Y_{12}^{BIR}}\right]_2 = \frac{\tau_d C_{bej}+(\tau_d-\tau_{in})C_{bed}}{g_m}. \tag{3.25}$$

The total EB capacitance can be extracted using (3.24). $C_{bed}$ and $C_{bej}$ can be obtained using the splitting method in Section 3.3.5. Then $\tau_{tr} = C_{bed}/g_m$ for all biases.

**Extraction of NQS delay time $\tau_{in}$ and $\tau_d$**

We first extract the $\tau_{in}$, $\tau_d$ values at low to medium biases, where they are constants. We plot $g_m\Re\left[\frac{Y_{11}^{BIR}+Y_{12}^{BIR}}{Y_{21}^{BIR}-Y_{12}^{BIR}}\right]_2$ versus $C_{bed}$, the curve should be linear at low to medium biases, as shown in Fig. 3.17 for a 50 GHz SiGe HBT. The y-axis intercept gives $\tau_d C_{bej}$ and the slope gives $\tau_d - \tau_{in}$. Consequently both $\tau_{in}$ and $\tau_d$ values at low to medium biases are obtained. Now we assume that the ratios $\tau_{in}/\tau_{tr}$ and $\tau_{in}/\tau_{tr}$ are bias independent and can be obtained low bias values of $\tau_{in}$, $\tau_d$ and

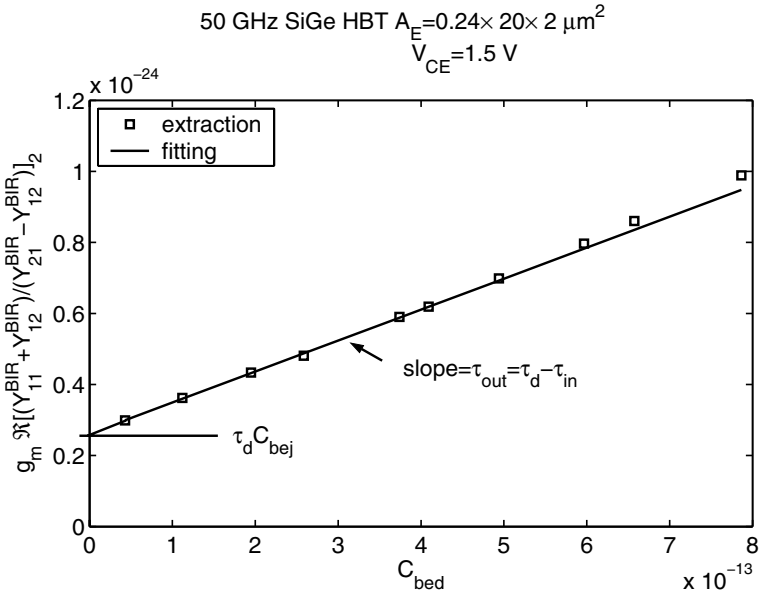


Figure 3.17: NQS delay time ($\tau_{in}$ and $\tau_d$ or $\tau_{out}$) extraction.

$\tau_{tr}$. The $\tau_{in}$, $\tau_d$ values of full bias range are determined by

$$\tau_{in} = \tau_{tr}\left(\frac{\tau_{in}}{\tau_{tr}}\right)_{low}, \quad \tau_d = \tau_{tr}\left(\frac{\tau_d}{\tau_{tr}}\right)_{low}. \tag{3.26}$$

**Extraction of bias dependent $r_{bi}$**

So far, the only unknown parameter for the intrinsic device without $r_{bi}$, or block $\boldsymbol{B_I}$, is $g_{be}$. Note that

$$\Re(Y_{11}^{BI})_0 = \frac{g_{be}}{1 + g_{be}r_{bi}}. \tag{3.27}$$

(3.27) does not give $g_{be}$ since $r_{bi}$ is unknown yet. Here we use the bias independent $r_{bi}$ value extracted in Section 3.3.3, i.e. $\overline{r_{bi}}$. $g_{be}$ then can be calculated as

$$g_{be} = \frac{\Re(Y_{11}^{BI})_0}{1 - \Re(Y_{11}^{BI})_0 \overline{r_{bi}}}. \tag{3.28}$$

Another simple but approximated way to obtain $g_{be}$ is to use $I_b/V_T$. Now the Y-parameters of block $B_I$ is totally known. $r_{bi}$ can be extracted from the $Y_{11}$ difference between block $B_I$ and $B_{IR}$, that is

$$r_{bi} = \frac{1}{Y_{11}^{BIR}} - \frac{1}{Y_{11}^{BI}} = \frac{1}{Y_{11}^{BIR}} - \frac{1}{g_{be} + j\omega \left( C_{bci} + C_{bej} + \frac{C_{bed}}{1+j\omega\tau_{in}} \right)}. \tag{3.29}$$

Fig. 3.18 shows the extracted bias dependent $r_{bi}$ compared with $\overline{r_{bi}}$ for (a) 50 GHz SiGe HBT and (b) 180 GHz SiGe HBTs. Since the $r_{bi}$ is significantly bias dependent for the 50 GHz SiGe HBT, the $\overline{r_{bi}}$ has noticeable error as shown in Fig. 3.18 (a). However, for the 180 GHz SiGe HBT, $r_{bi}$ is indeed weakly bias dependent. Consequently, the bias independent $r_{bi}$ extraction method gives accurate value.

### 3.6 Summary

In this chapter, we have examined small signal equivalent circuit modeling of input NQS effect including CB SCR delay. The input NQS effect is found to be more pronounced in scaled SiGe HBTs with higher built-in field, despite reduced total transit time and reduced absolute value of the input NQS delay time. A new direct parameter extraction method based on Taylor expansion of analytical Y/Z-parameter expressions has been developed and demonstrated for such circuit. The extracted parameters, such as intrinsic base resistance and excess phase delay time, are more physical than using conventional equivalent circuit without including input NQS effect. The frequency

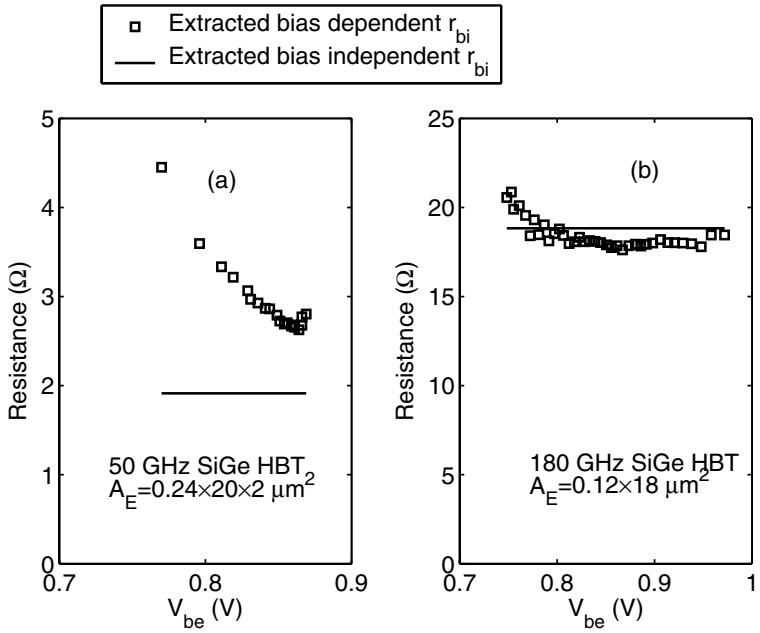


Figure 3.18: Bias dependent $r_{bi}$ compared with $\overline{r_{bi}}$ for (a) 50 GHz SiGe HBT and (b) 180 GHz SiGe HBTs.

dependence of the real part of intrinsic $Y_{11}$ is modeled and describes well the intrinsic base current noise de-embedded from experimental data. The extraction method has been verified for SiGe HBTs from different generations of technology.

# CHAPTER 4

## SEMI-EMPIRICAL NOISE MODEL BASED ON EXTRACTION

Present noise modeling approaches in current compact bipolar models uses uncorrelated $2qI$ shot noises for base and collector currents, and uses $4kT$ thermal noise for intrinsic base resistance based on QS input equivalent circuit [1]. As discussed in Chapter 2, such scenario is not accurate enough, particularly at the increasingly higher frequencies for robust circuit simulation, and must be refined to enable predictive low-noise RF circuit design. The straightforward and physical way to noise modeling is to propose better model for $S_{i_{rbi}}$ and correlated base and collector current noises using NQS equivalent circuit as done in Chapter 5.

This chapter, however, presents modeling of correlated RF noise in the intrinsic base and collector currents of SiGe HBTs, still using QS equivalent circuits. The purpose is to develop an improved noise model within the frame work of existing CAD tools. We use the improved $S_{i_{rbi}}$ model of (2.77), and then extract intrinsic noise $S_{ib}$, $S_{icib^*}$ and $S_{ic}$ from device noise parameters using standard noise de-embedding method [54]. We then develop semi-empirical equations to model these noise sources. The number of model parameters is the same as the previous noise modeling method, as we need in general four numbers to describe a noise correlation matrix. However, the $S_{ib}$ and $S_{ic}$ obtained are in general positive, which is an improvement over the previous method. The deviation caused by the use of a QS input equivalent circuit, and hence the lumping of input NQS resistance into $r_{bi}$, as well as the use of the improved $S_{i_{rbi}}$ model, is lumped into the intrinsic noise. The extracted $S_{ib}$ and $S_{ic}$ are thus not exactly the physical intrinsic transistor noises, which can only be obtained through higher order modeling that includes input NQS and noise crowding effects. The noise sources and their correlation, are first modeled as functions of

frequency ($\omega$). The coefficients are then extracted and modeled as a function of biasing current through $g_m$, as detailed below. The model is shown to work at frequencies up to at least half of the peak $f_T$, and at biasing currents below high injection $f_T$ roll off for devices with different emitter geometries.

In the following, we present the intrinsic noise de-embedding technique, the semi-empirical intrinsic noise model, geometry scaling ability, and model implementation in CAD tools.

## 4.1 Intrinsic noise extraction

### 4.1.1 Two basic noise de-embedding techniques

In Chapter 1, we introduced four two-port noise representations. For the case of SiGe HBT, only impedance (Z-) and admittance (Y-) representations are needed for noise de-embedding as shown below.

- Series block de-embedding

  In Fig. 4.1, block $N$ is in series with block A, B and C. Denote the final block as $N'$. The noise voltage of block A, B and C can be calculate by $4kT$ multiplied with the real part of Z-parameter of each block. If the noises of both $N$ and $N'$ are in Z-representation, the noise of inner block noise $S_N^Z$ can be calculated from total block noise by

$$S_N^Z = S_{N'}^Z - 4kT \begin{bmatrix} \Re(Z_A + Z_C) & \Re(Z_C) \\ \Re(Z_C) & \Re(Z_B + Z_C) \end{bmatrix}, \tag{4.1}$$

  where $Z_A$, $Z_B$ and $Z_C$ denote the impedances of block A, B and C respectively.

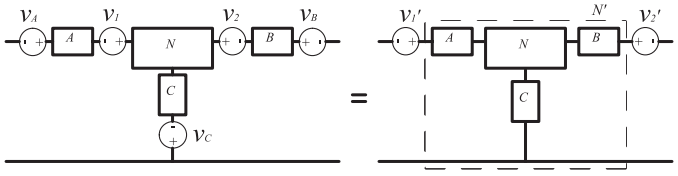


Figure 4.1: Series block de-embedding using impedance representation.

It is worth to note the Z-parameter de-embedding here:

$$Z_N = Z_{N'} - \begin{bmatrix} Z_A + Z_C & Z_C \\ Z_C & Z_B + Z_C \end{bmatrix}. \tag{4.2}$$

- Parallel block de-embedding

  In Fig. 4.2, block $N$ is paralleled with Block A, B and C. The final block is denoted as $N'$. The noise current of block A, B and C can be calculate by $4kT$ multiplied with the real part of Y-parameter of each block. If the noises of both $N$ and $N'$ are in Y-representation, the noise of inner block noise $S_N^Y$ can be calculated from total block noise by

$$S_N^Y = S_{N'}^Y - 4kT \begin{bmatrix} \Re(Y_A + Y_C) & -\Re(Y_C) \\ -\Re(Y_C) & \Re(Y_B + Y_C) \end{bmatrix}, \tag{4.3}$$

  where $Y_A$, $Y_B$ and $Y_C$ denote the admittances of block A, B and C respectively.

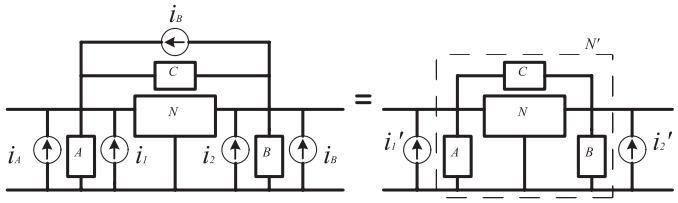


Figure 4.2: Parallel block de-embedding using admittance representation.

It is also worth to note the Y-parameter de-embedding for parallel configuration:

$$Y_N = Y_{N'} - \begin{bmatrix} Y_A + Y_C & -Y_C \\ -Y_C & Y_B + Y_C \end{bmatrix}. \tag{4.4}$$

### 4.1.2 SiGe HBT noise calculation

Fig. 4.3 shows the complete QS small signal equivalent circuit used in noise de-embedding. In our calculation, $C_{bc,p}$ is set to be zero. For the sake of convenience, we define six blocks (B1-B6) as shown in Fig. 4.3:

- B6: just the device under test.
- B5: exclude $L_B$, $L_C$, $L_E$ and $r_{cx}$ from B6.
- B4: exclude $C_{bc,p}$, $C_{cs}$ and $r_{cs}$ from B5.
- B3: exclude $r_{bx}$, $r_{ci}$ and $r_e$ from B4.
- B2: exclude $C_{be,x}$ and $C_{bc,x}$ from B3.
- B1: exclude $r_{bi}$ from B2. It is designated as the "intrinsic" transistor, which stands for the ideal 1-D transistor without intrinsic base resistance.

Based on these definitions, the noise de-embedding procedure is described below. Note that the noise calculation for whole transistor is exactly the inverse of noise de-embedding.

- STEP 1: Calculate the noise matrix of B6 in Z-representation from DUT noise parameters. De-embed $L_B$, $L_C$, $L_E$ and $r_{cx}$, which leads to the Z-representation noise matrix of B5.
- STEP 2: Transform Z-representation into Y-representation for B5. De-embed $C_{bc,p}$, $C_{cs}$, and $r_{cs}$. The Y-representation noise matrix of B4 is obtained.

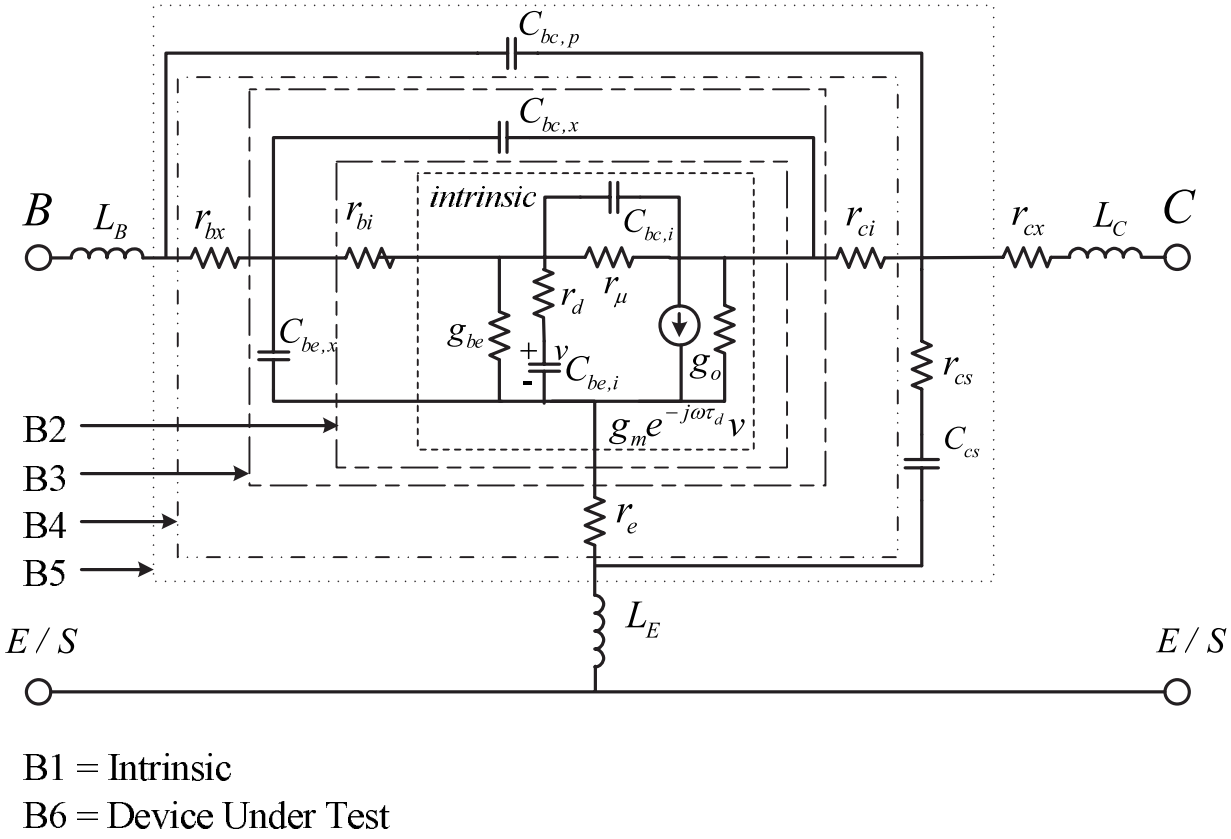


Figure 4.3: Small signal equivalent circuit of SiGe HBT used for Y-parameter and noise parameters de-embedding.

- STEP 3: Transform Y-representation into Z-representation for B4. De-embed $r_{bx}$, $r_{ci}$, and $r_e$. This gives Z-representation noise matrix of B3.

- STEP 4: Transform the Z-representation into Y-representation for B3. De-embed $C_{be,x}$ and $C_{bc,x}$ leading to the Y-representation noise matrix of B2.

- STEP 5: Transform Y-representation into Z-representation for B2. De-embed $r_{bi}$. As a consequence, the Z-representation noise matrix of intrinsic transistor is obtained. For convenience in intrinsic noise modeling, the Z-representation is transformed into Y-representation.

The MATLAB program for Y-parameter and noise de-embedding is shown in Appendix F.

### 4.1.3 Extracted intrinsic noise

S-parameters and noise parameters are measured for SiGe HBTs of different emitter geometries from a 50 GHz peak $f_T$ process, including $A_E = 0.24 \times 20 \times 2\mu m^2$, $A_E = 0.24 \times 20 \times 1\mu m^2$, $A_E = 0.24 \times 10 \times 2\mu m^2$ and $A_E = 0.48 \times 10 \times 1\mu m^2$. The data of $A_E = 0.24 \times 20 \times 2\mu m^2$ device is shown in Appendix F. These geometries allow us to investigate emitter length, width and finger number scaling. Unless specified, the experimental data of the $A_E = 0.24 \times 20 \times 2\mu m^2$ device is used below for illustration of model derivation. Noise simulation data for a $0.5 \times 1 \times 1\mu m^2$ SiGe HBT with 30 GHz peak $f_T$ is also used for extraction to provide guidance to model equation development. The SiGe HBT structure used in simulation does not correspond to the measured HBTs.

The S-parameters are measured on-chip using a 8510C Vector Network Analyzer (VNA) from 2-26 GHz. The noise parameters are measured using an ATN NP5 system from 2-25 GHz. Both S-parameters and noise parameters are de-embedded with the standard OPEN structure. The measurement is made across a wide biasing current range up to the peak $f_T$ point. The noise simulation is performed using DESSIS [67].

For a given bias, we first determine the equivalent circuit parameters from measured S-parameters using the direct extraction method in Chapter 3. Note that $r_{bi}$ is extracted using the input impedance circle fitting method with the Y-parameters of the equivalent circuit that consists of $r_{bi}$ and block B1 in Fig. 4.3. The same $r_{bi}$ is used for all noise models. Excellent fitting of measured S-parameters is achieved across a wide biasing current range for all of the frequencies measured. The extracted biasing dependence of equivalent circuit parameters is consistent with device physics based expectations. Table 4.1 gives the equivalent circuit parameter extraction results. Three biases representing low, medium and high biasing currents are shown. The extracted $\tau_d$ value is not strictly monotonous, but the variation is small. The extraction of $\tau_d$ at low biases is difficult because of the small values of the intrinsic $\Im(Y_{21})$. $C_{cs}$ is bias independent as $V_{CE}$ is fixed

Table 4.1: Extracted small signal parameter values of $0.24 \times 20 \times 2\mu m^2$ SiGe HBT

| | $V_{CE}$=1.5V<br>$I_C$=4.9mA<br>$I_B$=28$\mu$A | $V_{CE}$=1.5V<br>$I_C$=9.7mA<br>$I_B$=66$\mu$A | $V_{CE}$=1.5V<br>$I_C$=17.9mA<br>$I_B$=124$\mu$A |
|---|---|---|---|
| $r_{bx}(\Omega)$ | 2.70 | 2.70 | 2.70 |
| $r_{bi}(\Omega)$ | 3.20 | 2.89 | 2.66 |
| $r_e(\Omega)$ | 0.63 | 0.63 | 0.63 |
| $r_c(\Omega)$ | 10.1 | 10.1 | 10.1 |
| $r_u(\mathrm{K}\Omega)$ | 3150 | 421 | 139 |
| $g_{be}(\mathrm{S})$ | 0.0011 | 0.0025 | 0.0048 |
| $g_m(\mathrm{S})$ | 0.1730 | 0.3649 | 0.6338 |
| $\tau_d(\mathrm{ps})$ | 1.010 | 0.9450 | 0.9465 |
| $C_{be,i}(\mathrm{pF})$ | 0.5977 | 0.8854 | 1.5424 |
| $C_{bc,x}(\mathrm{fF})$ | 31.000 | 31.000 | 31.000 |
| $C_{bc,i}(\mathrm{fF})$ | 12.338 | 12.633 | 14.604 |
| $C_{CS}(\mathrm{fF})$ | 16.000 | 16.000 | 16.000 |
| $L_B(\mathrm{pH})$ | 48.0 | 48.0 | 48.0 |
| $L_C(\mathrm{pH})$ | 48.0 | 48.0 | 48.0 |
| $L_E(\mathrm{pH})$ | 11.2 | 11.2 | 11.2 |

in the measurement, leading to a fixed collector-to-substrate junction bias. $r_u$ decreases with bias since the neutral base recombination current modulation by $V_{CB}$ is a strong function of $I_C$ [68]. At frequencies above 1 GHz, the effect of $r_u$ is not significant for either Y-parameters or RF noise.

Using Table 4.1, we find that the $2qI_B/3$ to $4kT/r_{bi}$ ratio is 0.25% at peak $f_T$ point and less at lower biases. The $2qI_B/3$ term in improved $S_{i,rbi}$ model is thus negligible for SiGe HBTs because of the heavily doped base and hence a small $r_{bi}$, as well as a high $\beta$ and hence a low $I_B$.

Next, the noise correlation matrix for the whole transistor, including all of the parasitics, is calculated from measured $NF_{min}$, $Y_{opt}$ and $R_n$ as described in Chapter 1. The noise correlation matrix for the intrinsic transistor is then determined using noise de-embedding technique. After de-embedding $r_{bi}$, the PSDs of $i_b$, $i_c$ and $i_c i_b^*$ are obtained from the Y-representation noise correlation matrix of the intrinsic transistor. Fig. 4.4 shows the extracted intrinsic noise sources together with different noise model fits at $I_C$=17.9 mA. The data marked with circle are the extraction results. The dash line represents the SPICE model, the dot line represents the van Vliet model and the

dash-dot line represents the transport model. The solid line, representing the new model, will be discussed in detail in Section III. Note that the results of van Vliet model are shown only for reference as we use QS equivalent circuit. A few important observations can be made from Fig. 4.4:

- The extracted $S_{ib}$ has a strong frequency dependence and is much larger than $2qI_B$ at high frequencies. The van Vliet model $S_{ib}$ is $2qI_B$, the same as the SPICE model, as the input NQS effect is not explicitly modeled. The transport noise model $S_{ib}$ is fitted to the extraction result with parameter $\tau_n$ and overlaps with the new model. Note that $\tau_n$ is bias dependent and equals 3.5 ps at $I_C$=17.9 mA.

- For $S_{ic}$, all models except for the new model give $2qI_C$, and hence overlap with each other. Note that the extracted $S_{ic}$ is larger than $2qI_C$. The excess $S_{ic}$ is not due to avalanche multiplication due to the low $V_{CE}$. $S_{ib}$ would have also been affected if it was due to avalanche multiplication. The higher than $2qI_C$ value of $S_{ic}$ can be attributed to an simplified base hole model for $S_{irbi}$.

- The extraction shows a strongly frequency dependent correlation $S_{icib^*}$, which is assumed to be zero in the SPICE model. The van Vliet model $S_{icib^*}$ shows a frequency dependence due to the excess phase $\tau_d$, but the value is underestimated. The transport model $S_{icib^*}$ improves the frequency dependence a lot. However, its $\Im(S_{icib^*})$ is not well modeled, as $\tau_n$ is used to fit $S_{ib}$ only. It is also shown that with only one $\tau_n$, simultaneous fitting of $\Re(S_{icib^*})$ and $\Im(S_{icib^*})$ is difficult.

Fig. 4.4 shows that the extracted intrinsic noise and cannot be well described by all the old models. Clearly the new semi-empirical noise model gives the best intrinsic noise. The development of the new model is detailed below.

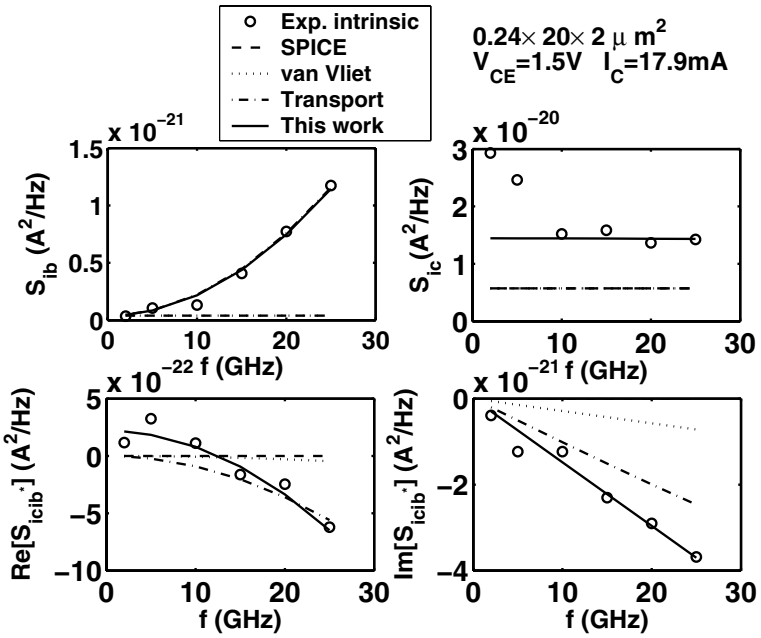


Figure 4.4: Extracted intrinsic noise sources as a function of frequency.

## 4.2 Semi-empirical intrinsic noise model

Based on the noise source extraction results, we now develop a new noise compact model that is aimed at circuit noise simulation, which requires accurate modeling over both bias and frequency. We will also compare the expressions of the proposed model with other popular models.

### 4.2.1 $S_{ib}$

An inspection of the extracted $S_{ib}$ in Fig. 4.4 shows that $S_{ib}$ increases with frequency. At low frequencies, $S_{ib}$=$2qI_B$, the conventional shot noise. At a given bias, we found that $S_{ib}$ can be expressed as the sum of a shot noise component $2qI_B$ and a frequency dependent component as:

$$S_{ib} = 2qI_B + C_{ib}\omega^2, \tag{4.5}$$

where $C_{ib}$ is a coefficient that varies with bias. At low frequencies, (4.5) reduces into $2qI_B$. In Fig. 4.5 (a), the excess base current noise, defined as $S_{ib} - 2qI_B$, is plotted as a function of $\omega^2$ for two representative biases. The excess base current noise increases with $\omega^2$ in a linear fashion. The data shows that (4.5) works well for all frequencies and biases measured. The $2qI_B$ term is a direct result of emitter hole velocity fluctuation. The $C_{ib}\omega^2$ term is, mainly, a result of base electron velocity and hence current density fluctuations, which induce diffusive capacitive charging, leading to the $\omega^2$ dependence. This is similar to the $\omega^2$ dependence of the induced gate noise in FETs caused by capacitive coupling between gate and channel. The functional form of the new $S_{ib}$ expression can be linked to the $S_{ib}$ expression of the transport noise model, particularly regarding the $\omega^2$ dependence:

$$\begin{aligned} S_{ib}^{Tran} &= 2qI_B + 4qI_C[1 - \Re(e^{j\omega\tau_n})] \\ &= 2qI_B + 4qI_C[1 - 1 + \frac{\tau_n^2\omega^2}{2} + o(\omega^2)] \\ &\approx 2qI_B + 2qI_C\tau_n^2\omega^2, \end{aligned} \tag{4.6}$$

where $\omega << 1/\tau_n$ is assumed. The $\omega^2$ dependence of the excess $S_{ib}$ can also be shown from the van Vliet model by assuming a first order input NQS model, e.g. the model of Winkel [37]. Using NQS equivalent circuit and noting that $g_{be}$ is approximately equal to $qI_B/(kT)$, one has

$$\begin{aligned} S_{ib}^{van} &= 4kT\Re(Y_{11}) - 2qI_B \\ &= 4kTg_{be} - 2qI_B + 4kT\Re(Y_{11} - g_{be}) \\ &\approx 2qI_B + 4kTC_{bed}^2 r_d\omega^2. \end{aligned} \tag{4.7}$$

For each bias, the coefficient $C_{ib}$ is extracted by plotting $S_{ib} - 2qI_B$ as a function of $\omega^2$, as illustrated in Fig. 4.5 (a). A careful inspection of the extracted $C_{ib}$ shows that the biasing

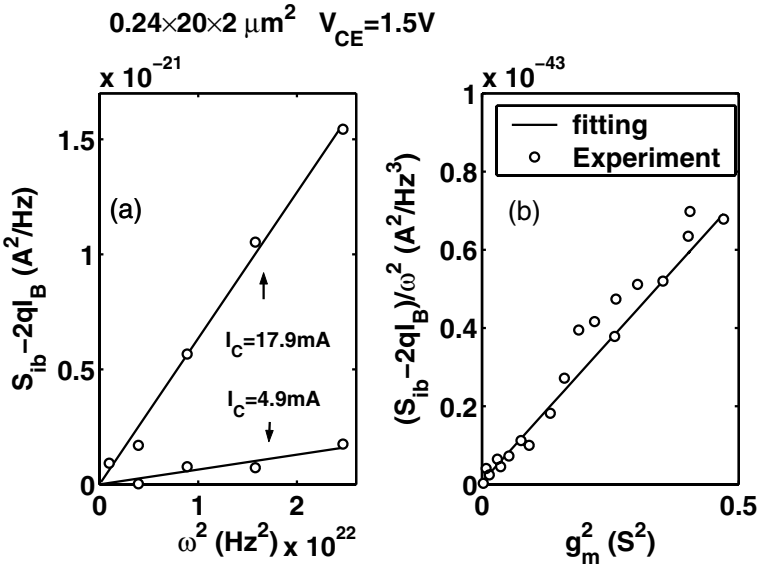


Figure 4.5: (a) $(S_{ib} - 2qI_B)$ versus $\omega^2$ at $I_c$=4.9 mA and 17.9 mA. (b) $C_{ib}$ (denoted as $(S_{ib} - 2qI_B)/\omega^2$) versus $g_m$.

dependence of $C_{ib}$ can be adequately described through $g_m^2$:

$$C_{ib} = K_{bb^*} g_m^2, \tag{4.8}$$

where $K_{bb^*}$ is a bias independent parameter. Fig. 4.5 (b) shows the extracted $C_{ib}$ (denoted as $S_{ib}/\omega^2$) versus $g_m^2$. The slope of the fitting line gives $K_{bb^*}$.

Substituting (4.8) into (4.5) leads to:

$$S_{ib} = 2qI_B + K_{bb^*} g_m^2 \omega^2. \tag{4.9}$$

Equating (4.6) with (4.9) and noticing that $g_m$ is a nearly linear function of $I_C$, we find that $\tau_n$ is bias dependent as shown in [45] and [54]. In the van Vliet model, if we assume that the input NQS delay time $C_{bed} r_d$ is constant, $(S_{ib} - 2qI_B) \propto g_m$, clear different from (4.9).

### 4.2.2 $S_{ic}$

In the SPICE model, the van Vliet model and the transport model, $S_{ic}$ is shot like and frequency independent, with a PSD of $2qI_C$. The $S_{ic}$ extracted from both experimental and simulation data, however, indicates that $S_{ic}$ is higher than $2qI_C$ and frequency dependent. Further, the extraction results show that $S_{ic}$ is proportional to the real part of the intrinsic $Y_{21}$:

$$S_{ic} = C_{ic}\Re(Y_{21}), \tag{4.10}$$

where $C_{ic}$ is a bias dependent coefficient. The frequency dependence of $S_{ic}$ is described by the frequency dependence of $\Re(Y_{21})$. For each bias, $C_{ic}$ is extracted using least square fitting. Fig. 4.6 (a) shows the $S_{ic}$ extracted from measurement data, together with modeling results, at low, medium and high biasing currents. The fitting is not good at low frequencies, as the $S_{ic}$ extraction is less accurate. The main reason is that noise figure is very low at low frequencies, and the system noise plays a bigger role in the noise parameter fitting procedure during measurement. To verify (4.10) without measurement noise problem, we use the simulation data. Very good fitting can be achieved as shown in Fig. 4.7 for all biases and all frequencies up to 30 GHz, the peak $f_T$.

Fig. 4.6 (b) shows the extracted $C_{ic}$, denoted as $S_{ic}/\Re(Y_{21})$, as a function of $g_m$. Note that a linear relation is observed. Thus $C_{ic}$ can be modeled as a function of $g_m$ as

$$C_{ic} = K_{cc^*}g_m + B_{cc^*}, \tag{4.11}$$

where $K_{cc^*}$ and $B_{cc^*}$ are bias independent parameters. The slope and intercept of the fitting line give $K_{cc^*}$ and $B_{cc^*}$ respectively. Substituting (4.11) into (4.10), we obtain the new model equation for $S_{ic}$ as

$$S_{ic} = (K_{cc^*}g_m + B_{cc^*})\Re(Y_{21}). \tag{4.12}$$

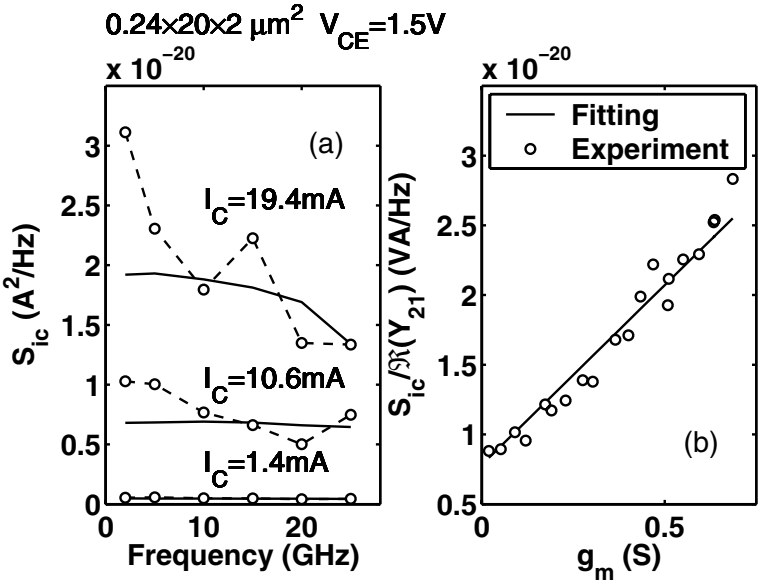


Figure 4.6: (a) Measured $S_{ic}$ versus frequency at $I_c$=1.40 mA, 10.6 mA and 19.4 mA. (b) $C_{ic}$ (denoted as $S_{ic}/\Re(Y_{21})$) versus $g_m$.

Note that at low bias $S_{ic}$ reduces to the ideal value $2qI_C$, this indicates that $B_{cc^*} \approx 2kT$. In the van Vliet model, $S_{ic} \approx 2qI_C$ as $\Re(Y_{22})$ is negligible in SiGe HBTs due to high Early voltage. Neither the van Vliet model nor the transport noise model can be used to describe the extracted $S_{ic}$.

### 4.2.3 Imaginary part of $S_{icib^*}$ [$\Im(S_{icib^*})$]

Fig. 4.8 (a) plots $\Im(S_{icib^*})$ as a function of $\omega$ at representative low and high biasing currents. A linear dependence on $\omega$ is observed at all biasing currents. We can thus model $\Im(S_{icib^*})$ as:

$$\Im(S_{icib^*}) = -C^i_{icib^*}\omega, \tag{4.13}$$

where $C^i_{icib^*}$ is a bias dependent coefficient that is determined from the slope of the fitting line. The functional form of (4.13) is consistent with the van Vliet model when $\omega << 1/\tau_d$, and consistent

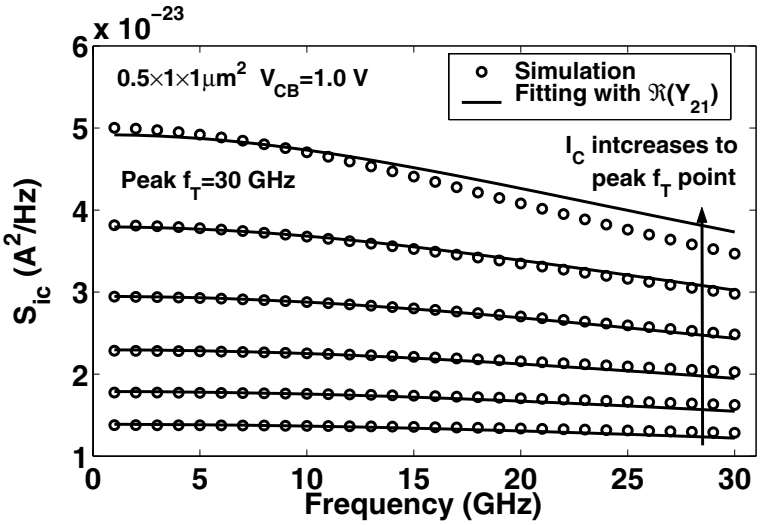


Figure 4.7: Simulated $S_{ic}$ versus frequency at different $I_c$ level.

with the transport noise model when $\omega << 1/\tau_n$. In the van Vliet model,

$$\begin{aligned}\Im(S^{van}_{icib^*}) &= \Im[2kT(Y_{21} + Y^*_{12} - g_m)] \\ &\approx \Im(2kTY_{21}) = \Im(2kTg_m e^{-j\omega\tau_d}) \\ &\approx -2kTg_m\tau_d\omega. \end{aligned} \tag{4.14}$$

In the transport noise model,

$$\begin{aligned}\Im(S^{tran}_{icib^*}) &= \Im[2qI_C(e^{-j\omega\tau_n} - 1)] \\ &\approx -2qI_C\tau_n\omega. \end{aligned} \tag{4.15}$$

The bias dependence of $C^i_{icib^*}$ extracted from measurement data differs from predictions by both the van Vliet model and the transport noise model. For the van Vliet model, assuming that $\tau_d$

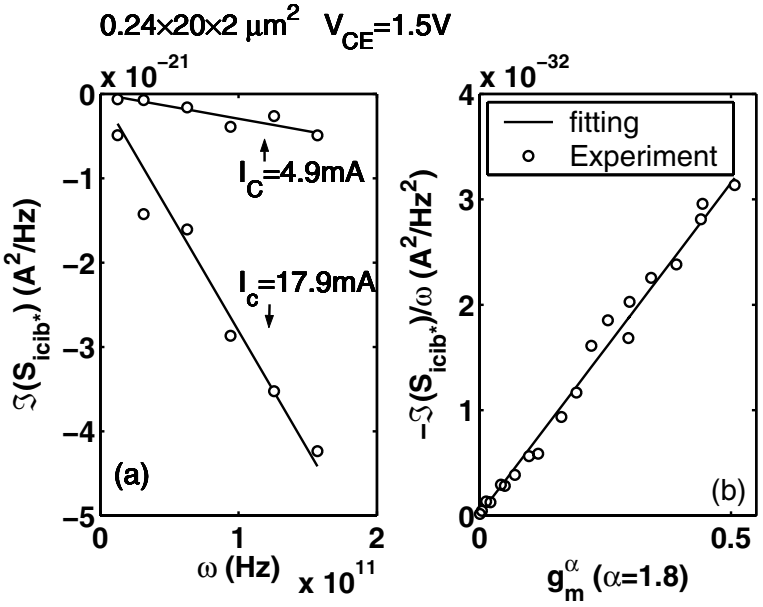


Figure 4.8: (a) $\Im(S_{icib^*})$ versus $\omega$ at $I_C$=4.9 mA and 17.9 mA. (b) $C^i_{icib^*}$ (denoted as $\Im(S_{icib^*}/\omega)$) versus $g_m^{1.8}$.

is bias independent, an inspection of (4.14) shows that:

$$C^{i_van}_{icib^*} = 2kTg_m\tau_d, \tag{4.16}$$

which is proportional to $g_m$. For the transport noise model, the bias dependent $\tau_n$ gives a more complex bias dependence of $\Im(S_{icib^*})$ according to (4.15).

Fig. 4.8 (b) plots $C^i_{icib^*}$ versus $g_m^{1.8}$. Note that a good linear relation is observed. Thus $C^i_{icib^*}$ can be modeled as a function of biasing current through $g_m$ as:

$$C^i_{icib^*} = K^i_{cb^*}g_m^{1.8}. \tag{4.17}$$

The $C^i_{icib^*}$ in these three cases can be expressed in a single functional form as

$$C^i_{icib^*} = K^i_{cb^*} g_m^{\alpha^i_{cb^*}}, \tag{4.18}$$

where $\alpha^i_{cb^*}$ and $K^i_{cb^*}$ are bias independent parameters. Substituting (4.18) into (4.13), we obtain a new model equation for $\Im(S_{icib^*})$:

$$S_{icib^*} = -(K^i_{cb^*} g_m^{\alpha^i_{cb^*}})\omega. \tag{4.19}$$

### 4.2.4 Real Part of $S_{icib^*}$ [$\Re(S_{icib^*})$]

Based on the $\Re(S_{icib^*})$ extracted, we model $\Re(S_{icib^*})$ as a linear function of $\omega^2$ as follows:

$$\Re(S_{icib^*}) = C^{r1}_{icib^*} - C^{r2}_{icib^*}\omega^2, \tag{4.20}$$

where $C^{r2}_{icib^*}$ and $C^{r1}_{icib^*}$ are two bias dependent coefficients. Fig. 4.9 shows $\Re(S_{icib^*})$ versus $\omega^2$ at low and high biases respectively. The slope of the fitting line gives $C^{r2}_{icib^*}$ while the intercept gives $C^{r1}_{icib^*}$.

The $\omega^2$ dependence of $\Re(S_{icib^*})$ is consistent with both the van Vliet model and the transport noise model. In the van Vliet model,

$$\begin{aligned}\Re(S^{van}_{icib^*}) &= \Re[2kT(Y_{21} + Y^*_{12} - g_m)] \\ &\approx \Re(g_m e^{-j\omega\tau_d} - g_m) \\ &\approx -2kT g_m \tau_d^2 \omega^2,\end{aligned} \tag{4.21}$$

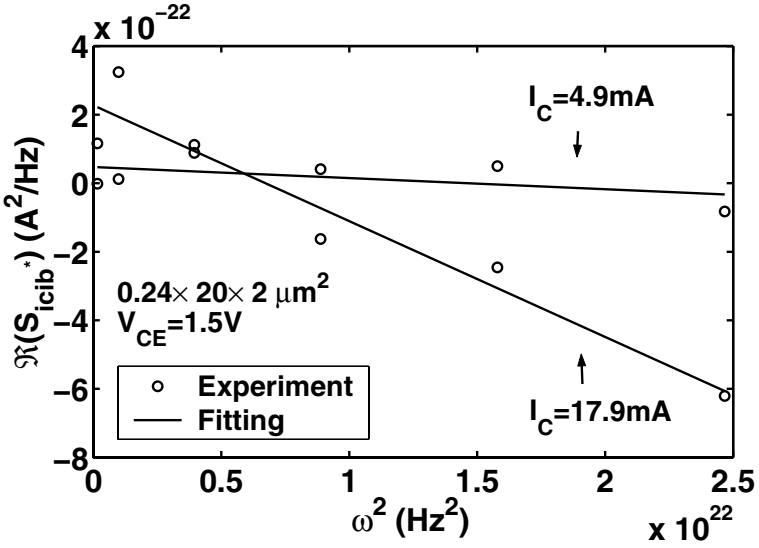


Figure 4.9: $\Re(S_{icib^*})$ versus $\omega^2$ at $I_c$=4.9 mA and 17.9 mA.

which is proportional to $\omega^2$. In the transport noise model,

$$\begin{aligned}\Re(S^{tran}_{icib^*}) &= \Re[2qI_C(e^{-j\omega\tau_n}-1)] \\ &\approx -qI_C\tau_n^2\omega^2, \end{aligned} \tag{4.22}$$

which is also proportional to $\omega^2$. Here $\omega << 1/\tau_n$ is assumed. However, the $C^{r1}_{icib^*}$ parameter in (4.20) would be zero for both the van Vliet model and the transport noise model, as can be seen from (4.21) and (4.22).

To model the bias dependence, the $C^{r2}_{icib^*}$ extracted is observed to be a linear function of $g_m^2$, as illustrated in Fig. 4.10 (a). Thus $C^{r2}_{icib^*}$ can be modeled as

$$C^{r2}_{icib^*} = K^{kr}_{cb^*} g_m^2, \tag{4.23}$$

where $K^{kr}_{cb^*}$ is a bias independent parameter.

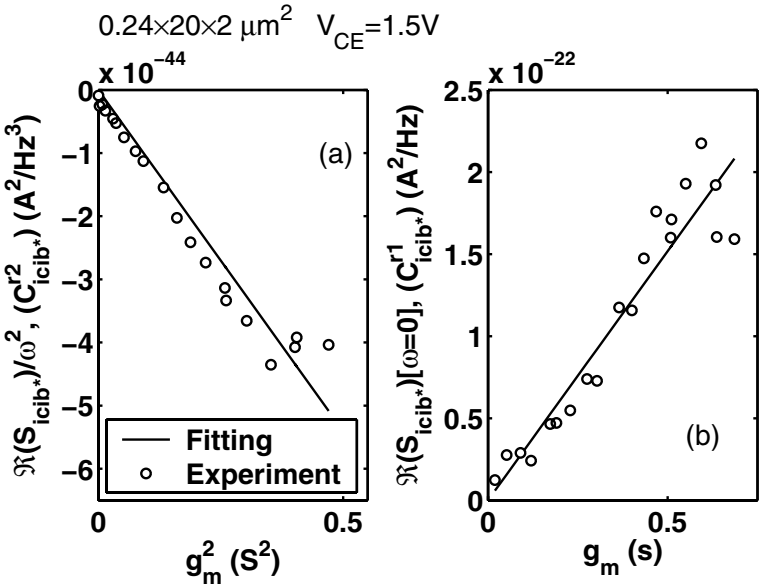


Figure 4.10: (a) $C^{r2}_{icib^*}$ (denoted as $\Re(S_{icib^*})/\omega^2$) versus $g_m^2$. (b) $C^{r1}_{icib^*}$ (denoted as $\Re(S_{icib^*})[\omega = 0]$) versus $g_m$.

Fig. 4.10 (b) shows the extracted $C^{r1}_{icib^*}$ versus $g_m$. A linear relation is observed, thus $C^{r1}_{icib^*}$ can be modeled as a function of biasing by:

$$C^{r1}_{icib^*} = K^{br}_{cb^*} g_m, \tag{4.24}$$

where $K^{br}_{cb^*}$ is a bias independent parameter.

Substituting (4.23) and (4.24) into (4.20) gives the new model equation for $\Re(S_{icib^*})$:

$$\Re(S_{icib^*}) = K^{br}_{cb^*} g_m - (K^{kr}_{cb^*} g_m^2)\omega^2. \tag{4.25}$$

### 4.2.5 Generalized Model Equations

So far we have shown that the correlated noise sources extracted from noise measurement data can be well modeled using (4.9), (4.12), (4.19) and (4.25). The modeling results fit the

experimental results well, as can be seen from Fig. 4.4 for $I_C$=17.9 mA. Application of the model equations to measured noise data and microscopic noise simulation data suggests the following generalized model expressions:

$$S_{ib} = 2qI_b + \omega^2(K_{bb^*} g_m^{\alpha_{bb^*}} + B_{bb^*}), \tag{4.26}$$

$$S_{ic} = (K_{cc^*} g_m^{\alpha_{cc^*}} + B_{cc^*})\Re(Y_{21}), \tag{4.27}$$

$$\Re(S_{icib^*}) = K_{cb^*}^{br} g_m - \omega^2 K_{cb^*}^{kr} g_m^2, \tag{4.28}$$

$$\Im(S_{icib^*}) = -\omega(K_{cb^*}^{i} g_m^{\alpha_{cb^*}^{i}} + B_{cb^*}^{i}). \tag{4.29}$$

In general, we found that:

- $\alpha_{bb^*}$, $\alpha_{cb^*}^{i}$ is between 1 and 2, and $\alpha_{cc^*} \approx 1$.
- $B_{cc^*}$ can be approximated by $2kT$.
- $\Re(S_{icib^*})$ is less important than other noise terms as detailed below.

(4.26)—(4.29) give a set of model equations with a total of 11 model parameters. The $\Re(S_{icib^*})$ is much less important than $\Im(S_{icib^*})$, we can set $\Re(S_{icib^*})$=0 with only a slight accuracy loss in $Y_{opt}$ at high frequencies as shown below in Section IV. Such a simplification further reduces two parameters. The $B_{bb^*}$ and $B_{cb^*}^{i}$ parameters are primarily introduced for low bias fitting. Their effects on $NF_{min}$, $R_n$ and $G_{opt}$ are opposite, therefore in most cases we only need one of these two parameters. $B_{bb^*}$ is used in this work.

So far we have individually examined the extraction results and proposed models for $S_{ib}$, $S_{ic}$, $\Re(S_{icib^*})$ and $\Im(S_{icib^*})$. These PSDs, however, according to random process statistics, are not completely independent. Instead, the normalized correlation $c$, defined as $c \equiv S_{icib^*}/\sqrt{S_{ib}S_{ic}}$, must have a magnitude no larger than unity, i.e. $|c| \leq 1$ [47, 69]. The new model equations do

not guarantee $|c| \leq 1$. Mathematical conditioning can be used during model implementation to ensure $|c| \leq 1$. However, during parameter extraction, this should not be used, as $|c| > 1$ indicates a problem with either noise measurement or equivalent circuit parameter extraction.

Fig. 4.11 (a) shows the real and imaginary part of $c$ versus frequency at $I_C$=17.9 mA. Fig. 4.11 (b) shows the magnitude of $c$ versus frequency at $I_C$=17.9 mA. Fig. 4.11 (c) shows the real and imaginary part of $c$ versus $I_C$ at $f$=25 GHz. Fig. 4.11 (d) shows the magnitude of $c$ versus $I_C$ at $f$=25 GHz. In most cases, $|c| \leq 1$ is satisfied as shown in Fig. 4.11 (b) and (d). Observe that the magnitude of $c$ is close to unity in many cases, therefore the correlation in SiGe HBTs is important and cannot be neglected. Another related observation is that $\Re(c)$ is nearly one order of magnitude smaller than $\Im(c)$ in practice for frequencies less than half of $f_T$. This is also true for noise simulation results. As a result, $\Re(S_{icib^*})$ is much less important than $\Im(S_{icib^*})$, which is further supported by the sensitivity analysis given below.

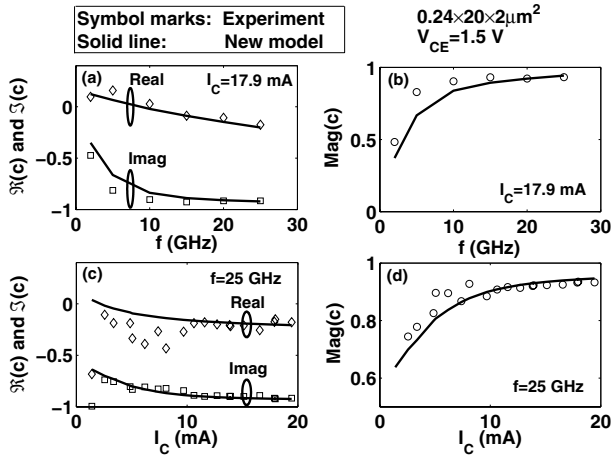


Figure 4.11: Normalized correlation $c$ of the extracted intrinsic noise for $0.24 \times 20 \times 2\mu m^2$ device: (a) $\Re(c)$ and $\Im(c)$ versus frequency at $I_c$=17.9 mA; (b) Magnitude of $c$ versus frequency at $I_c$=17.9 mA; (c) $\Re(c)$ and $\Im(c)$ versus $I_c$ at $f$=25 GHz; (d) Magnitude of $c$ versus $I_c$ at $f$=25 GHz.

Table 4.2: Parameter values of the simplified noise model for Experiment $0.24 \times 20 \times 2\ \mu m^2$ 50 GHz SiGe HBT .

| Parameter | Value | Parameter | Value |
|---|---|---|---|
| $\alpha_{bb^*}$ | 2 | $K_{bb^*}$ | $1.3934 \times 10^{-43}$ |
| $\alpha^i_{cb^*}$ | 1.8 | $K^i_{cb^*}$ | $6.2936 \times 10^{-32}$ |
| $\alpha_{cc^*}$ | 1 | $K_{cc^*}$ | $2.5782 \times 10^{-20}$ |
| $B_{bb^*}$ | $1 \times 10^{-60}$ | $B^i_{cb^*}$ | 0 |
| $K^{br}_{cb^*}$ | $3.0348 \times 10^{-22}$ | $K^{kr}_{cb^*}$ | $1.0809 \times 10^{-43}$ |
| $B_{cc^*}$ | $7.8210 \times 10^{-21}$ | | |

### 4.2.6 Noise Parameter Modeling Results

Using the methods described above, the 11 bias independent noise model parameters are extracted. Table 4.2 lists the parameters values (in MKS units) for the measured $0.24 \times 20 \times 2\ \mu m^2$ SiGe HBT.

Fig. 4.12 shows the modeled and measured noise parameters versus frequency at $I_C$=17.9 mA. $\Re(S_{icib^*})$ is much smaller than $\Im(S_{icib^*})$, making it possible to neglect $\Re(S_{icib^*})$. We thus also calculate the noise parameters with $\Re(S_{icib^*})$=0. The data marked with circle is the measurement. The dash line represents the SPICE model, the solid line represents the new model with $\Re(S_{icib^*})$ and the dash dot line represents the new model with $\Re(S_{icib^*})$=0. Fig. 4.13 shows the noise parameters of the same device as functions of collector current at $f$=25 GHz. It is inconsistent to implement the van Vliet model using a QS equivalent circuit, thus noise parameters are not shown for the van Vliet model. Similarly, the transport noise model result is not shown either due to its limitations in noise source modeling.

Using the proposed new model, excellent fitting is obtained for all of the four noise parameters, at all frequencies and across all biasing currents. Even with $\Re(S_{icib^*})$=0, only $Y_{opt}$ is slightly affected at frequencies above 20 GHz. This is beneficial as we can save two noise model parameters related to $\Re(S_{icib^*})$ by setting $\Re(S_{icib^*})$=0. To quantify errors from using current CAD tools, we

also show results obtained using the SPICE model. At low current level, the SPICE model works well, as was shown in [69]. However, at high current level, $NF_{min}$, $G_{opt}$ and $B_{opt}$ are overestimated.

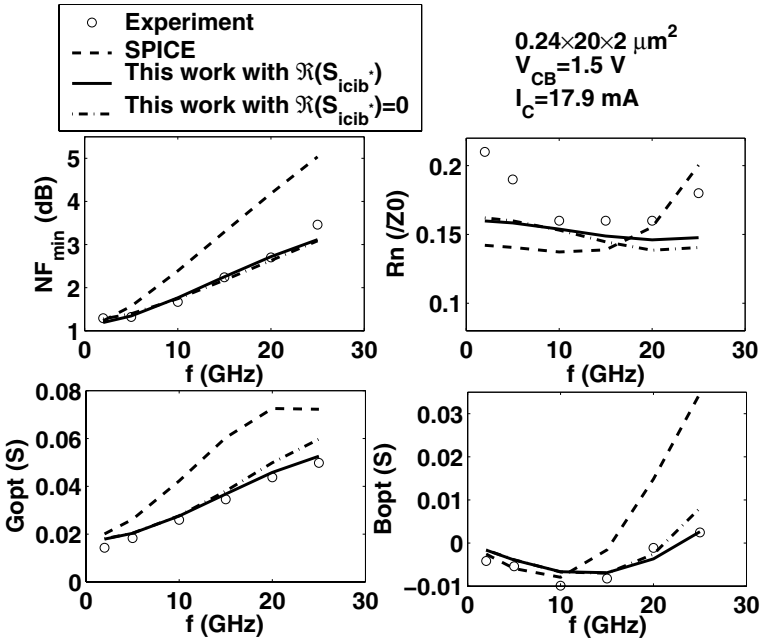


Figure 4.12: Noise parameters versus frequency for the measured noise data. $I_c$=17.9 mA. $A_E$=0.24 × 20 × 2$\mu m^2$.

So far we have used the $A_E$=0.24 × 20 × 2$\mu m^2$ device as an example. A natural question is how the noise sources scale with geometry. For ideal scaling, $S_{ib}$, $S_{ic}$ and $S_{icib^*}$ should all scale with the emitter area $A_E$ for the same biasing current density. This is indeed the case according to the extracted data from various geometries as shown below. Nonideal noise parameter scaling with geometry is mostly from nonideal scaling of resistances, such as $r_{bx}$ and $r_{bi}$.

### 4.2.7 Sensitivity Analysis

For understanding of model to data correlation and model parameter extraction, it is useful to calculate the sensitivity of noise parameters ($NF_{min}$, $R_n$ and $Y_{opt}$) to the intrinsic noise model parameters. Table 4.3 gives the percentage change of noise parameters responding to 5% change

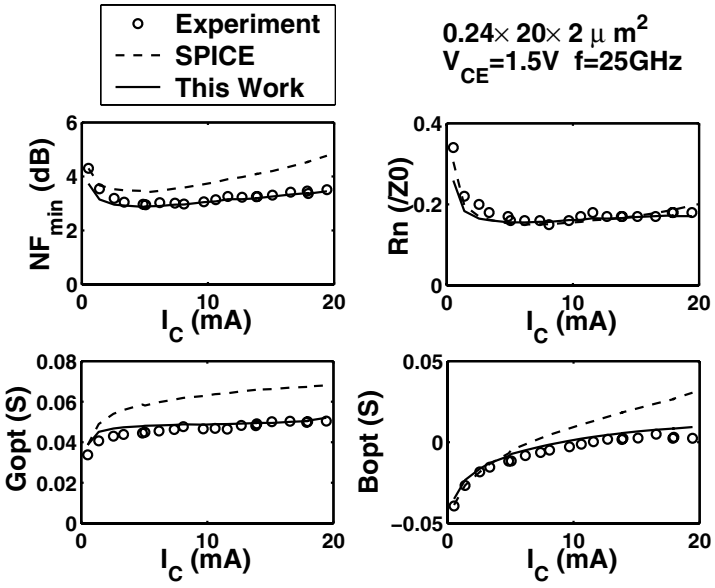


Figure 4.13: Noise parameters versus collector current for the measured noise data. $f$=25 GHz. $A_E$=0.24 × 20 × 2$\mu m^2$.

of the intrinsic noise model parameters. $I_C$=17.9 mA, $f$=25 GHz. $A_E$=0.24 × 20 × 2$\mu m^2$. We list only the noise model parameters that have a large impact on the noise parameters at higher biasing currents and higher frequencies. $B_{bb^*}$, $B^i_{cb^*}$ and $B_{cc^*}$ mainly affect low bias noise parameters and thus are not listed. The sensitivity analysis shows that:

- The noise parameters are sensitive to model parameters for $\Im(S_{icib^*})$, including $K^i_{cb^*}$ and $\alpha^i_{cb^*}$.
- $S_{ic}$ (through $K_{cc^*}$) is as important as $S_{ib}$ (through $K_{bb^*}$) at high frequencies.
- The noise parameters are not sensitive to $\Re(S_{icib^*})$ (through $K^{br}_{cb^*}$ and $K^{kr}_{cb^*}$). This explains why $\Re(S_{icib^*})$ can be set to zero and produce good noise parameter fitting.

Table 4.3: Parameter sensitivity at $I_C$=17.9mA, $f$=25GHz. $A_E$=0.24 × 20 × 2$\mu m^2$. Percentage variance of noise parameters responding to 5% variance of the noise model parameters.

| | $NF_{min}$ | $R_n$ | $G_{opt}$ | $B_{opt}$ |
|---|---|---|---|---|
| $K^i_{cb^*}$ | 29.10% | 10.17% | 22.5% | 233.3% |
| $\alpha^i_{cb}$ | 22.58% | 8.6% | 21.25% | 175.0% |
| $K_{bb^*}$ | 7.94% | 4.94% | 4.14% | 78.82% |
| $K_{cc^*}$ | 7.94% | 3.48% | 5.79% | 50% |
| $\alpha_{bb}$ | 7.62% | 4.94% | 4.72% | 78.57% |
| $\alpha_{cc}$ | 3.29% | 0.3% | 2.92% | 23.5% |
| $K^{kr}_{cb^*}$ | 0.14% | 0.33% | 0.61% | 5.25% |
| $K^{br}_{cb^*}$ | 0.035% | 0.12% | 2.63% | 1.3% |

## 4.3 Emitter geometry scaling

Optimal transistor sizing and biasing are important for high performance RF low-noise amplifier design using SiGe HBTs. This calls for accurate understanding and modeling of the emitter geometry scaling behavior of RF noise sources, including the correlated intrinsic base and collector current noises, their correlation, the thermal-like noise of intrinsic base resistance and the well know $4kTR$ thermal noises due to extrinsic terminal resistances. In SiGe HBTs, the crowding effect on noise voltage of rbi is negligible because of the high base doping, therefore the $r_{bi}$ noise can be approximated with $4kTr_{bi}$.

The study of scaling issue is based on experimental data of SiGe HBTs with different emitter geometries, indicates emitter length (LE), emitter width (WE) and emitter finger number (NE) scaling respectively. We first extract the small signal equivalent circuit parameters from measured s-parameters, and then extract the intrinsic base and collector current noises using standard noise de-embedding method [2] from measured noise parameters. With the extraction results, different scaling effects on intrinsic noise and resistance noise are discussed. The geometry scalability of our semi-empirical model is examined.

### 4.3.1 Intrinsic noise scaling

Ideally for transistors of the same vertical profile, if they are biased to have the same collector current density $J_C$, their *dc* currents, *ac* currents and Y-parameters are proportional to emitter area $A_E(= W_E \times L_E \times N_E)$, where $W_E$, $L_E$ and $N_E$ are the emitter width, length and number of fingers respectively. Using a given emitter area $A_{E0}$ as a reference, $I_B$, $I_C$, $g_m$ and $\Re(Y_{21})$ for other emitter geometries can be calculated using corresponding emitter area scaling factor $M(= A_E/A_{E0})$. Similarly, the PSDs of the intrinsic base and collector current noise and their correlations scale linearly with $A_E$ in this ideal case. Here the $0.24 \times 20 \times 2\mu m^2$ device is used as a reference. Our noise extraction results for different emitter geometries indeed show that the intrinsic noise PSDs obey such ideal scaling rule. In Fig. 4.14, the extracted intrinsic noises for each device are divided by its M factor and plotted versus $I_C/M$ at $f$=15 GHz. For $S_{ib}$, $S_{ic}$ and $\Im(S_{icib^*})$, the normalized data of the four devices overlap well. The trend is not obvious for $\Re(S_{icib^*})$, primarily due to extraction difficulties. $\Re(S_{icib^*})$ is one order of magnitude lower than $\Im(S_{icib^*})$, and has much weaker effect on noise parameters. Therefore $\Re(S_{icib^*})$ is easily affected by measurement noise. Furthermore we found that all $\alpha$ terms in the model are approximately emitter geometry independent. This leads to the following scaling rule for the $K$ and $B$ terms in the proposed noise model as

$$K_{bb^*} = K_{bb^*0} M^{1-\alpha_{bb^*}}, B_{bb^*} = B_{bb^*0} M, \tag{4.30}$$

$$K_{cc^*} = K_{cc^*0} M^{-\alpha_{cc^*}}, \; B_{cc^*} = B_{cc^*0}, \tag{4.31}$$

$$K^{br}_{cb^*} = K^{br}_{cb^*0}, \qquad K^{kr}_{cb^*} = K^{kr}_{cb^*0}/M, \tag{4.32}$$

$$K^{i}_{cb^*} = K^{i}_{cb^*0} M^{1-\alpha^{i}_{cb^*}}, B^{i}_{cb^*} = B^{i}_{cb^*0} M. \tag{4.33}$$

where the subscript 0 denotes the reference transistor. Since all of the noise current PSDs scale linearly with the emitter area, the normalized correlation $c$ does not change, $|c| \leq 1$ is kept satisfied.

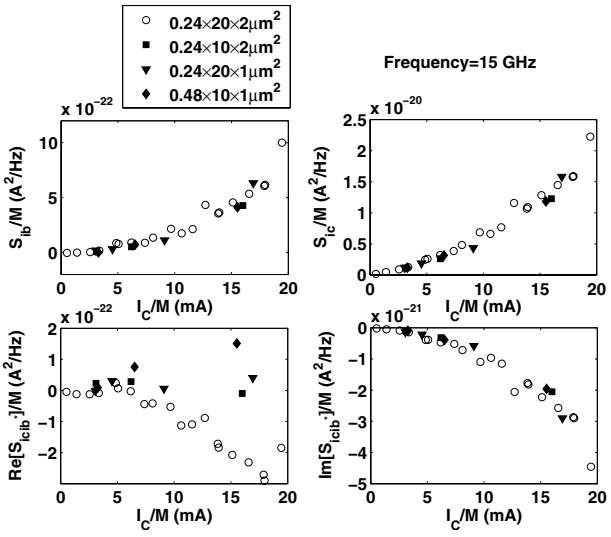


Figure 4.14: Extracted intrinsic noise divided by M vs $I_c/M$ at $f$=15 GHz, where M is the emitter geometry scaling factor.

We now verify the geometry scaling ability of the new model with measured noise data of different emitter geometries. The $0.24 \times 20 \times 2\mu m^2$ device is used as a reference. We use $0.24 \times 10 \times 2\mu m^2$ for emitter length scaling, $0.24 \times 20 \times 1\mu m^2$ for number of emitter finger scaling and $0.48 \times 10 \times 1\mu m^2$ for emitter width scaling. The model parameters for all devices satisfy the scaling rule given by (4.30)—(4.33). Note that the emitter area scaling factor M is 2 for all three scaled devices. The noise figures are shown in Figs. 5.18, 4.16, 4.17 for $A_E = 0.24 \times 10 \times 2\mu m^2$, $A_E = 0.24 \times 20 \times 1\mu m^2$ and $A_E = 0.48 \times 10 \times 1\mu m^2$ respectively. For each emitter geometry, a low bias and a high bias point are shown. Excellent agreement between modeling and measurement has been achieved for all of the four noise parameters and for all of the emitter geometries. Note that the collector voltage $V_{CE}$ of different size devices are different. The $V_{CE}$ effect has been taken into account by the small signal parameters.

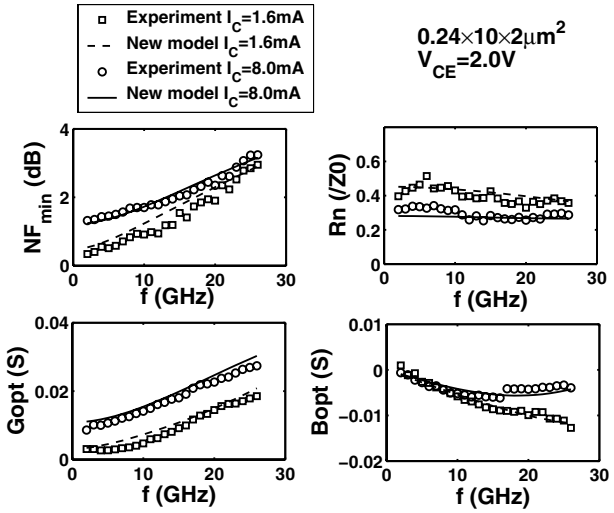


Figure 4.15: Noise parameters versus frequency for $0.24 \times 10 \times 2\mu m^2$ SiGe HBT at $I_c$=1.6 mA and 8.0 mA. $V_{CE}$=2.0 V.

Table 4.4: Extracted $r_{bx}$, $r_{bi}$ for 50 GHz SiGe HBTs with different emitter geometries

| Emitter geometry ($\mu m^2$) | M - | $r_{bx}$ ($\Omega$) | $r_{bi}$ at peak $f_T$ ($\Omega$) | $r_{bx} \times LE \times NE$ ($\Omega\mu m$) | $r_{bi} \times LE \times NE$ ($\Omega\mu m$) |
|---|---|---|---|---|---|
| $0.24 \times 20 \times 2$ | Ref. | 2.70 | 2.68 | 108 | 107.2 |
| $0.24 \times 10 \times 2$ | 1/2 | 3.70 | 5.75 | 74 | 115 |
| $0.24 \times 20 \times 1$ | 1/2 | 11.5 | 10.5 | 230 | 210 |
| $0.48 \times 10 \times 1$ | 1/2 | 13.0 | 21.1 | - | - |

### 4.3.2 Extrinsic noise scaling

Now we consider the geometry scaling of noises due to parasitic resistances. For SiGe HBT noise, $r_{cx}$ is less important and re is relatively small, hence only $r_{bx}$ and $r_{bi}$ are considered here. Since the intrinsic noise has shown to scale with AE ideally, if both $r_{bx}$ and $r_{bi}$ inversely scale with AE, the four normalized noise parameters, i.e., $NF_{min}$, $R_n \times M$, $G_{opt}/M$ and $B_{opt}/M$, will nearly be geometry independent [1]. This will make optimal transistor sizing easier in LNA design.

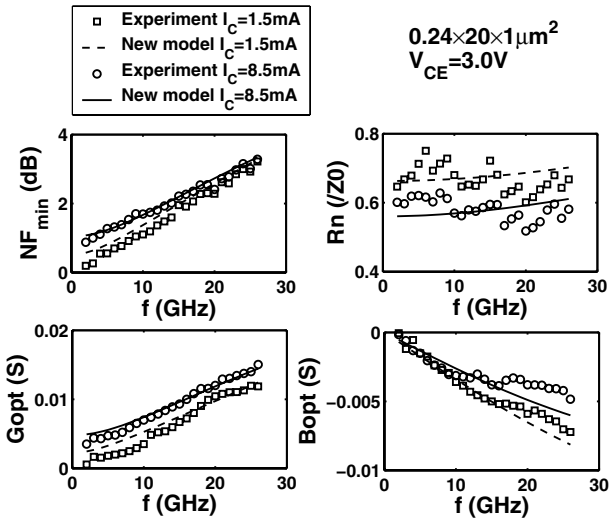


Figure 4.16: Noise parameters versus frequency for $0.24 \times 20 \times 1\mu m^2$ SiGe HBT at $I_c$=1.6 mA and 8.0 mA. $V_{CE}$=3.0 V.

Table 4.4 shows the extracted $r_{bx}$, $r_{bi}$ for SiGe HBTs with different geometries. For base resistance, as WE scaling is quite different with LE and NE scaling, we do not evaluate the normalized resistance values for WE case. For LE scaling, we compare the $0.24 \times 10 \times 2\mu m^2$ HBT with the $0.24 \times 20 \times 2\mu m^2$ reference device. Their normalized base resistances are close to each other as shown in Table 4.4 suggesting a near ideal LE scaling. Consequently, the four normalized noise parameters overlap with each other as shown in Fig. 4.18. Next we consider NE scaling by comparing the $0.24 \times 20 \times 1\mu m^2$ HBT with the $0.24 \times 20 \times 2\mu m^2$ reference. Their normalized $r_b$ values have a large difference due to the path resistances connected to base, leading to the discrepancy of normalized noise parameters. $NF_{min}$ is reduced using multiple emitter fingers as shown in Fig. 4.18. For the three scaling strategies, only emitter length scaling is near ideal and should be primarily considered during noise matching.

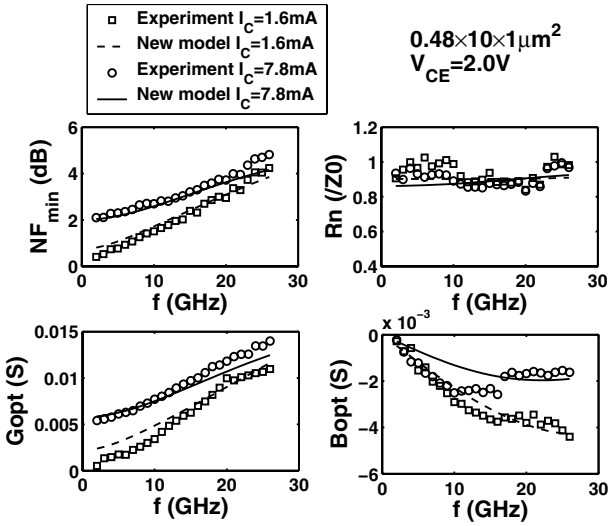


Figure 4.17: Noise parameters versus frequency for $0.48 \times 10 \times 1\mu m^2$ SiGe HBT at $I_c$=1.6 mA and 7.8 mA. $V_{CE}$=2.0 V.

### 4.3.3 Comparison of intrinsic noise with resistance noise

To compare the relative importance of noise sources in SiGe HBTs, we calculate three types of $NF_{min}$ versus $I_C$ as shown in Fig. 4.19. The solid line is calculated including both intrinsic noise and resistance noise, the dash line is calculated including only intrinsic noise and the dash dot line is calculated including only resistance noise. Note these $NF_{min}$ do not have simple relation. For all the devices examined, the intrinsic noise contributes more noise. The bias dependence of $NF_{min}$ mainly comes from the bias dependence of intrinsic noise. The resistance noise adds about 1dB to $NF_{min}$ for all the four devices and is important. Once their values are well modeled, we can model the noise parameters accurately.

## 4.4 Implementation in CAD tools

The semi-empirical model can be easily applied in present CAD tools. Here we demonstrate its implementation in VBIC model using Analog-A language for Advanced Design System (ADS), Agilent Technologies.

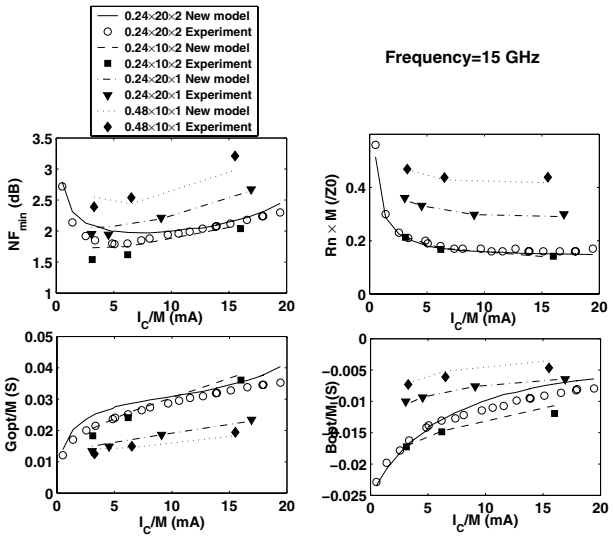


Figure 4.18: Normalized noise parameters versus $I_c/M$ at f=15 GHz.

Fig. 4.20 illustrates the technique to introduce correlated intrinsic transistor noise sources that give PSDs in (4.26)–(4.29) for VBIC model. We add two isolated nodes $v_a$ and $v_b$, each of them is connected to ground through a 1 Ohm noiseless conductance. Unity white noise currents $i_a$ and $i_b$ are injected into node $v_a$ and $v_b$ respectively, producing noise voltage $v_a$ and $v_b$. We have

$$S_{v_a} = S_{i_a} = 1, \quad S_{v_b} = S_{i_a} = 1. \tag{4.34}$$

We add $2qI_b$ shot noise current and $g_1\texttt{ddt}(v_a)$ noise current between base node $bi$ and emitter node $ei$. Note that the time derivative operator `ddt` in Analog-A generates $j\omega$ factor in frequency domain, leading to the frequency dependence of noise source. We then add two noise currents $g_2 v_a$

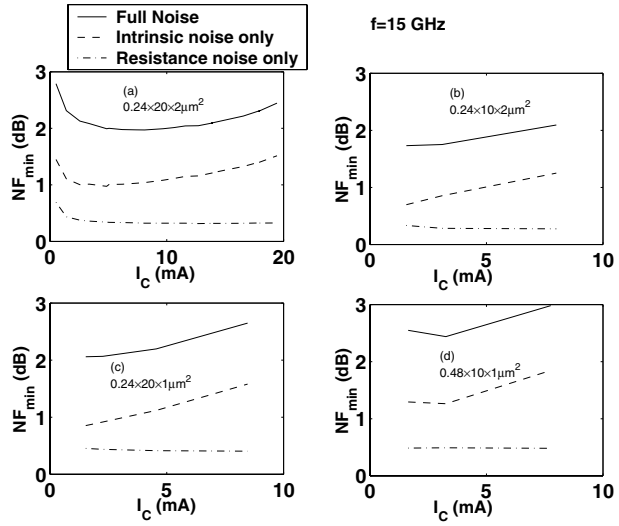


Figure 4.19: $NF_{min}$ versus $I_c$, determined by intrinsic noise only, resistance noise only and both of intrinsic and resistance noise for different geometry SiGe HBTs: (a) $0.24 \times 20 \times 2\mu m^2$; (b)$0.24 \times 10 \times 2\mu m^2$; (c) $0.24 \times 20 \times 1\mu m^2$; (d) $0.48 \times 10 \times 1\mu m^2$ .

and $g_3 v_a$ between collector node $ci$ and emitter node $ei$. We have

$$
\begin{aligned}
S_{ib} &= 2qI_b + S_{v_a} g_1^2 \omega^2 = 2qI_b + \omega^2 g_1^2, \\
S_{ic} &= S_{v_a} g_2^2 + S_{v_b} g_3^2 = g_2^2 + g_3^2, \\
S_{icib^*} &= S_{v_a}(-j\omega g_2 g_1) = -j\omega g_2 g_1.
\end{aligned} \tag{4.35}
$$

The correlation between base and collector current noises thus is obtained by the controlled noise currents $g_1 \texttt{ddt}(v_a)$ and $g_2 v_a$. Now we need to find the expressions of $g_1$, $g_2$ and $g_3$. For simplicity, $\Re(S_{icib*})$ is set to zero. The frequency dependence of $S_{ic}$ are neglected. $\Re(Y_{21})$ and $g_m$ are replaced with $qI_C/kT$ since $g_m$ is not referable in Analog-A of present versions. Comparing (4.35) with

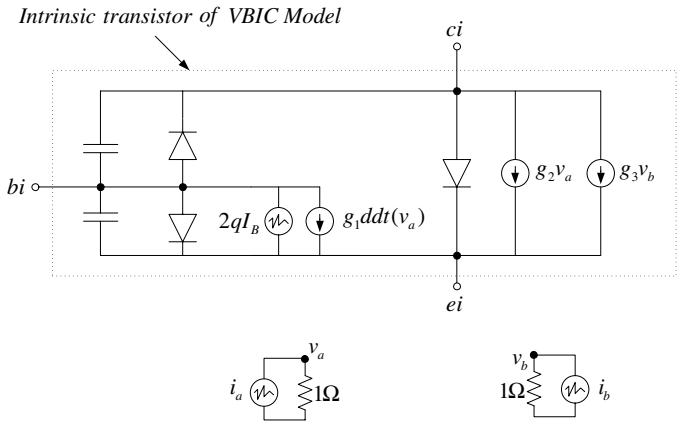


Figure 4.20: Technique of insertion of correlated noise sources into the intrinsic transistor of VBIC model.

(4.26)–(4.29), we have

$$g_1 = \sqrt{K_{bb^*} g_m^{\alpha_{bb^*}} + B_{bb^*}}, \tag{4.36}$$

$$g_2 = \frac{K^i_{cb^*} g_m^{\alpha^i_{cb^*}}}{\sqrt{K_{bb^*} g_m^{\alpha_{bb^*}} + B_{bb^*}}}, \tag{4.37}$$

$$g_3 = \sqrt{(K_{cc^*} g_m^{\alpha_{cc^*}} + B_{cc^*})\Re(Y_{21}) - \frac{(K^i_{cb^*} g_m^{\alpha^i_{cb^*}})^2}{K_{bb^*} g_m^{\alpha_{bb^*}} + B_{bb^*}}}. \tag{4.38}$$

A similar method of introducing correlated $i_b$ and $i_c$ noise is given in [70], where noise correlation $i_b i_c^*$ is introduced while $i_b$ and $i_c$ are still $2qI_b$ and $2qI_c$ white shot noise. This clearly is non-physical. As discussed in Chapter 2, $2qI_b$ is mainly contributed by emitter hole noise for modern transistors. It is the base electron noise that produces significant correlation between $i_b$ and $i_c$. The electron noise will inevitably produce frequency dependent excess noise current to $i_b$. It is this excess noise current of $i_b$ correlated with $i_c$. In our method, the electron noise is described by $g_1$, $g_2$ and $g_3$.

The Analog-A code for implementation of (4.36)–(4.38) in VBIC model is given in Appendix G. Figs. 4.21, 4.22 show the noise parameters versus frequency simulated by ADS using semi-empirical noise model and SPICE noise model respectively at $I_C$=15.1 mA. Clearly the new model improves noise modeling and gives the same results calculated by MATLAB in the previous section.

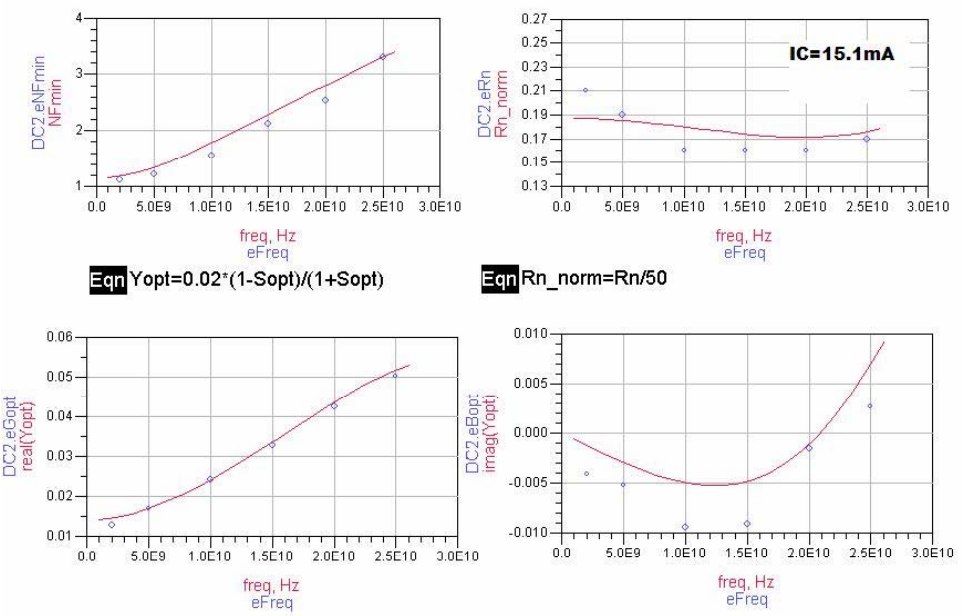


Figure 4.21: Noise parameters versus frequency simulated by ADS using semi-empirical noise model at $I_C$=15.1 mA.

## 4.5 Summary

We have presented the noise de-embedding method for SiGe HBTs using a QS input equivalent circuit. The intrinsic transistor noises are then extracted through noise de-embedding method, and modeled as functions of bias and frequency based on inspection of extraction results. The modeling methodology is demonstrated using noise parameters measured from 2 to 25 GHz on SiGe HBTs featuring a 50 GHz peak $f_T$. The imaginary part of the correlation $\Im(S_{icib^*})$ is found

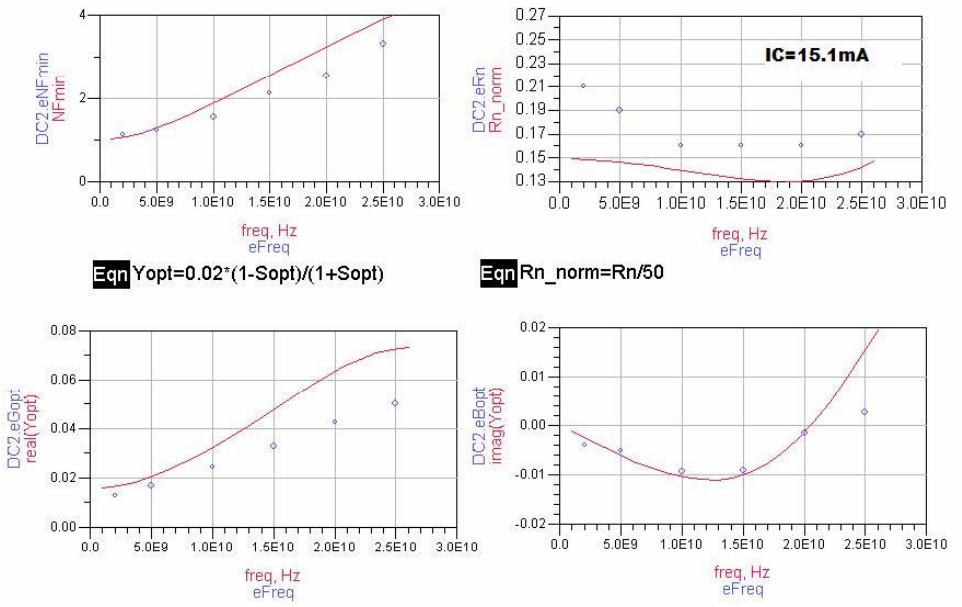


Figure 4.22: Noise parameters versus frequency simulated by ADS using SPICE noise model at $I_C$=15.1 mA.

to be proportional to $\omega$. $S_{ib}$ and and the real part of the correlation $\Re(S_{icib^*})$ are found to be proportional to $\omega^2$. $S_{ic}$ is found to be proportional to $\Re(Y_{21})$. $\Im(S_{icib^*})$ is found to be much greater than $\Re(S_{icib^*})$, and has a much larger impact on noise parameters. The bias dependence of all of the noise terms can all be modeled using $g_m$. Excellent fitting of both Y-parameters and noise parameters has been achieved. The new semi-empirical model is capable of geometry scaling and can be implemented in present CAD tools.

# CHAPTER 5

# IMPROVED PHYSICAL NOISE MODEL

With the technology advances, transistors are scaled, and have narrower base width and emitter width. Some effects related to BC and BE junctions are non-negligible any longer. This chapter improves compact RF noise modeling for SiGe HBTs based on NQS equivalent circuit by taking in account some of these effects. The impact of CB SCR on electron RF noise is examined to be important for scaled SiGe HBTs. The van Vliet model is then improved to account for the CB SCR effect. The impact of fringe BE junction on base hole noise is further investigated. Due to fringe effect, the base hole noise should be modeled with correlated noise voltage source and noise current source in hybrid representation. The base noise resistance is found to be different from AC intrinsic base resistance, and thus is modeled by an extra parameter. With four bias-independent model parameters in total, the combination of electron and hole noise model provides excellent noise parameter fittings for frequencies up to 26 GHz and all biases before $f_T$ roll off for three generations of SiGe HBTs. The new model is also capable of emitter geometry scaling.

## 5.1 CB SCR effect on electron noise

As reviewed in Chapter 2, the van Vliet model solves the microscopic noise transport equation for base minority carrier (electrons for NPN considered here). Van Vliet's derivation of base and collector current noise PSDs assumed adiabatic boundary condition i.e. $\widetilde{n}$=0 or zero electron density fluctuation at both ends of the base, and did not consider electron transport in the CB SCR. For scaled bipolar transistors, e.g. SiGe HBTs of 200 GHz peak $f_T$, CB SCR electron transport

becomes more significant than base electron transport, calling for an investigation of its impact on transistor noise.

The extremely useful result of van Vliet's derivation is that the base and collector current noise and their correlation can be related to the Y-parameters due to intrinsic base electron transport, $Y^B$. As shown in (2.69), the van Vliet model can be extended to include emitter hole noise by replacing $Y^B$ with the Y-parameters of base and emitter region $Y^{EB}$. In the literature, the van Vliet model is often applied using Y-parameters of the whole intrinsic transistor, e.g. in [2] and [47], as opposed to $Y^{EB}$, for which the model was derived. Physically speaking, both the Y-parameters and the noise parameters are modified by electron transport through the CB SCR, it is not clear at all what the relation between Y-parameters and transistor noise should be when the CB SCR is accounted for.

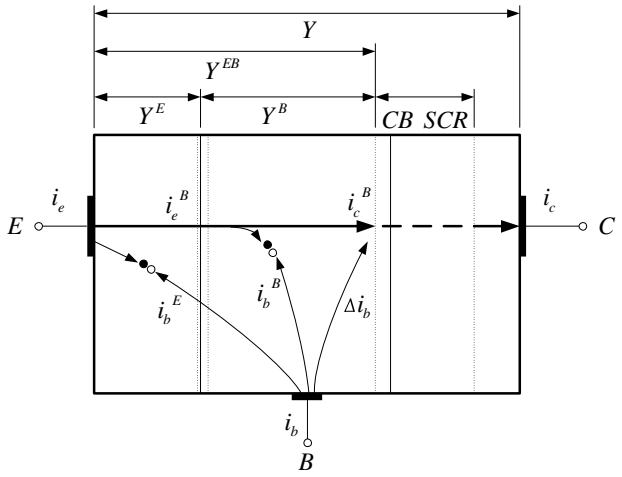


Figure 5.1: Illustration of AC or noise current flows in ideal 1-D intrinsic SiGe HBT.

Here we investigates the impact of CB SCR on transistor noise and derives an improved noise model including such impact. The CB SCR affects electron transport (and hence noise transport) in two ways. First, a velocity saturation boundary condition should be applied at the end of neutral base. Its effect on DC currents and base transit time, and noise has been investigated in Chapter

2. With a strong base built-in field, typically the case of graded SiGe HBTs, the van Vliet model can still correctly describe base electron noise. Therefore, we can continue to use van Vliet model for the relationship between noise and Y-parameters of the intrinsic base for graded SiGe HBTs. Secondly, electron transport through the CB SCR modifies both the Y-parameters and the noise parameters. The noise generated within CB SCR is neglected. The main CB SCR effect accounted is $\tau_c$ delay, which was briefly discussed in [5]. We derived a new set of relationship between noise currents and Y-parameters in presence of CB SCR delay based on van Vliet model. Here we note that $\tau_c$ effect was also included in [71]. However, the base region noise in [71] is derived from 1-D transmission line analogy without including base built-in field, and needs extra parameters (electron diffusion coefficient $D_n$, life time $\tau_n$ and base width $X_B$). Therefore it is much less general than our van Vliet model based result, which is based on Y-parameters that can be measured.

### 5.1.1 Model equation derivation

We denote the AC electron current injected into CB SCR as $i_c^B$ and the AC collector current as $i_c$. The electrons inside the CB SCR induce base hole accumulation at the SCR side of the base region and electron depletion at the SCR side of the collector region. The first part adds an extra base hole current $\Delta i_b$, which is $i_c^B - i_c$, to original base current $i_b^B$. Note that $i_c$ and $i_b$ take positive signs when they flow into the electrodes. Physics analysis [72] shows that $i_c$ and $i_c^B$ can be related by

$$\lambda(\omega) \equiv \frac{i_c}{i_c^B} = \frac{1 - e^{-2j\omega\tau_c}}{2j\omega\tau_c},$$

where $\tau_c$ is the collector transit time. The total AC/noise base and collector currents can be derived as

$$i_b = (i_b^E + i_b^B) + (1 - \lambda) i_c^B, \qquad i_c = \lambda i_c^B. \tag{5.1}$$

With (5.1) and by neglecting $Y_{12}^{EB}$ and $Y_{22}^{EB}$, we obtain the Y-parameters of the whole intrinsic transistor including CB SCR as

$$Y_{11} = Y_{11}^{EB} + (1-\lambda)Y_{21}^{EB}, \qquad Y_{21} = \lambda Y_{21}^{EB}. \tag{5.2}$$

The noise PSDs including CB SCR transport are derived from (5.1) as

$$\begin{aligned} S_{ib} &\equiv < i_b i_b^* > = S_{ib}^{EB} + 2\Re[(1-\lambda)S_{icib^*}^{EB}] + |1-\lambda|^2 S_{ic}^{EB}, \\ S_{ic} &\equiv < i_c i_c^* > = |\lambda|^2 S_{ic}^{EB}. \\ S_{icib^*} &\equiv < i_c i_b^* > = \lambda S_{icib^*}^{EB} + \lambda(1-\lambda^*)S_{ic}^{EB}. \end{aligned} \tag{5.3}$$

Here $S^{EB}$ is given in (2.69). Fig. 5.2 shows the effect of $\tau_c$ on noise, $\tau_c$=0 for the dash lines and $\tau_c$=0.75$\tau_{tr}$ for the solid lines. Emitter hole noise is not included. Clearly the base current noise is significantly *enlarged* due to CB SCR electron transport, particularly with increasing frequency. It is a direct result of increase of AC base current caused by CB SCR effect.

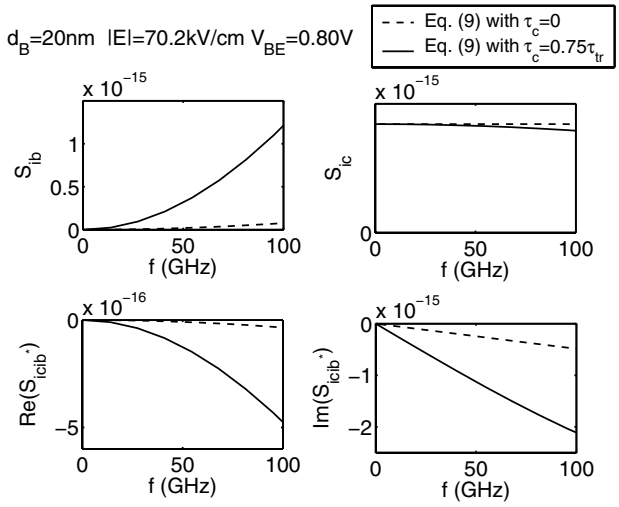


Figure 5.2: Comparison of the intrinsic noise with $\tau_c$=0 and $\tau_c$=0.75$\tau_{tr}$. For $\tau_c$=0.75$\tau_{tr}$, $f_T$=174 GHz. Emitter hole noise is not included.

For various reasons discussed above, it is highly desirable to express the noise PSDs in (5.3) in terms of the Y-parameters for the whole intrinsic transistor $Y$. A set of such expressions are derived below

$$\begin{aligned}
S_{ib} =& 4kT\Re(Y_{11}^{EB}) - 2qI_b + 4kT\Re[(1-\lambda)Y_{21}^{EB}] - 4kT\Re(1-\lambda)g_m + |1-\lambda|^2 S_{ic}^{EB} \\
=& 4kT\Re(Y_{11}) - 2qI_b - 4kT\Re(1-\lambda)g_m + |1-\lambda|^2 2qI_c \\
=& \{4kT\Re(Y_{11}) - 2qI_b\} + 2qI_c|1-\lambda|^2 - 4kTg_m\Re(1-\lambda), \\
S_{ic} =& \{2qI_c\}|\lambda|^2, \\
S_{icib^*} =& \lambda 2kTY_{21}^{EB} - \lambda 2kTg_m + \lambda(1-\lambda^*)S_{ic}^{EB} \\
=& \{2kTY_{21} - \lambda 2kTg_m\} + \lambda(1-\lambda^*)2qI_c \\
=& \{2kT(Y_{21} - g_m)\} + 2qI_c(\lambda - |\lambda|^2) + 2kTg_m(1-\lambda).
\end{aligned} \tag{5.4}$$

We illustrate the $S_{ib}$ derivation as an example. The first step is obtained directly from (5.3) and (2.69). The second step is obtained using (5.2). Note that the terms enclosed by {} in (5.4) are the noise expressed by van Vliet model using the Y-parameters of whole transistor, a brutal force application of van Vliet model (using $Y$ despite that it needs $Y^{EB}$ – often used without justification). The additional terms in our new model, (5.4), represent the error introduced by using the van Vliet model with the overall transistor Y-parameters.

Fig. 5.3 compares the improved model, the brutal use of van Vliet model and the exact result, that is, Langevin equation solution used with (5.3). The improved model works very well, and gives results nearly identical to the exact result. $S_{ib}$ and $|\Re(S_{icib^*})|$ are overestimated by the brutal use of van Vliet model, while $|\Im(S_{icib^*})|$ is correctly modeled for the analytical result where $g_m = I_c/V_T$. For practical SiGe HBTs, $g_m$ is typically smaller than $I_c/V_T$ at high current levels [1]. Consequently, the brutal use of van Vliet model cannot correctly model $|\Im(S_{icib^*})|$ at high $I_c$. The inconsistent modeling of $S_{ib}$ and $|\Im(S_{icib^*})|$ results in an overestimation of $NF_{min}$ for the brutal

Table 5.1: Extracted delay time from DESSIS simulation data

| Peak $f_T$ (GHz) | Device ($\mu m^2$) | $\tau_c$ (ps) | $\tau_{tr}$ (ps) | $\tau_c/\tau_{tr}$ |
|---|---|---|---|---|
| 65 | 0.5 × 1 | 0.57 | 2.1 | 27% |
| 85 | 0.2 × 1 | 0.55 | 1.5 | 37% |
| 183 | 0.12 × 1 | 0.58 | 0.86 | 67% |

use of van Vliet model. The magnitude of derivation depends on the ratio $\tau_c/\tau_{tr}$, which increases with scaling. Table 5.1 shows the extracted $\tau_c/\tau_{tr}$ ratio from DESSIS simulated three generations of SiGe HBTs using the method of [73]. The ratio increases with device scaling, indicating that the BC SCR has more significant impact on higher $f_T$ devices. Even though the differences look small on the plots shown, the resulting differences in noise parameters of the intrinsic transistor ($NF_{min}$, $R_n$, and $Y_{opt}$) are significant, making them important to model. For transistors in which base resistance is large, the final impact on overall transistor noise parameters is smaller, simply because of the less importance of intrinsic transistor noise.

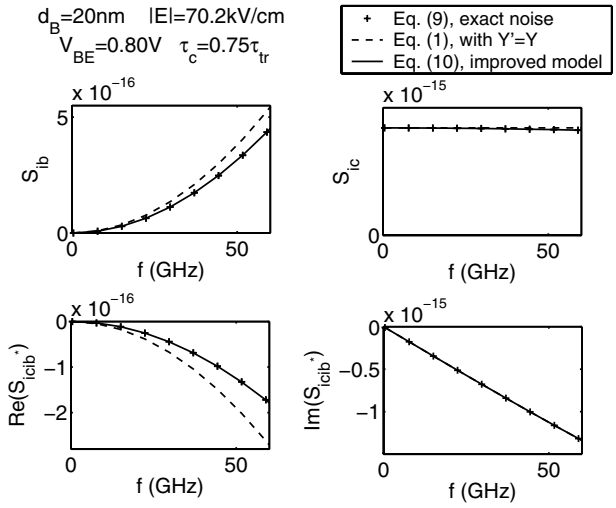


Figure 5.3: Comparison between the brutal used van Vliet model and the improved model under $\tau_c$=0.75$\tau_{tr}$. $f_T$=174 GHz.

### 5.1.2 Verification and discussion

To verify our derivations, we examine the new model using hydrodynamic DESSIS noise simulation. The device has 184 GHz peak $f_T$ with effective $d_B$=20nm. At $V_{BE} = 0.79V$, $\tau_c$=0.75($\tau_b$+$\tau_c$), $f_T$=155 GHz. Fig. 5.4 compares the improved model with the extracted $\tau_c$, the brutal use of van Vliet model and the extracted intrinsic base electron noise. The new model improves $S_{ib}$ and $\Re(S_{icib^*})$ modeling. The DESSIS simulated $S_{ic} < 2qI_C$ is a direct result of hydrodynamic simulation.

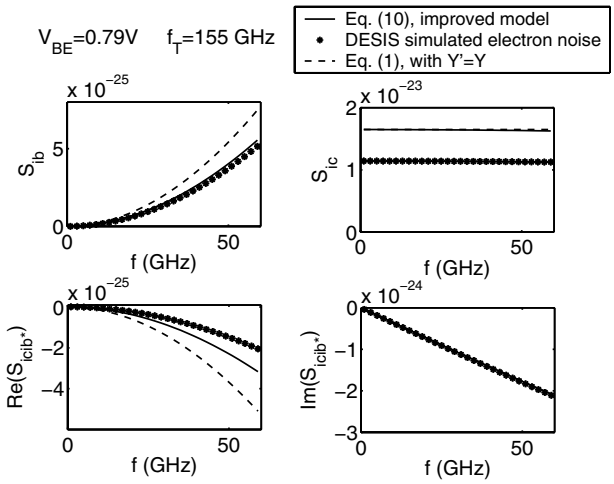


Figure 5.4: Comparison between van Vliet model, new model and the extracted intrinsic noise from DESIS simulation results. $\tau_c$=0.75($\tau_b$+$\tau_c$) is used in the new model. Effective $d_B$=20nm, $\eta$=5.4, $|E|$=70.2 kV/cm.

We approximate (5.4) up to the second order of $\omega$. $g_{be} = I_b/V_T$ are assumed. The frequency dependence of $S_{ib}$ caused by emitter hole noise is negligible compared to that of base electron

noise (see Fig. 2.14). We have

$$
\begin{aligned}
S_{ib} \approx & 2qI_b + \omega^2 \left[ 4kTg_m \left( \tau_{tr}\tau_{in} - \frac{2}{3}\tau_c^2 \right) + 2qI_c\tau_c^2 \right], \\
S_{ic} \approx & 2qI_c - \omega^2(2/3qI_c\tau_c^2), \\
S_{icib^*} \approx & -j\omega \left[ 2kTg_m(\tau_{in} + \tau_{out} - \tau_c) + 2qI_c\tau_c \right] - \omega^2 \left[ 2kTg_m \left( \tau_{in}^2 + \tau_{in}\tau_{out} + \frac{1}{2}\tau_{out}^2 - \frac{2}{3}\tau_c^2 \right) + \frac{2}{3}qI_c\tau_c^2 \right].
\end{aligned}
\tag{5.5}
$$

Clearly for general case where $g_m \neq I_c/V_T$, (5.5) cannot be simplified using three or four lumped model parameters.

Now we consider an extreme case, i.e. $\tau_c >> \tau_b$ or $\tau_c \approx \tau_{tr}$ . This eventually becomes the physical scenario described by the transport noise model [44] [43]. Under such condition, $\tau_{in} \to 2/3\tau_{tr}$ and $\tau_{out} \to 1/3\tau_{tr}$ as discussed in Chapter 3. We then have

$$
\begin{aligned}
S_{ib} \approx & 2qI_b + \omega^2(2qI_c\tau_c^2), \\
S_{ic} \approx & 2qI_c - \omega^2(2/3qI_c\tau_c^2), \\
S_{icib^*} \approx & -j\omega(2qI_c\tau_c) - \omega^2 \left( \frac{1}{9}kTg_m + \frac{2}{3}qI_c \right) \tau_c^2.
\end{aligned}
\tag{5.6}
$$

Comparing with the Taylor expression of transport model equations in Chapter 4, we found that

$$
\begin{aligned}
S_{ib} \approx & S_{ib}^{tran}, \\
S_{ic} \approx & S_{ic}^{tran} + 2/3\Re(S_{icib^*}^{tran}), \\
S_{icib^*} \approx & S_{icib^*}^{tran} - 4/9\Re(S_{icib^*}^{tran}).
\end{aligned}
\tag{5.7}
$$

This shows that under $\tau_c >> \tau_b$ condition, the transport noise model does not well model the intrinsic noise. However, it is a good approximation as $S_{ib}$ and $\Im(S_{icib^*})$ have been correctly

modeled. The improved model thus provides a means of "bridging" the van Vliet model and the transport noise model.

## 5.2 Fringe BE junction effect on base hole noise

Base hole noise is another major noise source for SiGe HBTs. Traditionally this noise is modeled by the thermal noise of $r_{bx}$ and $r_{bi}$, the small signal base resistance for the extrinsic and intrinsic region respectively. $r_{bx}$ is the resistance of a true resistor whose noise can be well modeled with $4kTr_{bx}$. However, $r_{bi}$ is a lumped resistance. There are two kinds of $r_{bi}$, depending on whether QS equivalent circuit or NQS equivalent circuit is used. As discussed in Chapter 2 and Chapter 3, $r_{bi,nqs}$ is more physical and also smaller than $r_{bi,qs}$. We found problems of using $4kTr_{bi}$ for noise modeling based on either QS or NQS lumped equivalent circuit. Firstly, noise resistance $R_n$ cannot be well modeled, which is sensitive to base hole noise. One has to use an empirical $S_{ic}$ based on noise extraction, which is unphysically larger than $2qI_c$ for 50 GHz SiGe HBTs [2]. Another problem is that the absolute value of the imaginary part of noise parameter $Y_{opt}$, i.e. $B_{opt}$, is overestimated by van Vliet model based on NQS equivalent circuit. The deviation cannot be eliminated by choosing appropriate $r_{bi}$. This work aims to solve these two problems by modeling the distributive effect of base hole noise.

The distributive effect is a significant feature of intrinsic base hole noise [48]. The best way to examine this effect is through microscopic noise simulation. There exist two kinds of distributive effect, the fringe effect associated with the edge transistor and the crowding effect associated with the intrinsic transistor. To account for these effects, we divide the BE/BC junction into four segments $A_{1-4}$, leading to five equivalent base resistances of three types as shown in Fig. 5.5. Further analysis shows that at least four segments (five resistors) are needed. Type I resistances are for the edge transistors. Type III resistances are for the main intrinsic transistor. Type II resistances are a combination of resistances from the main and edge transistors. Because of the narrow emitter width

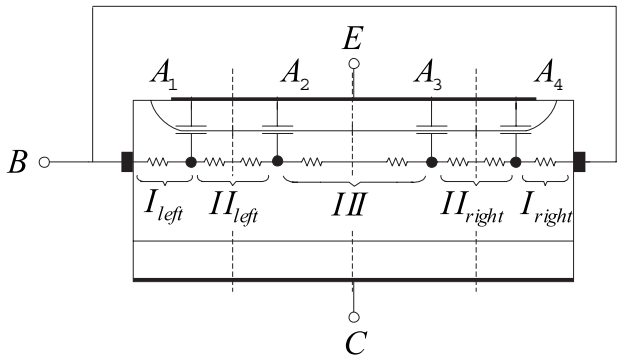


Figure 5.5: Illustration of base distribution effect by dividing the base resistances into five segments of three types. Double base contact is used.

and high base doping, DC crowding effect is negligible in practice. Hence the traditional $4kTr_{bi}$ description is theoretically true only for the main intrinsic transistor *without* the fringe region [41]. In lumped equivalent circuit based modeling, the fringe region or edge transistor is not explicitly separated from the main intrinsic region [2, 51, 52]. However it is unknown how the fringe effect affects base hole noise and how important the effect is.

We will show that the base hole noise should be modeled by a noise voltage source at the input and a correlated noise current source at the output due to the fringe effect. The $f_T$ is no longer assumed to be uniform across the whole BE junction as opposite to [41]. The fringe transistor has lower $f_T$ because of wider base at the edge of emitter and smaller $V_{BE}$. It is the correlation of the two noise sources that cause the $B_{opt}$) problem described above. The base noise resistance needed to fit noise data from both microscopic noise simulation and measurements is found to be not the same as $r_{bi}$, which cannot be explained by fringe effect. Such observation based on simulation was also reported in [46]. We hence use an extra parameter $R_{bn}$ as base noise resistance to improve $R_n$ fitting. DESSIS device simulation is used as guidance, as base hole and electron noises can be separated in simulation. Experimental data are used to verify the new model.

### 5.2.1 Physical considerations

The five resistance model has captured both the fringe effect and crowding effect of base hole noise in a lumped fashion. Fig. 5.6 shows the small signal equivalent circuit that corresponds to Fig. 5.5. The five resistances correspond to those five segments. The four capacitors and

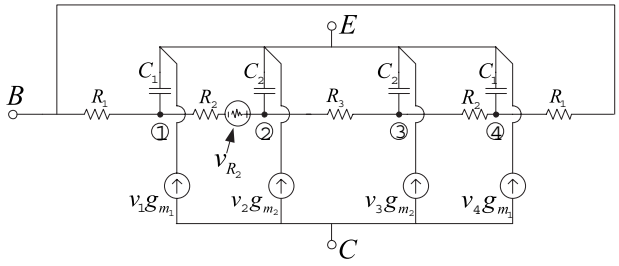


Figure 5.6: Small signal equivalent circuit of five segments model. Only the noise voltage source of left $R_2$ is shown. $g_{be}$ is neglected. Four nodes are labeled.

transconductances correspond to segment $A_{1-4}$ . Note that $g_{m2} >> g_{m1}$, $C_2 >> C_1$. $g_{be}$ is neglected in Fig. 5.6 which is only used for base hole noise derivation. The $g_{be}$ in the small signal equivalent circuit of SiGe HBT is not neglected. All the small signal components are connected through four inner nodes. The resulting equivalent circuit is symmetric.

Although the DC base-emitter bias is the same for $A_{1-4}$ segments, the local $f_T$ varies along the emitter junction. $A_2$ and $A_3$ have the same $f_T$. $A_1$ and $A_4$, however, have lower $f_T$ because of wider base of the edge transistor, meaning that $g_{m1}/C_1 < g_{m2}/C_2$. The smaller local $f_T$ does not affect the transistor $f_T$ much because of the small area of $A_1$ and $A_4$ compared to $A_2$ and $A_3$. However we will show that just because of the non-uniformity of $f_T$, base hole will produce noise current at the collector. This result cannot be obtained in [41] where uniform $f_T$ is assumed. Although chain representation of noise is directly related to noise parameters [20], for the directness of physics we will model the base hole noise using hybrid representation as shown in Fig. 1.4. $v_h$ and $i_h$ are the noise source for the hybrid representation, while $v_a$ and $i_a$ are the noise source for the chain representation. The hybrid representation noise is then transformed into chain representation

by [20]

$$
\begin{aligned}
S_{va} &= S_{vh} + \frac{S_{ih}}{|Y_{21}|^2} + 2\Re\left[\frac{S_{ihvh^*}}{Y_{21}}\right], \\
S_{ia} &= S_{ih}\left|\frac{Y_{11}}{Y_{21}}\right|^2, \\
S_{iava^*} &= S_{ihvh^*}\frac{Y_{11}}{Y_{21}} + S_{ih}\frac{Y_{11}}{|Y_{21}|^2}.
\end{aligned} \tag{5.8}
$$

where the Y-parameters are for the intrinsic transistor *including* $r_{bi}$.

### 5.2.2 Model equation derivation

We first use the five resistance model to derive model equations for the base hole noise. The equations include three model parameters $R_{bn}$, $K_1$ and $K_2$. We then examine the bias dependence of these model parameters using device simulation.

#### $v_h$ and $i_h$

To calculate $v_h$ and $i_h$, we float the base terminal and short the collector terminal to emitter in Fig. 5.6. The base terminal voltage gives $v_h$ and the collector output current gives $i_h$. Each resistance has $4kTR$ thermal noise. Contributions of each resistance to $v_h$ and $i_h$ can be calculated.

Because of the symmetry of the circuit in Fig. 5.6, the noise of $R_3$ does not contribute to either $v_h$ or $i_h$. Each $R_1$ gives $4kTR_1/4$ noise for $v_h$. The two $R_1$ totally contribute $4KTR_1/2$ noise to $v_h$. Again because of symmetry, $R_1$ does not contribute to $i_h$. The two $R_2$ resistors contribute to both $v_h$ and $i_h$.

Now consider the left $R_2$. We insert a test noise voltage source $v_{R2}$ into Fig. 5.6. $v_{R2}$ has a noise voltage PSD of $4kTR_2$. Solving the symmetric network,

$$v_1 + v_4 = -v_{R2}\frac{C_2}{C_1 + C_2 + j\omega R_2 C_1 C_2,} \tag{5.9}$$

$$v_2 + v_3 = v_{R2}\frac{C_1}{C_1 + C_2 + j\omega R_2 C_1 C_2.} \tag{5.10}$$

The equivalent hybrid representation noise sources for Fig. 5.6 are then obtained as

$$v_h = \frac{v_1 + v_4}{2}, \tag{5.11}$$

$$\begin{aligned} i_h &= -g_{m2}(v_2 + v_3) - g_{m1}(v_1 + v_4) \\ &= \left[\frac{g_{m2}}{C_2} - \frac{g_{m1}}{C_1}\right] C_1(v_1 + v_4). \end{aligned} \tag{5.12}$$

If the $f_T$ of $A_1$ and $A_2$ are the same, i.e., $g_{m2}/C_2 = g_{m1}/C_1$, then $i_h$=0. The base hole noise can be fully described by $v_h$. As discussed in Section II, $g_{m1}/C_1 < g_{m2}/C_2$, therefore $i_h$ has the same sign as $v_h$, leading to a positive $\Re(S_{ihvh*})$.

**Noise in hybrid representation**

For convenience, we define two partition factors

$$\lambda_c = \frac{C_1}{C_1 + C_2} < 1, \lambda_{gm} = \frac{g_{m1}}{g_{m1} + g_{m2}} < 1. \tag{5.13}$$

Note $\lambda_{gm} < \lambda_c$. As $C_2 << C_1$, we neglect the $\omega R_2 C_1 C_2$ term in both $v_h$ and $i_h$. The noise due to the left $R_2$ can be obtained as

$$\begin{aligned} S_{vh,R2} &=< v_h v_h^* >= 4kTR_2[\lambda_c^2/4], \\ S_{ih,R2} &=< i_h i_h^* >= 4kTR_2(g_{m1}+g_{m2})^2(1-\lambda_c-\lambda_{gm})^2, \\ S_{ihvh^*,R2} &=< i_h v_h^* >= 4kTR_2(g_{m1}+g_{m2})(1-\lambda_c)(\lambda_c-\lambda_{gm}). \end{aligned} \tag{5.14}$$

The right $R_2$ has the same noise as the left $R_2$, therefore the two $R_2$ contribute two times of the noise shown in (5.14). Now the overall noise can be obtained by adding the contributions of two $R_1$ and two $R_2$ in (5.14) as

$$\begin{aligned} S_{vh} &= 4kTR_{bn}, \\ S_{ih} &= 4kTR_{bn}g_m^2K_1, \\ S_{ihvh^*} &= 4kTR_{bn}g_mK_2, \end{aligned} \tag{5.15}$$

where

$$\begin{aligned} &g_m = 2(g_{m1}+g_{m2}),\ R_{bn} = [R_1 + R_2(1-\lambda_c)^2]/2, \\ &K_1 = \frac{R_2/2}{R_{bn}}(\lambda_c-\lambda_{gm})^2,\ K_2 = \frac{R_2/2}{R_{bn}}2(1-\lambda_c)(\lambda_c-\lambda_{gm}). \end{aligned} \tag{5.16}$$

We have lumped $R_1$, $R_2$, $\lambda_{gm}$ and $\lambda_c$ into three model parameters $R_{bn}$, $K_1$ and $K_2$. The following observations are noted:

- The thermal resistance $R_{bn}$ defined in (5.16) is actually the lumped intrinsic base resistance $r_{bi}$ of Fig. 5.6 . To provide this, we examine the BE input impedance of Fig. 5.6

$$\begin{aligned} Z_{BE} &= \frac{1}{2}\left[R_1 + \frac{1 + j\omega C_2 R_2}{j\omega(C_1 + C_2) - \omega^2 C_1 C_2 R_2}\right] \\ &\approx \frac{1}{2}\left[R_1 + R_2\left(\frac{C_2}{C_1 + C_2}\right)^2\right] + \frac{1}{j\omega(2C_1 + 2C_2)} \\ &= \left[R_1 + R_2(1 - \lambda_c)^2\right]/2 + \frac{1}{j\omega(2C_1 + 2C_2)} \\ &= r_{bi} + \frac{1}{j\omega(2C_1 + 2C_2)}. \end{aligned} \tag{5.17}$$

  (5.17) means that $Z_{BE}$ can be modeled by a resistance in series with total BE capacitance. Such resistance essentially is $r_{bi}$, and clearly equal to the $R_{bn}$ in (5.16). However, the $R_{bn}$ needed to fit experimental noise data is different from the $r_{bi}$ extracted either based on QS or NQS equivalent circuit as detailed below.

- According to stochastic physics, the normalized correlation should not exceed unity [2], meaning $K_2^2 \leq K_1$. If BE fringe effect is not taken in account, i.e. $\lambda_c = \lambda_{gm}$, then $K_1 = K_2 = 0$. The new model reduces to $4kTR_{bn} \approx 4kTr_{bi}$.

Fig. 5.7 shows the simulated base hole noise in hybrid representation with the new model at $V_{BE}$=0.90V. Note that $\Re(S_{ihvh*}) > 0$, which is consistent with $g_{m1}/C_1 < g_{m2}/C_2$. The spikes at low frequencies can be modeled at extra complexity if $g_{be}$ is included in Fig. 5.6. However, the spikes will disappear in chain representation due to the $Y_{11}$ factor in (5.8), which decreases as frequency decreases.

Fig. 5.8 shows the modeling results in chain representation using (5.8) at $V_{BE}$=0.90V. The new model correctly models $S_{va}$ and $\Im(S_{iava*})$. Note that the simulated $S_{ia}$ and $\Re(S_{iava^*})$ are nonzero at low frequencies. They are zero in the new model because $g_{be}$ was neglected. These low frequency errors are negligible compared to the large value of base electron noise and emitter

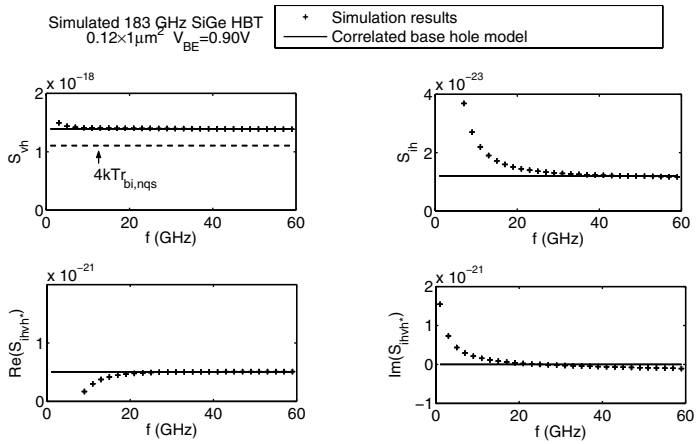


Figure 5.7: Comparison of simulation and new model for base hole noise in hybrid representation at one bias $V_{BE}$=0.90V.

hole noise. $S_{va}$ and $\Im(S_{iava*})$, however, are correctly modeled. The small error in $\Re(S_{iava*})$ is not important as $\Re(S_{iava*}) << \Im(S_{iava*})$.

**Bias dependence of $K_1$ and $K_2$**

We need to investigate the bias dependence of $K_1$ and $K_2$ because of the unknown bias dependence of $\lambda_c$ and $\lambda_{gm}$. We examined two SiGe HBTs simulated by DESSIS. One has 85 GHz peak $f_T$ and the other has 183 GHz peak $f_T$.

Fig. 5.9 (a) shows the bias dependence of $K_1$ for the two simulated devices. $K_1$ is nearly constant around peak $f_T$ for each device. For low biases, $S_{ih}$ is not important due to small $g_m$, hence the final noise is not sensitive to $K_1$. Further, the new model is proposed to improve noise modeling for biases before $f_T$ roll off, the $K_1$ value of peak $f_T$ bias can be used for all biases. Fig. 5.9 (b) shows the bias dependence of $K_2$ for the two devices. Again $K_2$ is nearly constant around peak $f_T$. Similarly, the $K_2$ value of peak $f_T$ bias can be used for all biases. Because of the weak bias dependence of $K_1$ and $K_2$, according to (5.15), $S_{ih}$ and $S_{ihvh^*}$ go to zero at low biases due to small $g_m$. The correlation of $v_h$ and $i_h$ affects mainly the biases around peak $f_T$.

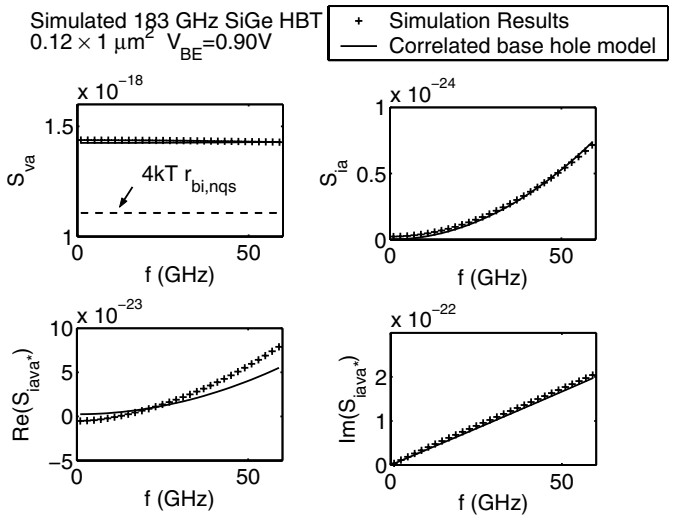


Figure 5.8: Comparison of simulation and new model for base hole noise in chain representation at one bias $V_{BE}$=0.90V.

### 5.2.3 $R_{bn}$, instead of $r_{bi}$, as base noise resistance

In DESSIS based microscopic noise simulation, the intrinsic base hole noise in hybrid representation can be obtained by integration of hole noise within intrinsic base. $R_{bn}$ can then be determined from $S_{v_h}/4kT$ according to (5.15). The $R_{bn}$ obtained is different from $r_{bi}$, no matter NQS or QS equivalent circuit is used. Fig. 5.13 shows $R_{bn}$ and $r_{bi}$ obtained using simulation for the 183 GHz SiGe HBT. Two different $r_{bi}$ extracted based on QS and NQS equivalent circuits are shown. The QS $r_{bi}$, extracted using circle method overestimates $R_{bn}$ at low biases and underestimates $R_{bn}$ at biases around peak $f_T$. The NQS $r_{bi}$, which is more physical, has a value close to $R_{bn}$ at low biases, however, underestimates $R_{bn}$ at high biases. It can also be observed that $R_{bn}$ has a weak bias dependence. Therefore $R_{bn}$ can be modeled as a constant, whose value can be approximated by the $r_{bi}$ value based on NQS equivalent circuit at *low* biases.

Experimentally, $R_{bn}$ can be extracted by fitting $R_n$, as detailed below. The difference between $R_{bn}$ and $r_{bi}$ was also observed using noise simulation in [46], where the total base resistance was

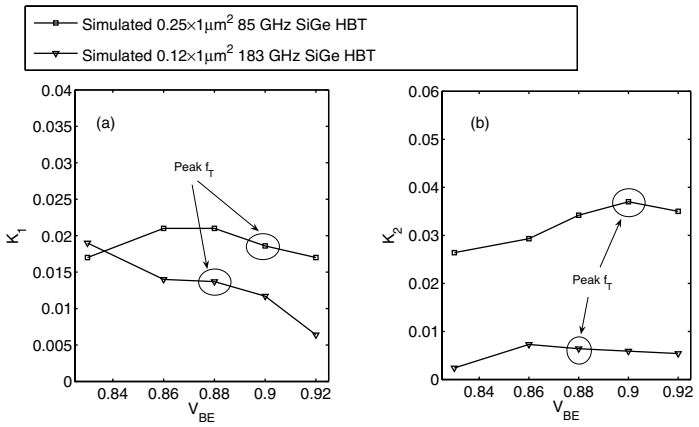


Figure 5.9: (a) $K_1$ extracted for simulated 85 GHz and 183 GHz peak $f_T$ SiGe HBTs. (b) $K_2$ extracted for simulated 85 GHz and 183 GHz peak $f_T$ SiGe HBTs

used. To our knowledge, at present, the physics behind such difference is not understood and needs further investigation.

## 5.3 Improved physical noise model

Our new noise model, the combination of improved electron noise and base hole noise models, can be implemented for SiGe HBTs with four model parameters, $\tau_c$, $R_{bn}$, $K_1$ and $K_2$. Details are given below.

### 5.3.1 Implementation technique

S-parameters and noise parameters are measured for SiGe HBTs from three generations of processes. The individual HBTs measured here have peak $f_T$ of 50 GHz, 90GHz and 160 GHz. Note that these experimental devices do not exactly correspond to the DESSIS simulated devices. Two devices of different emitter length from each generation are used, which allow us to investigate emitter length scaling. The S-parameters are measured on-chip using a 8510C Vector Network Analyzer (VNA) from 2-26 GHz. The noise parameters are measured using an ATN NP5 system

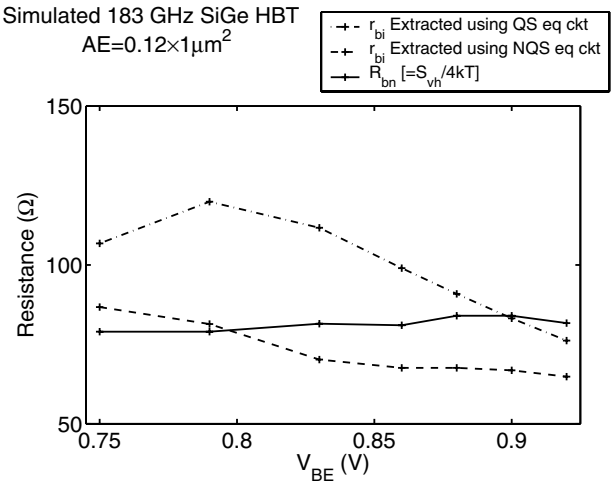


Figure 5.10: Comparison between thermal resistances $R_{bn}$ and small signal resistance $r_{bi}$.

for the same frequency range. Both S-parameters and noise parameters are de-embedded with standard OPEN/SHORT structures. The measurement is made across a wide biasing current range up to $f_T$ roll off point.

We first determine the equivalent circuit parameters from measured S-parameters for each bias using our direct extraction method described in Chapter 3. Excellent fitting of measured S-parameters is achieved across a wide biasing current range for all of the frequencies measured. The extracted biasing dependence of circuit parameters is consistent with device physics based expectations. The next step is to determine the four noise model parameters $\tau_c$, $R_{bn}$, $K_1$ and $K_2$. For DESSIS simulation data, they can be extracted directly. For experimental data, their values are determined by fitting the noise parameters. This is achievable as different model parameters affect different noise parameters as detailed below.

### 5.3.2 Modeling results

In this section, we show the modeling results for three generations of SiGe HBTs respectively. Emitter length scaling is also examined. Finally we summarize the effect of model parameters on noise parameters.

**50 GHz SiGe HBTs**

Fig. 5.11 shows the noise parameters versus frequency for an emitter area $A_E = 0.24 \times 20 \times 2\ \mu\text{m}^2$ SiGe HBT with 50 GHz peak $f_T$. $I_C$=19.4 mA. The solid line and dot line represent the results of using improved base hole model and electron model with $\tau_c$=0 ps and $\tau_c$=0.8 ps respectively. The dash dot line is calculated using $4kTr_{bi}$ for base hole noise and brutal use of van Vliet model for electron noise. The dash line is the result of using $S_{ib} = 2qI_b$, $S_{ic} = 2qI_c$, which is referred as SPICE model. Fig. 5.12 plots the noise parameters versus $I_c$ for the same

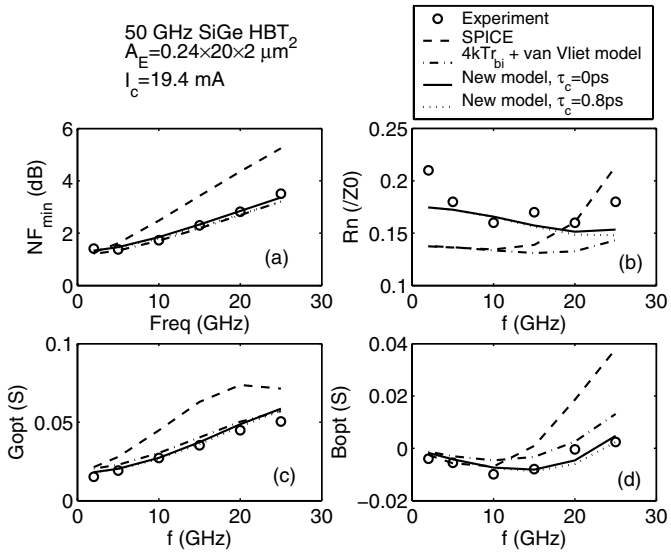


Figure 5.11: Noise parameters versus frequency for $A_E = 0.24 \times 20 \times 2\mu\text{m}^2$ 50 GHz SiGe HBT at $I_c$=19.4 mA.

device at $f$=15 GHz. The solid line is for the new model. The dash line is for the SPICE model.

The dot dash line is for the brutal use of van Vliet model with $4kTr_{bi}$ hole noise. As shown by

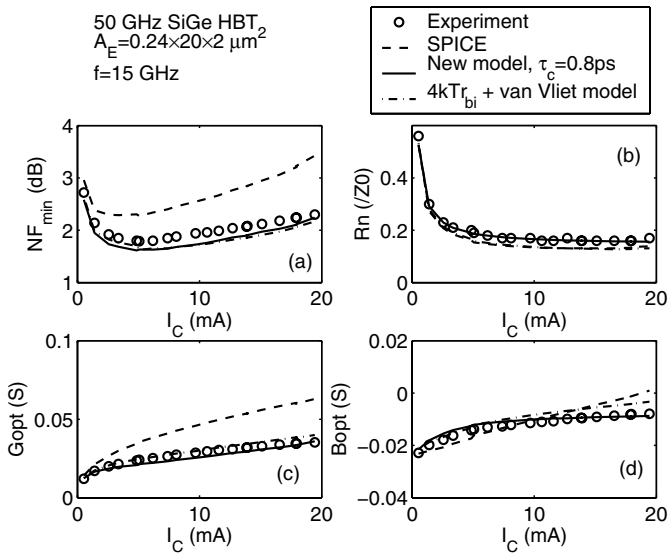


Figure 5.12: Noise parameters versus $I_C$ for $A_E = 0.24 \times 20 \times 2$ $\mu$m$^2$ 50 GHz SiGe HBT at f=15 GHz.

Fig. 5.11 and Fig. 5.12, the SPICE model overestimates $NF_{min}$ and $G_{opt}$. Compared to the van Vliet model with $4kTr_{bi}$, the new model is clearly better in modeling $R_n$ and $B_{opt}$, and provides excellent fitting for all noise parameters overall. We can make the following observations on the various effects involved:

- CB SCR effect

  $\tau_c$ has no significant effect. For this device, the total transit time $\tau_{tr}$ is 2.1 ps, which is dominated by base transit time. Therefore the brutal use of van Vliet model does not cause noticeable error.

- Fringe BE junction effect

  We find the fringe effect mainly affects $B_{opt}$ through correlation parameter $K_2$. An inspection of the difference between the solid line and the dash dot line in Fig. 5.11 (d) shows that the

correlation of base hole noise decreases $B_{opt}$. Fig. 5.12 (d) shows that such reduction can improve $B_{opt}$ modeling at high current levels.

- $R_{bn}$ instead of $r_{bi}$ as base noise resistance

  Since we choose small value for $K_1$ i.e. $K_1 = K_2^2$ as shown in Table 5.2, improvement of $R_n$ fitting is mainly achieved by choosing appropriate $R_{bn}$ value. A bias independent $R_{bn}$ is shown to be enough. Fig. 5.13 shows $R_{bn}$ together with $r_{bi}$ for the device examined. Two different $r_{bi}$ extracted based on QS and NQS equivalent circuits are shown. $R_{bn}$ is close to the low current $r_{bi}$ values and is larger than $r_{bi}$ at high current levels. As shown by Fig. 5.11

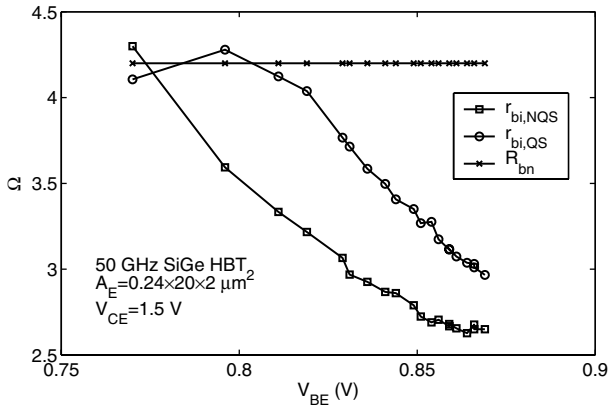


Figure 5.13: Comparison between thermal resistances $R_{bn}$ and small signal resistance $r_{bi}$.

(b) and Fig. 5.12 (b), a larger $R_{bn}$ increases $R_n$ at all frequencies and all biases. The $R_n$ curve is shifted upward in parallel.

**160 GHz SiGe HBTs**

Fig. 5.14 shows the noise parameters versus frequency for an $A_E = 0.12 \times 18$ $\mu$m$^2$ 160 GHz peak $f_T$ SiGe HBT. $I_c$=11.7 mA. The solid line and dot line represent the results of using improved base hole model and electron model with $\tau_c$=0.5 ps and $\tau_c$=0 ps respectively. The dash dot line is the result of new model with $K_1 = K_2 = 0$ and $\tau_c = 0.5$ ps. The dash line is the result of SPICE

model. For $R_n$, the dot line overlaps with the solid line. For $G_{opt}$, all of the lines almost overlap together and give good fitting. Fig. 5.15 plots the noise parameters versus $I_c$ for the same 160 GHz

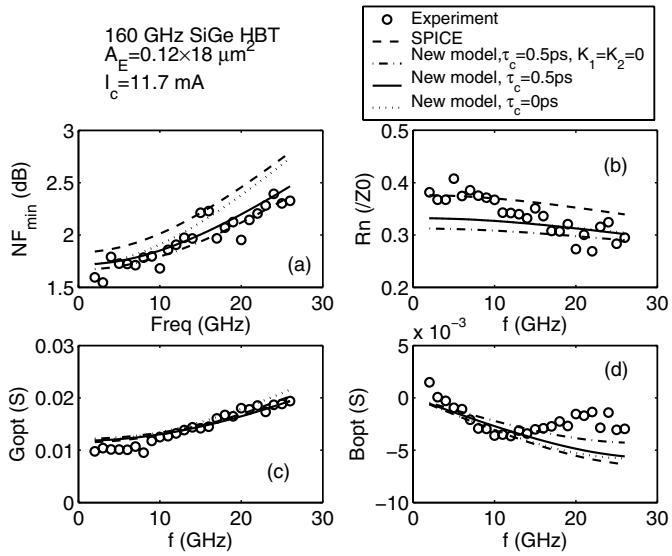


Figure 5.14: Noise parameters versus frequency for $A_E = 0.12 \times 18\ \mu\text{m}^2$ 160 GHz SiGe HBT at $I_c$=11.7 mA.

SiGe HBT at $f$=26 GHz. The line meanings are exactly the same as in Fig. 5.14. We can examine the various effects:

- CB SCR effect

  Fig. 5.14 (a) shows that $\tau_c$ reduces $NF_{min}$ at high frequencies as illustrated by the difference between the solid line and the dot line. Such reduction becomes more significant at high current levels as shown by Fig. 5.15 (a). Actually, the total transit time of this device is 0.58 ps. The 0.5 ps $\tau_c$ thus has noticeable impact on $NF_{min}$.

- Fringe BE junction effect

  Comparing the dash dot line and the solid line in Fig. 5.14 (d), we again find that the correlation parameter $K_2$ reduces $B_{opt}$. However because of the small value of $B_{opt}$ (<0.005) for

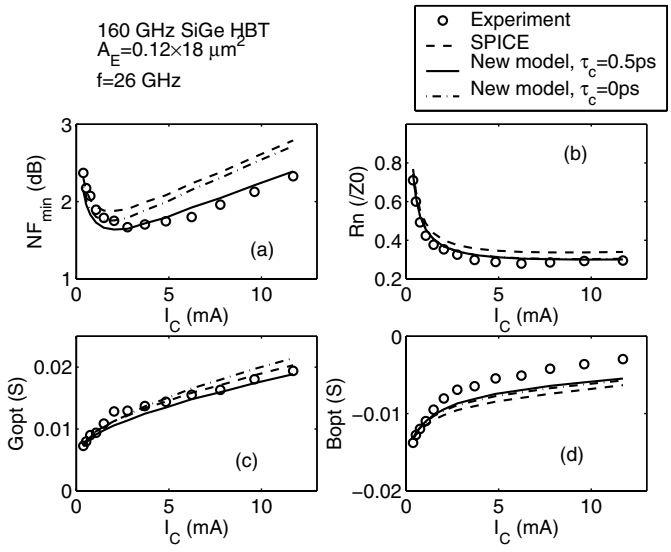


Figure 5.15: Noise parameters versus $I_c$ for $A_E = 0.12 \times 18$ $\mu$m$^2$ 160 GHz SiGe HBT at f=26 GHz.

this device, and the noisiness of measurement data, it is difficult to evaluate the importance of the fringe effect.

- $R_{bn}$ instead of $r_{bi}$ as base noise resistance

  $R_n$ fitting process shows that we need $R_{bn} < r_{bi}$ for this device. Consequently, the new model gives smaller $R_n$ as shown in Fig. 5.14 (b). The bias dependences for high frequencies are improved, as shown in Fig. 5.15 (b).

**90 GHz SiGe HBTs**

Fig. 5.16 shows the noise parameters versus frequency for $0.12 \times 20 \times 4$ Fig. 5.17 shows the noise parameters versus $I_C$ for $0.12 \times 20 \times 4$ 90 GHz SiGe HBT at f=20 GHz. The impact of CB SCR is between its impacts on the former two generations. The impact of the fringe effect is similar to that observed in 50 GHz device. For this generation, $R_{bn}$ is close to $r_{bi}$. Overall, the new

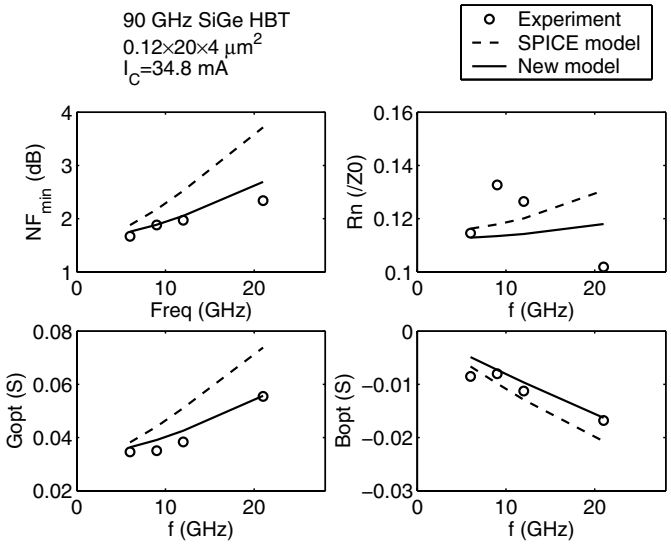


Figure 5.16: Noise parameters versus frequency for 0.12 × 20 × 4 90 GHz SiGe HBT at $I_C$=34.8 mA.

model gives excellent noise parameter fittings for all measured frequencies and biases before $f_T$ roll off.

### 5.3.3 Geometry scaling

Here we examine emitter length (LE) scaling. Ideally, $\tau_c$ should be constant versus LE. $K_1$ and $K_2$ should be also constant versus LE as the partition factor $\lambda_C$ and $\lambda_{gm}$ are independent on LE. $R_{bn}$ should scale closely like a resistance as discussed in [46] using noise simulation. Excellent fittings have been obtained for scaled devices of three generations. Figs. 5.18- 5.20 plots noise parameters versus frequency for scaled 50 GHz, 90 GHz and 160 GHz devices respectively. The solid line is the result of a high bias and the dash line is the result of a low bias. The experimental data has been well modeled for both biases of each generation.

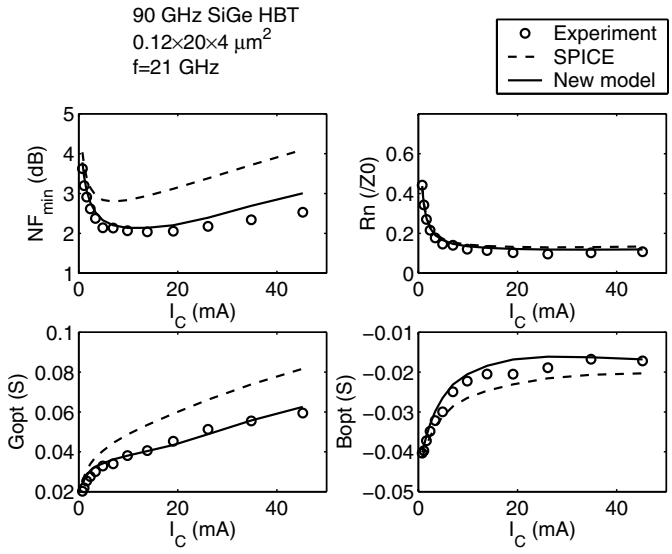


Figure 5.17: Noise parameters versus $I_C$ for 0.12 × 20 × 4 90 GHz SiGe HBT at f=20 GHz.

### 5.3.4 Model parameter impacts and extraction guidelines

- $\tau_c$ reduces high frequency $NF_{min}$ for high biases as shown by Fig. 5.14 (a) and Fig. 5.15 (a). It has more significant effect for highly scaled generations where $\tau_c > \tau_b$. The initial value can be estimated with $\tau_{tr}$. Its final value can be determined by $NF_{min}$ fitting.

- $R_{bn}$ mainly affects $R_n$ for all frequencies and all biases. How $R_{bn}$ compares to $r_{bi}$ depends on technology generation as shown by Fig. 5.12 (b) and Fig. 5.15 (b). Its initial value can be estimated with $r_{bi}$ at low current levels, and finally determined by $R_n$ fitting.

- $K_2$ reduces $B_{opt}$ for high biases and has little effect on other parameters as shown by Fig. 5.12. $K_2$, which involves $\lambda_C$, $\lambda_{gm}$ and $R_2/R_{bn}$ can be estimated with simulation. Experimentally, a small value, e.g. 0.01, should be used as initial guess. Its final values is determined by high current level $B_{opt}$ fitting.

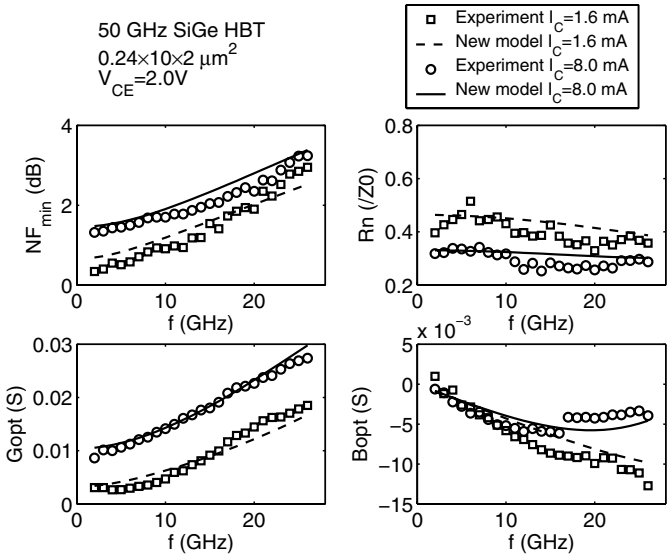


Figure 5.18: Noise parameters versus frequency for scaled 50 GHz SiGe HBTs ($A_E = 0.24 \times 10 \times 2\mu\text{m}^2$).

- $K_1$ can increase $NF_{min}$ and $R_n$ as shown by Fig. 5.14 (a) and (b). However, in model implementation, we choose $K_1 = K_2^2$ to simplify parameter determination, which is generally satisfactory.

Table 5.2 summarizes the model parameters for the previous results. $r_{bi}$ and $r_{bx}$ are also shown.

Table 5.2: Model parameters, $r_{bi}$* and $r_{bx}$* for reference

| $f_T$ | Device | $\tau_c$ | $K_1$ | $K_2$ | $R_{bn}$ | $r_{bi}$* | $r_{bx}$* |
|---|---|---|---|---|---|---|---|
| GHz | $\mu m^2$ | ps | - | - | Ω | Ω | Ω |
| 50 | 0.24 × 10 × 2 | 0.8 | 0.002 | 0.045 | 6.2 | 5.4 | 3.75 |
| | 0.24 × 20 × 2 | | | | 4.2 | 2.7 | 2.4 |
| 90 | 0.12 × 8 × 4 | 0.8 | 0.02 | 0.1 | 3.0 | 3.0 | 1.52 |
| | 0.12 × 20 × 4 | | | | 1.2 | 1.2 | 3.67 |
| 160 | 0.12 × 12 | 0.5 | 0.02 | 0.1 | 7.5 | 11.1 | 6.10 |
| | 0.12 × 18 | | | | 4.0 | 7.0 | 4.77 |

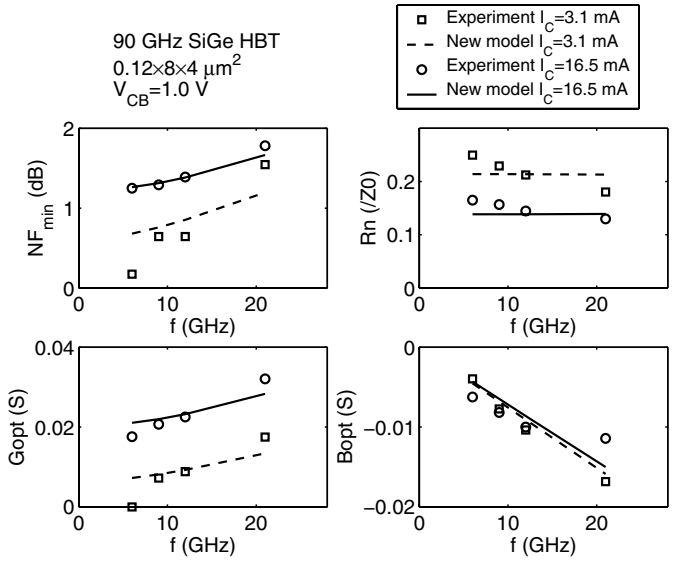


Figure 5.19: Noise parameters versus frequency for scaled 90 GHz SiGe HBTs ($A_E$=0.12 × 8 × 4$\mu m^2$).

## 5.4 Summary

We have presented an improved RF noise model for SiGe HBTs using NQS equivalent circuit. The van Vliet model has been extended to include both emitter hole noise and CB SCR effect for modern BJTs. The CB SCR delay time decreases high frequency $NF_{min}$ for high biases. The base hole noise is modeled by a noise voltage source and a correlated noise current source in hybrid representation due to fringe BE junction effect. The correlation between two noise sources decreases $B_{opt}$. The base noise resistance $R_{bn}$ is not always the same as the intrinsic base resistance $r_{bi}$, which cannot be explained by fringe effect. Model parameter extraction guidelines are given. The utility of the model has been demonstrated using experimental data of SiGe HBTs from three generations.

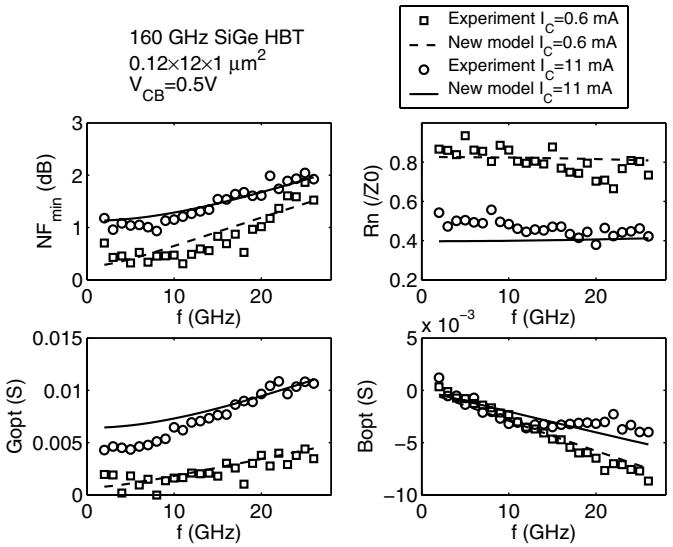


Figure 5.20: Noise parameters versus frequency for scaled 160 GHz SiGe HBTs ($A_E$=0.12 × $12\mu m^2$).

# BIBLIOGRAPHY


[1] J. D. Cressler and G. Niu, *Silicon-Germeanium Heterojunction Bipolar Transistors*. Artech House, 2003.

[2] K. Xia, G. Niu, D. Sheridan, and S. Sweeney, "Frequency and bias-dependent modeling of correlated base and collector current rf noise in sige hbts using quasi-static equivalent circuit," *IEEE Trans. Electron Devices*, vol. 53, pp. 515–522, March 2006.

[3] K. Xia, G. Niu, D. Sheridan, and W. E. Ansley, "Ratio based direct extraction of small-signal parameters for sige hbts," *Proc. of the IEEE BCTM*, pp. 144–147, September 2004.

[4] K. Xia, G. Niu, D. Sheridan, and S. Sweeney, "Input non-quasi static effect on small signal parameter extraction and noise modeling for sige hbts," *Proc. of the IEEE BCTM*, pp. 180–183, October 2005.

[5] K. Xia and G. Niu, "Impact of collector-base space charge region on rf noise in bipolar transistors," *Proc. of the IEEE BCTM*, pp. 166–169, October 2006.

[6] K. Xia and G. Niu, "Modeling of intrinsic base majority carrier thermal noise for sige hbts including fringe be junction effect," *Proc. of the IEEE BCTM*, pp. 283–286, October 2006.

[7] K. Xia, G. Niu, D. Sheridan, and S. Sweeney, "Emitter geometry scaling of rf noise in sige hbts," *Proc. of the IEEE SiRF*, pp. 16–19, January 2006.

[8] K. Xia and G. Niu, "Small signal parameter extraction for sige hbts including input non-quasistatic effect," *to be published*, 2006.

[9] K. Xia, G. Niu, and S. Sweeney, "Improving rf noise modeling for high speed sige hbts by including cb scr effect and fringe be junction effect based on non-quasistatic equivalent circuitt," *to be published*, 2006.

[10] H. Kroemer, "Zur theorie des diffusions und des drifttransistors. part iii," *Archiv der Elektrischen Ubertragungstechnik*, vol. 8, pp. 499–504, 1954.

[11] H. Kroemer, "Quasielectric and quasimagnetic fields in nonuniform semiconductors," *RCA Review*, vol. 18, pp. 332–342, 1957.

[12] G. Freeman, B. Jagannathan, S. J. Jeng, J. S. Rieh, A. Stricker, D. Ahlgren, and S. Subbanna, "Transistor design and application considerations for > 200-ghz sige hbts," *IEEE Trans. Electron Devices*, vol. 50, pp. 645–655, 2003.

[13] H. N. Yu, "Transistor with limited-area base-collector junction," *U. S. Patent Re. 27- 045*, no. Feb. 2, 1971.

[14] M. Nandakumar, A. Chatterjee, S. Sridhar, K. Joyner, M. Rodder, and I. C. Chen, "Shallow trench isolation for advanced ulsi cmos technologies," *Technical Digest of the IEEE IEDM*, pp. 133–136, 1998.

[15] C. T. Kirk, "A theory of transistor cutoff frequency ($f_t$) falloff at high current densities," *IEEE Trans. Electron Devices*, pp. 164–174, November 1962.

[16] S. S. Iyer, G. L. Patton, S. L. Delage, S. Tiwari, and J. M. C. Stork, "Silicon-germanium base heterojunction bipolar transistor by molecular beam epitaxy," *Technical Digest of the IEEE IEDM*, pp. 874–876, 1987.

[17] J. S. Rieh, D. Greenberg, M. Khater, K. T. Schonenberg, J. J. Jeng, F. Pagette, T. Adam, A. Chinthakindi, J. Flokey, B. Jagannahan, J. Johnson, R. Krishnasamy, D. Sanderson, C. Schnabel, P. Smith, A. Sricker, S. Sweeney, K. Caed, T. Yanagisawa, D. Ahlgren, K. Stein, and G. Freeman, "Sige hbts for millimeterwave applications with simultaneously optimized $f_t$ and $f_{max}$," *Proceedings of the IEEE RFIC symposium*, pp. 395–398, 2004.

[18] J. S. Rieh, B. Jagannathan, D. Greenberg, M. Meghelli, A. Rylyakov, F. Guarin, Z. Yang, D. Ahlgren, G. Freeman, P. Cottrell, and D. Harame, "Sige heterojunction bipolar transistors and circuits toward terahertz communication applications," *IEEE Trans. Microwave Theory and Techniques*, vol. 52, pp. 2390–2408, 2004.

[19] J. D. Cressler, ed., *Silicon Heterojunction Handbook - Materials, Fabrication, Devices, Circuits, and Applications of SiGe and Si Strained-Layer Epitaxy*. CRC Press, Taylor & Francis Group, 2006.

[20] H. A. Haus, W. R. Atkinson, W. H. Fonger, W. W. Mcleod, G. M. Branch, W. A. Harris, E. K. Stodola, W. B. D. Jr., S. W. Harrison, and T. E. Talpey, "Representation of noise in linear two ports," *Proc. IRE*, vol. 48, pp. 69–74, January 1960.

[21] C. M. van Vliet, "Macroscopic and microscopic methods for noise in devices," *IEEE Trans. Electron Devices*, vol. 41, pp. 1902–1915, November 1994.

[22] F. Bonani and G. Ghione, *Noise in Semiconductor Devices: Modeling and Simulation – Springer Series in Advanced Microelectronics*. Springer Series in Advanced Microelectronics, Berlin, Germany: Springer Verlag, 2001.

[23] M. Bixon and R. Zwanzig, "Boltzmann-langevin equation and hydrodynamic fluctuations," *Phys. Rev.*, vol. 187, p. 267, 1969.

[24] R. F. Fox and G. E. Uhlenbeck, "Contribution to nonequilibrium thermodynamics. ii fluctuation theory for the boltzmann equation," *Phys. Fluids.*, vol. 13, p. 2881, 1970.

[25] S. V. Gantsevich, V. L. Gurevich, and R. Katilius, "Theory of fluctuations in nonequilibrium electron gas," *II Nuovo Cimento (Rivista)*, vol. 2, pp. 1–87, 1979.

[26] J. P. Nougier and J. C. Vassiere, "Fluctuations of the hot-carrier state occupancy function in homogeneous semiconductors," *Phys. Rev.*, vol. B37, pp. 8882–8887, 1988.

[27] A. Einstein, "On the motion of small particles suspended in liquids at rest required by the molecular-kinetic theory of heat," *Annalen der Physik*, vol. 17, pp. 549–560, 1905.

[28] M. P. Langevin, "Sur la theorie du mouvement brownien, in english: On the theory of brownian motion," *C. R. Acad. Sci. (Paris)*, vol. 146, pp. 530–533, 1908.

[29] G. E. Uhlenbeck and L. S. Ornstein, "On the theory of the brownian motion," *Phys. Rev.*, vol. 36, pp. 823–841, 1930.

[30] S. Chandrasekar, "Stochatic problems in physics and astronomy," *Rev. Modern Phys.*, vol. 15, pp. 1–89, 1943.

[31] M. Reisch, *High-Frequency Bipolar Transistors*. Springer Series in Advanced Microelectronics, Berlin, Germany: Springer Verlag, 2002.

[32] C. W. Gardiner, *Handbook of stochastic methods*. New York: Springer-Verlag, 2nd edition ed., 1990.

[33] C. Jungemann, B. Neinhus, and B. Meinerzhagen, "Hierarchical 2-d dd and hd noise simulations of si and sige devices - part i: theory," *IEEE Trans. Electron Devices*, vol. 49, pp. 1250–1257, July 2002.

[34] W. Shockley, J. A. Copeland, and R. P. James, "The impedance-field method of noise calculation in active semiconductor device," *Quantum Theory of Atoms, Molecules, and the Solid State, P.O. Lowdin, Ed. New York: Academic*, pp. 537–563, 1966.

[35] K. M. van Vliet, "Noise sources in transport equations associated with ambipolar diffusion and shockley-read recombination," *Solid state electronics*, vol. 13, no. 5, p. 649, 1970.

[36] J. T. Winkel, "Extended charge-control model for bipolar transistor," *IEEE Trans. Electron Devices*, vol. 20, pp. 389–394, April 1973.

[37] J. T. Winkel, "Drift transistor, simplified electrical characterization," *Radio Electron. Eng.*, vol. 36, pp. 280–288, 1959.

[38] J. Seitchik, A. Chatterjee, and P. Yang, "An accurate bipolar model for large signal transient and ac applications," *IEDM Tech. Dig.*, pp. 244–247, 1987.

[39] K. M. van Vliet, "General transport theory of noise in pn junction-like devices-i. three-dimensional green's function formulation," *Solid state electronics*, vol. 15, pp. 1033–1053, October 1972.

[40] K. M. van Vliet, "Markov approach to density fluctuations due to transport and scattering. i. mathmetical formalism," *J. math. Phys.*, vol. 12, p. 1981, 1971.

[41] J. C. J. Paasschens, "Compact modeling of the noise of a bipolar transistor under dc and ac current crowding conditions," *IEEE Trans. Electron Devices*, vol. 51, pp. 1483 –1495, September 2004.

[42] A. Vladimirescu, A. R. Newton, and D. O. Pederson, "Spice version 2 user's guide," tech. rep., University of California, Berkeley, September 1980.

[43] G. Niu, J. D. Cressler, S. Zhang, W. E. Ansley, C. S. Webster, and D. L. Harame, "A unified approach to rf and microwave noise parameter modeling in bipolar transistors," *IEEE Trans. Electron Devices*, vol. 48, pp. 2568 – 2574, November 2001.

[44] M. Rudolph, R. Doerner, L. Klapproth, and P. Heymann, "An hbt noise model valid up to transit frequency," *IEEE Trans. Electron Device Letters*, vol. 20, pp. 24– 26, January 1999.

[45] J. Moller, B. Heinermann, and F. Herzel, "An improved model for high-frequency noise in bjts and hbts interpolating between the quasi-thermal approach and the correlated-shot-noise model," *Proc. of the IEEE BCTM*, pp. 228–231, 2002.

[46] C. Jungemann, B. Neinhus, B. Meinerzhagen, and R. Dutton, "Investigation of compact models for rf noise in sige hbts by hydrodynamic device simulation," *IEEE Trans. Electron Devices*, vol. 51, pp. 956–961, June 2004.

[47] J. C. J. Paasschens, R. J. Havens, and L. F. Tiemeijer, "Modeling the correlation in the high frequency noise of bipolar transistors using charge partitioning," *Proc. of the IEEE BCTM*, pp. 221–224, 2003.

[48] Y. Cui, G. Niu, and D. L. Harame, "An examination of bipolar transistor noise modeling and noise physics using microscopic noise simulation," *Proc. of the IEEE BCTM*, pp. 225–228, 2003.

[49] A. van der Ziel and G. Bosman, "Accurate expression for the noise temperature of common emitter microwave transistor," *IEEE Trans. Electron Devices*, vol. 31, pp. 1280–1283, September 1984.

[50] R. Pucel, T. Daniel, A. Kain, and R. Tayrani, "A bias and temperature dependent noise model of heterojunction bipolar transistors," *Tech. Digest of IEEE MTT-S*, pp. 141–144, 1998.

[51] Q. Cai, J. Gerber, U. L. Rohde, and T. Daniel, "Hbt high-frequency modeling and integrated parameter extraction," *IEEE Trans. Microwave Theory and Techniques*, vol. 45, pp. 2493–2502, December 1997.

[52] J. Roux, L. Escotte, R. Plana, J. Graddeuil, S. Delage, and H. Blanck, "Small signal and noise model extraction technique for heterojunction bipolar transistor at microwave frequencies," *IEEE Trans. Microwave Theory and Techniques*, vol. 43, pp. 293–298, Febrary 1995.

[53] T. Daniel and R. Tayrani, "Dc and high frequenct models for heterojunction bipolar transistor," *IEEE GaAs IC symposium*, pp. 299–302, 1996.

[54] G. Niu, K. J. Xia, D.Sheridan, and D. L. Harame, "Experimental extraction and model evaluation of base and collector rf noise in sige hbts," *Proc. RFIC*, vol. 36, pp. 615–618, June 2004.

[55] J. M. M. Rios, L. M. Lunardi, S. Chandrasekhar, and Y. Miyamoto, "A self-consistent method for complete small-signal parameter extraction of inp-based heterojunction bipolar transistors(hbt's)," *IEEE Trans. Microwave Theory and Techniques*, vol. 45, pp. 39–45, January 1997.

[56] B. Li and S. Prasad, "Basic expressions and approximations in small-signal parameter extraction for hbt's," *IEEE Trans. Microwave Theory and Techniques*, vol. 47, pp. 534–539, May 1999.

[57] M. Sotoodeh, L. Sozzi, A. Vinay, A. H. Khalid, Z. Hu, and A. A. Rezazadeh, "Stepping toward standard methods of small-signal parameter extraction for hbt's," *IEEE Trans. Electron Devices*, vol. 47, pp. 1139–1151, June 2000.

[58] T. S. Horng, J. M. Wu, and H. S. Huang, "An extrinsic-inductance independent approach for direct extraction of hbt intrinsic circuit parameters," *IEEE Trans. Microwave Theory and Techniques*, vol. 49, pp. 2300–2305, December 2001.

[59] A. Ouslimani, J. Gaubert, H. Hafdallah, A. Birafane, P. Pouvil, and H. Leier, "Direct extraction of linear hbt-model parameters using nine analytical expression blocks," *IEEE Trans. Microwave Theory and Techniques*, vol. 50, pp. 218–221, January 2002.

[60] S. Bousnina, P. Mandeville, A. G. Kouki, R. Surridge, and F. M. Ghannouchi, "Direct extraction of linear hbt-model parameters using nine analytical expression blocks," *IEEE Trans. Microwave Theory and Techniques*, vol. 50, pp. 529–536, Febrary 2002.

[61] H. Chen, K. Chen, G. Huang, and C. Chang, "Small-signal modeling of sige hbts using direct parameter-extraction method," *IEEE Trans. Electron Devices*, vol. 53, pp. 2287–2295, September 2006.

[62] I. E. Getrew, "Modeling the bipolar transistors," tech. rep., Tektronix Inc., 1978.

[63] Z. Huszka, E. Seebacher, and W. Pflanzi, "An extended two-port method for the determination of the base and emitter resistance," *Proc. of the IEEE BCTM*, pp. 188–191, October 2005.

[64] U. Basaran and M. Berroth, "An accurate method to determine the substrate network elements and base resistance," *Proc. of the IEEE BCTM*, pp. 93–96, September 2003.

[65] S. Lee, "A simple method to extract intrinsic and extrinsic base-collector capacitances of bipolar transistors," *IEEE Trans. Electron Devices*, vol. 51, pp. 647–650, April 2004.

[66] M. W. Dvorak and C. R. Bolognesi, "On the accuracy of direct extraction of the heterojunction-bipolar-transistor equivalent-circuit model parameters $c_\pi$, $c_{BC}$, and $r_e$," *IEEE Trans. Microwave Theory and Techniques*, vol. 51, pp. 1640–1649, June 2003.

[67] I. S. Engineering, "Manual of dessis, ise tcad release 9.0," tech. rep., 2003.

[68] G. F. Niu, J. D. Cressler, U. Gogineni, and A. J. Joseph, "A new common-emitter hybrid-$\pi$ small-signal equivalent circuit for bipolar transistors with significant neutral base recombination," *IEEE Trans. Electron Devices*, vol. 46, pp. 1166–1173, June 1999.

[69] G. Niu, W. E. Ansley, S. M. Zhang, J. D. Cressler, C. S. Webster, and R. A. Groves, "Noise parameter optimization of uhv/cvd sige hbt's for rf and microwave applications," *IEEE Trans. Electron Devices*, vol. 46, pp. 1589–1597, August 1999.

[70] A. C. P. Sakalas, J. Herricht and M. Schroter, "Compact modeling of high frequency correlated noise in hbts," *Proc. of the IEEE BCTM*, pp. 279–282, October 2006.

[71] A. Huber, D. Huber, C. Bergamaschi, T. Morf, and H. Jackel, "Noise model of inp-ingaas shbts for rf circuit design," *IEEE Trans. Microwave Theory and Techniques*, vol. 50, July 2002.

[72] R. Pritchard, *Electrical Characteristics of Transistors*. New York: McGraw-Hill, 1967.

[73] Y. Shi, *Design and optimization of nano-scaled Silicon-Germanium heterojunction bipolar transistors*. Auburn University: PhD. dissertation, August 2005.

APPENDIX A

REPRESENTATION TRANSFORMATION FOR TWO-PORT NETWORK

## A.1 T-matrix for noise representation transformation

Table A.1: Transformation Matrices to Calculate Noise Matrices

| $T$ | | Original Representation: Y- | Original Representation: Z- | Original Representation: A- |
|---|---|---|---|---|
| Resulting | Y- | $\begin{bmatrix} 1 & 0 \\ 0 & 1 \end{bmatrix}$ | $\begin{bmatrix} Y_{11} & Y_{12} \\ Y_{21} & Y_{22} \end{bmatrix}$ | $\begin{bmatrix} -Y_{11} & 1 \\ -Y_{21} & 0 \end{bmatrix}$ |
| | Z- | $\begin{bmatrix} Z_{11} & Z_{12} \\ Z_{21} & Z_{22} \end{bmatrix}$ | $\begin{bmatrix} 1 & 0 \\ 0 & 1 \end{bmatrix}$ | $\begin{bmatrix} 1 & -Z_{11} \\ 0 & -Z_{21} \end{bmatrix}$ |
| | A- | $\begin{bmatrix} 0 & A_{12} \\ 1 & A_{22} \end{bmatrix}$ | $\begin{bmatrix} 1 & -A_{11} \\ 0 & -A_{21} \end{bmatrix}$ | $\begin{bmatrix} 1 & 0 \\ 0 & 1 \end{bmatrix}$ |

## A.2 Derivation of Noise Parameters

According to (1.4), we have

$$NF = \frac{S_s/N_s}{S_o/N_o} = \frac{N_o}{N_s G} = 1 + \frac{N_{added}}{N_s G} = 1 + \frac{N_{added}/G}{N_s}. \tag{A.1}$$

This means that $NF$ can be calculated at *any point* of circuit by 1 plus a ratio (Noise added by two-port network divided by noise from signal source). Fig. A.1 shows the circuit configuration used for derivation. We denote the input admittance of the two-port network as $Y_I$. $Y_S = G_S + jB_S$. We choose node B for derivation.

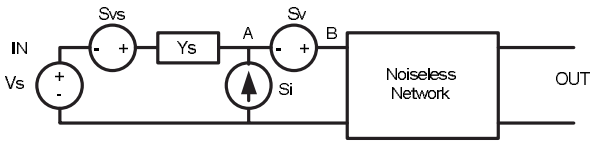


Figure A.1: Noise Figure

We have

$$v_{added} = v_a \frac{Y_S}{Y_I + Y_S} + \frac{i_a}{Y_I + Y_S}, \quad v_s = \frac{i_s}{Y_I + Y_S}.$$

which means

$$N_{added} \equiv < v_{added} v^*_{added} > = S_v \left| \frac{Y_S}{Y_I + Y_S} \right|^2 + \frac{S_i}{|Y_I + Y_S|^2} + \frac{2\Re(Y^*_S S_{iv^*})}{|Y_I + Y_S|^2},$$
$$N_s \equiv < v_s v^*_s > = \frac{4kTRe(Y_S)}{|Y_I + Y_S|^2} = \frac{4kTG_S}{|Y_I + Y_S|^2}.$$

Therefore

$$NF = 1 + \frac{S_v}{4kTG_S} \left[ \frac{S_i}{S_v} + 2\Re \left( Y^*_S \frac{S_{iv^*}}{S_v} \right) + |Y_S|^2 \right] \tag{A.2}$$

With some algebra maniplutation, (A.2) can be simplified into (1.5) with relations in (1.8). Note that generally we have two opposite values for $G_{opt}$ from a square root, however only the positive value is chosen because of the resistivity of signal source admittance.

# APPENDIX B

# APPROXIMATION OF INTRINSIC BASE RESISTANCE NOISE CONSIDERING CURRENT CROWDING EFFECT

## B.1 General Principles

The approximation for the intrinsic base resistance noise current PSD, $S_{irbi}$, is based on J. C. J. Paasschens's theorectical analysis of BJT noise considering both *dc* and *ac* crowding [41]. In [41], the intrinsic base resistance noise was described using $V_{B_xB_i}$, the *dc* voltage drop cross the equivalent base resistance representing *dc* current crowding. To avoid $V_{B_xB_i}$ extraction, we relate the intrinsic base resistance noise to its small signal value $r_{bi}$ and *dc* current $I_B$. This is helpful when modeling noise based on small signal equivalent circuit.

Carefully observing the $I_B$ and $S_{irbi}$ expressions for both circular and rectangular emitter BJTs, (see (37), (41), (52) and (56) in [41]), we found that all these terms are inversely proportional to $R_{BV}$ and the remaining part of these expressions excluding $R_{BV}$ only depends on $V_{B_xB_i}$. Here $R_{BV}$ is the low current limit of $V_{B_xB_i}/I_B$. Therefore we can make an approximation for $S_{irbi}$ using a linear combination of $4kTg_{bi}$ and $qI_B$ as

$$S_{irbi,appr} = (\lambda_1 4kTg_{bi} - \lambda_2 qI_B)\Delta f. \tag{B.1}$$

where $g_{bi} = 1/r_{bi}$. Note that the error is *independent* of $R_{BV}$. Therefore the two coefficients are general for any crowding strength. In the following we will obtain these two coefficients for circular and rectangular emitters respectively.

## B.2 Circular Emitter BJT

For circular emitter BJT [41],

$$I_B = \frac{V_T(e^{V_{B_x B_i}/V_T} - 1)}{R_{BV}}. \tag{B.2}$$

$g_{bi}$ is obtained by

$$g_{bi} = \frac{dI_B}{dV_{B_x B_i}} = \frac{e^{V_{B_x B_i}/V_T}}{R_{BV}}. \tag{B.3}$$

The base resistance noise is given in (2.75) by [41] Substitute (B.2), (B.3) and (2.75) into (B.1), one has

$$4\lambda_1 + \lambda_2 = 10/3, \tag{B.4}$$

$$\lambda_2 = 2/3. \tag{B.5}$$

This gives $\lambda_1 = 1$ and $\lambda_2 = 2/3$. Therefore, we get an exact expression for $S_{irbi}$ as

$$S_{irbi,appr} = \left[4kT/r_{bi} - 2qI_B/3\right] \Delta f. \tag{B.6}$$

To make (B.6) positive, we need

$$r_{bi} < 6(V_T/I_B) = 6r_{\pi,e}.$$

This is easily satisfied in practice.

### B.3 Rectangular Emitter BJT

For rectangular emitter BJT [41],

$$I_B = \frac{2V_T(e^{V_{B_x B_i}/V_T} - 1) + V_{B_x B_i}}{3R_{BV}}. \tag{B.7}$$

$g_{bi}$ is thus

$$g_{bi} = \frac{dI_B}{dV_{B_x B_i}} = \frac{2e^{V_{B_x B_i}/V_T} + 1}{3R_{BV}}. \tag{B.8}$$

The noise $S_{irbi}$ is given in (2.76) by [41] If $V_{B_x B_i} >> V_T$, $S_{irbi}$ will be proportional to $e^{V_{B_x B_i}/V_T}$, the same as $I_B$ and $g_{bi}$. Therefore the error using approximation (B.1) at large $V_{B_x B_i}$ will saturate to a constant. Because of the exponential term, $V_{B_x B_i} = 10V_T$ is sufficient to cause such saturation of error. Therefore we only need to consider $V_{B_x B_i} \in [0 \;\; 10V_T]$. We optimize $\lambda_1$ and $\lambda_2$ to minimize the error defined by

$$Err = |(S_{irbi,theory} - S_{irbi,appr})/S_{irbi,theory}|.$$

We found $\lambda_1 = 1.0149$ and $\lambda_2 = 0.6772$. The solid line in Fig. B.1 shows the error from approximations. The error is smaller than 1.5% for all $V_{B_x B_i}$. These two coefficients are very close to the values of the circular case. The dash line in Fig. B.1 shows the error using $\lambda_1 = 1$ and $\lambda_2 = 2/3$. The error is less than 3%. Therefore we can unify these two cases using (B.6) with little loss in accuracy. Fig. B.2 shows the ratio of calculated noise to the theoretical noise using this method and traditional $4kT/r_{bi}$ method. The error has been much decreased using the proposed method. For the SiGe HBTs used in this work, $V_{B_x B_i}/V_T$ is less than 0.8 at peak $f_T$, making the crowding effect indeed unimportant for practical purposes. This is in part by design, as the HBTs are typically designed to keep the crowding effect under control.

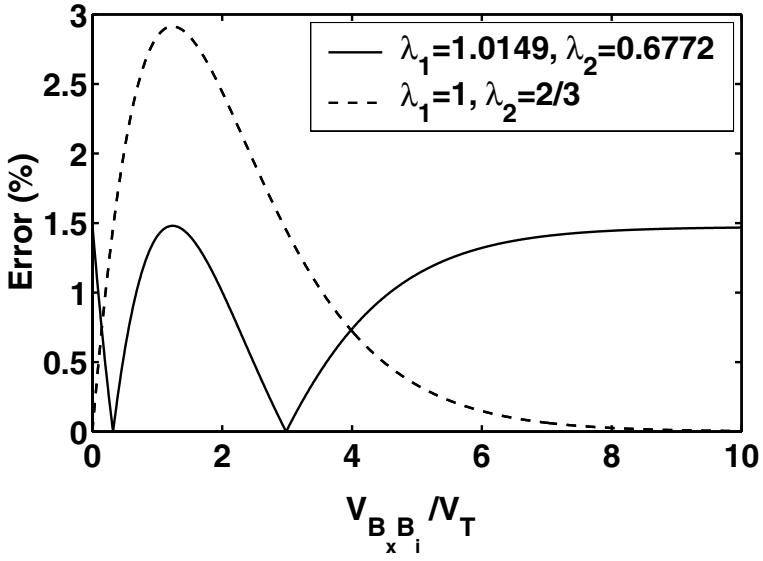


Figure B.1: Approximation induced error versus $V_{B_x B_i}$ for rectangular emitter BJT.

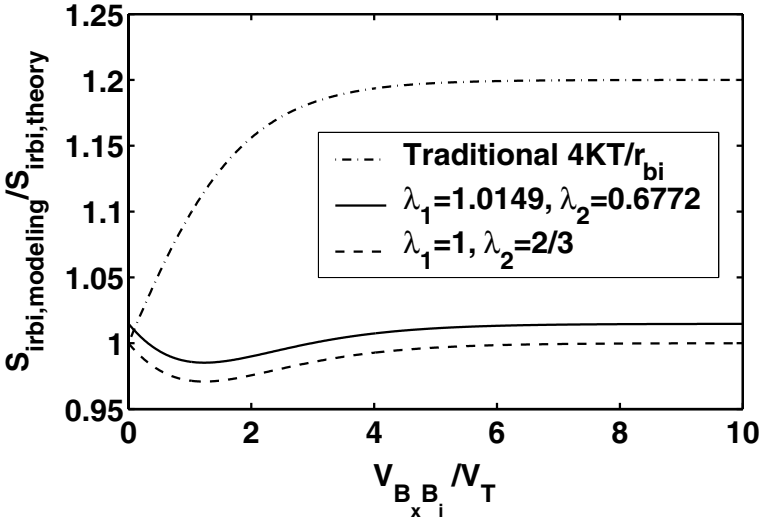


Figure B.2: Comparison between approximation method and the traditional $4kT/r_{bi}$ method for rectangular emitter BJT.

## APPENDIX C

## DERIVATION OF NQS DELAY TIME WITH CB SCR

We can drive (3.3) by approximating (3.2) with the functional form of (3.1) using Taylor expansion analysis method. We use Arabic numeral subscripts to indicate the order of the Taylor expansion coefficients, as was done in Section III. The first order coefficients for $\Im(Y_{11})$ without and with CB SCR delay are

$$\begin{aligned}
\Im(Y_{11}^{bs})_1 &= C_{bej} + C_{bed}^{b}, \\
\Im(Y_{11}^{al})_1 &= C_{bej} + C_{bed}^{b} + g_m\tau_c \equiv C_{bej} + C_{bed},
\end{aligned} \tag{C.1}$$

respectively. (C.1) means $C_{bed} = C_{bed}^{b} + g_m\tau_c$. With the definitions of $\tau_{tr}$ and $\tau_{tr}^{b}$, we obtain the $\tau_{tr}$ expression in (3.3). The second order coefficients of $\Re(Y_{21})$ for the base and the whole intrinsic transistor are

$$\begin{aligned}
\Re(Y_{21}^{bs})_2 &= g_m\tau_{tr}^{b}\tau_{in}^{b}, \\
\Re(Y_{21}^{al})_2 &= g_m\tau_{tr}\left[\tau_{in}^{b} + \tau_c\frac{\tau_{out}^{b} + 2\tau_c/3}{\tau_{tr}}\right] \equiv g_m\tau_{tr}\tau_{in}.
\end{aligned} \tag{C.2}$$

(C.2) directly gives the $\tau_{in}$ expression in (3.3). Similarly, by comparing $\Im(Y_{21}^{bs})_1$ and $\Im(Y_{21}^{al})_1$, we have $\tau_{in} + \tau_{out} = \tau_{in}^{b} + \tau_{out}^{b} + \tau_c$. With the $\tau_{in}$ expression already known, the $\tau_{out}$ expression in (3.3) can then be obtained through substraction.

# APPENDIX D

## ANALYTICAL Y-PARAMETERS

In the following, we derive the analytical Y-parameters for different blocks related to the small signal equivalent circuit in Fig. 3.4 using two methods.

### D.1 Manual Derivation of Analytical Y-parameters

We define $Y_I$ and $G_M$ as

$$Y_I \equiv g_{be} + j\omega C_{bej} + \frac{j\omega C_{bed}}{1 + j\omega C_{bed} r_d}, \quad G_M \equiv g_m e^{-j\omega\tau_d}. \tag{D.1}$$

We have

$$Y_{11}^{BI} = Y_I + j\omega C_{bci}, \quad Y_{12}^{BI} = -j\omega C_{bci}, \quad Y_{21}^{BI} = G_M - j\omega C_{bci}, \quad Y_{22}^{BI} = j\omega C_{bci}. \tag{D.2}$$

then

$$\begin{aligned} Y_{11}^{BIR} &= \frac{Y_I + j\omega C_{bci}}{1 + Y_I r_{bi} + j\omega C_{bci} r_{bi}}, \quad Y_{12}^{BIR} = \frac{-j\omega C_{bci}}{1 + Y_I r_{bi} + j\omega C_{bci} r_{bi}}, \\ Y_{21}^{BIR} &= \frac{G_M - j\omega C_{bci}}{1 + Y_I r_{bi} + j\omega C_{bci} r_{bi}}, \quad Y_{22}^{BIR} = \frac{j\omega C_{bci}(1 + Y_I r_{bi} + G_M r_{bi})}{1 + Y_I r_{bi} + j\omega C_{bci} r_{bi}}. \end{aligned} \tag{D.3}$$

We further define

$$\begin{aligned} &\Delta \equiv Y_{11}^{BIR} Y_{22}^{BIR} - Y_{12}^{BIR} Y_{21}^{BIR} + j\omega C_{bcx}(Y_{11}^{BIR} + Y_{22}^{BIR} + Y_{12}^{BIR} + Y_{21}^{BIR}) + j\omega C_{bex} Y_{22}^{BIR} - \omega^2 C_{bex} C_{bcx} \\ &T \equiv 1 + Y_{11}^{BIR} r_{bx} + Y_{22}^{BIR} r_c + \Delta r_{bx} r_c + j\omega(r_{bx} C_{bex} + r_{bx} C_{bcx} + r_c C_{bcx}), \end{aligned} \tag{D.4}$$

we have

$$Y_{11}^{BM} = \frac{Y_{11}^{BIR} + j\omega C_{bex} + j\omega C_{bcx} + \Delta r_c}{T}, \quad Y_{12}^{BM} = \frac{Y_{12}^{BIR} - j\omega C_{bcx}}{T},$$
$$Y_{21}^{BM} = \frac{Y_{21}^{BIR} - j\omega C_{bcx}}{T}, \quad Y_{22}^{BM} = \frac{Y_{22}^{BIR} + j\omega C_{bcx} + \Delta r_{bx}}{T}. \tag{D.5}$$

## D.2 MATLAB Code for Analytical Y-parameters Derivation

For the Taylor expansion analysis, $g_{be}$ is neglected.

```
% w    -- omega
% gbe  -- EB conductance
% Cd   -- EB diffusion capacitance
% Cj   -- EB depletion capacitance
% Cs   -- Cbci, Ci is a reserved symbol of MATLAB
% Cx   -- Cbcx
% Cbex -- extrinsic EB capacitance
% gm   -- transconductance
% t    -- total output delay time (tau_in+tau_out)
% Rb   -- rbi
% Rd   -- delay resistance rd
% Rc   -- rci+rcx
% Rx   -- rbx

clear all;
syms w gbe Cd Cj Cs Cx Cbex gm t Rb Rd Rc Rx real
YI=j*w*Cd/(1+j*w*Rd*Cd)+j*w*Cj;%+gbe;
GM=gm*exp(-j*w*t);
Ybci=j*w*Cs;
Ybcx=j*w*Cx;
Y=[YI+Ybci -Ybci
    GM-Ybci Ybci];
% Y -- Y-parameters of BI block

Z=inv(Y);
Z(1,1)=Z(1,1)+Rb;
% Z -- Z-parameters of BIR block

YY=inv(Z);
YY(1,1)=YY(1,1)+Ybcx+j*w*Cbex;
YY(1,2)=YY(1,2)-Ybcx;
YY(2,1)=YY(2,1)-Ybcx;
YY(2,2)=YY(2,2)+Ybcx;
simple(YY);
% YY -- Y-parameters of BM block without rbx

detYY=YY(1,1)*YY(2,2)-YY(1,2)*YY(2,1);
T=1+Rx*YY(1,1);
YYx(1,1)=YY(1,1)/T;
YYx(2,2)=(YY(2,2)+Rx*detYY)/T;
YYx(1,2)=YY(1,2)/T;
```

```
YYx(2,1)=YY(2,1)/T;
% YYx -- Y-parameters of BM block with rbx

detYY=YY(1,1)*YY(2,2)-YY(1,2)*YY(2,1);
T=1+Rx*YY(1,1)+Rc*YY(2,2)+detYY*Rx*Rc;
YYY(1,1)=(YY(1,1)+Rc*detYY)/T;
YYY(2,2)=(YY(2,2)+Rx*detYY)/T;
YYY(1,2)=YY(1,2)/T;
YYY(2,1)=YY(2,1)/T;
ZZZ=inv(YYY);
% YYY/ZZZ -- Y/Z-parameters of BX block
```

### D.3 MATLAB code for Taylor expansion

For (3.8)-(3.10),

```
AA=1/(ZZZ(2,2)-ZZZ(2,1));
BB=1/ZZZ(1,2);

imAA=taylor(imag(AA),w,2);
simple(imAA);
pretty(imAA);
% imAA -- the first order coefficient of Im(AA)

reAA=taylor(real(AA),w,3);
simple(reAA);
pretty(reAA);
% reAA -- the second order coefficient of Re(AA)

reBB=taylor(real(BB),w,1);
simple(reBB);
% reBB -- the zero order coefficient of Re(BB)
```

For (3.13)-(3.15) and (3.17)

```
imAA=taylor(imag(YYx(1,1)+YYx(1,2)),w,2);
simple(imAA);
pretty(imAA);
% imAA -- the first order coefficient of Im(Y11^BM+Y12^BM)

imAA=taylor(imag(YYx(2,1)-YYx(1,2)),w,2);
simple(imAA);
pretty(imAA);
% imAA -- the first order coefficient of Im(Y21^BM-Y12^BM)

imAA=taylor(imag(YYx(2,2)),w,2);
simple(imAA);
pretty(imAA);
% imAA -- the first order coefficient of Im(Y22^BM)

reAA=taylor(real(YYx(1,1)+YYx(1,2)),w,3);
simple(reAA);
pretty(reAA);
% imAA -- the second order coefficient of Re(Y11^BM+Y12^BM)
```

For (3.21)-(3.22), $g_{be}$ should be added, then the Y-parameters should be re-calculated.

```
imAA=taylor(imag(Y(1,1)+Y(1,2)),w,2);
simple(imAA);
pretty(imAA);
% imAA -- the first order coefficient of Im(Y11^BI+Y12^BI)

imAA=taylor(imag(Y(2,1)-Y(1,2)),w,2);
simple(imAA);
pretty(imAA);
% imAA -- the first order coefficient of Im(Y21^BI-Y12^BI)

reAA=taylor(real(Y(1,1)),w,1);
simple(reAA);
pretty(reAA);
% imAA -- the zero order coefficient of Re(Y11^BI)

reAA=taylor(real(Y(1,1))-gbe,w,3);
simple(reAA);
pretty(reAA);
% imAA -- the second order coefficient of Re(Y11^BI)
```

# APPENDIX E

## MATLAB CODE FOR SMALL SIGNAL PARAMETER EXTRACTION

The following MATLAB code extracts the small signal parameters for a 50 GHz SiGe HBT with $A_E = 0.24 \times 20 \times 2\ \mu m^2$.

```
HasCbi=0;  % Cbi is the crowding cap paralleled with rbi. 0: no Cbe
HasCrowdingnoise=0; % 0: Sirbi=4kT/rbi, otherwise 4kT/rbi-2qIb/3

% Data: Fixed Vce=1.5 V, Vbe=0.77-0.869 V, freq 2-26 GHz, num_bias=20;
% Data: peakfT 50GHz at bias 19. Ae=0.24x20x2 um^2. Open de-embedded.

load_data_26G;
f=Y_cell_exp{step}(:,1); Omega=2*pi*f;

%=============Deembedding Lb Lc Le =====
for step=1:1:num_bias
    Lb(step)=4.8e-11;
    Lc(step)=4.8e-11;
    Le(step)=1.12e-11;
    Ydlc=Y_cell_exp{step}(:,2:5);
    Zdlc=Y_to_Z(Ydlc);
    Zdlc(:,1)=Zdlc(:,1)-j*Omega*Lb(step)-j*Omega*Le(step);
    Zdlc(:,4)=Zdlc(:,4)-j*Omega*Lc(step)-j*Omega*Le(step);
    Zdlc(:,2)=Zdlc(:,2)-j*Omega*Le(step);
    Zdlc(:,3)=Zdlc(:,3)-j*Omega*Le(step);
    Ydlc=Z_to_Y(Zdlc);
    Y_cell_exp{step}(:,2:5)=Ydlc;
end;

%===De Ccs rcs =============
for step=1:1:num_bias
    Ccs(step)=1.80e-14;  % obtained from cold measurement
    Rcs(step)=180;       % obtained from cold measurement
    Ccs2(step)=0;
    Y=Y_cell_exp{step}(:,2:5);
    Ys=j.*Omega.*Ccs(step)./(1+j.*Omega.*Ccs(step).*Rcs(step));
    Y(:,4)=Y(:,4)-Ys;
    Y_cell_exp{step}(:,2:5)=Y;
end;

%== extract  Re ==========
for step=1:1:num_bias
    Ybeta=Y_cell_exp{step}(:,2:5);
    Zbeta=Y_to_Z(Ybeta);
    z12(step)=real(Zbeta(1,2));
```

```
    y21(step)=real(Ybeta(1,3));
    %plot(Omega,real(Ybeta(:,3))); hold on;
end;
%     ben=17; enn=18;
%     xx=1./Ic_tmp;%;
%     k_b=polyfit(xx(ben:enn),z12(ben:enn),1); %intercept gives Re
%     plot(xx,re_gm,xx,xx.*k_b(1)+k_b(2),'+-'); hold on;

%== De-embed Re, extract Cbct tt gm ==========
for step=1:1:num_bias
    Re(step)=0.66;   % determined from above method
    Y=Y_cell_exp{step}(:,2:5);
    Y=com_Y_re(Y,-Re(step));
    Y_cell_exp{step}(:,2:5)=Y;
    Z=Y_to_Z(Y);
    H=Z(:,4)-Z(:,3);
    G=Z(:,1)-Z(:,2);
    Q=Z(:,2)-Z(:,3);
    k_b=linefit(Omega,imag(1./H),1,20,1,0,'+-','r');
    Cbct(step)=k_b(1);
    k_b=linefit(Omega.^2,real(1./H),1,20,-1,0,'+-','r');
    tt(step)=k_b(1)/Cbct(step)^2;
    k_b=linefit(Omega.^2,real(1./Z(:,2)),5,15,1,0,'+-','r');
    gm0(step)=k_b(2);
end;
% smooth tt (for rcx)
tt(1)=tt(2);
tt(5:num_bias)=tt(5:num_bias).*0+tt(4);
tt=fitcurv(tt.',0.3)';

%===== De   Rcx ========
for step=1:1:num_bias
    Rcx(step)=tt(step);
    Y=Y_cell_exp{step}(:,2:5);
    Y=com_Y_rc(Y,-Rcx(step));
    Y_cell_exp{step}(:,2:5)=Y;
end;

%===taylor method for  Rbx ====
for step=1:1:num_bias
    Y=Y_cell_exp{step}(:,2:5);
    %--imag y12
    k_b=linefit(Omega.^2,imag(Y(:,2))./Omega,1,5,1,0,'+-','r');
    Cbctt(step)=-k_b(2);
    %--imag y11
    k_b=linefit(Omega.^2,imag(Y(:,1))./Omega,1,3,1,0,'+-','r');
    Ct(step)=k_b(2);
    %--real Y12
    k_b=linefit(Omega.^2,real(Y(:,2)),1,2,-1,0,'+-','r');
    ReY12_2(step)=-k_b(1);
    %--imag Y22
    k_b=linefit(Omega.^2,imag(Y(:,4))./Omega,1,4,1,0,'+-','r');
    ImY22_1(step)=k_b(2);
    %--real Y21
    k_b=linefit(Omega.^2,real(Y(:,3)),1,4,1,0,'+-','r');
    gm(step)=k_b(2);
    %--imagY2112
```

```
    k_b=linefit(Omega,imag(Y(:,3)-Y(:,2)),1,5,-1,0,'+-','r');
    ImY2112(step)=-k_b(1);
    %--real Y11+Y12
    k_b=linefit(Omega.^2,real(Y(:,1)+Y(:,2)),1,5,1,0,'+-','r');
    ReY1112(step)=k_b(1);
end;

%===== Extract Rbx Cbex Cbcx Cbci ====
k_b=linefit(gm0.*Cbct,ImY22_1,1,8,1,0,'+','r');     Rx_rRi=k_b(1);
k_b=linefit(Ct-Cbct,ImY2112./gm0,1,num_bias,1,0,'+','b');Rx_Ri=k_b(1);

r=0.3;  % Cbci/Cbct, extracted from cold measurement

Ri=(Rx_Ri-Rx_rRi)/(1-r); Rx=Rx_Ri-Ri;
Cbcx=Cbct.*(1-r);        Cbci=Cbct.*r;
k_b=linefit(gm0,Ct-Cbct,1,8,1,0,'+','b');           cj=k_b(2);
k_b=linefit(gm0,ReY1112,2,3,1,0,'+','r');           test=k_b(2);
aa=Ri; bb=r.*Ri.*Cbctt; cc=-test+Rx.*cj.*(cj+Cbctt);
xx=(-bb+sqrt(bb.^2-4.*aa.*cc))./(2.*aa);
Cbex=(Cbct-Cbct+cj-xx(1));
Cbej=cj-Cbex;

%==== De  Rbx Cbcx Cbex ======
for step=1:1:num_bias
    Rbx(step)=Rx;
    Y=Y_cell_exp{step}(:,2:5);
    Y=com_Y_rb(Y,-Rbx(step));
    Y=Y-[j*Omega*Cbcx(step) -j*Omega*Cbcx(step)...
     -j*Omega*Cbcx(step) j*Omega*Cbcx(step)];
    rbi_QSx(step)=circle(1./Y(:,1));
    Y(:,1)=Y(:,1)-j.*Omega.*Cbex(step);
    rbi_QS(step)=circle(1./Y(:,1));
    Y_cell_exp{step}(:,2:5)=Y;
end;

%==== Extract and de go =====
for step=1:1:num_bias
     Y=Y_cell_exp{step}(:,2:5);
     go(step)=0;%real(Y(1,4));
     %figure(100); plot(Omega,real(Y(:,4)),Omega,Omega-Omega+go(step));
     Y(:,4)=Y(:,4)-go(step);     Y_cell_exp{step}(:,2:5)=Y;
end;

%%%==== Extraction  for QS rbi and intrinsic para======
%--de-embed rbi_QS, then extract gbe, gm ,Cbet and Taud
for step=1:1:num_bias
    Y=Y_cell_exp{step}(:,2:5);
    Y=com_Y_rb(Y,-rbi_QS(step));
    y11=Y(:,1)+Y(:,2);
    y21=Y(:,3)-Y(:,2);
    %--- Cbet_QS
    ben=1; enn=15;
    k_b=polyfit(Omega(ben:enn).^2,imag(y11(ben:enn))./Omega(ben:enn),1);
    %plot(Omega.^2,imag(y11)./Omega,Omega.^2,Omega.^2*k_b(1)+k_b(2));
    Cbet_QS(step)=k_b(2);
    %--- gm_QS
    ben=1; enn=15;
```

```
    k_b=polyfit(Omega(ben:enn).^2,real(y21(ben:enn)),1);
    %plot(Omega.^2,real(y21),Omega.^2,Omega.^2*k_b(1)+k_b(2)); hold on;
    gm_QS(step)=k_b(2);
    %--- gbe_QS
    ben=1; enn=5;
    k_b=polyfit(Omega(ben:enn).^2,real(y11(ben:enn)),1);
    %plot(Omega.^2,real(y11),Omega.^2,Omega.^2*k_b(1)+k_b(2)); hold on;
    gbe_QS(step)=k_b(2);
    %--- Taud_QS
    ben=1; enn=15;
    k_b=polyfit(Omega(ben:enn).^2,imag(y21(ben:enn))./Omega(ben:enn),1);
    %plot(Omega.^2,imag(y21)./Omega,Omega.^2,Omega.^2*k_b(1)+k_b(2));
    Taud_QS_old(step)=-k_b(2)/gm_QS(step);
    %plot(Omega,-imag(log(y21))./Omega); hold on;
    k_b=slopefit(Omega(ben:enn),imag(y21(ben:enn)));
    Taud_QS_old(step)=-k_b/gm_QS(step);
    %plot(Omega,imag(y21),Omega,Omega*k_b); hold on;
end;
Taud_QS_old(1)=Taud_QS_old(2);
Taud_QS=fitcurv(Taud_QS_old',1)';
gbe_QS=Ib_tmp./0.026;
%%%===Extraction for QS end===


%==== NQS tau extraction ======
for step=1:1:num_bias
    Y=Y_cell_exp{step}(:,2:5);
    Z=Y_to_Z(Y);
    H=Z(:,4)-Z(:,3);
    Q=Z(:,2)-Z(:,3);
    k_b=linefit(Omega.^2,real(H./Q),1,20,1,0,'+-','r');
    ReHQ(step)=-k_b(1).*gm0(step);
    k_b=linefit(Omega,imag(H./Q),1,20,-1,0,'+-','r');
    ImHQ(step)=k_b(1).*gm0(step);
end;
k_b=linefit(gm0,ImHQ,1,6,1,0,'+','r');
Cbei0=gm0.*k_b(1); Cbej0=ImHQ-Cbei0;
fn=num_bias-7;
Cbej0(fn:num_bias)=Cbej0(fn:num_bias).*0+Cbej0(fn-1);
Cbei0=ImHQ-Cbej0;
%plot(gm0,Cbei0,gm0,Cbej0);
k_b=linefit(Cbei0(1:10),ReHQ(1:10),1,6,1,1,'ks','k');
Tautr0=Cbei0./gm0;
Taud0=k_b(2)/Cbej0(8)/Tautr0(1).*Tautr0;
Tauin0=(Taud0(1)-k_b(1))/Tautr0(1).*Tautr0;
%plot(gm0,Tautr0,gm0,Tauin0,gm0,Taud0);

%====== extract rbi ==========
gbe=Ib_tmp./0.026;

for step=1:1:num_bias
    Y=Y_cell_exp{step}(:,2:5);
    Y11=gbe(step)+j.*Omega*(Cbej0(step)+Cbci(step))...
        +j.*Omega.*Cbei0(step)./(1+j.*Omega.*Tauin0(step));
    Ybi=1./(1./Y(:,1)-1./Y11);

    Rbi(step)=sum(1./real(Ybi(11:15)))/(15-11+1);
```

```
   % subplot(1,2,1);
   % plot(Omega,1./real(Ybi),Omega,Omega+Rbi(step)-Omega); hold on;
   % subplot(1,2,2);
   % plot(Omega,imag(Ybi)./Omega,Omega,Omega.*0+(Cbei0(step))/5);
end

Rci=Rbi-Rbi; % set to be zero

%=== If rbi bias dependent method, use the following block
  %Tau_in=Tauin0;   Rd=Tau_in./Cbei;
  %Tau_out_all=Taud0;
  %Taud=Tau_out_all-Tau_in;
  %Cbei=Cbei0;
  %gm=gm0;
  %Cbej=Cbej0;
% ====== over ====


%=== If rbi bias independent, cnt ====
%=== de Rbi Cbi, Rci ======
for step=1:1:num_bias
    rbi(step)=Ri;  % bias independent value
    Y=Y_cell_exp{step}(:,2:5);
    if(HasCbi==1)
        Cbi(step)=(Cbci(step)+Cbet_QS(step))./5;
        Zrbi=Rbi(step)./(1+j.*Omega.*Rbi(step).*Cbi(step));
    else
        Zrbi=Omega-Omega+Rbi(step);
    end;
    Y=com_Y_rb(Y,-Zrbi);
    Y=com_Y_rc(Y,-Rci(step));
    Y_cell_exp_sav{step}(:,2:5)=Y;
end;

%=== Extracion of the intrinsic transistor
%    for bias independent rbi method =======

  for step=1:1:num_bias
    ytmp=Y_cell_exp_sav{step}(:,2:5);

    %--- Cbci
    ben=1; enn=6;
    k_b=polyfit(Omega(ben:enn).^2,imag(ytmp(ben:enn,2))./Omega(ben:enn),1);
    %plot(Omega.^2,imag(ytmp(:,2))./Omega,Omega.^2,Omega.^2*k_b(1)+k_b(2));
    %Cbci(step)=-k_b(2);

    %--- ru
    ben=1; enn=4;
    k_b=polyfit(Omega(ben:enn).^2,real(ytmp(ben:enn,2)),1);
    Ru(step)=abs(1./k_b(2));
    Ru(step)=1.5e6;
    %plot(Omega.^2,real(ytmp(:,2)),Omega.^2,Omega.^2*k_b(1)+k_b(2));


    %=== de Cbci (Y12)===
    ytmp=ytmp-[-ytmp(:,2) ytmp(:,2) ytmp(:,2) -ytmp(:,2)];
    Y_cell_exp{step}(:,2:5)=ytmp;
```

```
    %plot(Omega,real(ytmp(:,1))); hold on;

    %--- gbe
    ben=1; enn=5;
    k_b=polyfit(Omega(ben:enn).^2,real(ytmp(ben:enn,1)),1);
    %plot(Omega.^2,real(ytmp(:,1)),Omega.^2,Omega.^2*k_b(1)+k_b(2));
    gbe_ex(step)=k_b(2);

    %--- Cd*Cd*Rd
    ben=1; enn=15;
    k_b=polyfit(Omega(ben:enn).^2,real(ytmp(ben:enn,1)),1);
    %plot(Omega,real(ytmp(:,1)),Omega,Omega.^2*k_b(1)+k_b(2)); hold on;
    CdCdRd(step)=k_b(1);

    %--- Cbet
    ben=1; enn=6;
    k_b=polyfit(Omega(ben:enn).^2,imag(ytmp(ben:enn,1))./Omega(ben:enn),1);
    %plot(Omega.^2,imag(ytmp(:,1))./Omega,Omega.^2,Omega.^2*k_b(1)+k_b(2));
    Cbet(step)=k_b(2);
    CdCdCdRdRd(step)=-k_b(1);

    %--- gm
    ben=1; enn=6;
    k_b=polyfit(Omega(ben:enn).^2,real(ytmp(ben:enn,3)),1);
    %plot(Omega.^2,real(ytmp(:,3)),Omega.^2,Omega.^2*k_b(1)+k_b(2));
    gm_ex(step)=k_b(2);

    %--- Taud+Tau_in = Tau_out_all
    ben=10; enn=20;
    k_b=polyfit(Omega(ben:enn).^2,imag(ytmp(ben:enn,3))./Omega(ben:enn),1);
    %plot(Omega.^2,imag(ytmp(:,3))./Omega,Omega.^2,Omega.^2*k_b(1)+k_b(2));
    Tau_out_all(step)=-k_b(2)/gm_ex(step);

    gm(step)=gm_ex(step);
    %gbe(step)=gbe_ex(step);
    gbe(step)=Ib_tmp(step)./(k*bias_cell{step}(5)/q);%gbe_ex(step);
  end;

%=== split Cbet into Cbei and Cbej
  k_b=polyfit(gm(1:10),Cbet(1:10),1);
  %plot(gm,Cbet,gm,gm*k_b(1)+k_b(2));
  for step=1:1:num_bias;
    Cbej(step)=k_b(2);
    Cbei(step)=Cbet(step)-Cbej(step);
    Tau_in(step)=CdCdRd(step)/Cbei(step);
  end;
  Tau_in(1)=Tau_in(3);
  Tau_in(2)=Tau_in(3);
  Rd=Tau_in./Cbei;
  Taud_old=Tau_out_all-Tau_in;
  Taud=fitcurv(Taud_old',1)';

  %plot(Vbe(1:num_bias),Tau_in,'r*',Vbe(1:num_bias),Tau_out_all,'rs',...
  %    Vbe(1:num_bias),Taud_QS,'gv',Vbe(1:num_bias),Cbei./gm); hold on;
```

# APPENDIX F

## MATLAB CODE FOR INTRINSIC NOISE EXTRACTION

The following MATLAB code is used to extract the intrinsic noise for a 50 GHz SiGe HBT with $A_E = 0.24 \times 20 \times 2\ \mu m^2$. `N_exp_adm_cell_intr` is the full PSD of intrinsic base and collector current noises. `N_exp_adm_cell_base` is the PSD of base electron noise, i.e. the $2qI_b$ removed version of `N_exp_adm_cell_intr`.

### F.1 MATLAB code

```
load_data_26G;
num_b=1;
num_e=20;
Omega=Y_cell_exp{step}(:,1).*2.*pi;

index=[1 4 9 14 19 24];  %Noise frequency points

for step=num_b:1:num_e
    %de-embeded Y parameters
    N_Y_exp=select_row(Y_cell_exp{step},index);
    f_N=N_Y_exp(:,1);
    Omega_N=f_N*2*pi;
    N_Y_6=N_Y_exp(:,2:5);

    N_Y_5=com_Y_rc(N_Y_6,-j*Omega_N*Lc(step)-Rcx(step)); %Lc Rcx
    N_Y_5=com_Y_rb(N_Y_5,-j*Omega_N*Lb(step)); %Lb
    N_Y_5=com_Y_re(N_Y_5,-j*Omega_N*Le(step)); %Le

    N_Y_4=N_Y_5;
    N_Y_4(:,4)=N_Y_4(:,4)...
    -j*Omega_N.*Ccs(step)./(1+j*Omega_N*Ccs(step)*Rcs(step));%Rcs Ccs
    N_Y_4=N_Y_4-[j*Omega_N*Cbco(step) ...
                 -j*Omega_N*Cbco(step) ...
                 -j*Omega_N*Cbco(step) ...
                 j*Omega_N*Cbco(step)]; %Cbco

    N_Y_3=com_Y_rb(N_Y_4,-Rbx(step)); %Rbx
    N_Y_3=com_Y_rc(N_Y_3,-Rci(step)); %Rci
    N_Y_3=com_Y_re(N_Y_3,-Re(step)); %Re
    N_Y_2=N_Y_3;

    N_Y_2(:,1)=N_Y_2(:,1)-j*Omega_N*Cbex(step)-gbex(step); %Cbex
```

```
N_Y_2=N_Y_2-[j*Omega_N*Cbcx(step) ...
             -j*Omega_N*Cbcx(step) ...
             -j*Omega_N*Cbcx(step) ...
             j*Omega_N*Cbcx(step)]; %Cbcx

if(HasCbi==1)
    Zrbi=Rbi(step)./(1+j.*Omega_N.*Rbi(step).*Cbi(step));
else
    Zrbi=Rbi(step);
end;
N_Yintrinsic=com_Y_rb(N_Y_2,-Zrbi); %Rbi Cbi

N_Ybase=N_Yintrinsic;
N_Ybase(:,1)=N_Ybase(:,1)-gbe(step)-j*Omega_N*Cbej(step);

N_Yintr_cell_exp{step}=[f_N N_Yintrinsic];
N_Ybase_cell_exp{step}=[f_N N_Ybase];

%Noise de-embedding
T=bias_cell{step}(5);
N_exp_6=FRY_to_Svi(10.^(N_cell_exp{step}(:,2)./10),...
         N_cell_exp{step}(:,3)*get_Z0,N_cell_exp{step}(:,4),T_noise);

N_exp_5=cha_to_imp_noise(N_exp_6,Y_to_Z(N_Y_6));
N_exp_5(:,4)=N_exp_5(:,4)-4*k*T*Rcx(step);    %Rcx

N_exp_4=imp_to_adm_noise(N_exp_5,N_Y_5);
N_exp_4(:,4)=N_exp_4(:,4)-...
4*k*T*real(j*Omega_N.*Ccs(step)./(1+j*Omega_N*Ccs(step)*Rcs(step)));%Rcs

N_exp_3=adm_to_imp_noise(N_exp_4,Y_to_Z(N_Y_4));
N_exp_3(:,1)=N_exp_3(:,1)-4*k*T*(Re(step)+Rbx(step)); % Rbx re
N_exp_3(:,4)=N_exp_3(:,4)-4*k*T*(Re(step)+Rci(step)); % Rci re
N_exp_3(:,2)=N_exp_3(:,2)-4*k*T*(Re(step));  %re
N_exp_3(:,3)=N_exp_3(:,3)-4*k*T*(Re(step));  %re

N_exp_2=imp_to_adm_noise(N_exp_3,N_Y_3);
N_exp_2(:,1)=N_exp_2(:,1)-2.*k.*T.*gbex(step); %gbex
N_exp_1=adm_to_imp_noise(N_exp_2,Y_to_Z(N_Y_2));
if(HasCbi==1)
    Zrbi=Rbi(step)./(1+j.*Omega_N.*Rbi(step).*Cbi(step));
else
    Zrbi=Rbi(step);
end;
if(HasCrowdingnoise==1)
  noiserbiv=(4.*k.*T./Rbi(step)-2.*q.*Ib_tmp(step)./3).*Zrbi.*conj(Zrbi);
else
  noiserbiv=4.*k.*T./Rbi(step).*Zrbi.*conj(Zrbi);
end;
N_exp_1(:,1)=N_exp_1(:,1)-noiserbiv;  %Rbi

N_exp_intrinsic=imp_to_adm_noise(N_exp_1,N_Yintrinsic);

N_exp_base=N_exp_intrinsic;
N_exp_base(:,1)=N_exp_base(:,1)-2*q*Ib_tmp(step);

N_exp_adm_cell{step}=[f_N N_exp_intrinsic]; % for noise calculateion
```

```
    N_exp_adm_cell_intr{step}=[f_N N_exp_intrinsic]; % intrinsic
    N_exp_adm_cell_base{step}=[f_N N_exp_base]; % base

end;
```

### F.2 Data of S-parameters and noise

The following is the S-parameters and noise data de-embedded with OPEN structure for the 50 GHz SiGe HBT with $A_E = 0.24 \times 20 \times 2\ \mu m^2$.

```
!
! S-Parameters vs Frequency vs Bias
!M NOISE: M:PS;A:16;C:16;DC:1;H:0;P:1;DOT:DUT_NF_M;
!
!Bias# 1
!Bias Values Read:
!Vb:.770 V, Ib:.002 mA
!Vc:1.500 V, Ic:.520 mA
!Date: 27 Mar 2003
!Time: 15:52:30
!Deembedding: ON
!
!  Freq    S11 Mag  S11 Ang  S21 Mag  S21 Ang  S12 Mag  S12 Ang  S22 Mag  S22 Ang
!  (GHz)             (Deg)             (Deg)             (Deg)             (Deg)
!-------- -------- -------- -------- -------- -------- -------- -------- --------
!
  2.0000     .978    -24.1    1.921    160.8     .051     74.7     .978     -7.7
  3.0000     .957    -35.8    1.755    152.0     .075     67.5     .959    -10.9
  4.0000     .935    -46.7    1.724    143.6     .095     60.9     .937    -13.8
  5.0000     .919    -56.8    1.630    136.2     .113     54.9     .914    -16.6
  6.0000     .897    -66.4    1.457    128.2     .129     49.4     .896    -18.5
  7.0000     .878    -75.0    1.472    122.3     .141     44.0     .869    -21.3
  8.0000     .858    -83.4    1.403    115.8     .151     39.3     .848    -23.3
  9.0000     .843    -90.4    1.312    110.1     .161     35.2     .831    -25.0
 10.0000     .826    -97.5    1.233    104.7     .167     31.3     .814    -26.7
 11.0000     .820   -102.1    1.200     99.8     .177     28.2     .794    -28.5
 12.0000     .797   -109.1    1.110     94.8     .179     24.7     .783    -29.8
 13.0000     .790   -114.9    1.047     90.0     .182     21.5     .770    -31.2
 14.0000     .780   -119.2    1.000     85.6     .186     18.6     .758    -32.7
 15.0000     .770   -124.1     .938     81.7     .187     16.1     .750    -34.1
 16.0000     .760   -127.8     .931     77.8     .190     13.6     .733    -35.7
 17.0000     .751   -131.9     .876     74.2     .191     11.6     .725    -37.0
 18.0000     .749   -135.7     .834     70.6     .193      9.2     .718    -38.4
 19.0000     .739   -137.6     .815     67.8     .195      7.4     .706    -40.1
 20.0000     .741   -141.7     .787     64.1     .195      4.8     .698    -41.3
 21.0000     .737   -145.4     .750     61.0     .188      2.8     .693    -42.6
 22.0000     .734   -147.3     .724     57.6     .192       .5     .686    -43.8
 23.0000     .722   -150.4     .697     55.4     .189       .1     .678    -45.6
 24.0000     .723   -152.8     .668     52.1     .191     -2.1     .670    -46.7
 25.0000     .721   -155.3     .644     49.8     .189     -3.5     .666    -48.6
 26.0000     .723   -157.5     .618     47.4     .186     -5.1     .665    -49.7
!
! Noise Parameters vs Frequency vs Bias
!M NOISE: M:PS;A:16;C:16;DC:1;H:0;P:1;DOT:DUT_NF_M;
!
!  Freq     F(min)    Gamma Opt  Gamma Opt Normalized Associated
!  (GHz)    Fitted     Fitted     Fitted    Rn Z0=50   Gain (dB)
!           (dB)        Mag       Angle      Fitted     Fitted
!-------- ---------- ---------- ---------- ---------- ----------
!
```

```
 2.0000        .23       .770        8.2        .66      15.57
 5.0000        .66       .801       36.8        .70       9.72
10.0000       1.25       .704       77.5        .61       6.92
15.0000       2.72       .614      106.4        .56       4.47
20.0000       3.19       .600      130.1        .39       2.86
25.0000       4.30       .625      145.5        .34        .93
!
! S-Parameters vs Frequency vs Bias
!M NOISE: M:PS;A:16;C:16;DC:1;H:0;P:1;DOT:DUT_NF_M;
!
!Bias# 2
!Bias Values Read:
!Vb:.796 V, Ib:.008 mA
!Vc:1.500 V, Ic:1.400 mA
!Date: 27 Mar 2003
!Time: 15:52:32
!Deembedding: ON
!
!  Freq    S11 Mag  S11 Ang  S21 Mag  S21 Ang  S12 Mag  S12 Ang  S22 Mag  S22 Ang
!  (GHz)             (Deg)             (Deg)             (Deg)             (Deg)
!-------- -------- -------- -------- -------- -------- -------- -------- --------
 2.0000      .949    -34.5    4.789    155.8      .050     69.6      .952    -12.2
 3.0000      .912    -50.5    4.283    145.9      .070     60.5      .909    -16.8
 4.0000      .880    -64.5    4.020    136.6      .086     52.9      .863    -20.7
 5.0000      .859    -76.6    3.686    129.1      .099     46.3      .818    -24.0
 6.0000      .832    -87.8    3.233    121.7      .109     40.5      .785    -25.7
 7.0000      .814    -97.1    3.122    115.7      .116     35.6      .741    -28.6
 8.0000      .796   -106.0    2.885    109.9      .121     31.0      .708    -30.3
 9.0000      .782   -112.9    2.640    105.1      .126     27.7      .685    -31.6
10.0000      .766   -119.7    2.433    100.5      .128     24.4      .664    -32.8
11.0000      .764   -123.4    2.310     96.3      .135     22.1      .637    -34.3
12.0000      .748   -130.2    2.111     92.5      .134     19.3      .626    -35.1
13.0000      .743   -135.2    1.968     88.8      .134     16.9      .612    -36.1
14.0000      .738   -138.9    1.853     85.5      .136     14.6      .600    -37.1
15.0000      .731   -143.3    1.723     82.3      .136     12.9      .592    -38.0
16.0000      .726   -146.3    1.676     79.0      .138     10.9      .571    -39.3
17.0000      .720   -150.0    1.566     76.2      .138      9.3      .565    -40.3
18.0000      .720   -152.8    1.483     73.6      .138      7.6      .559    -41.5
19.0000      .711   -153.9    1.426     71.4      .140      6.7      .547    -42.8
20.0000      .714   -158.0    1.367     68.2      .138      4.5      .539    -43.8
21.0000      .710   -161.5    1.294     65.6      .132      3.9      .537    -44.6
22.0000      .714   -162.5    1.242     63.2      .136      1.7      .529    -45.7
23.0000      .701   -165.1    1.192     61.3      .135      1.6      .522    -47.2
24.0000      .704   -167.2    1.132     58.9      .134        .2     .516    -48.1
25.0000      .701   -168.9    1.092     56.5      .133        .1     .514    -49.8
26.0000      .705   -171.3    1.036     54.8      .131      -1.7     .514    -51.1
!
! Noise Parameters vs Frequency vs Bias
!M NOISE: M:PS;A:16;C:16;DC:1;H:0;P:1;DOT:DUT_NF_M;
!
!  Freq     F(min)    Gamma Opt  Gamma Opt Normalized Associated
!  (GHz)    Fitted     Fitted     Fitted    Rn Z0=50   Gain (dB)
!           (dB)         Mag      Angle      Fitted     Fitted
!-------- ---------- ---------- ---------- ---------- ----------
 2.0000       -0.00       .905        7.2        .37      14.10
 5.0000         .65       .608       33.7        .39      13.81
10.0000        1.02       .545       78.9        .32      10.06
15.0000        2.14       .476      109.7        .30       7.54
20.0000        2.56       .466      136.9        .23       5.98
25.0000        3.54       .509      151.5        .22       4.13
!
! S-Parameters vs Frequency vs Bias
!M NOISE: M:PS;A:16;C:16;DC:1;H:0;P:1;DOT:DUT_NF_M;
!
!Bias# 3
!Bias Values Read:
!Vb:.811 V, Ib:.014 mA
!Vc:1.500 V, Ic:2.560 mA
!Date: 27 Mar 2003
!Time: 15:52:35
!Deembedding: ON
!
!  Freq    S11 Mag  S11 Ang  S21 Mag  S21 Ang  S12 Mag  S12 Ang  S22 Mag  S22 Ang
```

```
!  (GHz)             (Deg)             (Deg)             (Deg)             (Deg)
!-------- -------- -------- -------- -------- -------- -------- -------- --------
!
  2.0000     .914    -45.0    7.683    150.5     .048     64.7     .917    -16.9
  3.0000     .869    -64.5    6.708    139.5     .064     54.2     .849    -22.6
  4.0000     .836    -80.2    6.041    129.7     .076     46.3     .781    -26.9
  5.0000     .815    -93.5    5.388    122.1     .085     39.7     .721    -30.1
  6.0000     .791   -104.9    4.658    115.2     .091     34.4     .680    -31.4
  7.0000     .776   -114.1    4.355    109.5     .096     30.0     .629    -34.0
  8.0000     .763   -122.5    3.952    104.4     .098     26.2     .594    -35.2
  9.0000     .754   -128.7    3.579    100.1     .101     23.4     .571    -36.0
 10.0000     .743   -134.9    3.267     96.1     .101     20.9     .550    -36.8
 11.0000     .742   -138.0    3.060     92.3     .107     19.1     .522    -37.9
 12.0000     .732   -144.0    2.787     89.2     .105     17.1     .513    -38.4
 13.0000     .731   -148.4    2.584     86.0     .105     15.3     .501    -38.9
 14.0000     .728   -151.5    2.420     83.2     .106     13.4     .489    -39.7
 15.0000     .723   -155.3    2.250     80.5     .105     12.3     .483    -40.4
 16.0000     .716   -157.9    2.165     77.6     .106     10.8     .463    -41.6
 17.0000     .714   -160.8    2.021     75.3     .106     10.1     .458    -42.2
 18.0000     .714   -163.2    1.911     73.0     .106      8.9     .452    -43.3
 19.0000     .709   -164.3    1.829     71.1     .108      8.1     .441    -44.3
 20.0000     .712   -167.5    1.748     68.3     .106      6.8     .432    -45.2
 21.0000     .713   -170.3    1.652     66.3     .101      7.2     .433    -45.8
 22.0000     .710   -171.4    1.581     64.0     .104      5.2     .426    -46.7
 23.0000     .701   -173.1    1.509     62.4     .104      5.3     .419    -48.2
 24.0000     .702   -175.0    1.440     60.3     .103      4.5     .417    -49.1
 25.0000     .708   -177.1    1.385     58.6     .103      5.6     .413    -50.5
 26.0000     .709   -178.4    1.319     56.8     .100      3.5     .414    -51.8
!
! Noise Parameters vs Frequency vs Bias
!M NOISE: M:PS;A:16;C:16;DC:1;H:0;P:1;DOT:DUT_NF_M;
!
!  Freq     F(min)    Gamma Opt  Gamma Opt Normalized Associated
!  (GHz)    Fitted     Fitted     Fitted    Rn Z0=50   Gain (dB)
!           (dB)        Mag       Angle      Fitted     Fitted
!-------- ---------- ---------- ---------- ---------- ----------
!
  2.0000        .21       .893        5.9        .29      15.54
  5.0000        .65       .533       32.1        .30      15.35
 10.0000        .97       .460       80.5        .25      11.51
 15.0000       1.92       .407      114.1        .23       9.02
 20.0000       2.33       .397      143.3        .19       7.42
 25.0000       3.19       .448      157.7        .20       5.66
!
! S-Parameters vs Frequency vs Bias
!M NOISE: M:PS;A:16;C:16;DC:1;H:0;P:1;DOT:DUT_NF_M;
!
!Bias# 4
!Bias Values Read:
!Vb:.819 V, Ib:.022 mA
!Vc:1.500 V, Ic:3.360 mA
!Date: 27 Mar 2003
!Time: 15:52:37
!Deembedding: ON
!
!  Freq    S11 Mag  S11 Ang  S21 Mag  S21 Ang  S12 Mag  S12 Ang  S22 Mag  S22 Ang
!  (GHz)             (Deg)             (Deg)             (Deg)             (Deg)
!-------- -------- -------- -------- -------- -------- -------- -------- --------
!
  2.0000     .891    -52.0    9.538    147.1     .046     61.4     .889    -20.0
  3.0000     .844    -73.3    8.175    135.5     .060     50.7     .806    -26.2
  4.0000     .814    -89.7    7.186    125.6     .070     42.5     .726    -30.4
  5.0000     .793   -103.2    6.308    118.1     .077     36.2     .661    -33.5
  6.0000     .773   -114.4    5.420    111.7     .081     31.4     .618    -34.4
  7.0000     .761   -123.0    4.980    106.2     .084     27.4     .566    -36.7
  8.0000     .753   -131.0    4.484    101.4     .086     24.2     .532    -37.6
  9.0000     .744   -136.7    4.042     97.5     .088     21.9     .510    -38.1
 10.0000     .737   -142.3    3.673     93.8     .089     19.7     .490    -38.7
 11.0000     .736   -145.3    3.418     90.3     .093     18.1     .464    -39.6
 12.0000     .729   -150.6    3.115     87.5     .091     16.5     .456    -39.8
 13.0000     .729   -154.6    2.884     84.6     .091     15.4     .444    -40.3
 14.0000     .725   -157.3    2.695     81.9     .092     13.8     .434    -40.9
 15.0000     .722   -160.7    2.505     79.5     .091     13.1     .428    -41.5
 16.0000     .719   -163.1    2.397     76.8     .092     11.9     .409    -42.5
 17.0000     .715   -165.7    2.240     74.7     .091     11.4     .405    -43.0
 18.0000     .717   -168.0    2.115     72.7     .091     10.1     .401    -44.2
```

```
 19.0000     .706   -169.0    2.017     70.8     .093      9.7     .390    -45.1
 20.0000     .714   -171.9    1.933     68.2     .092      8.5     .383    -45.8
 21.0000     .711   -174.6    1.828     66.3     .087      9.4     .383    -46.4
 22.0000     .712   -175.3    1.746     64.2     .090      7.9     .377    -47.2
 23.0000     .699   -177.3    1.662     62.7     .090      9.0     .372    -48.6
 24.0000     .714   -178.9    1.590     60.6     .089      7.5     .367    -49.4
 25.0000     .715    179.6    1.531     58.8     .089      8.4     .366    -50.8
 26.0000     .708    178.4    1.453     57.3     .087      7.3     .364    -51.9
!
! Noise Parameters vs Frequency vs Bias
!M NOISE: M:PS;A:16;C:16;DC:1;H:0;P:1;DOT:DUT_NF_M;
!
!  Freq     F(min)    Gamma Opt  Gamma Opt Normalized Associated
!  (GHz)    Fitted     Fitted     Fitted    Rn Z0=50   Gain (dB)
!            (dB)       Mag       Angle      Fitted     Fitted
!-------- ---------- ---------- ---------- ---------- ----------
!
  2.0000        .25       .908        8.2        .26      15.64
  5.0000        .71       .498       32.6        .27      16.11
 10.0000       1.02       .419       81.8        .22      12.15
 15.0000       1.85       .366      116.6        .21       9.66
 20.0000       2.26       .384      147.3        .16       8.09
 25.0000       3.05       .432      160.7        .18       6.35
!
! S-Parameters vs Frequency vs Bias
!M NOISE: M:PS;A:16;C:16;DC:1;H:0;P:1;DOT:DUT_NF_M;
!
!Bias# 5
!Bias Values Read:
!Vb:.829 V, Ib:.028 mA
!Vc:1.500 V, Ic:4.860 mA
!Date: 27 Mar 2003
!Time: 15:52:39
!Deembedding: ON
!
!  Freq    S11 Mag  S11 Ang  S21 Mag  S21 Ang  S12 Mag  S12 Ang  S22 Mag  S22 Ang
!  (GHz)             (Deg)             (Deg)             (Deg)             (Deg)
!-------- -------- -------- -------- -------- -------- -------- -------- --------
!
  2.0000     .855    -63.1   12.354    141.9     .043     56.4     .840    -24.8
  3.0000     .810    -86.6   10.258    129.7     .054     45.3     .734    -31.3
  4.0000     .787   -103.3    8.721    119.9     .061     37.6     .644    -35.3
  5.0000     .771   -116.4    7.502    112.8     .066     31.9     .576    -37.8
  6.0000     .758   -126.7    6.392    107.0     .068     28.0     .533    -38.2
  7.0000     .750   -134.5    5.758    102.0     .070     24.9     .484    -40.0
  8.0000     .745   -141.5    5.137     97.8     .071     22.3     .453    -40.4
  9.0000     .740   -146.6    4.608     94.2     .072     20.6     .432    -40.5
 10.0000     .735   -151.4    4.172     90.9     .073     19.1     .415    -40.8
 11.0000     .734   -154.1    3.856     87.8     .076     18.1     .391    -41.5
 12.0000     .730   -158.6    3.516     85.3     .074     16.4     .384    -41.5
 13.0000     .730   -161.8    3.250     82.7     .074     16.1     .375    -41.8
 14.0000     .728   -164.2    3.031     80.3     .075     14.8     .365    -42.3
 15.0000     .727   -167.2    2.817     78.1     .074     14.6     .359    -42.6
 16.0000     .724   -169.4    2.680     75.7     .075     14.1     .343    -43.6
 17.0000     .726   -171.5    2.508     73.8     .075     13.6     .340    -44.0
 18.0000     .723   -173.6    2.361     71.9     .075     13.4     .336    -45.2
 19.0000     .718   -174.6    2.257     70.2     .075     13.4     .328    -45.9
 20.0000     .719   -176.9    2.150     67.9     .075     12.3     .320    -46.5
 21.0000     .723   -179.1    2.038     66.0     .072     14.2     .321    -47.0
 22.0000     .717   -179.8    1.944     64.1     .074     11.8     .316    -47.6
 23.0000     .714    178.5    1.859     62.9     .074     13.1     .310    -49.3
 24.0000     .722    177.0    1.772     60.9     .075     13.1     .305    -50.2
 25.0000     .716    175.7    1.700     59.4     .073     13.1     .304    -51.1
 26.0000     .719    174.6    1.621     57.7     .075     13.6     .304    -52.8
!
! Noise Parameters vs Frequency vs Bias
!M NOISE: M:PS;A:16;C:16;DC:1;H:0;P:1;DOT:DUT_NF_M;
!
!  Freq     F(min)    Gamma Opt  Gamma Opt Normalized Associated
!  (GHz)    Fitted     Fitted     Fitted    Rn Z0=50   Gain (dB)
!            (dB)       Mag       Angle      Fitted     Fitted
!-------- ---------- ---------- ---------- ---------- ----------
!
  2.0000        .11       .941       11.0        .25      14.47
```

```
 5.0000        .78       .450       38.8        .22      17.31
10.0000       1.07       .354       85.9        .20      13.04
15.0000       1.80       .319      122.4        .20      10.45
20.0000       2.18       .352      154.5        .16       8.83
25.0000       2.97       .414      164.8        .17       7.04
!
! S-Parameters vs Frequency vs Bias
!M NOISE: M:PS;A:16;C:16;DC:1;H:0;P:1;DOT:DUT_NF_M;
!
!Bias# 6
!Bias Values Read:
!Vb:.831 V, Ib:.036 mA
!Vc:1.500 V, Ic:5.060 mA
!Date: 27 Mar 2003
!Time: 15:52:42
!Deembedding: ON
!
!  Freq    S11 Mag  S11 Ang  S21 Mag  S21 Ang  S12 Mag  S12 Ang  S22 Mag  S22 Ang
!  (GHz)             (Deg)             (Deg)             (Deg)             (Deg)
!-------- -------- -------- -------- -------- -------- -------- -------- --------
!
 2.0000     .844    -66.3   13.111    140.5     .042     55.1     .825    -26.1
 3.0000     .802    -90.2   10.793    128.1     .052     44.0     .714    -32.7
 4.0000     .781   -106.8    9.103    118.5     .059     36.4     .622    -36.5
 5.0000     .767   -119.7    7.789    111.5     .063     31.1     .554    -38.9
 6.0000     .755   -129.8    6.624    105.8     .065     27.1     .511    -39.2
 7.0000     .748   -137.3    5.938    100.9     .067     24.2     .463    -40.7
 8.0000     .744   -144.1    5.288     96.8     .067     21.9     .433    -41.1
 9.0000     .739   -148.9    4.739     93.4     .069     20.3     .413    -41.1
10.0000     .735   -153.6    4.289     90.2     .069     19.2     .397    -41.2
11.0000     .735   -156.3    3.958     87.1     .072     18.1     .374    -41.9
12.0000     .729   -160.5    3.606     84.7     .070     17.1     .367    -41.9
13.0000     .732   -163.6    3.337     82.2     .070     16.4     .358    -42.1
14.0000     .728   -165.9    3.108     79.9     .071     15.6     .349    -42.6
15.0000     .730   -168.7    2.891     77.7     .070     15.1     .343    -43.0
16.0000     .725   -170.7    2.745     75.4     .071     15.1     .328    -43.8
17.0000     .725   -173.0    2.564     73.5     .071     14.5     .325    -44.3
18.0000     .725   -174.8    2.421     71.7     .071     14.1     .322    -45.4
19.0000     .722   -176.0    2.311     70.0     .072     13.9     .313    -46.1
20.0000     .722   -178.1    2.198     67.8     .072     13.8     .305    -46.9
21.0000     .723    180.0    2.087     66.0     .068     14.4     .307    -47.4
22.0000     .718    178.8    1.991     64.1     .071     13.7     .302    -47.9
23.0000     .711    177.6    1.899     62.9     .070     15.1     .296    -49.3
24.0000     .720    176.1    1.809     61.0     .071     14.3     .292    -50.0
25.0000     .721    175.0    1.744     59.4     .071     16.2     .291    -51.5
26.0000     .719    173.8    1.662     57.9     .071     15.7     .287    -52.6
!
! Noise Parameters vs Frequency vs Bias
!M NOISE: M:PS;A:16;C:16;DC:1;H:0;P:1;DOT:DUT_NF_M;
!
!  Freq     F(min)    Gamma Opt  Gamma Opt Normalized Associated
!  (GHz)    Fitted     Fitted     Fitted    Rn Z0=50   Gain (dB)
!           (dB)        Mag       Angle      Fitted     Fitted
!-------- ---------- ---------- ---------- ---------- ----------
!
 2.0000        .27       .845       15.6        .24      19.41
 5.0000        .89       .386       29.1        .24      17.42
10.0000       1.08       .338       87.0        .19      13.24
15.0000       1.79       .312      123.9        .19      10.63
20.0000       2.17       .347      156.5        .16       9.00
25.0000       2.95       .417      165.2        .16       7.26
!
! S-Parameters vs Frequency vs Bias
!M NOISE: M:PS;A:16;C:16;DC:1;H:0;P:1;DOT:DUT_NF_M;
!
!Bias# 7
!Bias Values Read:
!Vb:.836 V, Ib:.042 mA
!Vc:1.500 V, Ic:6.180 mA
!Date: 27 Mar 2003
!Time: 15:52:44
!Deembedding: ON
!
!  Freq    S11 Mag  S11 Ang  S21 Mag  S21 Ang  S12 Mag  S12 Ang  S22 Mag  S22 Ang
```

| (GHz) | | (Deg) | | (Deg) | | (Deg) | | (Deg) |
|---|---|---|---|---|---|---|---|---|
| 2.0000 | .825 | -72.9 | 14.618 | 137.6 | .040 | 52.4 | .793 | -28.8 |
| 3.0000 | .787 | -97.4 | 11.808 | 125.1 | .049 | 41.4 | .673 | -35.3 |
| 4.0000 | .771 | -113.7 | 9.801 | 115.7 | .054 | 34.1 | .579 | -38.8 |
| 5.0000 | .760 | -126.0 | 8.305 | 109.0 | .057 | 29.3 | .512 | -40.8 |
| 6.0000 | .751 | -135.5 | 7.044 | 103.7 | .059 | 26.0 | .470 | -40.8 |
| 7.0000 | .745 | -142.5 | 6.261 | 99.0 | .060 | 23.4 | .425 | -42.0 |
| 8.0000 | .743 | -148.7 | 5.559 | 95.2 | .060 | 21.5 | .397 | -42.2 |
| 9.0000 | .740 | -153.2 | 4.976 | 92.0 | .062 | 20.4 | .379 | -42.0 |
| 10.0000 | .735 | -157.5 | 4.496 | 88.9 | .062 | 19.3 | .363 | -42.1 |
| 11.0000 | .737 | -160.1 | 4.137 | 86.0 | .064 | 18.6 | .342 | -42.6 |
| 12.0000 | .734 | -163.9 | 3.775 | 83.8 | .063 | 18.1 | .337 | -42.5 |
| 13.0000 | .735 | -166.6 | 3.486 | 81.4 | .063 | 17.5 | .328 | -42.7 |
| 14.0000 | .731 | -168.8 | 3.247 | 79.1 | .063 | 16.8 | .320 | -43.1 |
| 15.0000 | .731 | -171.3 | 3.023 | 77.1 | .063 | 17.1 | .314 | -43.5 |
| 16.0000 | .729 | -173.3 | 2.862 | 74.8 | .064 | 16.6 | .300 | -44.2 |
| 17.0000 | .728 | -175.3 | 2.677 | 73.1 | .064 | 16.3 | .296 | -44.5 |
| 18.0000 | .729 | -177.2 | 2.523 | 71.3 | .064 | 16.6 | .293 | -45.8 |
| 19.0000 | .725 | -178.2 | 2.408 | 69.6 | .064 | 16.7 | .286 | -46.3 |
| 20.0000 | .725 | 179.7 | 2.292 | 67.6 | .065 | 16.4 | .278 | -47.2 |
| 21.0000 | .733 | 177.3 | 2.174 | 65.7 | .062 | 17.7 | .279 | -47.6 |
| 22.0000 | .726 | 177.1 | 2.069 | 63.9 | .064 | 16.6 | .275 | -47.9 |
| 23.0000 | .719 | 175.7 | 1.980 | 62.6 | .063 | 17.7 | .271 | -49.6 |
| 24.0000 | .723 | 174.1 | 1.889 | 61.0 | .065 | 17.6 | .266 | -50.3 |
| 25.0000 | .724 | 172.9 | 1.803 | 59.5 | .064 | 19.2 | .266 | -51.7 |
| 26.0000 | .723 | 172.1 | 1.728 | 58.0 | .065 | 18.4 | .262 | -53.0 |

! Noise Parameters vs Frequency vs Bias
!M NOISE: M:PS;A:16;C:16;DC:1;H:0;P:1;DOT:DUT_NF_M;

| Freq (GHz) | F(min) Fitted (dB) | Gamma Opt Fitted Mag | Gamma Opt Fitted Angle | Normalized Associated Rn Z0=50 Fitted | Gain (dB) Fitted |
|---|---|---|---|---|---|
| 2.0000 | .50 | .649 | 17.4 | .23 | 23.42 |
| 5.0000 | .84 | .390 | 42.0 | .21 | 18.13 |
| 10.0000 | 1.16 | .319 | 89.9 | .18 | 13.59 |
| 15.0000 | 1.80 | .299 | 127.7 | .18 | 10.98 |
| 20.0000 | 2.15 | .337 | 161.1 | .16 | 9.33 |
| 25.0000 | 3.03 | .406 | 169.3 | .16 | 7.52 |

! S-Parameters vs Frequency vs Bias
!M NOISE: M:PS;A:16;C:16;DC:1;H:0;P:1;DOT:DUT_NF_M;

!Bias# 8
!Bias Values Read:
!Vb:.841 V, Ib:.050 mA
!Vc:1.500 V, Ic:7.380 mA
!Date: 27 Mar 2003
!Time: 15:52:47
!Deembedding: ON

| Freq (GHz) | S11 Mag | S11 Ang (Deg) | S21 Mag | S21 Ang (Deg) | S12 Mag | S12 Ang (Deg) | S22 Mag | S22 Ang (Deg) |
|---|---|---|---|---|---|---|---|---|
| 2.0000 | .805 | -80.0 | 16.115 | 134.5 | .038 | 49.8 | .757 | -31.5 |
| 3.0000 | .775 | -104.6 | 12.772 | 122.0 | .045 | 39.0 | .630 | -37.8 |
| 4.0000 | .763 | -120.4 | 10.449 | 113.0 | .049 | 32.3 | .536 | -40.8 |
| 5.0000 | .755 | -132.1 | 8.774 | 106.7 | .052 | 27.8 | .471 | -42.5 |
| 6.0000 | .748 | -140.9 | 7.425 | 101.6 | .053 | 25.0 | .431 | -42.3 |
| 7.0000 | .745 | -147.4 | 6.552 | 97.3 | .054 | 23.0 | .390 | -43.1 |
| 8.0000 | .743 | -153.1 | 5.802 | 93.7 | .054 | 21.6 | .363 | -43.1 |
| 9.0000 | .740 | -157.1 | 5.185 | 90.6 | .055 | 20.4 | .347 | -42.8 |
| 10.0000 | .738 | -161.0 | 4.680 | 87.7 | .056 | 19.9 | .332 | -42.7 |
| 11.0000 | .739 | -163.5 | 4.293 | 85.0 | .057 | 19.2 | .313 | -43.1 |
| 12.0000 | .735 | -166.9 | 3.917 | 82.8 | .057 | 19.0 | .308 | -43.0 |
| 13.0000 | .739 | -169.5 | 3.620 | 80.6 | .057 | 18.7 | .299 | -43.1 |
| 14.0000 | .735 | -171.5 | 3.368 | 78.5 | .057 | 18.3 | .292 | -43.3 |
| 15.0000 | .735 | -173.9 | 3.137 | 76.5 | .057 | 18.7 | .287 | -43.7 |
| 16.0000 | .732 | -175.8 | 2.963 | 74.4 | .058 | 18.4 | .273 | -44.6 |
| 17.0000 | .730 | -177.7 | 2.773 | 72.6 | .058 | 19.4 | .271 | -44.6 |
| 18.0000 | .733 | -179.1 | 2.615 | 70.9 | .058 | 19.3 | .269 | -45.8 |

```
 19.0000     .729    179.8    2.493     69.4     .059     19.2     .261    -46.8
 20.0000     .730    177.9    2.367     67.3     .059     19.4     .253    -47.4
 21.0000     .732    175.6    2.252     65.6     .057     20.3     .255    -48.1
 22.0000     .728    175.4    2.145     63.7     .059     19.7     .252    -48.2
 23.0000     .725    173.5    2.046     62.6     .058     22.2     .247    -49.2
 24.0000     .725    172.7    1.950     60.7     .060     22.2     .243    -50.7
 25.0000     .729    171.6    1.877     59.7     .060     23.4     .242    -52.0
 26.0000     .728    170.7    1.796     58.2     .059     24.0     .240    -53.7
!
! Noise Parameters vs Frequency vs Bias
!M NOISE: M:PS;A:16;C:16;DC:1;H:0;P:1;DOT:DUT_NF_M;
!
!  Freq     F(min)    Gamma Opt  Gamma Opt Normalized Associated
!  (GHz)    Fitted     Fitted     Fitted    Rn Z0=50   Gain (dB)
!            (dB)       Mag       Angle      Fitted     Fitted
!-------- ---------- ---------- ---------- ---------- ----------
!
  2.0000        .66       .529       19.5        .23      25.02
  5.0000       1.00       .298       31.2        .23      18.48
 10.0000       1.23       .294       94.4        .18      13.97
 15.0000       1.85       .296      132.2        .17      11.31
 20.0000       2.21       .331      165.0        .16       9.59
 25.0000       3.01       .406      171.9        .16       7.88
!
! S-Parameters vs Frequency vs Bias
!M NOISE: M:PS;A:16;C:16;DC:1;H:0;P:1;DOT:DUT_NF_M;
!
!Bias# 9
!Bias Values Read:
!Vb:.844 V, Ib:.054 mA
!Vc:1.500 V, Ic:8.100 mA
!Date: 27 Mar 2003
!Time: 15:52:49
!Deembedding: ON
!
!  Freq    S11 Mag  S11 Ang  S21 Mag  S21 Ang  S12 Mag  S12 Ang  S22 Mag  S22 Ang
!  (GHz)             (Deg)             (Deg)             (Deg)             (Deg)
!-------- -------- -------- -------- -------- -------- -------- -------- --------
!
  2.0000     .795    -83.7   16.853    133.0     .036     48.4     .739    -32.9
  3.0000     .769   -108.3   13.226    120.5     .043     37.8     .608    -39.1
  4.0000     .759   -123.7   10.747    111.7     .047     31.2     .515    -41.8
  5.0000     .753   -135.0    8.983    105.5     .049     27.4     .451    -43.3
  6.0000     .747   -143.5    7.597    100.6     .050     24.7     .412    -42.9
  7.0000     .744   -149.8    6.679     96.4     .051     22.6     .372    -43.6
  8.0000     .743   -155.1    5.908     92.9     .051     21.6     .348    -43.5
  9.0000     .742   -159.1    5.277     89.9     .052     20.8     .331    -43.0
 10.0000     .738   -162.8    4.766     87.1     .053     20.1     .318    -42.9
 11.0000     .741   -165.1    4.362     84.4     .054     19.9     .299    -43.2
 12.0000     .736   -168.5    3.984     82.3     .054     19.8     .294    -43.1
 13.0000     .740   -170.9    3.678     80.1     .054     19.9     .285    -43.2
 14.0000     .738   -172.9    3.422     78.0     .055     19.4     .279    -43.5
 15.0000     .738   -175.2    3.185     76.1     .054     19.8     .274    -43.7
 16.0000     .734   -177.0    3.007     74.0     .055     19.4     .262    -44.7
 17.0000     .733   -178.8    2.815     72.3     .055     20.0     .259    -44.9
 18.0000     .734    179.8    2.658     70.6     .055     20.6     .256    -46.1
 19.0000     .730    178.6    2.530     69.1     .056     21.2     .250    -47.0
 20.0000     .731    177.0    2.405     67.0     .056     21.0     .244    -47.6
 21.0000     .734    174.9    2.288     65.5     .054     23.4     .245    -48.0
 22.0000     .733    174.5    2.173     63.8     .055     21.2     .241    -48.6
 23.0000     .725    172.2    2.078     62.3     .056     22.3     .235    -49.8
 24.0000     .726    172.0    1.985     60.7     .057     23.6     .233    -50.9
 25.0000     .737    170.6    1.908     59.0     .057     24.8     .229    -52.5
 26.0000     .727    169.9    1.827     58.1     .058     25.0     .227    -53.0
!
! Noise Parameters vs Frequency vs Bias
!M NOISE: M:PS;A:16;C:16;DC:1;H:0;P:1;DOT:DUT_NF_M;
!
!  Freq     F(min)    Gamma Opt  Gamma Opt Normalized Associated
!  (GHz)    Fitted     Fitted     Fitted    Rn Z0=50   Gain (dB)
!            (dB)       Mag       Angle      Fitted     Fitted
!-------- ---------- ---------- ---------- ---------- ----------
!
  2.0000        .72       .486       21.1        .22      25.56
```

```
 5.0000       1.02       .277       32.6        .22      18.73
10.0000       1.26       .280       97.3        .17      14.17
15.0000       1.88       .291      135.6        .17      11.48
20.0000       2.23       .330      166.5        .16       9.71
25.0000       2.98       .414      174.1        .15       8.10
!
! S-Parameters vs Frequency vs Bias
!M NOISE: M:PS;A:16;C:16;DC:1;H:0;P:1;DOT:DUT_NF_M;
!
!Bias# 10
!Bias Values Read:
!Vb:.849 V, Ib:.066 mA
!Vc:1.500 V, Ic:9.680 mA
!Date: 27 Mar 2003
!Time: 15:52:52
!Deembedding: ON
!
!  Freq    S11 Mag  S11 Ang  S21 Mag  S21 Ang  S12 Mag  S12 Ang  S22 Mag  S22 Ang
!  (GHz)             (Deg)             (Deg)             (Deg)             (Deg)
!-------- -------- -------- -------- -------- -------- -------- -------- --------
!
 2.0000     .778    -91.2   18.241    129.9     .034     45.6     .699    -35.5
 3.0000     .759   -115.4   14.048    117.6     .040     35.6     .566    -41.3
 4.0000     .754   -130.0   11.269    109.2     .042     29.6     .474    -43.5
 5.0000     .750   -140.5    9.351    103.4     .044     26.3     .414    -44.5
 6.0000     .747   -148.3    7.898     98.8     .045     24.2     .377    -43.9
 7.0000     .745   -154.0    6.901     94.8     .046     22.8     .341    -44.2
 8.0000     .745   -158.9    6.093     91.5     .046     21.8     .319    -44.0
 9.0000     .744   -162.4    5.438     88.7     .047     21.5     .304    -43.4
10.0000     .741   -165.9    4.906     86.0     .047     21.4     .291    -43.2
11.0000     .744   -168.1    4.480     83.5     .049     20.9     .274    -43.4
12.0000     .740   -171.0    4.099     81.5     .048     21.2     .270    -43.3
13.0000     .742   -173.2    3.783     79.5     .048     21.8     .263    -43.4
14.0000     .740   -175.1    3.513     77.5     .049     21.7     .256    -43.5
15.0000     .741   -177.1    3.272     75.6     .049     22.2     .252    -43.9
16.0000     .740   -179.0    3.081     73.6     .050     22.6     .240    -44.7
17.0000     .738    179.5    2.890     72.0     .050     23.2     .238    -44.9
18.0000     .738    178.1    2.726     70.4     .050     23.6     .236    -46.3
19.0000     .735    176.8    2.594     68.8     .051     24.2     .228    -46.8
20.0000     .736    175.4    2.461     66.9     .052     23.9     .223    -47.6
21.0000     .729    173.6    2.332     65.3     .050     24.9     .226    -48.1
22.0000     .733    173.0    2.239     63.5     .051     24.4     .221    -48.1
23.0000     .730    171.3    2.136     62.4     .052     27.5     .216    -49.5
24.0000     .735    170.5    2.029     60.9     .054     27.2     .211    -50.5
25.0000     .731    169.5    1.962     59.1     .056     30.3     .213    -52.9
26.0000     .736    168.5    1.866     58.0     .055     29.5     .209    -53.3
!
! Noise Parameters vs Frequency vs Bias
!M NOISE: M:PS;A:16;C:16;DC:1;H:0;P:1;DOT:DUT_NF_M;
!
!  Freq     F(min)    Gamma Opt  Gamma Opt Normalized Associated
!  (GHz)    Fitted     Fitted     Fitted    Rn Z0=50   Gain (dB)
!           (dB)        Mag       Angle      Fitted     Fitted
!-------- ---------- ---------- ---------- ---------- ----------
!
 2.0000         .84       .411       25.4        .22      26.47
 5.0000        1.01       .259       43.3        .21      19.24
10.0000        1.33       .258      104.1        .17      14.52
15.0000        1.94       .287      140.3        .17      11.75
20.0000        2.29       .335      170.4        .16       9.95
25.0000        3.06       .401      176.4        .16       8.25
!
! S-Parameters vs Frequency vs Bias
!M NOISE: M:PS;A:16;C:16;DC:1;H:0;P:1;DOT:DUT_NF_M;
!
!Bias# 11
!Bias Values Read:
!Vb:.851 V, Ib:.074 mA
!Vc:1.500 V, Ic:10.620 mA
!Date: 27 Mar 2003
!Time: 15:52:54
!Deembedding: ON
!
!  Freq    S11 Mag  S11 Ang  S21 Mag  S21 Ang  S12 Mag  S12 Ang  S22 Mag  S22 Ang
```

```
!  (GHz)             (Deg)             (Deg)             (Deg)             (Deg)
!-------- -------- -------- -------- -------- -------- -------- -------- --------
!
  2.0000     .770    -95.1   18.885    128.3     .033     44.3     .679    -36.8
  3.0000     .755   -118.9   14.414    116.2     .038     34.7     .545    -42.3
  4.0000     .752   -133.0   11.499    108.0     .040     29.0     .455    -44.2
  5.0000     .751   -143.2    9.509    102.3     .042     25.9     .396    -45.0
  6.0000     .748   -150.5    8.027     97.9     .043     24.1     .361    -44.3
  7.0000     .746   -155.9    6.993     94.0     .043     23.0     .327    -44.5
  8.0000     .746   -160.7    6.170     90.9     .043     22.4     .306    -44.1
  9.0000     .746   -164.1    5.501     88.1     .044     21.9     .292    -43.4
 10.0000     .743   -167.4    4.966     85.5     .045     22.1     .279    -43.1
 11.0000     .745   -169.4    4.529     83.0     .046     21.9     .263    -43.4
 12.0000     .743   -172.4    4.146     81.1     .046     22.0     .259    -43.4
 13.0000     .746   -174.3    3.822     79.0     .046     22.2     .252    -43.1
 14.0000     .742   -176.4    3.554     77.0     .047     22.5     .246    -43.7
 15.0000     .743   -178.2    3.314     75.2     .047     23.6     .241    -43.8
 16.0000     .741   -180.0    3.111     73.3     .047     23.7     .231    -44.8
 17.0000     .740    178.3    2.917     71.6     .048     24.5     .228    -44.9
 18.0000     .742    177.1    2.753     70.1     .049     25.0     .227    -46.2
 19.0000     .740    175.7    2.619     68.4     .050     26.1     .220    -47.2
 20.0000     .739    174.7    2.481     66.7     .049     25.4     .216    -47.7
 21.0000     .736    172.5    2.362     65.0     .050     28.0     .216    -48.2
 22.0000     .739    172.3    2.251     63.4     .050     27.8     .212    -48.0
 23.0000     .730    170.3    2.148     62.2     .050     28.1     .207    -49.8
 24.0000     .736    169.8    2.047     60.6     .051     29.0     .203    -50.3
 25.0000     .731    168.5    1.969     59.4     .052     31.0     .202    -51.9
 26.0000     .741    167.6    1.893     57.8     .052     30.5     .199    -53.2
!
! Noise Parameters vs Frequency vs Bias
!M NOISE: M:PS;A:16;C:16;DC:1;H:0;P:1;DOT:DUT_NF_M;
!
!  Freq     F(min)    Gamma Opt  Gamma Opt Normalized Associated
!  (GHz)    Fitted     Fitted     Fitted    Rn Z0=50   Gain (dB)
!           (dB)        Mag       Angle      Fitted     Fitted
!-------- ---------- ---------- ---------- ---------- ----------
!
  2.0000        .90       .376       27.4        .21      26.83
  5.0000       1.05       .233       46.2        .20      19.49
 10.0000       1.36       .246      107.9        .17      14.68
 15.0000       1.96       .287      143.4        .16      11.90
 20.0000       2.34       .341      172.2        .15      10.07
 25.0000       3.14       .402      178.4        .17       8.28
!
! S-Parameters vs Frequency vs Bias
!M NOISE: M:PS;A:16;C:16;DC:1;H:0;P:1;DOT:DUT_NF_M;
!
!Bias# 12
!Bias Values Read:
!Vb:.854 V, Ib:.082 mA
!Vc:1.500 V, Ic:11.580 mA
!Date: 27 Mar 2003
!Time: 15:52:57
!Deembedding: ON
!
!  Freq    S11 Mag  S11 Ang  S21 Mag  S21 Ang  S12 Mag  S12 Ang  S22 Mag  S22 Ang
!  (GHz)             (Deg)             (Deg)             (Deg)             (Deg)
!-------- -------- -------- -------- -------- -------- -------- -------- --------
!
  2.0000     .763    -98.7   19.462    126.8     .032     42.9     .659    -38.0
  3.0000     .752   -122.1   14.733    114.9     .036     33.5     .524    -43.2
  4.0000     .751   -135.8   11.686    107.0     .038     28.6     .437    -44.8
  5.0000     .750   -145.4    9.640    101.5     .040     25.7     .381    -45.4
  6.0000     .748   -152.5    8.132     97.2     .041     24.1     .346    -44.5
  7.0000     .747   -157.7    7.066     93.4     .041     23.2     .314    -44.6
  8.0000     .747   -162.1    6.229     90.3     .041     22.7     .294    -44.1
  9.0000     .747   -165.4    5.555     87.7     .042     22.5     .280    -43.4
 10.0000     .744   -168.6    5.011     85.1     .043     22.7     .269    -43.1
 11.0000     .747   -170.6    4.565     82.6     .044     22.8     .254    -43.3
 12.0000     .745   -173.3    4.180     80.8     .044     22.9     .250    -43.2
 13.0000     .748   -175.3    3.857     78.7     .044     23.3     .242    -43.3
 14.0000     .744   -177.1    3.584     76.8     .045     23.9     .237    -43.6
 15.0000     .745   -178.9    3.343     75.1     .045     24.7     .232    -43.7
 16.0000     .743    179.3    3.135     73.1     .045     25.1     .222    -44.8
 17.0000     .742    177.7    2.939     71.5     .046     26.3     .220    -44.8
 18.0000     .745    176.5    2.774     70.0     .047     25.9     .218    -46.1
```

```
 19.0000     .739    175.2    2.634     68.6     .047     28.1     .213    -46.7
 20.0000     .740    174.0    2.498     66.7     .048     27.7     .207    -47.6
 21.0000     .742    172.1    2.382     65.2     .048     30.4     .209    -47.9
 22.0000     .737    171.6    2.273     63.3     .048     29.4     .204    -47.8
 23.0000     .734    170.2    2.175     62.2     .048     31.9     .201    -49.4
 24.0000     .734    169.4    2.072     60.7     .050     31.9     .196    -50.7
 25.0000     .729    167.7    1.971     59.6     .052     31.8     .195    -51.8
 26.0000     .739    167.4    1.906     57.7     .051     33.8     .192    -53.9
!
! Noise Parameters vs Frequency vs Bias
!M NOISE: M:PS;A:16;C:16;DC:1;H:0;P:1;DOT:DUT_NF_M;
!
!  Freq     F(min)    Gamma Opt  Gamma Opt Normalized Associated
!  (GHz)    Fitted     Fitted     Fitted    Rn Z0=50   Gain (dB)
!            (dB)       Mag       Angle      Fitted     Fitted
!-------- ---------- ---------- ---------- ---------- ----------
!
  2.0000        .96       .349       29.4        .21      27.08
  5.0000       1.08       .218       51.2        .20      19.72
 10.0000       1.41       .242      111.5        .17      14.81
 15.0000       1.99       .290      146.1        .16      12.03
 20.0000       2.39       .343      173.9        .16      10.14
 25.0000       3.26       .398     -179.6        .18       8.28
!
! S-Parameters vs Frequency vs Bias
!M NOISE: M:PS;A:16;C:16;DC:1;H:0;P:1;DOT:DUT_NF_M;
!
!Bias# 13
!Bias Values Read:
!Vb:.856 V, Ib:.084 mA
!Vc:1.500 V, Ic:12.700 mA
!Date: 27 Mar 2003
!Time: 15:52:59
!Deembedding: ON
!
!  Freq    S11 Mag  S11 Ang  S21 Mag  S21 Ang  S12 Mag  S12 Ang  S22 Mag  S22 Ang
!  (GHz)             (Deg)             (Deg)             (Deg)             (Deg)
!-------- -------- -------- -------- -------- -------- -------- -------- --------
!
  2.0000     .756   -102.5   19.995    125.3     .030     41.7     .639    -39.1
  3.0000     .750   -125.4   15.013    113.6     .034     32.7     .505    -44.0
  4.0000     .750   -138.5   11.847    105.9     .036     28.0     .419    -45.3
  5.0000     .751   -147.8    9.747    100.5     .038     25.2     .365    -45.6
  6.0000     .749   -154.6    8.218     96.4     .039     24.2     .332    -44.7
  7.0000     .748   -159.6    7.126     92.7     .039     23.1     .301    -44.5
  8.0000     .748   -163.8    6.278     89.7     .039     23.1     .283    -44.1
  9.0000     .748   -166.8    5.595     87.1     .040     23.1     .269    -43.3
 10.0000     .745   -169.9    5.046     84.6     .041     23.3     .259    -42.9
 11.0000     .748   -171.9    4.592     82.2     .042     23.7     .245    -43.1
 12.0000     .746   -174.6    4.207     80.3     .042     24.1     .240    -43.0
 13.0000     .750   -176.3    3.880     78.3     .042     25.2     .233    -43.1
 14.0000     .745   -178.1    3.609     76.5     .043     25.8     .229    -43.3
 15.0000     .748   -179.9    3.363     74.7     .043     25.6     .225    -43.6
 16.0000     .746    178.5    3.151     72.8     .043     26.7     .215    -44.6
 17.0000     .743    176.4    2.957     71.0     .044     26.9     .211    -44.5
 18.0000     .747    175.8    2.791     69.7     .045     28.2     .211    -45.9
 19.0000     .740    174.2    2.641     68.2     .045     29.4     .205    -46.9
 20.0000     .743    173.5    2.512     66.3     .046     28.9     .199    -47.4
 21.0000     .741    171.2    2.394     64.8     .045     30.6     .202    -47.8
 22.0000     .741    171.0    2.284     63.1     .047     30.7     .198    -47.5
 23.0000     .741    168.8    2.184     61.7     .048     33.5     .194    -49.6
 24.0000     .741    168.6    2.081     60.2     .049     31.3     .185    -50.0
 25.0000     .740    167.2    1.991     59.1     .050     34.6     .188    -52.4
 26.0000     .736    166.5    1.914     58.0     .050     34.4     .184    -54.0
!
! Noise Parameters vs Frequency vs Bias
!M NOISE: M:PS;A:16;C:16;DC:1;H:0;P:1;DOT:DUT_NF_M;
!
!  Freq     F(min)    Gamma Opt  Gamma Opt Normalized Associated
!  (GHz)    Fitted     Fitted     Fitted    Rn Z0=50   Gain (dB)
!            (dB)       Mag       Angle      Fitted     Fitted
!-------- ---------- ---------- ---------- ---------- ----------
!
  2.0000       1.02       .317       32.0        .21      27.35
```

```
 5.0000       1.13       .197       55.6        .20      19.91
10.0000       1.46       .233      115.9        .17      14.93
15.0000       2.04       .284      148.9        .17      12.10
20.0000       2.43       .351      175.2        .16      10.23
25.0000       3.23       .415     -177.8        .17       8.51
!
! S-Parameters vs Frequency vs Bias
!M NOISE: M:PS;A:16;C:16;DC:1;H:0;P:1;DOT:DUT_NF_M;
!
!Bias# 14
!Bias Values Read:
!Vb:.859 V, Ib:.096 mA
!Vc:1.500 V, Ic:13.920 mA
!Date: 27 Mar 2003
!Time: 15:53:01
!Deembedding: ON
!
!  Freq    S11 Mag  S11 Ang  S21 Mag  S21 Ang  S12 Mag  S12 Ang  S22 Mag  S22 Ang
!  (GHz)             (Deg)             (Deg)             (Deg)             (Deg)
!-------- -------- -------- -------- -------- -------- -------- -------- --------
!
 2.0000     .750   -106.4   20.474    123.8     .029      40.6     .618    -40.2
 3.0000     .748   -128.6   15.251    112.3     .033      32.0     .485    -44.7
 4.0000     .749   -141.2   11.977    104.8     .035      27.5     .402    -45.6
 5.0000     .751   -150.0    9.831     99.6     .036      25.3     .350    -45.8
 6.0000     .750   -156.5    8.287     95.6     .036      24.2     .319    -44.7
 7.0000     .750   -161.2    7.167     92.1     .037      23.7     .290    -44.4
 8.0000     .750   -165.1    6.312     89.1     .037      23.8     .272    -43.7
 9.0000     .750   -168.2    5.623     86.6     .038      23.8     .260    -43.0
10.0000     .747   -171.1    5.073     84.1     .039      24.4     .250    -42.7
11.0000     .750   -173.0    4.607     81.8     .040      24.8     .236    -42.8
12.0000     .748   -175.6    4.225     80.0     .040      25.6     .232    -42.7
13.0000     .751   -177.2    3.899     78.0     .040      25.8     .225    -42.8
14.0000     .748   -179.1    3.621     76.1     .041      26.5     .222    -43.0
15.0000     .751    179.4    3.379     74.4     .041      27.5     .216    -43.4
16.0000     .748    177.6    3.163     72.5     .042      28.0     .209    -44.3
17.0000     .745    175.8    2.968     70.9     .042      28.9     .205    -44.0
18.0000     .748    175.0    2.803     69.4     .043      29.4     .204    -45.8
19.0000     .745    173.6    2.664     68.0     .044      30.9     .199    -47.0
20.0000     .745    172.8    2.522     66.2     .045      31.2     .193    -47.0
21.0000     .741    170.5    2.397     64.6     .044      33.0     .195    -47.8
22.0000     .743    170.5    2.295     62.9     .045      32.5     .192    -47.2
23.0000     .743    168.6    2.186     61.7     .046      33.6     .187    -49.6
24.0000     .743    168.1    2.091     60.2     .047      33.9     .182    -50.1
25.0000     .746    167.0    1.999     58.5     .048      35.2     .183    -52.2
26.0000     .735    166.0    1.926     57.8     .049      38.1     .175    -52.2
!
! Noise Parameters vs Frequency vs Bias
!M NOISE: M:PS;A:16;C:16;DC:1;H:0;P:1;DOT:DUT_NF_M;
!
!  Freq     F(min)    Gamma Opt  Gamma Opt Normalized Associated
!  (GHz)    Fitted     Fitted     Fitted    Rn Z0=50   Gain (dB)
!           (dB)        Mag       Angle      Fitted     Fitted
!-------- ---------- ---------- ---------- ---------- ----------
!
 2.0000       1.06       .284       34.7        .21      27.59
 5.0000       1.17       .181       61.2        .19      20.08
10.0000       1.51       .228      120.9        .16      15.06
15.0000       2.08       .290      151.9        .16      12.22
20.0000       2.47       .354      176.1        .16      10.28
25.0000       3.26       .422     -177.3        .17       8.60
!
! S-Parameters vs Frequency vs Bias
!M NOISE: M:PS;A:16;C:16;DC:1;H:0;P:1;DOT:DUT_NF_M;
!
!Bias# 15
!Bias Values Read:
!Vb:.859 V, Ib:.096 mA
!Vc:1.500 V, Ic:13.840 mA
!Date: 27 Mar 2003
!Time: 15:53:04
!Deembedding: ON
!
!  Freq    S11 Mag  S11 Ang  S21 Mag  S21 Ang  S12 Mag  S12 Ang  S22 Mag  S22 Ang
```

```
!  (GHz)             (Deg)             (Deg)             (Deg)             (Deg)
!-------- -------- -------- -------- -------- -------- -------- -------- --------
!
  2.0000     .750   -106.4   20.471    123.8     .029     40.7     .618    -40.2
  3.0000     .748   -128.6   15.248    112.3     .033     31.8     .485    -44.7
  4.0000     .749   -141.2   11.976    104.8     .035     27.5     .402    -45.6
  5.0000     .750   -150.0    9.830     99.6     .036     25.4     .351    -45.7
  6.0000     .750   -156.5    8.284     95.6     .036     24.0     .319    -44.7
  7.0000     .750   -161.2    7.168     92.0     .037     23.5     .290    -44.4
  8.0000     .750   -165.2    6.312     89.1     .038     23.4     .272    -43.7
  9.0000     .750   -168.2    5.622     86.6     .038     23.8     .260    -43.1
 10.0000     .746   -171.1    5.069     84.1     .039     24.2     .250    -42.7
 11.0000     .751   -173.0    4.608     81.8     .040     24.8     .236    -42.8
 12.0000     .748   -175.5    4.226     80.0     .040     25.3     .232    -42.7
 13.0000     .752   -177.3    3.898     78.0     .040     26.3     .225    -42.9
 14.0000     .749   -179.1    3.622     76.2     .041     26.8     .222    -43.1
 15.0000     .751    179.3    3.380     74.4     .042     27.5     .216    -43.3
 16.0000     .748    177.6    3.163     72.6     .042     28.4     .208    -44.1
 17.0000     .744    175.9    2.964     70.9     .041     29.1     .205    -44.0
 18.0000     .748    175.1    2.804     69.5     .043     29.9     .203    -45.9
 19.0000     .745    173.8    2.659     68.0     .043     31.7     .199    -46.3
 20.0000     .745    172.8    2.519     66.2     .045     30.7     .194    -47.2
 21.0000     .747    170.7    2.408     64.6     .044     32.9     .195    -47.8
 22.0000     .743    170.8    2.291     63.0     .045     31.7     .192    -47.0
 23.0000     .738    168.3    2.183     61.6     .046     34.4     .187    -48.9
 24.0000     .741    168.0    2.082     60.3     .046     35.0     .180    -50.0
 25.0000     .737    167.3    2.009     59.3     .048     36.5     .182    -51.7
 26.0000     .739    166.6    1.919     57.9     .048     37.3     .179    -54.1
!
! Noise Parameters vs Frequency vs Bias
!M NOISE: M:PS;A:16;C:16;DC:1;H:0;P:1;DOT:DUT_NF_M;
!
!  Freq     F(min)    Gamma Opt  Gamma Opt Normalized Associated
!  (GHz)    Fitted     Fitted     Fitted    Rn Z0=50   Gain (dB)
!           (dB)        Mag       Angle      Fitted     Fitted
!-------- ---------- ---------- ---------- ---------- ----------
!
  2.0000       1.05       .282       34.8        .21      27.60
  5.0000       1.17       .181       60.9        .19      20.08
 10.0000       1.51       .228      120.2        .16      15.04
 15.0000       2.07       .288      151.8        .16      12.21
 20.0000       2.49       .356      175.9        .15      10.28
 25.0000       3.25       .414     -178.0        .17       8.55
!
! S-Parameters vs Frequency vs Bias
!M NOISE: M:PS;A:16;C:16;DC:1;H:0;P:1;DOT:DUT_NF_M;
!
!Bias# 16
!Bias Values Read:
!Vb:.861 V, Ib:.106 mA
!Vc:1.500 V, Ic:15.120 mA
!Date: 27 Mar 2003
!Time: 15:53:06
!Deembedding: ON
!
!  Freq    S11 Mag  S11 Ang  S21 Mag  S21 Ang  S12 Mag  S12 Ang  S22 Mag  S22 Ang
!  (GHz)             (Deg)             (Deg)             (Deg)             (Deg)
!-------- -------- -------- -------- -------- -------- -------- -------- --------
!
  2.0000     .746   -110.0   20.851    122.4     .028     39.5     .599    -41.1
  3.0000     .747   -131.6   15.427    111.1     .031     31.2     .467    -45.2
  4.0000     .749   -143.7   12.063    103.9     .033     27.2     .386    -45.9
  5.0000     .751   -152.1    9.879     98.8     .034     25.0     .337    -45.7
  6.0000     .751   -158.2    8.328     94.9     .035     24.4     .307    -44.5
  7.0000     .751   -162.7    7.187     91.5     .035     24.1     .280    -44.0
  8.0000     .752   -166.4    6.326     88.6     .035     24.1     .264    -43.5
  9.0000     .752   -169.3    5.634     86.1     .036     24.5     .252    -42.6
 10.0000     .750   -172.1    5.083     83.7     .037     25.2     .242    -42.2
 11.0000     .753   -174.0    4.614     81.4     .038     25.9     .228    -42.4
 12.0000     .748   -176.4    4.232     79.7     .038     26.4     .226    -42.4
 13.0000     .753   -178.1    3.904     77.8     .039     27.3     .219    -42.4
 14.0000     .751   -179.7    3.629     75.9     .039     27.9     .216    -42.6
 15.0000     .752    178.7    3.384     74.2     .039     29.2     .211    -42.9
 16.0000     .749    177.1    3.164     72.3     .040     29.7     .204    -43.9
 17.0000     .747    175.4    2.974     70.7     .041     31.1     .200    -44.0
 18.0000     .751    174.6    2.808     69.3     .041     31.5     .200    -45.3
```

| | | | | | | | | |
|---|---|---|---|---|---|---|---|---|
| 19.0000 | .748 | 173.3 | 2.661 | 67.9 | .043 | 32.3 | .195 | -46.6 |
| 20.0000 | .746 | 172.2 | 2.521 | 66.0 | .044 | 32.2 | .189 | -47.0 |
| 21.0000 | .748 | 169.8 | 2.405 | 64.4 | .043 | 34.2 | .190 | -47.8 |
| 22.0000 | .744 | 170.1 | 2.288 | 62.9 | .045 | 35.0 | .186 | -47.5 |
| 23.0000 | .740 | 168.3 | 2.196 | 61.6 | .045 | 36.4 | .181 | -48.7 |
| 24.0000 | .746 | 167.6 | 2.088 | 60.1 | .047 | 36.3 | .178 | -49.9 |
| 25.0000 | .748 | 167.1 | 2.001 | 58.7 | .047 | 37.1 | .177 | -51.8 |
| 26.0000 | .739 | 165.7 | 1.924 | 57.5 | .048 | 37.6 | .173 | -52.5 |

! Noise Parameters vs Frequency vs Bias
!M NOISE: M:PS;A:16;C:16;DC:1;H:0;P:1;DOT:DUT_NF_M;

| Freq (GHz) | F(min) Fitted (dB) | Gamma Opt Fitted Mag | Gamma Opt Fitted Angle | Normalized Associated Rn Z0=50 Fitted | Gain (dB) Fitted |
|---|---|---|---|---|---|
| 2.0000 | 1.12 | .255 | 37.1 | .21 | 27.74 |
| 5.0000 | 1.22 | .166 | 67.0 | .19 | 20.22 |
| 10.0000 | 1.55 | .228 | 125.7 | .16 | 15.17 |
| 15.0000 | 2.12 | .293 | 154.4 | .16 | 12.28 |
| 20.0000 | 2.54 | .360 | 177.4 | .16 | 10.32 |
| 25.0000 | 3.31 | .431 | -177.2 | .17 | 8.65 |

! S-Parameters vs Frequency vs Bias
!M NOISE: M:PS;A:16;C:16;DC:1;H:0;P:1;DOT:DUT_NF_M;

!Bias# 17
!Bias Values Read:
!Vb:.864 V, Ib:.114 mA
!Vc:1.500 V, Ic:16.560 mA
!Date: 27 Mar 2003
!Time: 15:53:09
!Deembedding: ON

| Freq (GHz) | S11 Mag | S11 Ang (Deg) | S21 Mag | S21 Ang (Deg) | S12 Mag | S12 Ang (Deg) | S22 Mag | S22 Ang (Deg) |
|---|---|---|---|---|---|---|---|---|
| 2.0000 | .741 | -113.7 | 21.133 | 120.9 | .027 | 38.4 | .578 | -41.9 |
| 3.0000 | .745 | -134.6 | 15.540 | 109.9 | .030 | 30.4 | .448 | -45.6 |
| 4.0000 | .750 | -146.1 | 12.096 | 102.9 | .031 | 27.0 | .371 | -45.7 |
| 5.0000 | .752 | -154.0 | 9.893 | 98.1 | .032 | 25.4 | .325 | -45.4 |
| 6.0000 | .752 | -159.8 | 8.338 | 94.3 | .033 | 24.8 | .296 | -44.2 |
| 7.0000 | .752 | -164.1 | 7.180 | 91.0 | .033 | 24.9 | .271 | -43.5 |
| 8.0000 | .754 | -167.7 | 6.317 | 88.2 | .034 | 24.9 | .255 | -42.9 |
| 9.0000 | .753 | -170.4 | 5.628 | 85.7 | .035 | 25.8 | .244 | -42.0 |
| 10.0000 | .752 | -173.1 | 5.071 | 83.4 | .035 | 26.1 | .235 | -41.6 |
| 11.0000 | .754 | -174.8 | 4.599 | 81.2 | .036 | 26.9 | .222 | -41.6 |
| 12.0000 | .752 | -177.0 | 4.225 | 79.4 | .036 | 27.5 | .219 | -41.6 |
| 13.0000 | .755 | -178.8 | 3.896 | 77.5 | .037 | 28.9 | .214 | -41.8 |
| 14.0000 | .752 | 179.5 | 3.621 | 75.7 | .037 | 29.1 | .210 | -42.0 |
| 15.0000 | .753 | 178.1 | 3.378 | 74.1 | .038 | 30.8 | .206 | -42.3 |
| 16.0000 | .752 | 176.4 | 3.152 | 72.2 | .039 | 31.1 | .197 | -43.1 |
| 17.0000 | .748 | 174.9 | 2.968 | 70.7 | .039 | 32.6 | .195 | -43.1 |
| 18.0000 | .752 | 173.9 | 2.804 | 69.2 | .040 | 33.2 | .194 | -44.9 |
| 19.0000 | .749 | 172.9 | 2.656 | 67.8 | .041 | 33.4 | .189 | -45.6 |
| 20.0000 | .748 | 171.8 | 2.513 | 66.0 | .042 | 34.3 | .184 | -46.0 |
| 21.0000 | .748 | 170.3 | 2.398 | 64.5 | .042 | 36.9 | .185 | -47.1 |
| 22.0000 | .748 | 169.7 | 2.286 | 62.9 | .042 | 36.7 | .184 | -47.1 |
| 23.0000 | .749 | 167.7 | 2.186 | 61.7 | .044 | 37.6 | .177 | -48.5 |
| 24.0000 | .745 | 167.5 | 2.087 | 59.9 | .046 | 38.6 | .174 | -49.2 |
| 25.0000 | .749 | 166.3 | 1.987 | 58.8 | .047 | 40.4 | .176 | -50.7 |
| 26.0000 | .746 | 165.8 | 1.925 | 58.0 | .048 | 41.3 | .168 | -52.9 |

! Noise Parameters vs Frequency vs Bias
!M NOISE: M:PS;A:16;C:16;DC:1;H:0;P:1;DOT:DUT_NF_M;

| Freq (GHz) | F(min) Fitted (dB) | Gamma Opt Fitted Mag | Gamma Opt Fitted Angle | Normalized Associated Rn Z0=50 Fitted | Gain (dB) Fitted |
|---|---|---|---|---|---|
| 2.0000 | 1.20 | .228 | 39.9 | .21 | 27.84 |

```
 5.0000       1.27       .154       74.1        .19      20.33
10.0000       1.61       .231      130.0        .16      15.22
15.0000       2.18       .299      157.1        .16      12.33
20.0000       2.62       .365      178.5        .16      10.32
25.0000       3.42       .436     -174.8        .17       8.65
!
! S-Parameters vs Frequency vs Bias
!M NOISE: M:PS;A:16;C:16;DC:1;H:0;P:1;DOT:DUT_NF_M;
!
!Bias# 18
!Bias Values Read:
!Vb:.866 V, Ib:.124 mA
!Vc:1.500 V, Ic:17.960 mA
!Date: 27 Mar 2003
!Time: 15:53:11
!Deembedding: ON
!
!  Freq    S11 Mag  S11 Ang  S21 Mag  S21 Ang  S12 Mag  S12 Ang  S22 Mag  S22 Ang
!  (GHz)             (Deg)             (Deg)             (Deg)             (Deg)
!-------- -------- -------- -------- -------- -------- -------- -------- --------
!
 2.0000     .738   -117.3   21.263    119.5     .026      37.3     .558    -42.5
 3.0000     .745   -137.3   15.569    108.9     .029      30.0     .432    -45.7
 4.0000     .750   -148.2   12.064    102.1     .030      26.6     .358    -45.4
 5.0000     .753   -155.8    9.863     97.4     .031      25.1     .313    -44.8
 6.0000     .754   -161.3    8.315     93.8     .031      25.3     .287    -43.5
 7.0000     .753   -165.3    7.142     90.5     .032      25.4     .263    -42.7
 8.0000     .757   -168.8    6.280     87.8     .032      25.7     .249    -42.0
 9.0000     .755   -171.4    5.594     85.4     .033      26.0     .239    -41.1
10.0000     .754   -173.8    5.042     83.2     .034      27.5     .230    -40.8
11.0000     .755   -175.6    4.565     80.9     .035      28.1     .219    -40.8
12.0000     .753   -177.5    4.197     79.3     .035      29.4     .215    -40.8
13.0000     .755   -179.3    3.877     77.5     .035      30.2     .211    -40.7
14.0000     .754    179.0    3.598     75.7     .036      31.0     .206    -41.0
15.0000     .754    177.5    3.357     74.0     .037      32.2     .202    -41.2
16.0000     .752    176.2    3.125     72.3     .037      32.5     .194    -42.4
17.0000     .750    175.1    2.950     70.9     .039      34.7     .194    -42.9
18.0000     .750    173.5    2.784     69.4     .040      34.7     .191    -43.8
19.0000     .749    173.3    2.649     68.0     .040      36.5     .187    -44.4
20.0000     .750    171.5    2.487     66.0     .041      35.8     .182    -45.5
21.0000     .750    171.0    2.390     64.7     .040      39.5     .181    -45.5
22.0000     .751    169.4    2.265     63.0     .042      37.9     .179    -46.4
23.0000     .750    169.0    2.179     62.3     .043      40.9     .176    -47.4
24.0000     .750    167.3    2.066     60.5     .045      40.5     .171    -48.9
25.0000     .747    167.2    2.009     59.2     .047      41.7     .173    -51.3
26.0000     .747    166.1    1.901     57.8     .047      41.6     .168    -52.0
!
! Noise Parameters vs Frequency vs Bias
!M NOISE: M:PS;A:16;C:16;DC:1;H:0;P:1;DOT:DUT_NF_M;
!
!  Freq     F(min)    Gamma Opt  Gamma Opt Normalized Associated
!  (GHz)    Fitted     Fitted     Fitted    Rn Z0=50   Gain (dB)
!           (dB)        Mag       Angle      Fitted     Fitted
!-------- ---------- ---------- ---------- ---------- ----------
!
 2.0000       1.28       .203       43.4        .21      27.88
 5.0000       1.32       .146       81.9        .18      20.40
10.0000       1.66       .236      134.0        .16      15.26
15.0000       2.24       .302      159.5        .16      12.33
20.0000       2.72       .373      179.2        .16      10.28
25.0000       3.37       .432     -176.7        .18       8.69
!
! S-Parameters vs Frequency vs Bias
!M NOISE: M:PS;A:16;C:16;DC:1;H:0;P:1;DOT:DUT_NF_M;
!
!Bias# 19
!Bias Values Read:
!Vb:.866 V, Ib:.124 mA
!Vc:1.500 V, Ic:17.880 mA
!Date: 27 Mar 2003
!Time: 15:53:13
!Deembedding: ON
!
!  Freq    S11 Mag  S11 Ang  S21 Mag  S21 Ang  S12 Mag  S12 Ang  S22 Mag  S22 Ang
```

```
!  (GHz)             (Deg)             (Deg)             (Deg)             (Deg)
!-------- -------- -------- -------- -------- -------- -------- -------- --------
!
  2.0000     .738   -117.3   21.255    119.5     .026     37.4     .558    -42.5
  3.0000     .745   -137.2   15.570    108.9     .029     30.0     .432    -45.7
  4.0000     .751   -148.1   12.059    102.2     .030     26.7     .358    -45.4
  5.0000     .753   -155.6    9.866     97.5     .031     25.4     .314    -44.8
  6.0000     .754   -161.1    8.312     94.0     .031     25.1     .287    -43.4
  7.0000     .753   -165.2    7.144     90.7     .032     25.3     .264    -42.5
  8.0000     .757   -168.5    6.277     88.0     .032     25.9     .248    -41.8
  9.0000     .754   -171.3    5.597     85.6     .033     26.4     .238    -41.0
 10.0000     .756   -173.4    5.039     83.5     .034     27.4     .229    -40.7
 11.0000     .755   -175.4    4.569     81.2     .035     28.5     .219    -40.6
 12.0000     .753   -177.0    4.199     79.7     .035     30.0     .216    -40.5
 13.0000     .753   -179.2    3.879     77.8     .036     30.3     .212    -40.6
 14.0000     .755    179.5    3.596     76.0     .036     31.9     .206    -40.8
 15.0000     .754    177.6    3.359     74.4     .037     32.1     .202    -41.1
 16.0000     .751    176.5    3.125     72.5     .037     33.1     .194    -42.0
 17.0000     .752    175.6    2.956     71.3     .038     35.5     .195    -42.1
 18.0000     .749    173.8    2.788     69.7     .039     35.5     .191    -43.0
 19.0000     .744    174.1    2.651     68.8     .040     36.7     .188    -43.8
 20.0000     .750    171.8    2.490     66.3     .040     36.7     .180    -45.2
 21.0000     .756    171.6    2.383     65.5     .041     39.8     .180    -44.9
 22.0000     .755    169.9    2.260     63.4     .041     38.5     .175    -47.5
 23.0000     .747    170.7    2.182     62.8     .043     42.3     .177    -47.1
 24.0000     .756    167.8    2.075     60.9     .043     41.5     .175    -48.9
 25.0000     .742    167.6    1.992     60.1     .046     43.8     .175    -49.5
 26.0000     .755    166.4    1.918     58.4     .046     42.7     .174    -51.8
!
! Noise Parameters vs Frequency vs Bias
!M NOISE: M:PS;A:16;C:16;DC:1;H:0;P:1;DOT:DUT_NF_M;
!
!  Freq     F(min)    Gamma Opt  Gamma Opt Normalized Associated
!  (GHz)    Fitted     Fitted     Fitted    Rn Z0=50   Gain (dB)
!            (dB)       Mag       Angle     Fitted     Fitted
!-------- ---------- ---------- ---------- ---------- ----------
!
  2.0000       1.29       .204       43.2        .21      27.88
  5.0000       1.32       .146       80.8        .19      20.39
 10.0000       1.67       .246      133.3        .16      15.28
 15.0000       2.24       .303      159.1        .16      12.33
 20.0000       2.70       .373      178.3        .16      10.28
 25.0000       3.46       .428     -177.3        .18       8.56
!
! S-Parameters vs Frequency vs Bias
!M NOISE: M:PS;A:16;C:16;DC:1;H:0;P:1;DOT:DUT_NF_M;
!
!Bias# 20
!Bias Values Read:
!Vb:.869 V, Ib:.136 mA
!Vc:1.500 V, Ic:19.440 mA
!Date: 27 Mar 2003
!Time: 15:53:16
!Deembedding: ON
!
!  Freq    S11 Mag  S11 Ang  S21 Mag  S21 Ang  S12 Mag  S12 Ang  S22 Mag  S22 Ang
!  (GHz)             (Deg)             (Deg)             (Deg)             (Deg)
!-------- -------- -------- -------- -------- -------- -------- -------- --------
!
  2.0000     .735   -121.1   21.178    118.0     .025     36.3     .537    -42.9
  3.0000     .745   -140.0   15.478    107.8     .027     29.2     .415    -45.5
  4.0000     .752   -150.3   11.930    101.3     .028     26.8     .344    -44.7
  5.0000     .753   -157.4    9.761     96.9     .029     25.7     .304    -43.9
  6.0000     .755   -162.5    8.232     93.4     .030     25.9     .279    -42.4
  7.0000     .754   -166.3    7.052     90.2     .030     26.0     .257    -41.4
  8.0000     .758   -169.6    6.194     87.7     .031     26.7     .243    -40.7
  9.0000     .756   -172.2    5.523     85.3     .032     27.4     .234    -39.8
 10.0000     .759   -174.2    4.972     83.2     .032     28.9     .225    -39.6
 11.0000     .755   -176.2    4.497     81.0     .033     29.7     .216    -39.4
 12.0000     .755   -177.5    4.140     79.5     .033     31.0     .212    -39.2
 13.0000     .755   -179.8    3.831     77.7     .034     32.1     .209    -39.6
 14.0000     .757    179.0    3.550     75.9     .035     32.5     .204    -39.7
 15.0000     .753    177.3    3.319     74.3     .036     34.0     .201    -40.3
 16.0000     .753    176.4    3.071     72.6     .036     35.4     .192    -40.9
 17.0000     .755    175.8    2.914     71.4     .037     36.2     .193    -41.4
 18.0000     .749    173.4    2.749     69.7     .038     37.5     .189    -41.5
```

```
 19.0000     .747    174.6    2.625     69.1     .038     38.5     .187    -42.4
 20.0000     .752    171.4    2.446     66.3     .040     38.4     .179    -44.0
 21.0000     .767    172.5    2.357     65.7     .040     40.3     .178    -44.6
 22.0000     .756    169.8    2.223     63.5     .040     40.5     .173    -46.8
 23.0000     .748    171.6    2.152     63.2     .043     45.0     .176    -47.0
 24.0000     .762    167.6    2.037     60.9     .042     43.2     .174    -47.4
 25.0000     .742    167.8    1.972     60.5     .045     45.3     .177    -46.9
 26.0000     .757    166.3    1.879     58.9     .045     45.6     .173    -51.6
!
! Noise Parameters vs Frequency vs Bias
!M NOISE: M:PS;A:16;C:16;DC:1;H:0;P:1;DOT:DUT_NF_M;
!
!  Freq     F(min)     Gamma Opt  Gamma Opt Normalized Associated
!  (GHz)    Fitted     Fitted     Fitted    Rn Z0=50   Gain (dB)
!           (dB)         Mag      Angle      Fitted     Fitted
!-------- ---------- ---------- ---------- ---------- ----------
!
  2.0000       1.41       .176       46.2        .21      27.80
  5.0000       1.38       .141       89.5        .18      20.40
 10.0000       1.73       .254      137.6        .16      15.28
 15.0000       2.30       .308      160.7        .17      12.27
 20.0000       2.82       .383      179.4        .16      10.19
 25.0000       3.51       .433     -177.4        .18       8.51
```

## APPENDIX G

## VERILOG-A CODE OF VBIC MODEL FOR SEMI-EMPIRICAL NOISE MODEL IMPLEMENTATION

Only the noise block is given, which is relavant to the semi-empirical noise model. Branch *n_ia* and *n_ib* consist of 1 Ohm resistance respectively. Branch *b_bei* is the intrinsic BE diode. Branch *b_cei* is the intrinsic CB current flow path.

```
...
// begin noise block

n_gm     = abs(Itzf)/(nf_t*Vtv);                    // added by kejun
n_cSib   = n_Kbb*pow(n_gm,n_abb)+n_Bbb+1e-60;       // added by kejun
n_cSic   = (n_Kcc*pow(n_gm,n_acc)+n_Bcc)*n_gm;      // added by kejun
n_cSicib = n_Kcb*pow(n_gm,n_acb)+n_Bcb;             // added by kejun
n_cVib   = n_cSic-n_cSicib*n_cSicib/n_cSib;         // added by kejun
n_cVib   = n_cVib>0.0 ? sqrt(n_cVib) : 0.0;         // added by kejun

I(n_ia)  <+ white_noise(1);                         // added by kejun
I(n_ib)  <+ white_noise(1);                         // added by kejun
I(n_ia)  <+ V(n_ia);                                // added by kejun
I(n_ib)  <+ V(n_ib);                                // added by kejun
I(b_bei) <+ ddt(V(n_ia))*sqrt(n_cSib);              // added by kejun
I(b_cei) <+ V(n_ia)*n_cSicib/sqrt(n_cSib);          // changed by kejun
I(b_cei) <+ V(n_ib)*n_cVib;                         // changed by kejun
I(b_bei) <+ white_noise(2*`QQ*abs(Ibe))
          +flicker_noise(kfn*pow(abs(Ibe),afn),bfn);
I(b_bex) <+ white_noise(2*`QQ*abs(Ibex))
          +flicker_noise(kfn*pow(abs(Ibex),afn),bfn);
I(b_bep) <+ white_noise(2*`QQ*abs(Ibep))
          +flicker_noise(kfn*pow(abs(Ibep),afn),bfn);
I(b_rcx) <+ white_noise(4*`KB*Tdev*Gcx);
I(b_rci) <+ white_noise(4*`KB*Tdev*((abs(Irci)
                      +1.0e-10*Gci)/(abs(Vrci)+1.0e-10)));
I(b_rbx) <+ white_noise(4*`KB*Tdev*Gbx);
I(b_rbi) <+ white_noise(4*`KB*Tdev*qb*Gbi);
I(b_re)  <+ white_noise(4*`KB*Tdev*Ge);
I(b_rbp) <+ white_noise(4*`KB*Tdev*qbp*Gbp);
I(b_cep) <+ white_noise(2*`QQ*abs(Iccp));
I(b_rs)  <+ white_noise(4*`KB*Tdev*Gs);

// end noise block
...
```

# APPENDIX H

# DERIVATION OF LOW INJECTION VAN VLIET MODEL IN ADMITTANCE REPRESENTATION

## H.1 Fundamentals

### H.1.1 Operator

We define inner product

$$< f, g >\equiv \int f g^* dv.$$

For operator $L$, its adjoint operator, $\widetilde{L}$, is defined as

$$< Lf, g > - < f, \widetilde{L}g >= \oint C[f, g] \cdot d\sigma. \tag{H.1}$$

That is, there is only a surface integration for the difference of inner products. The surface integral is along the inner surface. Note that $\widetilde{L} = (L^T)^*$, where $L^T$ is the transpose of $L$, superscript * denotes conjugate. If $L = \widetilde{L}$, $L$ is called self-adjoint operator. If the surface integration of a self-adjoint operator vanishes, $L$ is a Hermitian operator.

For carrier transport in semiconductor, carrier continuity equations like (2.40), (2.44) and (2.49) should be satisfied. The carrier changing rate operators for electron and hole in frequency domain are

$$L_n = s + 1/\tau_n - \bigtriangledown \cdot \mu\vec{E} - D\bigtriangledown^2, \tag{H.2}$$

$$L_p = s + 1/\tau_p + \bigtriangledown \cdot \mu\vec{E} - D\bigtriangledown^2, \tag{H.3}$$

where $s = j\omega$. The diffusion coefficient $D$ is assumed to be position independent, while the electric field is not subjected to such constraint. Their adjoint operators are

$$\widetilde{L}_n = -s + 1/\tau_n + \mu\overrightarrow{E} \cdot \bigtriangledown - D\bigtriangledown^2, \tag{H.4}$$

$$\widetilde{L}_p = -s + 1/\tau_p - \mu\overrightarrow{E} \cdot \bigtriangledown - D \bigtriangledown^2 . \tag{H.5}$$

The adjoint operators are simple because the electrical field is in front of $\bigtriangledown$. Further, in accord with [39], we write $\Lambda$ the spatial parts of these operators, i.e. $L = \Lambda + s$ and $\widetilde{L} = \widetilde{\Lambda} + s^*$. For example, the $\Lambda$ of hole carrier is

$$\Lambda_p = 1/\tau_p + \bigtriangledown \cdot \mu\overrightarrow{E} - D\bigtriangledown^2, \tag{H.6}$$

$$\widetilde{\Lambda}_p = 1/\tau_p - \mu\overrightarrow{E} \cdot \bigtriangledown - D \bigtriangledown^2 . \tag{H.7}$$

### H.1.2 Green's theorem for $L_p$

The Green's theorem for $L_p$ is that for any two functions $\alpha(r)$ and $\beta(r)$, (H.1) is satisfied, explicitly

$$\int \beta^* L_p \alpha dv - \int \alpha \widetilde{L}_p^* \beta^* dv = \oint [-\beta^* (D \bigtriangledown_0 - \mu\overrightarrow{E}_0)\alpha + \alpha D \bigtriangledown_0 \beta^*] \cdot d\sigma. \tag{H.8}$$

The surface integral is along the inner surface.

### H.1.3 Dirac delta function

The bulk delta function $\delta(r - r')$ is zero at any position except $r'$ and $\int \delta(r - r')dv = 1$. There are many analytical $\delta(r-r')$ functions, for example $-\bigtriangledown^2[1/(4\pi|r-r'|)]$. $\delta(r-r')$ has the following

properties:

$$\begin{aligned}
\phi(r')\delta(r-r') &= \phi(r)\delta(r-r'),\\
\bigtriangledown\delta(r-r') &= -\bigtriangledown'\delta(r-r'),\\
\phi(r')\bigtriangledown\delta(r-r') &= \phi(r)\bigtriangledown\delta(r-r') + [\bigtriangledown\phi(r)]\delta(r-r'),\\
\int \delta(r_0-r)\phi(r)dv &= \phi(r_0)/2,
\end{aligned} \tag{H.9}$$

where $\phi(r)$ can be any function, and $r_0$ is a point on the *smooth* boundary surface of given integration volume.

### H.1.4 $\Lambda$ theorem

$\Lambda$ is the spatial part of operator $L$. The $\Lambda$ theorem derived by van Vliet in [40] gives the connection between the covariance $\Gamma(r,r') \equiv < \Delta p(r,t)\Delta p(r',t) >$ and the noise source $\xi(r,t)$ with strength $\Xi(r,r') = \frac{1}{2}S_{bulk}$, that is

$$(\Lambda_r + \Lambda_{r'})\Gamma(r,r') = \frac{1}{2}S_{bulk}(r,r'). \tag{H.10}$$

Note $\Gamma(r,r') = \Gamma(r',r)$ and $S_{bulk}(r,r') = S_{bulk}(r',r)$. Certain boundary conditions can be stated which indicate that $\Gamma$ often satisfies delta-type singularities at the surface of volume $V$. The solution *inside* V stemming from the volume sources only will be denoted as $\Gamma'$.

## H.2 Problem setup for base low injection noise of PNP transistor

We consider the low injection minority carrier (i.e. hole) noise for the base region of a PNP transistor as shown in Fig. H.1. $S_\alpha$ and $S_\beta$ are the neutral base ending surface at EB and CB junctions. $S_f$ is the free surface of base. $S_c$ is the base contact surface. We allow position dependent

built-in field $E(r)$ and life time $\tau(r)$, while a position independent diffusion coefficient $D$. $E(r)$ should not depend on the carrier density.

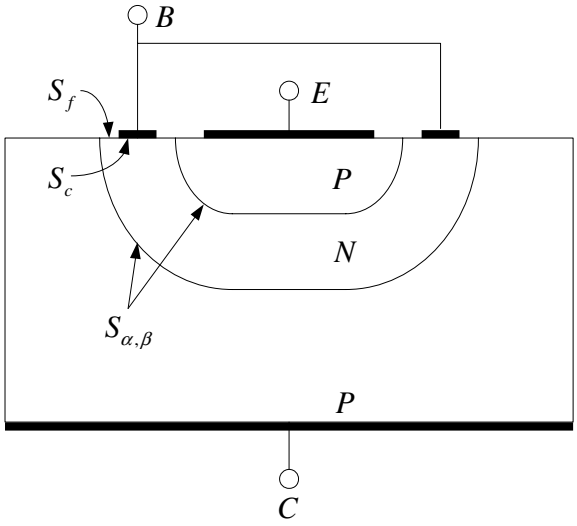


Figure H.1: Schematic geometry of a PNP transistor.

The hole continuity equation with *homogenous boundary condition* is

$$L_p p = \xi(r, s), \quad \xi(r, s) = \zeta(r, s) + \bigtriangledown \cdot \gamma(r, s), \tag{H.11}$$

$$p|_{\sigma=S_\alpha,S_\beta} = 0, \tag{H.12}$$

where $L_p$ is given in (H.3), $p$ is the hole density fluctuation. $\gamma(r, s)$ is the diffusion noise with PSD (in flux density representation, i.e. no charge units $e$)

$$S_\gamma(r, r') = 4Dp_s(r)\delta(r - r')\mathbb{I}, \tag{H.13}$$

according to (2.35), where $p_s(r)$ is the total DC hole density. $\zeta(r, s)$ is the GR noise with PSD

$$S_\zeta(r, r') = \left\{ \frac{4p_s(r)}{\tau_p} - 2D \bigtriangledown^2 p_s(r) + 2 \bigtriangledown \cdot [\mu \vec{E}(r) p_s(r)] \right\} \delta(r - r') \tag{H.14}$$

Note (H.14) is equivalent to (2.36) once $p_s(r) >> p_{s0}(r)$, a condition well satisfied when the transistor is forward biased. $p_{s0}(r)$ is the hole density at zero bias. To provide this, we consider the DC continuity equation, which is $\Lambda_p p_s(r) = 0$. Hence,

$$S_\zeta(r, r') = \left[\frac{2p_s(r)}{\tau_p} - 2\Lambda_p p_s(r)\right]\delta(r - r') = \frac{2p_s(r)}{\tau_p}\delta(r - r') \approx \frac{2[p_s(r) + p_{s0}(r)]}{\tau_p}\delta(r - r').$$

The reason of using (H.14) instead of (2.36) will be clear when applying $\Lambda$ theorem below. The total noise spectrum is

$$\begin{aligned} S_\xi(r, r') =& S_\zeta(r, r') + \bigtriangledown \cdot \bigtriangledown' \cdot S_\gamma(r, r') \\ =& \left\{\frac{4p_s(r)}{\tau_p} - 2D\bigtriangledown^2 p_s(r) + 2\bigtriangledown\cdot[\mu\vec{E}(r)p_s(r)]\right\}\delta(r - r') + 4D\bigtriangledown\cdot\bigtriangledown'[p_s(r)\delta(r - r')]. \end{aligned} \tag{H.15}$$

*Due to the assumption $p_s(r) >> p_{s0}(r)$, the van Vliet model is not correct at zero bias. Clearly finite exit velocity effect at CB junction is not considered as of the homogenous boundary condition used.*

### H.3 Green's function of homogeneous boundary

Define the homogeneous boundary Green's function $G^s$ as

$$L_p G^s(r, r', s) = \delta(r - r'), \quad G^s(r_0, r', s) = 0|_{r_0 \in S_c, S_f, S_\alpha, S_\beta}. \tag{H.16}$$

If the surface recombination velocity of $S_c$ and $S_f$ are not infinite, boundary conditions in (H.16) are not correct. However, theoretical analysis shows that the noise results will not change [39]. Define the adjoint Green's function $\widetilde{G}^s$ as

$$\widetilde{L}_p \widetilde{G}^s(r, r'', s) = \delta(r - r''). \tag{H.17}$$

Here $r'$ and $r''$ are source positions within the volume of integration. The Green's functions are not defined when the source positions are on the boundary yet. A "good" boundary condition for $\widetilde{G}^s$ should be chosen so that reciprocity

$$G^s(r, r', s) = \widetilde{G}^{s*}(r', r, s)$$

holds. This means that $\oint C[G^s(r_0, r', j\omega), \widetilde{G}^{s*}(r_0, r'', s)]d\sigma$ must vanish. To provide this, $\widetilde{G}^s$ should satisfy the boundary condition according to (H.8)

$$\widetilde{G}^s(r_0, r'', s) = 0|_{r_0 \in S_c, S_f, S_\alpha, S_\beta}.$$

Due to the reciprocity condition,

$$G^s(r', r_0, s) = 0|_{r_0 \in S_c, S_f, S_\alpha, S_\beta}, \quad \widetilde{G}^s(r'', r_0, s) = 0|_{r_0 \in S_c, S_f, S_\alpha, S_\beta}.$$

So far the Green's functions are fully defined.

$G(r, r', s)$ has the following property: for $r = r_\alpha$ and $r' \to r_\alpha^+$,

$$\oint\!\!\!\!\bigcirc (D \bigtriangledown_\alpha - \mu \vec{E}_\alpha) G^s(r_\alpha, r_\alpha^+, s) \cdot d\sigma_\alpha = -1, \tag{H.18}$$

where $r$ is a point on surface $\alpha$, and $r'$ approaches to the surface $\alpha$ from the inside. To provide this, consider an infinite small volume $\Delta V$ enclosed by surface $\alpha$ and surface $t$ as shown in Fig. H.2. The surface $t$ is a auxiliary surface infinitely close to surface $\alpha$. $r' \to r_\alpha^+$ is contained by $\Delta V$. According to the boundary condition of $G(r, r', s)$,

$$G(r_\alpha, r_\alpha^+, s) = 0, \qquad G(r_t, r_\alpha^+, s) = 0. \tag{H.19}$$

and then take a volume integral of (H.16) inside $\Delta V$,

$$\int \bigtriangledown \cdot (\mu \vec{E} - D \bigtriangledown) G(r, r', s) dv = \int \delta(r - r') dv = 1. \tag{H.20}$$

By using the Gauss theorem for the left side of (H.20), the volume integral can be transformed into a surface integral. Noticing that the surface integral on surface $t$ is infinite small, (H.18) is then obtained. Physically, (H.18) means that when the delta current injection position is very close to surface $\alpha$, then all the injected current will be collected by surface $\alpha$.

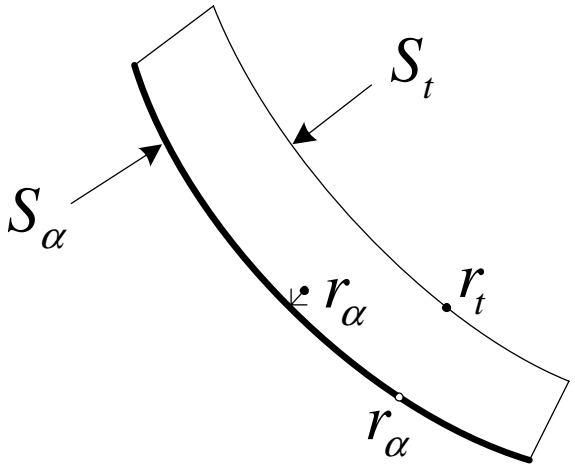


Figure H.2: Illustration of surface integral.

### H.4 Hole concentration fluctuation and its spectrum

The Green's theorem with $\alpha = p(r, s)$ and $\beta = \widetilde{G}^s(r, r', s)$ gives

$$\begin{aligned} p(r', s) = & \int \widetilde{G}^{s*}(r, r', s) \xi(r, s) dv \\ & + \oint [\widetilde{G}^{s*}(r_0, r', s)(D \bigtriangledown_0 - \mu \vec{E}_0) p(r_0, s) - p(r_0, s) D \bigtriangledown_0 \widetilde{G}^{s*}(r_0, r', s)] \cdot d\sigma. \end{aligned} \tag{H.21}$$

Making the changes $r' \to r$, $r \to r''$ and using the reciprocity, the hole concentration fluctuation can be obtained as

$$p(r, s) = \int G^s(r, r'', s)\xi(r'', s)dv + \oint [G^s(r, r_0, s)(D \bigtriangledown_0 - \mu\vec{E}_0)p(r_0, s) - p(r_0, s)D \bigtriangledown_0 G^s(r, r_0, s)] \cdot d\sigma. \tag{H.22}$$

(H.22) is valid for $G^s$ with any boundary condition. Especially for the homogeneous boundary condition defined for $G^s$, (H.22) reduces to

$$p(r, s) = \int G^s(r, r'', s)\xi(r'', s)dv. \tag{H.23}$$

From (H.23), the noise spectrum of the correlation between $p(r, s)$ and $p(r', s)$ can be obtained

$$\begin{aligned} S_p(r, r', \omega) \equiv < p^*(r, s)p(r', s) > &= \int\int G^s(r, r_1, -s) < \xi^*(r_1, s)\xi(r_2, s) > G^s(r', r_2, s)dv_1dv_2 \\ &= \int\int G^s(r, r_1, -s)S_\xi(r_1, r_2)G^s(r', r_2, s)dv_1dv_2. \end{aligned} \tag{H.24}$$

(H.24) is quadratic in Green's function, and should be transformed to be linear in Green's function using the $\Lambda$ theorem.

### H.4.1 van Vliet - Fasset form of noise spectrum

According to (H.10), the bulk covariance $\Gamma'(r_1, r_2)$ satisfies

$$(L^*_{p,r_1} + L_{p,r_2})\Gamma'(r_1, r_2) = (\Lambda_{p,r_1} + \Lambda_{p,r_2})\Gamma'(r_1, r_2) = \frac{1}{2}S_\xi(r_1, r_2), \tag{H.25}$$

so that

$$S_p(r, r', \omega) = 2 \int\int G^s(r, r_1, -s) G^s(r', r_2, s) [L^*_{p,r_1} + L_{p,r_2}] \Gamma'(r_1, r_2) dv_1 dv_2. \tag{H.26}$$

Changing $r \to r_2$ and making $\alpha = \Gamma'(r_1, r_2)$ and $\beta^* = G^s(r, r_1, -s) G^s(r', r_2, s)$, the Green's theorem gives

$$\begin{aligned} \int G^s(r, r_1, -s) G^s(r', r_2, s) L_{p,r_2} \Gamma'(r_1, r_2) dv_2 = & \int \Gamma'(r_1, r_2) \widetilde{L}^*_{p,r_2} G^s(r, r_1, -s) G^s(r', r_2, s) dv_2 \\ & + \oint [-G^s(r, r_1, -s) G^s(r', r_0, s) (D \bigtriangledown_0 - \mu \vec{E}_0) \Gamma'(r_1, r_0)] \cdot d\sigma \\ & + \oint [\Gamma'(r_1, r_0) D \bigtriangledown_0 G^s(r, r_1, -s) G^s(r', r_0, s)] \cdot d\sigma. \end{aligned} \tag{H.27}$$

Similarly, Changing $r \to r_1$ and making $\alpha^* = \Gamma'(r_1, r_2)$ and $\beta = G^s(r, r_1, -s) G^s(r', r_2, s)$, the conjugate Green's theorem gives

$$\begin{aligned} \int G^s(r, r_1, -s) G^s(r', r_2, s) L^*_{p,r_1} \Gamma'(r_1, r_2) dv_1 = & \int \Gamma'(r_1, r_2) \widetilde{L}_{p,r_1} G^s(r, r_1, -s) G^s(r', r_2, s) dv_1 \\ & + \oint [-G^s(r, r_0, -s) G^s(r', r_2, s) (D \bigtriangledown_0 - \mu \vec{E}_0) \Gamma'(r_0, r_2)] \cdot d\sigma \\ & + \oint [\Gamma'(r_0, r_2) D \bigtriangledown_0 G^s(r, r_0, -s) G^s(r', r_2, s)] \cdot d\sigma. \end{aligned} \tag{H.28}$$

Now using (H.27) and (H.28), (H.26) becomes

$$
\begin{aligned}
S_p(r,r',\omega) =& 2\int\int \Gamma'(r_1,r_2)[\widetilde{L}_{p,r_1}+\widetilde{L}^*_{p,r_2}]\widetilde{G}^s(r_1,r,s)\widetilde{G}^{s*}(r_2,r',s)dv_1dv_2 \\
&+2\oint\int -G^s(r,r'',-s)G^s(r',r_0,s)(D\bigtriangledown_0-\mu\vec{E}_0)\Gamma'(r'',r_0)dv''\cdot d\sigma \\
&+2\oint\int \Gamma'(r'',r_0)D\bigtriangledown_0 G^s(r,r'',-s)G^s(r',r_0,s)dv''\cdot d\sigma \\
&+2\oint\int -G^s(r,r_0,-s)G^s(r',r'',s)(D\bigtriangledown_0-\mu\vec{E}_0)\Gamma'(r_0,r'')dv''\cdot d\sigma \\
&+2\oint\int \Gamma'(r_0,r'')D\bigtriangledown_0 G^s(r,r_0,-s)G^s(r',r'',s)dv''\cdot d\sigma. \qquad \text{(H.29)}
\end{aligned}
$$

Note that the bulk part of (H.29) can be further reduced using the definition of Green's functions

$$
\begin{aligned}
S_p(r,r',\omega)|_{bulk} =& 2\int\int \widetilde{G}^{s*}(r_2,r',s)\Gamma'(r_1,r_2)[\widetilde{L}_{p,r_1}\widetilde{G}^s(r_1,r,s)]dv_1dv_2 \\
&+2\int\int \widetilde{G}^s(r_1,r,s)\Gamma'(r_1,r_2)[\widetilde{L}^*_{p,r_2}\widetilde{G}^{s*}(r_2,r',s)]dv_1dv_2 \\
=& 2\int\int \widetilde{G}^{s*}(r_2,r',s)\Gamma'(r_1,r_2)\delta(r_1-r)dv_1dv_2 \\
&+2\int\int \widetilde{G}^s(r_1,r,s)\Gamma'(r_1,r_2)\delta(r_2-r')dv_1dv_2 \\
=& 2\int[\Gamma'(r,r'')G^s(r',r'',s)+\Gamma'(r'',r')G^s(r,r'',-s)dv'', \qquad \text{(H.30)}
\end{aligned}
$$

so that

$$
\begin{aligned}
S_p(r,r',\omega) =& 2\int[\Gamma'(r,r'')G^s(r',r'',s)+\Gamma'(r'',r')G^s(r,r'',-s)dv'' \\
&+2\oint\int -G^s(r,r'',-s)G^s(r',r_0,s)(D\bigtriangledown_0-\mu\vec{E}_0)\Gamma'(r'',r_0)dv''\cdot d\sigma \\
&+2\oint\int \Gamma'(r'',r_0)D\bigtriangledown_0 G^s(r,r'',-s)G^s(r',r_0,s)dv''\cdot d\sigma \\
&+2\oint\int -G^s(r,r_0,-s)G^s(r',r'',s)(D\bigtriangledown_0-\mu\vec{E}_0)\Gamma'(r_0,r'')dv''\cdot d\sigma \\
&+2\oint\int \Gamma'(r_0,r'')D\bigtriangledown_0 G^s(r,r_0,-s)G^s(r',r'',s)dv''\cdot d\sigma. \qquad \text{(H.31)}
\end{aligned}
$$

This is the van-Fasset form whose main part is linear in Green's functions. (H.31) is valid for $G^s$ with any boundary condition for the hole density fluctuation caused by *bulk* noise sources. Particularly, for the homogeneous boundary condition of $G^s$, $G^s(r, r_0, s) = 0$. All surface integrals in (H.31) vanish, therefore

$$S_p(r, r', \omega) = 2 \int [\Gamma'(r, r'') G^s(r', r'', s) + \Gamma'(r'', r') G^s(r, r'', -s) dv''. \tag{H.32}$$

### H.4.2 Solution for $\Lambda$ theorem at low injection

For low injection, the $\Lambda$ theorem with the source (H.15) and $\Lambda$ (H.7) is

$$\begin{aligned} &\left[ \frac{2}{\tau_p} + \bigtriangledown \cdot \mu \vec{E}(r) - D \bigtriangledown^2 + \bigtriangledown' \cdot \mu \vec{E}(r') - D \bigtriangledown'^2 \right] \Gamma'(r, r') \\ &= \left\{ \frac{2 p_s(r)}{\tau_p} - D \bigtriangledown^2 p_s(r) + \bigtriangledown \cdot [\mu \vec{E}(r) p_s(r)] \right\} \delta(r - r') + 2D \bigtriangledown \cdot \bigtriangledown' [p_s(r) \delta(r - r')]. \end{aligned} \tag{H.33}$$

Using the properties of delta function in (H.9), one finds that (H.33) admits the solution

$$\Gamma'(r, r') = p_s(r) \delta(r - r'). \tag{H.34}$$

The derivation manifests the value of using $\Lambda p_s(r) = 0$ in the GR noise source as discussed in Section H.2. With (H.34) and (H.32), the spectrum of hole fluctuation for homogeneous boundary condition is

$$S_p(r, r', \omega) = 2 p_s(r) G^s(r', r, s) + 2 p_s(r') G^s(r, r', -s). \tag{H.35}$$

### H.5 Terminal noise current spectrum

The operator to transform carrier density into current density is $(e\mu\overrightarrow{E} - eD\bigtriangledown)$ for hole. The total hole current density at given point $r$ is

$$j(r,t) = e(\mu\overrightarrow{E} - D\bigtriangledown)p(r,t) - e\gamma(r,t) = j^o(r,t) - e\gamma(r,t), \tag{H.36}$$

where $j^o(r,t)$ is the response fluctuation current density

$$j^o(r,t) = e(\mu\overrightarrow{E} - D\bigtriangledown)p(r,t). \tag{H.37}$$

Therefore, the spectrum of is

$$S_j(r,r',\omega) = S_{j^o}(r,r',\omega) - S_{j^{o*},e\gamma}(r,r',\omega) - S_{e\gamma^*,j^o}(r,r',\omega) + e^2 S_\gamma(r,r',\omega). \tag{H.38}$$

The current spectrum due to $\gamma$ is

$$S_{j_\gamma}(\omega) = e^2 \oint\oint S_\gamma(r_\alpha, r_\alpha^+, \omega)\cdot d\sigma_\alpha \cdot d\sigma_\alpha^+ = e^2 \oint\oint 4Dp_s(r_\alpha)\delta(r_\alpha - r_\alpha^+) d\sigma_\alpha \cdot d\sigma_\alpha^+ = 0. \tag{H.39}$$

In the following, the rest three components are calculated.

### H.5.1 Spectrum due to $j^o$

The correlation spectrum of $j^o$, $< j^{o*}(r)j^o(r') >$, is

$$\begin{aligned}
S_{j^o}(r,r',\omega) =& 2e^2(\mu\overrightarrow{E} - D\bigtriangledown)(\mu\overrightarrow{E}' - D\bigtriangledown')[p_s(r)G^s(r',r,s) + p_s(r')G^s(r,r',-s)] \\
=& 2e^2 p_s(r')(D\bigtriangledown - \mu\overrightarrow{E})D\bigtriangledown' G^s(r,r',-s) \\
&+ 2e^2\left\{(D\bigtriangledown' - \mu\overrightarrow{E}')p_s(r')\right\}(D\bigtriangledown - \mu\overrightarrow{E})G^s(r,r',-s) \\
&+ 2e^2 p_s(r)(D\bigtriangledown' - \mu\overrightarrow{E}')D\bigtriangledown G^s(r',r,s) \\
&+ 2e^2\left\{(D\bigtriangledown - \mu\overrightarrow{E})p_s(r)\right\}(D\bigtriangledown' - \mu\overrightarrow{E}')G^s(r',r,s) \qquad \text{(H.40)}
\end{aligned}$$

The reason of separation will be clear when it is connected to Y-parameters below.

Now the correlation PSD of two different terminal $\alpha$ and terminal $\beta$ ($\alpha \neq \beta$) is,

$$\begin{aligned}
S_{i_\alpha^{o*} i_\beta^o}(\omega) =& \oint\!\!\oint S_{j^o}(r,r',\omega)\cdot d\sigma_\alpha \cdot d\sigma_\beta \Big|_{r=r_\alpha, r'=r_\beta} \\
=& \oint\!\!\oint 2e^2 p_s(r_\beta)(D\bigtriangledown_\alpha - \mu\overrightarrow{E}_\alpha)D\bigtriangledown_\beta G^s(r_\alpha, r_\beta, -s)\cdot d\sigma_\alpha \cdot d\sigma_\beta \\
&+ \oint\!\!\oint 2e^2 p_s(r_\alpha)(D\bigtriangledown_\beta - \mu\overrightarrow{E}_\beta)D\bigtriangledown_\alpha G^s(r_\beta, r_\alpha, s)\cdot d\sigma_\alpha \cdot d\sigma_\beta. \qquad \text{(H.41)}
\end{aligned}$$

For the auto-correlation PSD of terminal $\alpha$, $r = r_\alpha$ and $r' = r_\alpha$ cannot be set simultaneously, since the derivative of $G(r_\alpha, r_\alpha, s)$ cannot be defined. The trick is to set $r = r_\alpha$ and let $r' \to r_\alpha^+$ (or to set $r' = r_\alpha$ and let $r \to r_\alpha^+$). Here the superscript + indicates that the surface position is approached from the inside (consistent with the Green's theorem). Note that

$$e(D\bigtriangledown_\alpha - \mu\overrightarrow{E}_\alpha)p_s(r_\alpha) = -J_\alpha^{DC}(r_\alpha), \qquad \oint J_\alpha^{DC}(r_\alpha)\cdot d\sigma_\alpha = I_\alpha$$

Then the auto-correlation PSD of terminal $\alpha$ is

$$\begin{aligned}
S_{i_\alpha^{o*} i_\alpha^o}(\omega) &= \oint\oint S_{j^o}(r, r', \omega) \cdot d\sigma_\alpha \cdot d\sigma_\alpha|_{r=r_\alpha, r'\to r_\alpha^+} \\
&= \oint\oint 2e^2 p_s(r_\alpha^+)(D \bigtriangledown_\alpha - \mu\vec{E}_\alpha) D \bigtriangledown_\alpha^+ G^s(r_\alpha, r_\alpha^+, -s) \cdot d\sigma_\alpha \cdot d\sigma_\alpha^+ \\
&\quad + \oint\oint 2e^2 p_s(r_\alpha)(D \bigtriangledown_\alpha^+ - \mu\vec{E}_\alpha^+) D \bigtriangledown_\alpha G^s(r_\alpha^+, r_\alpha, s) \cdot d\sigma_\alpha \cdot d\sigma_\alpha^+ \\
&\quad - \oint 2eJ_\alpha^{DC}(r_\alpha) \oint (D \bigtriangledown_\alpha - \mu\vec{E}_\alpha) G^s(r_\alpha, r_\alpha^+, -s) \cdot d\sigma_\alpha \cdot d\sigma_\alpha^+ \\
&= \oint\oint 2e^2 p_s(r_\alpha^+)(D \bigtriangledown_\alpha - \mu\vec{E}_\alpha) D \bigtriangledown_\alpha^+ G^s(r_\alpha, r_\alpha^+, -s) \cdot d\sigma_\alpha \cdot d\sigma_\alpha^+ \\
&\quad + \oint\oint 2e^2 p_s(r_\alpha)(D \bigtriangledown_\alpha^+ - \mu\vec{E}_\alpha^+) D \bigtriangledown_\alpha G^s(r_\alpha^+, r_\alpha, s) \cdot d\sigma_\alpha \cdot d\sigma_\alpha^+ \\
&\quad + 2eI_\alpha. \qquad \text{(H.42)}
\end{aligned}$$

### H.5.2 Spectrum due to correlation of $j^o$ and $\gamma$

Similar to the derivation of $S_p(r, r', \omega)$, using (H.23) and (2.35), $S_{p^*,\gamma}(r, r', \omega)$ can be obtained as

$$S_{p^*,\gamma}(r, r', \omega) = 4D \int G^s(r, r'', -s) \bigtriangledown'' [p_s(r')\delta(r'' - r')] = -4Dp_s(r') \bigtriangledown' G^s(r, r', -s), \qquad \text{(H.43)}$$

since the surface integral vanishes. Further,

$$S_{j^{o*},\gamma}(r_\alpha, r_\beta, \omega) = 4eDp_s(r_\beta)(D \bigtriangledown_\alpha - \mu\vec{E}_\alpha) \bigtriangledown_\beta G^s(r_\alpha, r_\beta, -s), \qquad \text{(H.44)}$$

and finally

$$S_{i_\alpha^{o*}, e\int \gamma_\beta \cdot d\sigma_\beta}(\omega) = e^2 \oint\oint 4Dp_s(r_\beta)(\mu\vec{E}_\alpha - D\bigtriangledown_\alpha) \bigtriangledown_\beta G^s(r_\alpha, r_\beta, -s) \cdot d\sigma_\alpha \cdot d\sigma_\beta. \qquad \text{(H.45)}$$

Similarly,

$$S_{e\int\gamma_\alpha^*\cdot d\sigma_\alpha, i_\beta^o}(\omega) = e^2 \oint\!\!\oint 4Dp_s(r_\alpha)(\mu\vec{E}_\beta - D\bigtriangledown\beta) \bigtriangledown_\alpha G^s(r_\beta, r_\alpha, s)\cdot d\sigma_\beta \cdot d\sigma_\alpha. \tag{H.46}$$

### H.5.3 Terminal total noise current density spectrum

The correlation PSD of two different terminal $\alpha$ and terminal $\beta$ ($\alpha \neq \beta$) is,

$$\begin{aligned} S_{i_\alpha^*, i_\beta}(\omega) =& S_{i_\alpha^{o*} i_\beta^o}(\omega) - S_{i_\alpha^{o*}, e\int\gamma_\beta\cdot d\sigma_\beta}(\omega) - S_{e\int\gamma_\alpha^*\cdot d\sigma_\alpha, i_\beta^o}(\omega) \\ =& -\oint\!\!\oint 2e^2 p_s(r_\beta)(D\bigtriangledown_\alpha - \mu\vec{E}_\alpha) D\bigtriangledown_\beta G^s(r_\alpha, r_\beta, -s)\cdot d\sigma_\alpha \cdot d\sigma_\beta \\ & -\oint\!\!\oint 2e^2 p_s(r_\alpha)(D\bigtriangledown_\beta - \mu\vec{E}_\beta) D\bigtriangledown_\alpha G^s(r_\beta, r_\alpha, s)\cdot d\sigma_\alpha \cdot d\sigma_\beta. \end{aligned} \tag{H.47}$$

The auto-correlation PSD of terminal $\alpha$ is,

$$\begin{aligned} S_{i_\alpha^*, i_\alpha}(\omega) =& S_{i_\alpha^{o*} i_\alpha^o}(\omega) - S_{i_\alpha^{o*}, e\int\gamma_\beta\cdot d\sigma_\beta}(\omega)|_{r_\beta = r_\alpha^+} - S_{e\int\gamma_\alpha^*\cdot d\sigma_\alpha, i_\beta^o}(\omega)|_{r_\beta = r_\alpha^+} \\ =& -\oint\!\!\oint 2e^2 p_s(r_\alpha^+)(D\bigtriangledown_\alpha - \mu\vec{E}_\alpha) D\bigtriangledown_\alpha^+ G^s(r_\alpha, r_\alpha^+, -s)\cdot d\sigma_\alpha \cdot d\sigma_\alpha^+ \\ & -\oint\!\!\oint 2e^2 p_s(r_\alpha)(D\bigtriangledown_\alpha^+ - \mu\vec{E}_\alpha^+) D\bigtriangledown_\alpha G^s(r_\alpha^+, r_\alpha, s)\cdot d\sigma_\alpha \cdot d\sigma_\alpha^+ \\ & + 2eI_\alpha. \end{aligned} \tag{H.48}$$

## H.6 Y-parameters in homogeneous Green's function

We supply small signal $v_\beta$ at surface $\beta$ and measure the small signal current that flows into surface $\alpha$, then $Y_{\alpha\beta} \equiv i_\alpha / v_\beta$. Denote the small signal hole carrier density $p(r)$. We need to solve $p(r)$ for equation

$$L_p p(r) = 0, \quad p(r_\alpha) = 0, \quad p(r_\beta) = ep_s(r_\beta)/kTv_\beta.$$

To do this, we insert $\alpha = p(r)$, $\beta = \widetilde{G}^s(r, r', s)$ into (H.8), with boundary condition of both $p(r)$ and Green's function, we at once obtain ($r'$ is substituted with $r$)

$$p(r) = -\oint p(r_\beta) D \bigtriangledown_\beta G^s(r, r_\beta, s) \cdot d\sigma_\beta. \tag{H.49}$$

With the current operator $(e\mu\vec{E} - eD\bigtriangledown)$ for hole carrier, we obtain the Y-parameter as

$$Y_{\alpha\beta} = -\frac{e^2}{kT} \oint\oint p_s(r_\beta)(D \bigtriangledown_\alpha - \mu\vec{E}_\alpha) D \bigtriangledown_\beta G^s(r, r_\beta, s) \cdot d\sigma_\alpha \cdot d\sigma_\beta. \tag{H.50}$$

Let $\beta \to \alpha^+$ for (H.50), $Y_{\alpha\alpha}$ can be obtained as

$$\begin{aligned} Y_{\alpha\alpha} &= -\frac{e^2}{kT} \oint\oint p_s(r_\alpha^+)(D \bigtriangledown_\alpha - \mu\vec{E}_\alpha) D \bigtriangledown_\alpha^+ G^s(r, r_\alpha^+, s) \cdot d\sigma_\alpha \cdot d\sigma_\alpha^+ \\ &= -\frac{e^2}{kT} \oint\oint p_s(r_\alpha)(D \bigtriangledown_\alpha^+ - \mu\vec{E}_\alpha^+) D \bigtriangledown_\alpha G^s(r, r_\alpha, s) \cdot d\sigma_\alpha \cdot d\sigma_\alpha^+. \end{aligned} \tag{H.51}$$

The second step of (H.51) follows from symmetry.

### H.7 Relation between Y-parameter and noise spectrum

Comparing the Y-parameters in (H.51) and (eq:Yab) with the noise spectrum in (H.48) and (H.47), their relation can be summarized as

$$Si_\alpha^*, i_\beta(\omega) = 2kT(Y_{\beta\alpha} + Y_{\alpha\beta}^*) + \delta_{\alpha\beta} 2eI_\alpha, \tag{H.52}$$

where $\delta_{\alpha\beta}$ is the Kronecker delta. (H.52) is the van Vliet model in common-base configuration. Note the terminal DC current $I_\alpha$ takes the positive sign when it flows outward from the device and the $e$ should be $-e$ for NPN transistor.

### H.7.1 Common-base noise for BJTs

The PSD of $i_e^{CB}$ and $i_c^{CB}$ noise currents for BJTs in common-base configuration as shown in Fig. H.3 (a) can be obtained from (H.52) directly

$$\begin{aligned} S_{ie}^{CB} &= 4kT\Re(Y_{11}^{CB}) - 2qI_E, \\ S_{ic,ie^*}^{CB} &= 2kT(Y_{21}^{CB} + Y_{12}^{*CB}), \\ S_{ic}^{CB} &= 4kT\Re(Y_{22}^{CB}) + 2qI_C. \end{aligned} \tag{H.53}$$

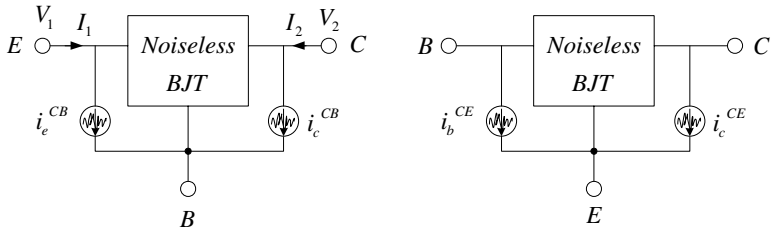


(*a*) *common base* (*b*) *common emitter*

Figure H.3: Admittance representation for BJT noise: (a) Common-base; (b) Common-emitter.

### H.7.2 Common-emitter noise for BJTs

Comparing Fig. H.3 (a) with Fig. H.3 (a), we have $i_b^{CE} = -i_e^{CB} - i_c^{CB}$ and $i_c^{CE} = i_c^{CB}$. Therefore the PSD of $i_b^{CE}$ and $i_c^{CE}$ is

$$\begin{aligned} S_{ib}^{CE} &= S_{ie}^{CB} + S_{ic}^{CB} + 2\Re[S_{ic,ie^*}^{CB}] = 4kT\Re(Y_{11}^{CB} + Y_{21}^{CB} + Y_{12}^{CB} + Y_{22}^{CB}) - 2qI_B, \\ S_{ic,ib^*}^{CE} &= -S_{ic}^{CB} - S_{ic,ie^*}^{CB} = -2kT(Y_{21}^{CB} + Y_{22}^{CB} + Y_{12}^{*CB} + Y_{22}^{*CB}) - 2qI_C, \\ S_{ic}^{CE} &= S_{ic}^{CB} = 4kT\Re(Y_{22}^{CB}) + 2qI_C. \end{aligned} \tag{H.54}$$

Now derive the Y-parameter relations between the common-base and common-emitter configurations. $V_1$, $V_2$, $I_1$ and $I_2$ defined in Fig. H.3 (a) satisfy

$$\begin{bmatrix} I_1 \\ I_2 \end{bmatrix} = \begin{bmatrix} Y_{11}^{CB} & Y_{12}^{CB} \\ Y_{21}^{CB} & Y_{22}^{CB} \end{bmatrix} \begin{bmatrix} V_1 \\ V_2 \end{bmatrix}. \tag{H.55}$$

$V_1$, $V_2$, $I_1$ and $I_2$ also satisfy

$$\begin{bmatrix} -I_1 - I_2 \\ I_2 \end{bmatrix} = \begin{bmatrix} Y_{11}^{CE} & Y_{12}^{CE} \\ Y_{21}^{CE} & Y_{22}^{CE} \end{bmatrix} \begin{bmatrix} -V_1 \\ V_2 - V_1 \end{bmatrix}. \tag{H.56}$$

According to (H.55) and (H.56),

$$\begin{bmatrix} Y_{11}^{CE} & Y_{12}^{CE} \\ Y_{21}^{CE} & Y_{22}^{CE} \end{bmatrix} = \begin{bmatrix} Y_{11}^{CB} + Y_{12}^{CB} + Y_{21}^{CB} + Y_{22}^{CB} & -Y_{12}^{CB} - Y_{22}^{CB} \\ -Y_{21}^{CB} - Y_{22}^{CB} & Y_{22}^{CB} \end{bmatrix}. \tag{H.57}$$

Finally, with (H.57) and (H.54), the van Vliet model in common-emitter configuration can be obtained

$$\begin{aligned} S_{ib}^{CE} &= 4kT\Re(Y_{11}^{CE}) - 2qI_B, \\ S_{ic,ib^*}^{CE} &= 2kT(Y_{21}^{CE} + Y_{12}^{*CE}) - 2qI_C, \\ S_{ic}^{CE} &= 4kT\Re(Y_{22}^{CE}) + 2qI_C. \end{aligned} \tag{H.58}$$